



**HAL**  
open science

# Modelling the temperature effect on phytoplankton : from acclimation to adaptation

Ghjuvan Micaelu Grimaud

► **To cite this version:**

Ghjuvan Micaelu Grimaud. Modelling the temperature effect on phytoplankton : from acclimation to adaptation. Other. Université Nice Sophia Antipolis, 2016. English. NNT : 2016NICE4025 . tel-01383294

**HAL Id: tel-01383294**

**<https://theses.hal.science/tel-01383294>**

Submitted on 18 Oct 2016

**HAL** is a multi-disciplinary open access archive for the deposit and dissemination of scientific research documents, whether they are published or not. The documents may come from teaching and research institutions in France or abroad, or from public or private research centers.

L'archive ouverte pluridisciplinaire **HAL**, est destinée au dépôt et à la diffusion de documents scientifiques de niveau recherche, publiés ou non, émanant des établissements d'enseignement et de recherche français ou étrangers, des laboratoires publics ou privés.

UNIVERSITÉ NICE SOPHIA-ANTIPOLIS - UFR SCIENCES

École Doctorale

SCIENCES ET TECHNOLOGIES DE L'INFORMATION ET DE LA COMMUNICATION

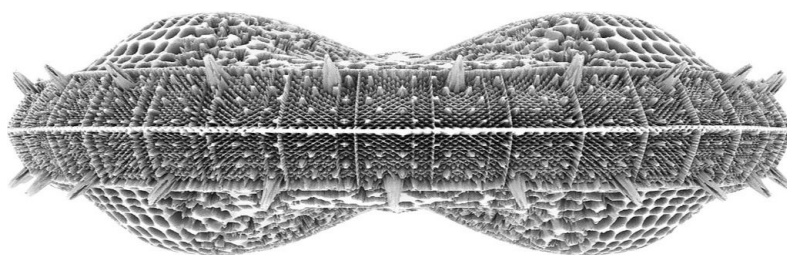
# THÈSE

pour obtenir le grade de

DOCTEUR DE L'UNIVERSITÉ NICE SOPHIA-ANTIPOLIS

Mention

AUTOMATIQUE, TRAITEMENT DU SIGNAL ET DES IMAGES



présentée par

**Ghjuvan Micaelu GRIMAUD**

Titre de la thèse

**Modélisation de l'effet de la température sur le  
phytoplancton: de l'acclimatation à l'adaptation**

**Modelling the temperature effect on phytoplankton:  
from acclimation to adaptation**

Thèse préparée dans le projet BIOCORE, INRIA Sophia-Antipolis

Dirigée par Olivier BERNARD, Antoine SCIANDRA, Francis MAIRET

Soutenue le 14 juin 2016 devant le jury composé de:

Président	Jean-Pierre GATTUSO	Université Pierre et Marie Curie
Rapporteur	Jean-Marc GUARINI	Université Pierre et Marie Curie
Rapporteur	Jean-Christophe POGGIALE	Aix-Marseille Université
Examineur	Jef HUISMAN	University of Amsterdam
Directeur de thèse	Olivier BERNARD	INRIA
Co-Directeur de thèse	Antoine SCIANDRA	Université Pierre et Marie Curie
Encadrant	Francis MAIRET	INRIA
Encadrant	Sophie RABOUILLE	Université Pierre et Marie Curie

Cover picture: artist's fractal view of a diatom microalgae  
©Markos Kay. Individual Diatom. 16 January 2010. Online image. Flickr. 9 September 2015.  
<https://www.flickr.com/photos/mrkism/4279102097/>

Pè Babò & Baba  
*U chjassu di vostri voci ricuccà in stu scrittu*

A Papou  
*'Dans l'eau que je puise scintille le début du printemps'*



## Remerciements



Sisyphus, 'Tableaux du temple des muses', Michel de Marolles, Paris, 1655.

Je tiens à remercier en premier lieu les rapporteurs de cette thèse d'avoir accepté avec patience de lire et de juger ce manuscrit. Merci à Jean-Marc Guarini et à Jean-Christophe Poggiale.

Merci à Jean-Pierre Gattuso d'avoir accepté de présider ce jury. C'est à mes yeux un privilège.

*I also would like to gratefully thank Jeff Huissman, who accepted to be part of my jury, which is a great honor.*

Merci à mes encadrants de thèse, qui m'ont donné l'accès tant attendu au monde de la recherche. Je remercie Olivier Bernard, qui est à mon humble avis un chercheur particulièrement brillant aux qualités humaines et humanistes époustouflantes et d'autant plus précieuses qu'elles se font rare dans un milieu si compétitif. Merci Olivier pour ton coaching scientifique et pour ces trois années. Je remercie chaleureusement Antoine Sciandra, qui a l'étonnante capacité d'être absolument polyvalent. Merci Antoine de m'avoir accueilli dans cette grande famille qu'est le LOV et d'avoir enrichi mon savoir et mes compétences en Océanographie. Je remercie Francis Mairet qui est un incroyable chercheur et une très belle personne. Merci de m'avoir soutenu pendant ces trois ans et de m'avoir fait progresser en modélisation. Enfin, je remercie Sophie Rabouille pour m'avoir également ouvert les portes du LOV et pour son expertise enrichissante sur les cyanobactéries diazotrophes et la biogéochimie marine.

Je remercie les membres de l'équipe BIOCORE, Jean-Luc Gouzé, Frédéric Grognard, Rafael Muñoz-Tamayo et toute la team pour ces échanges scientifiques et humains. Merci à Stéphanie Sorres pour ses compétences et sa

bonne humeur. Pour les même raison, merci aux membres du LOV, Lars Stemann, Fabien Lombard, Christophe Migon et tant d'autres chercheurs.

Merci aux enseignants, tous niveaux confondus, qui ont enrichi mon savoir: merci Cécile Guidicelli et France Colombani, avant tout. Merci à l'Université di Corti, à Magali Cannac, Anne Luciani, Bernard Marchand, Christophe Mori, Alain Muselli, Antoine Orsini, Gérard Pergent, Sylvia Agostini, Jacques Maury, Vanina Pasqualini. Un merci spécial à Marie Garrido qui devait faire partie de ce jury mais qui est appelée par d'autres aventures. Merci à l'Université Aix-Marseille II, à Charles-François Boudouresque, Daniela Banaru, David Nerini, Jean Christophe Poggiale, Mathias Gauduchon pour leurs enseignements si précieux.

Je remercie mes collègues et amis : Hubert la malice (en particulier pour son aide et ses conseils précieux, et notamment pour la partie matériel et méthode à laquelle il a très largement contribué), Simon, Martin, Sakina (qui m'a poussé à partir aux USA et je l'en remercie), Valérie valoche (qui est une fille formidable), Quentin, Caroline, Fabio, Orens, Raphaëlle, Margaux, Lisa, Yann l'artiste, Sophie, Ulysse, Tiphaine. Un grand merci à Amélie Talec, Eric Pruvost et Christophe Vasseur pour leurs conseils éclairés. Je remercie Andreas et Andrea d'avoir dompté le grand requin blanc en ma compagnie en Afrique du Sud. Merci à mon binôme officiel Robin Failletaz, aussi farfelu que sympathique. Merci à Anthony Dron qui fût un 'ainé' extra. Merci au physicien Allemand Philipp Hartmann, qui est un personnage génial.

Je remercie mes amis, Sébastien dit 'El Gancho', Benjamin, Morgan Fant, Mathieu, Antoine toto, Christoffe, Leslie, Johana, Gabie, Perle, Doudou, Mélanie pour la partie détente qu'ils ont remplie parfaitement. *Vi ringraziau fratellucci*. Je remercie grandement Orezza<sup>®</sup>, AirCorsica<sup>®</sup>, Freddy du WiC<sup>®</sup>.

Un merci particulier à Charlotte Combe, qui a partagé cette expérience avec moi. J'espère que ton aventure Air-liquidienne te portera où tu le souhaites.

Je remercie ma famille: Daniel, Isabelle, Marine; ma grand-mère, mes oncles et mes cugini. Merci tonton et tata Rose pour cette filiation.

Merci aux Marincais d'hier et d'aujourd'hui...

Je remercie mon extraordinaire grande soeur avec qui j'ai partagé de nombreuses aventures sous-marines mémorables.

Enfin, je souhaite remercier mes sponsors pour leur bienveillance et leur présence indéfectibles et fondamentales, sans lesquels je vivrais reclus dans un abri de fortune en bord de mer. Merci infiniment Dumè&Nathalie.

*'Chaque fois que la science avance d'un pas, c'est qu'un imbécile la pousse, sans le faire exprès'. Emile Zola*

*'L'optimiste est un imbécile heureux'. Georges Bernanos*

# Publications

## In peer reviewed journal articles

- Bonnefond, H., Grimaud, G.M., Rumin, J., Pruvost, E., Bernard, O., Sciandra, A. (Submitted) Continuous pressure of selection to improve temperature response of *Tisochrysis Lutea*. Plos One.
- Grimaud, G.M., Mairet, F., LeGuenec, V., Ayata, S.D., Sciandra, A., Bernard, O. (in preparation) A modelling approach to understand how phytoplankton faces temperature change in the global ocean.
- Grimaud, G.M., Mairet, F., Bonnefond, H., Sciandra, A., Bernard, O. (in preparation) Modelling the temperature effect on unicellular organisms from heterotrophic bacteria to autotrophic eukaryotes: a review.
- Grimaud, G.M., Rabouille, S., Dron, A., Sciandra, A., Bernard, O. (2014) Modelling the dynamics of carbon-nitrogen metabolism in the unicellular diazotrophic cyanobacterium *Crocospaera watsonii* WH8501 under variable light regimes. Ecological Modelling 291, 121-133.

## In peer reviewed conference proceedings

- Grimaud, G.M., LeGuenec, V., Ayata, S.D., Mairet, F., Bernard, O. (2015) Modelling the temperature effect on phytoplankton growth across the global Ocean. Mathmod 2015, Vienna
- Grimaud, G.M., Mairet, F., Bernard, O. (2014) Modelling thermal adaptation in microalgae: an Adaptive Dynamics point of view. IFAC 2014, Cape Town, South Africa
- Grimaud, G.M., Dron, A., Rabouille, S., Sciandra, A., Bernard, O. (2013) Modelling photoperiod influence on the carbon-nitrogen metabolism in a unicellular diazotrophic cyanobacterium. Computer Application to Biotechnology 2013, Mumbai (Bombay)



## **PUBLICATIONS**

---

# Contents

<b>Publications</b>	<b>v</b>
<b>List of Figures</b>	<b>xi</b>
<b>List of Tables</b>	<b>xv</b>
<b>1 Introduction</b>	<b>1</b>
1.1 An ode to phytoplankton . . . . .	1
1.2 Phytoplankton and temperature . . . . .	2
1.2.1 The direct effect of temperature . . . . .	2
1.2.2 Phytoplankton in a changing climate . . . . .	3
1.2.3 A decisive parameter in biotechnological applications . . . . .	6
1.3 From acclimation to adaptation . . . . .	7
1.4 Objectives of the thesis . . . . .	9
<b>2 Material and methods</b>	<b>11</b>
2.1 Culture device and selection procedure . . . . .	11
2.1.1 The selectiostats . . . . .	11
2.1.2 Cultivation mode for selection experiments . . . . .	13
2.1.3 The TIP device . . . . .	13
2.2 Data compilation, parameters identification and models calibration . . . . .	14
2.2.1 Thermal growth curves compilation . . . . .	14
2.2.2 Species biovolume . . . . .	15
2.2.3 CTMI parameters determination . . . . .	15
2.2.4 Data sets selection . . . . .	16
2.2.5 Hinshelwood model calibration . . . . .	16
2.2.6 Data analysis . . . . .	17
2.2.6.1 Linear relationships between the cardinal temperatures . . . . .	17
2.2.6.2 Non-linear relationships between $T_{opt}$ and $\mu_{opt}$ . . . . .	17
2.2.6.3 Statistical tools for models comparison . . . . .	18

## CONTENTS

---

<b>3</b>	<b>Modelling the temperature effect on unicellular organisms from heterotrophic bacteria to autotrophic eukaryotes: a review</b>	<b>19</b>
3.1	Introduction . . . . .	19
3.2	Modelling the specific growth rate of unicellular organisms as a function of temperature . . . . .	22
3.2.1	Methodological clarification . . . . .	22
3.2.2	The Arrhenius model from Van't-Hoff to Eyring: . . . . .	23
3.2.3	Empirical approach . . . . .	25
3.2.4	Mechanistic approach . . . . .	26
3.2.5	The protein thermal stability challenge . . . . .	29
3.3	The special case of unicellular photosynthetic organisms . . . . .	34
3.3.1	The Eppley point of view for phytoplankton . . . . .	34
3.3.2	The link between photosynthesis and temperature in the models . . . . .	36
3.4	The dynamical effect of temperature on unicellular organisms . . . . .	37
3.4.1	The metabolic response to temperature acclimation . . . . .	37
3.4.2	The thermally-induced death . . . . .	39
3.5	Conclusion . . . . .	41
<b>4</b>	<b>Correlation between the cardinal temperatures: insight into thermal adaptation</b>	<b>45</b>
4.1	Introduction . . . . .	45
4.2	Relation between the cardinal temperatures . . . . .	46
4.2.1	Linear relationships . . . . .	46
4.2.2	Differences among the phylogenetic groups . . . . .	48
4.2.3	A closer look at microalgae . . . . .	53
4.3	Thermal adaptation and the thermal niche width . . . . .	55
4.4	Conclusion . . . . .	56
<b>5</b>	<b>Revisiting the Eppley hypothesis</b>	<b>61</b>
5.1	Introduction . . . . .	61
5.2	Hotter is not always faster . . . . .	62
5.2.1	Describing the relationship between $T_{opt}$ and $\mu_{opt}$ using quantile regression . . . . .	62
5.2.2	Group specificities . . . . .	64
5.2.3	Scaling law in the thermal growth curve . . . . .	64
5.3	The phytoplankton paradigm . . . . .	70
5.3.1	The revisited Eppley curve for phytoplankton . . . . .	70
5.3.2	A case study: the cyanobacteria <i>Synechococcus</i> sp. . . . .	73
5.4	Conclusion . . . . .	73
<b>6</b>	<b>Towards understanding the thermodynamical fundament of the thermal growth curve: a modelling approach</b>	<b>77</b>
6.1	Introduction . . . . .	77

6.2	The Hinshelwood model as a theoretical framework . . . . .	78
6.2.1	Metabolism represented as a set of n autocatalytic reactions . . . .	78
6.2.2	Data normalization and calibration of the Hinshelwood model . . .	80
6.3	Accounting for the enthalpy-entropy compensation . . . . .	80
6.3.1	Theoretical approach . . . . .	80
6.3.2	Calibration . . . . .	81
6.4	Accounting for the activity-stability trade-off . . . . .	81
6.4.1	Theoretical approach . . . . .	81
6.4.2	Calibration . . . . .	83
6.5	The two parameters Hinshelwood model . . . . .	83
6.5.1	Reducing the parameter number of the Hinshelwood model down to 2 . . . . .	83
6.5.2	Comparison between the reduced Hinshelwood and the reduced CTMI models . . . . .	85
6.5.3	Correlation between the cardinal temperatures . . . . .	85
6.6	Conclusion . . . . .	90
<b>7 Modelling thermal adaptation in microalgae: an adaptive dynamics</b>		
	<b>point of view</b>	<b>93</b>
7.1	Introduction . . . . .	93
7.2	Simple dynamical model describing the temperature effect on microalgae in chemostat . . . . .	94
7.2.1	The Monod model in chemostat . . . . .	94
7.2.2	The specific case of the Droop model in chemostat . . . . .	95
7.3	Evolutionary Model . . . . .	96
7.3.1	General case . . . . .	96
7.3.2	Modelling the evolution of the optimal temperature trait . . . . .	98
7.3.3	Structural link between adaptive traits . . . . .	99
7.4	Fluctuating temperature . . . . .	101
7.4.1	Ecological timescale . . . . .	101
7.4.2	Evolutionary timescale . . . . .	103
7.4.2.1	Case 1: $T_{opt}$ is varying only . . . . .	103
7.4.2.2	Case 2: the thermal niche width is kept constant . . . . .	105
7.4.3	Evolutionary Branching conditions . . . . .	106
7.5	Conclusion . . . . .	109
<b>8 Selecting thermal tolerant strains of the Haptophyceae <i>Tisochrysis</i></b>		
	<b><i>lutea</i></b>	<b>113</b>
8.1	Introduction . . . . .	113
8.2	Selection experiment in controlled systems . . . . .	114
8.2.1	Summary of the experiment . . . . .	114
8.2.2	Main results . . . . .	115
8.3	Modelling selection during the experiment . . . . .	118

## CONTENTS

---

8.3.1	Re-identification of the final thermal tolerance parameters . . . . .	118
8.3.1.1	Identification at the population scale . . . . .	118
8.3.1.2	Competition between two thermal phenotypes . . . . .	121
8.4	Modelling thermal adaptation during the experiment . . . . .	127
8.4.1	Determining the invasion fitness . . . . .	127
8.4.1.1	Population dynamics, invasion fitness and selection gradient in a turbidostat growth model . . . . .	128
8.4.1.2	Population dynamics, invasion fitness and selection gradient in a fed-batch growth model . . . . .	128
8.4.2	Evolutionary dynamics . . . . .	129
8.4.3	Evolutionary equilibrium . . . . .	132
8.5	Conclusion . . . . .	133
<b>9</b>	<b>Modelling the effect of temperature on phytoplankton growth across the global ocean</b> . . . . .	<b>135</b>
9.1	Introduction . . . . .	136
9.2	Evolutionary model for thermal adaptation . . . . .	137
9.2.1	Slow-fast dynamical system . . . . .	137
9.2.2	Evolutionary model using Adaptive Dynamics theory . . . . .	139
9.3	Global ocean scale simulations . . . . .	140
9.3.1	Evolutionary model with realistic temperature signal . . . . .	140
9.3.2	Global scale simulations . . . . .	141
9.3.3	Comparison with experimental data . . . . .	141
9.3.4	The warming scenario . . . . .	145
9.4	Conclusion . . . . .	146
<b>10</b>	<b>Conclusion &amp; Perspectives</b> . . . . .	<b>149</b>
10.1	The physiological impacts of temperature on phytoplankton . . . . .	149
10.1.1	From empirical models to thermodynamical insights . . . . .	149
10.1.2	The submerged iceberg of unknown: future works . . . . .	150
10.2	Capturing the evolutionary trajectories . . . . .	151
10.2.1	Selection experiments and evolutionary modelling . . . . .	151
10.2.2	Evolution in the ocean . . . . .	152
10.3	Conclusion . . . . .	153
<b>Annexes</b>		<b>155</b>
	Determining $T_{min}$ , $T_{opt}$ , $T_{max}$ and $\mu_{opt}$ in the Hinshelwood model . . . . .	155
	Autocatalytic view of the Hinshelwood model . . . . .	155
<b>Bibliography</b>		<b>157</b>

# List of Figures

1.1	Eukaryote phylogenetic tree . . . . .	2
1.2	Size range of phytoplankton . . . . .	3
1.3	Thermal growth curve . . . . .	4
1.4	Global warming trend . . . . .	5
1.5	Correlation between warming and Net Primary Production change . . . . .	6
1.6	Temperature variations in a raceway pond located in New Zealand . . . . .	8
1.7	Dallinger experiment . . . . .	9
1.8	Adaptation of the thermal growth curve . . . . .	10
2.1	Selectostat culture device . . . . .	12
2.2	TIP device . . . . .	14
3.1	Model fit . . . . .	20
3.2	Master reaction model (eq. 3.19) . . . . .	27
3.3	Hinshelwood model . . . . .	28
3.4	Modified master reaction model . . . . .	30
3.5	Free energy distribution . . . . .	32
3.6	Eppley curve . . . . .	35
3.7	Modified Eppley model . . . . .	36
3.8	Survival curves . . . . .	40
3.9	Coupled growth and death models . . . . .	42
3.10	Survival curves obtained at different temperatures . . . . .	43
4.1	Linear regression between the cardinal temperatures. . . . .	47
4.2	Linear regression between $T_{opt}$ and $T_{max}$ . . . . .	49
4.3	Linear regression between $T_{opt}$ and $T_{min}$ . . . . .	50
4.4	Linear regression between $T_{max}$ and $T_{min}$ . . . . .	51
4.5	Linear regression between $T_{opt}$ and $T_{min}$ , $T_{opt}$ and $T_{max}$ for phytoplankton (data from Thomas et al. [2015]) . . . . .	55
4.6	Thermal niche width box plot . . . . .	57
4.7	Thermal niche width box plot for Thomas et al. [2015] data set . . . . .	58
5.1	Maximal growth rate $\mu_{opt}$ as a function of $T_{opt}$ . . . . .	63

## LIST OF FIGURES

---

5.2	Normalized thermal envelope of the $\mu_{opt} = f(T_{opt})$ curve. . . . .	65
5.3	Maximal growth rate $\mu_{opt}$ as a function of $T_{opt}$ and 99th quantile regression with fourth degrees polynome for the 5 groups . . . . .	66
5.4	Log of cell biovolume $V$ as a function of $\mu_{opt}$ . . . . .	67
5.5	Maximal growth rate biovolume-adjusted $\mu_{opt}/V^\alpha$ as a function of $T_{opt}$ and third polynomial 99th quantile regression for the whole data set . . . . .	68
5.6	Maximal growth rate $\mu_{opt}$ as a function of $T_{opt}$ and 99th quantile regression for 4 microalgae subgroups . . . . .	71
5.7	Maximal growth rate $\mu_{opt}$ as a function of $T_{opt}$ , 99th quantile regression and CTMI model calibration for 4 microalgae subgroups . . . . .	72
5.8	Thermal growth curve of <i>Synechococcus</i> sp. strains. . . . .	74
6.1	Thermostability of <i>Escherichia coli</i> homoserine transsuccinylase . . . . .	78
6.2	Log-linear relation between $A_2$ and $E_2$ . . . . .	82
6.3	$E_1/E_2$ as a function of $T_{max}$ for bacteria and archaee . . . . .	84
6.4	Normalised model validation . . . . .	86
6.5	Model validation . . . . .	87
6.6	Histogram of $r^2$ distribution . . . . .	88
6.7	Predicted versus experimental growth rate . . . . .	89
6.8	Cardinal temperatures predicted by the Hinshelwood model . . . . .	90
7.1	Thermal growth curve obtained with the Droop model . . . . .	97
7.2	Thermal growth curve of <i>Nannochloropsis oceanica</i> . . . . .	100
7.3	Evolution of the thermal growth curve . . . . .	104
7.4	Evolution of $T_{opt}$ if the niche width is kept constant . . . . .	107
7.5	Pairwise Invasibility Plots . . . . .	108
7.6	Evolutionary branching of trait $a$ . . . . .	110
8.1	Thermal growth curves of the initial and adapted strains of <i>Tisochrysis lutea</i> . . . . .	116
8.2	Growth rates of the different strains during each cycle of the experiment . . . . .	117
8.3	Re-identified strains with one parameter for Turbidostat . . . . .	121
8.4	Re-identified strains with one parameter for Fed-batch . . . . .	122
8.5	Re-identified strains using method 5 . . . . .	123
8.6	Re-identified strains using method 7 . . . . .	124
8.7	Temperature applied to the turbidostat and fed-batch cultures . . . . .	126
8.8	Competition dynamics for the Fed-batch culture . . . . .	127
8.9	Adaptation during the selection experiment in turbidostat . . . . .	130
8.10	Adaptation during the selection experiment in fed-batch . . . . .	131
8.11	Thermal growth curve at the evolutionary equilibrium . . . . .	132
9.1	Global ocean scale simulations . . . . .	142
9.2	Model predictions . . . . .	143
9.3	Comparison to experimental data . . . . .	144

9.4 Global ocean scale simulations of  $T_{max}^*$ . . . . . 147



## LIST OF FIGURES

---

# List of Tables

3.1	Synthesis of the main models . . . . .	21
4.1	Parameters of the linear regression between cardinal temperatures and statistical descriptors. $\hat{a}$ and $\hat{b}$ correspond to the slope and to the intercept of the linear regression $y = \hat{a}x + \hat{b}$ . . . . .	52
4.2	Parameters of the linear regression between cardinal temperatures and statistical descriptors for Thomas et al. [2015] data set (microalgae). $\hat{a}$ and $\hat{b}$ correspond to the slope and to the intercept of the linear regression $y = \hat{a}x + \hat{b}$ . . . . .	54
5.1	Parameters of the fourth order polynomial function $\mu_{opt}(T) = \sum p_i T^i$ applied to the 5 groups. . . . .	64
5.2	Parameters of the CTMI model applied to the 5 groups. . . . .	65
5.3	Parameters of the CTMI model applied to microalgae groups. . . . .	71
6.1	Parameters of the activity/stability trade-off function . . . . .	83
6.2	Models comparison on normalised data sets . . . . .	85
7.1	Model parameters for evolutionary branching . . . . .	109
8.1	Bernard & Rémond model parameters for strains W2X, S-Turb and S-Fb. The error interval correspond to the mean $\pm$ standard deviation determined by a jackknife analysis as in Bernard and Rémond [2012]. . . . .	115
8.2	Re-identified parameters for strains S-Turb and S-Fb. The initial parameters which do not change appear in gray. . . . .	120
8.3	Thermal parameters of two-subpopulations competing (corresponding in average to strain S-Turb or strain S-Fb). The initial parameters which do not change appear in gray. . . . .	126

## GLOSSARY

---

# 1

## Introduction

### 1.1 An ode to phytoplankton

Light in the euphotic layer of the oceans supports the growth of unicellular autotrophic organisms. These organisms drifting with the current are called phytoplankton [Falkowski and Raven, 2013]. Phytoplankton constitute a polyphyletic group, gathering prokaryotes (*Cyanobacteria*) and various unicellular eukaryotes lineages (fig. 1.1), for which photosynthesis results from different evolutionary pathways of the chloroplast (*i.e.* the cellular organelle performing photosynthesis), which has travelled between eukaryote groups via endosymbiosis through the ages [Boudouresque, 2015]. For this reason, phytoplankton comprise very different organisms, with size ranging from 1 to  $10^4 \mu\text{m}$  (fig. 1.2), and a vast variety of metabolic functions shaping ocean biogeochemistry. Currently, the global ocean is dominated in cell number by *Cyanobacteria* of the genus *Prochlorococcus* and *Synechococcus* [Ting et al., 2002], which can annually reach, for example, a total of  $10^{27}$  and  $10^{26}$  cells on average in the Pacific Ocean, respectively [Flombaum et al., 2013].

By harvesting the solar energy, phytoplankton fuel the entire oceanic food web, forming a functional ecological group<sup>1</sup> responsible of approximately 45% of the worldwide primary production [Field et al., 1998]. In 1936, Alfred Redfield noticed a curious constant stoichiometry between carbon, nitrogen and phosphorus in the ocean [Redfield, 1934] (C:N:P=106:16:1) which puzzled scientists for several decades. We now know that phytoplankton are the guilty organisms, and, as underlined by Pr. Paul Falkowski: ‘*Phytoplankton not only reflected the chemical composition of the deep ocean, but created it.*’. Phytoplankton deeply control biogeochemical cycles of these key elements up to the depths of the oceans, and then indirectly drive climate [Boyd and Doney, 2003]. Dead sinking phytoplankton actively participate to the ‘biological carbon pump’ [Volk and Hoffert, 1985], a process by which inorganic carbon is incorporated to the biological biomass, exported to the depth, then remineralized and finally partially redistributed thousand to millions years later.

---

<sup>1</sup>We do not include predators, parasites and heterotrophic species in our phytoplankton definition

# 1. INTRODUCTION

Phytoplankton growth depends on various physico-chemical environmental factors. Light, obviously, is a fundamental factor driving growth and scientists even use it to infer phytoplankton world distribution by tracking the ocean colour [Antoine and Morel, 1996, Lin et al., 2016]. After light, temperature is also a very influencing factor, neglected for a long time, defining the biogeographical boundaries of major groups, from polar to tropical oceans [Longurst, 1998]. A recent global scale study deeply confirms the temperature role in phytoplankton growth and repartition [Sunagawa et al., 2015]. Finally, nutrients (*e.g.* N, P, Fe etc.) may also limit phytoplankton growth.

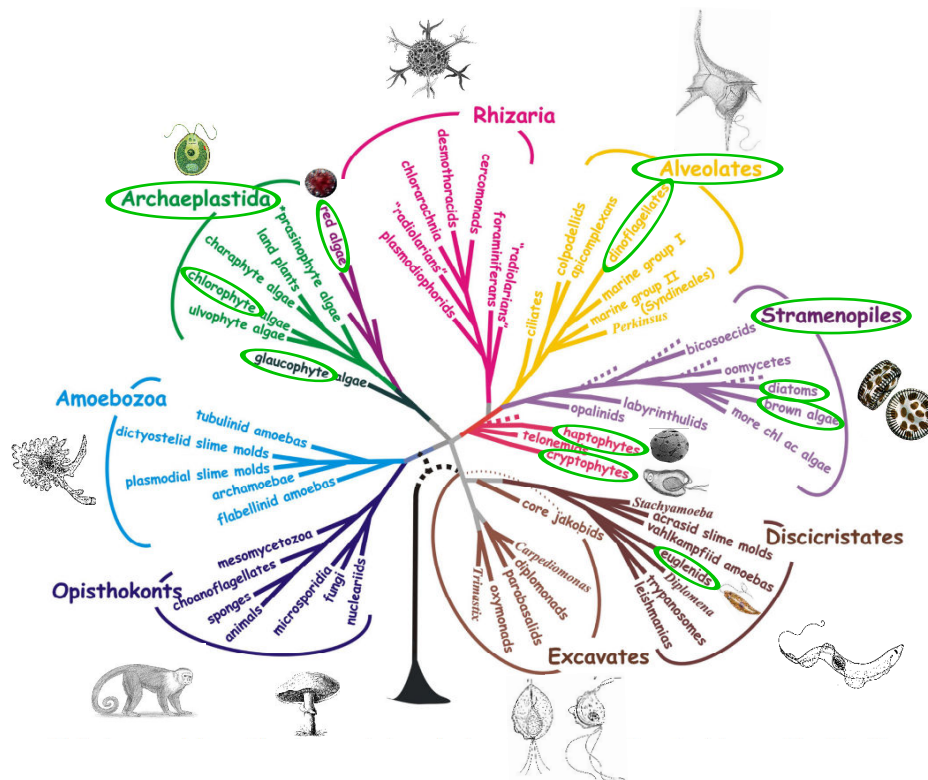


Figure 1.1: Eukaryote phylogenetic tree - Eukaryote phylogenetic tree (adapted from Baldauf [2008]). Phytoplankton groups are marked with green ellipses.

## 1.2 Phytoplankton and temperature

### 1.2.1 The direct effect of temperature

The direct effect of temperature on phytoplankton growth rate is represented by an asymmetric curve called the thermal growth curve or the thermal reaction norm

## 1.2 Phytoplankton and temperature

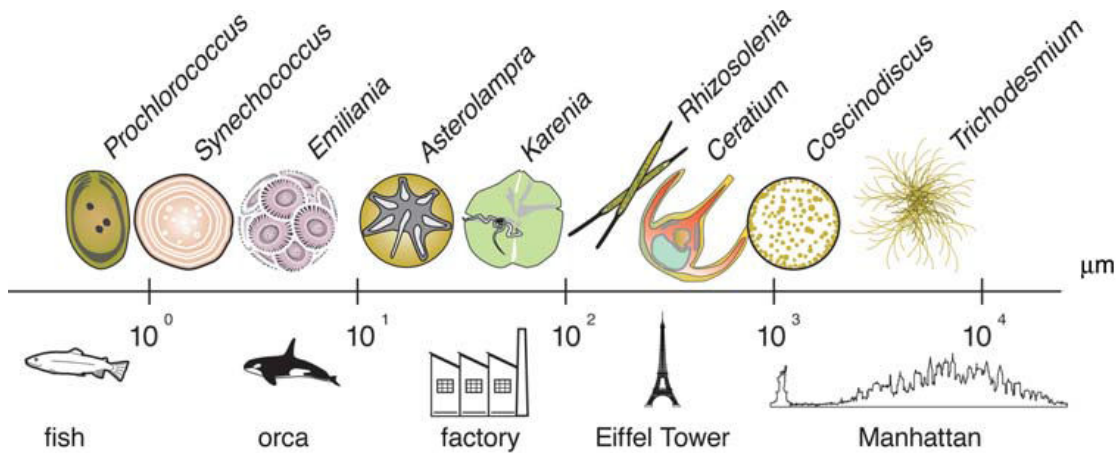


**Figure 1.2: Size range of phytoplankton** - Scale range of phytoplankton, from unicellular *Cyanobacteria* to giant Bacillariophyceae and colonial *Cyanobacteria* (adapted from Finkel et al. [2009]).

[Kingsolver, 2009] (fig. 1.3). The cardinal temperatures corresponding to the boundaries of thermal tolerance are defined as the minimal ( $T_{min}$ ), optimal ( $T_{opt}$ ) and maximal ( $T_{max}$ ) temperatures for growth. The growth rate obtained at  $T_{opt}$  is the theoretical maximal growth rate  $\mu_{opt}$  which may further depend on light. The thermal range on which a given phytoplankton species can thrive is called the thermal niche width (*i.e.*  $|T_{max} - T_{min}|$ ).

Phytoplankton can acclimate to temperature conditions (and then modify the shape of this curve) by increasing their RNA and modifying their chlorophyll content at low temperature, for example, or by expressing heat-shock proteins at high temperatures [Hoppenrath and Leander, 2010] and adapting membrane fluidity accordingly.

The thermal growth curve is also influenced by several other factors. In specific conditions, light and temperature can have coupled effects. For example, at low temperature, the enzymatic-dependent part of photosynthesis is lowered by temperature whereas the non-enzymatic dependent part is not, resulting in an energy imbalances participating in photoinhibition [Ras et al., 2013]. Similarly, nutrient starvation Thomas [2013] and salinity changes can temporarily modify the cardinal temperatures.

### 1.2.2 Phytoplankton in a changing climate

In the late 80's, a french team led by Pr. Claude Lorius brought back the proof from the Antarctic ices that earth was warming [Lorius et al., 1990]. According to Claude Lorius: *'Les fluctuations du CO<sub>2</sub> sont régulées par les océans, à travers des processus physiques, chimiques mais aussi biologiques, le monde vivant participant ainsi à l'évolution du climat. Depuis des centaines de milliers d'années, températures et concentrations en aérosols et en gaz à effet de serre varient entre des maxima et des minima relativement constants. Le climat terrestre s'auto-contrôle naturellement pour évoluer entre*

## 1. INTRODUCTION

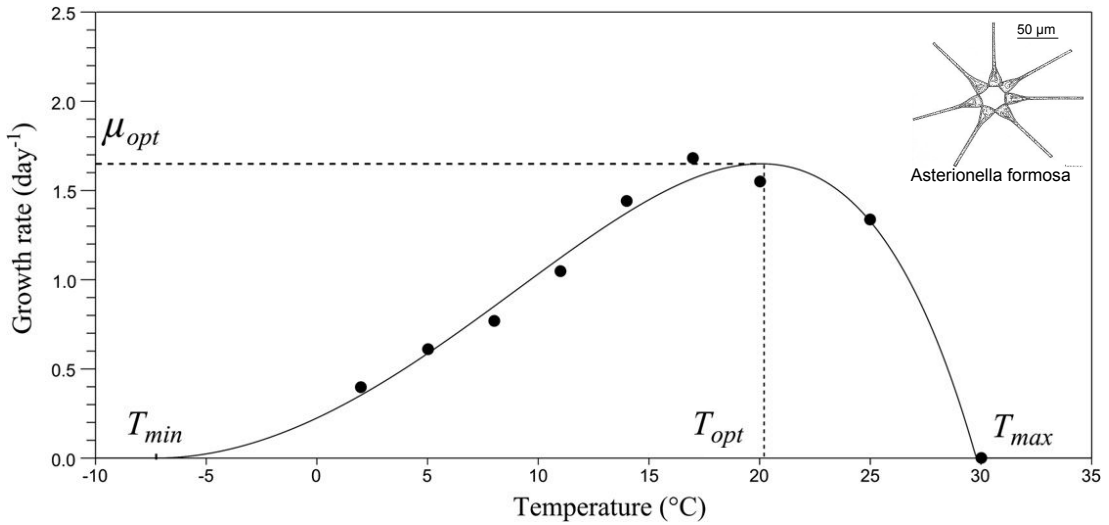


**Figure 1.3: Thermal growth curve** - Thermal growth curve for the phytoplankton species *Asterionella formosa* (adapted from Bernard and Rémond [2012]). Note the minimal temperature parameter  $T_{min}$  which is negative here while no data points are available below zero (see chapter 3).

*deux états stables bien définis. [...] les teneurs actuelles en gaz à effet de serre n'ont pas d'équivalent au cours des dernières centaines de milliers d'années et sont directement liées à l'impact anthropique sur la composition de l'atmosphère. Les conclusions tirées des archives glaciaires conduisent par conséquent à penser que la planète devrait sensiblement se réchauffer au cours du XXI<sup>e</sup> siècle, au risque d'affecter les ressources en eau, l'agriculture, la santé, la biodiversité et, d'une façon générale, les conditions de vie des humains.* This alarming report is a current reality; the year 2015 was, for example, the hottest year on record [Tollefson, 2016]. Recent estimations predict a global increase of 1°C to 5°C [Rogelj et al., 2012] for the year 2100 (fig. 1.4).

Global warming is materialized in the oceans by an increase of the average annual Sea Surface Temperature [Wijffels et al., 2016]. In this context, phytoplankton have to face different phenomena. Firstly, warming enhances upper ocean stratification and consequently lowers access to nutrient [Winder and Sommer, 2012]. Secondly, warming has a direct impact on phytoplankton physiology, specially during extreme thermal events. Behrenfeld et al. [2006] has found a correlation between the positive annual average temperature anomaly for the years 1999 to 2004 (corresponding to El Niño Southern Oscillations events) and the negative average annual anomaly of Net Primary Production (fig. 1.5). This is concerning because El Niño is thought to occur repetitively, and a extreme one is predicted for 2016 [Monastersky, 2016]. Recent studies claim that temperature strongly determines phytoplankton biogeographical repartition [Chen, 2015, Thomas et al., 2015, Yvon-Durocher et al., 2015]. These modified thermal regimes could induce community shifts in some areas, modifying the stoichiometry of fundamental el-

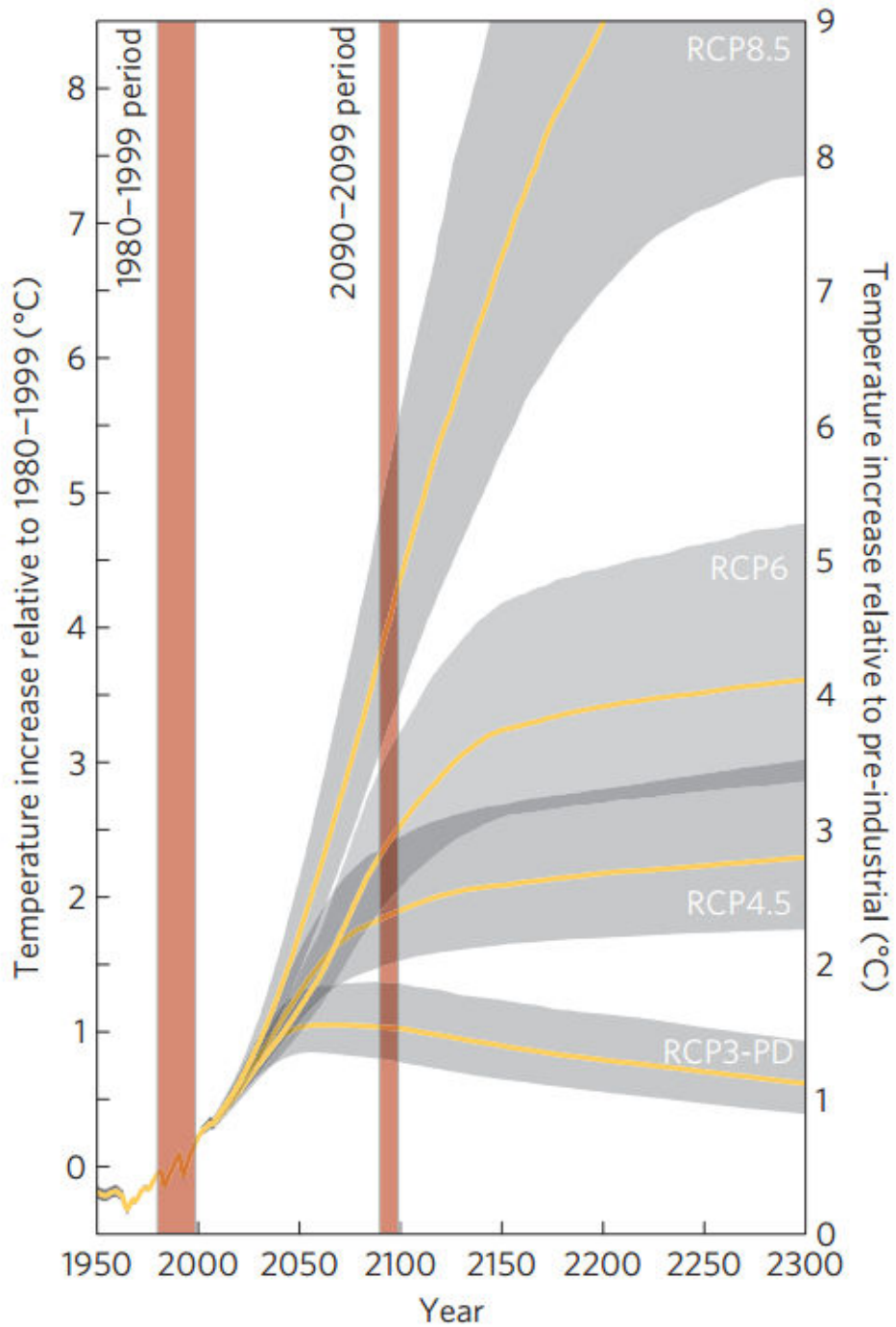


**Figure 1.4: Global warming trend** - Change in average temperature recorded and predicted according to different scenario of the Intergovernmental Panel on Climate Change (IPCC) (adapted from Rogelj et al. [2012]).



## 1. INTRODUCTION

---

elements such as the N:P ratio which is largely temperature dependent [Martiny et al., 2013] (at higher temperatures, the P-rich ribosome concentration in cells is lower and thus the N:P ratio is higher).

It is worth noting that global change induces several other environmental modifications in the ocean combined to warming, such as the extension of oxygen minimum zones (OMZ) [Wright et al., 2012] (*i.e.* oxygen depletion enhancement in certain areas), as well as ocean acidification Riebesell and Gattuso [2015]. The coupled effects of all these factors on phytoplankton are currently unknown and represent a challenge in marine sciences.

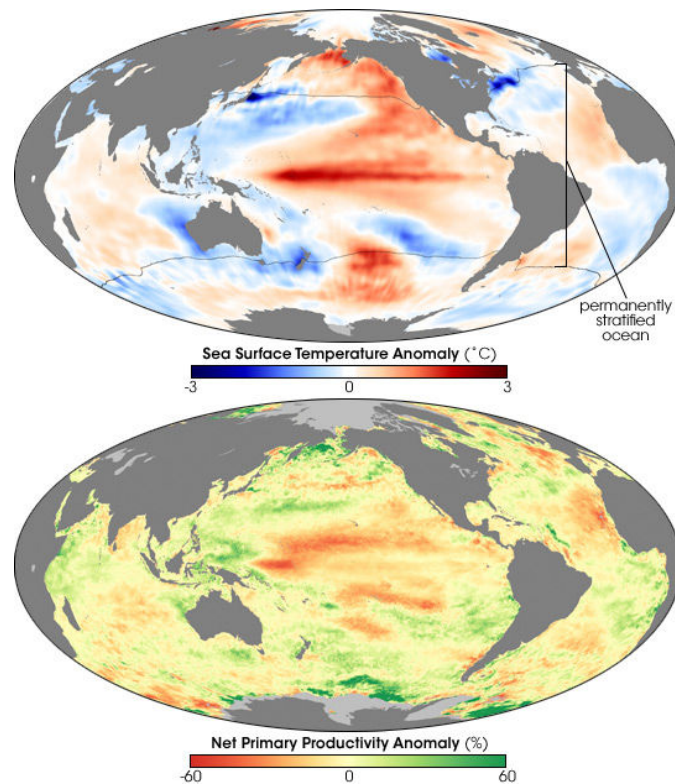


**Figure 1.5: Correlation between warming and Net Primary Production change** - Change in average Sea Surface Temperature (upper figure) and Net Primary Production (figure below) during the 1999 to 2004 period (adapted from Behrenfeld et al. [2006]).

### 1.2.3 A decisive parameter in biotechnological applications

Characterized by several attracting physiological specificities, phytoplankton, also called microalgae in the context of valorisation, are under the scientific spotlights. On top of their autotrophic growth requiring little nutrient input compared to heterotrophic unicellular eukaryotes, some of them are able to accumulate important amounts of neutral

lipids [Mata et al., 2010], which can be turned into biofuel. Others can store large quantities of carbohydrates, used for methane production. They are therefore a promising resource for future biotechnologies [Wijffels et al., 2013].

Microalgae are cultivated in a wide range of systems. For large scale industrial productions, the most common ones are outdoor open ponds called raceways (fig. 1.6 A). Pond daily temperature variations can reach high values far different from what is encountered in the natural environment, sometimes higher than 40°C [Bechet et al., 2010, Béchet et al., 2011] (fig. 1.6 B). Temperature then appears as a key factor for optimizing production and has to be controlled here for several purposes: maintain optimal temperature values in order to enhance productivity, limit thermally induced death during extreme thermal events, avoid light-saturation that occurs at low temperature [Béchet et al., 2011, Ras et al., 2013]. A recent modelling study trying to figure out the orders of magnitudes of phytoplankton large scale outdoor cultures productivity in France points toward a crucial role played by temperature, and particularly the negative impact of temperature daily fluctuations [De Rosbo and Bernard, 2014].

### 1.3 From acclimation to adaptation

The phytoplankton thermal growth curve is flexible, and phytoplankton can acclimate in a certain limit to temperature variations. However, when temperature variations overtake this limit, phytoplankton have to adapt through a process of evolution [Hofmann and Todgham, 2010]. Historically, Dallinger was the first to conduct a selection experiment to test for the adaptation limits of unicellular eukaryotes [Dallinger, 1887] (fig. 1.7). Dallinger progressively increased the environmental temperature of three Monads (fig. 1.7 right), and watched for their presence with a microscope. He found that, years after years, Monads were well adapting to their new temperatures and were still alive. This experiment is subjected to caution, because of possible contamination. However, in 2011, more than one century after Dallinger's experiment, Huertas et al. [2011] conducted a closely related one with phytoplankton (the so-called ratchet experiments). Huertas et al. [2011] concluded that phytoplankton did adapt to temperature *in silico*, at least to smooth temperature increase, and that this adaptation is highly group dependent.

Since Huertas et al. [2011], several studies have been conducted to define the ability of each species to adapt to temperature [Costas et al., 2014a,b, Padfield et al., 2015b]. It is however not known how the shape of the thermal growth curve evolves during adaptation, as well as the process by which cardinal temperatures change. Several hypotheses exist depending on the constraints playing a role during evolution [Angilletta, 2009, Knies et al., 2009] (fig. 1.8). If the species are not thermodynamically constrained (*i.e.* if the effect of warming does not favour growth in an Arrhenius-like way), then the thermal growth curve would only horizontally transpose (horizontal shift hypothesis). In the other case, higher temperatures are expected to sustain higher growth rates (higher is better hypothesis). The thermal niche width is not obviously constant, and thus can decrease (specialist-generalist hypothesis) or increase (hotter is broader hypothesis)

## 1. INTRODUCTION

---

A



B

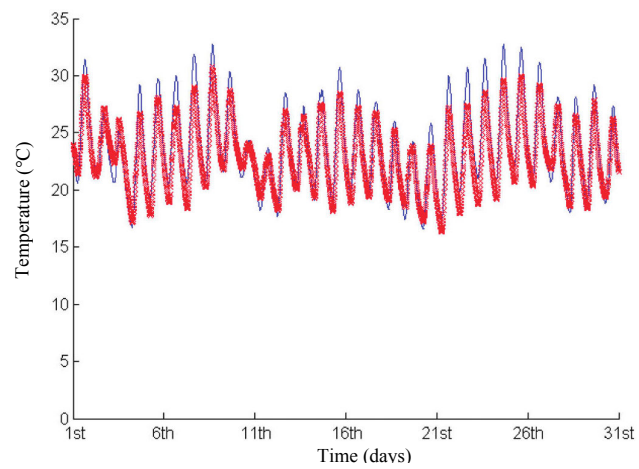


**Figure 1.6: Temperature variations in a raceway pond located in New Zealand - Raceway pond (A) and associated temperature variations (B) during August 2013 (adapted from Béchet et al. [2011]).** Experimental data are marked in red whereas the blue line corresponds to a dedicated model.

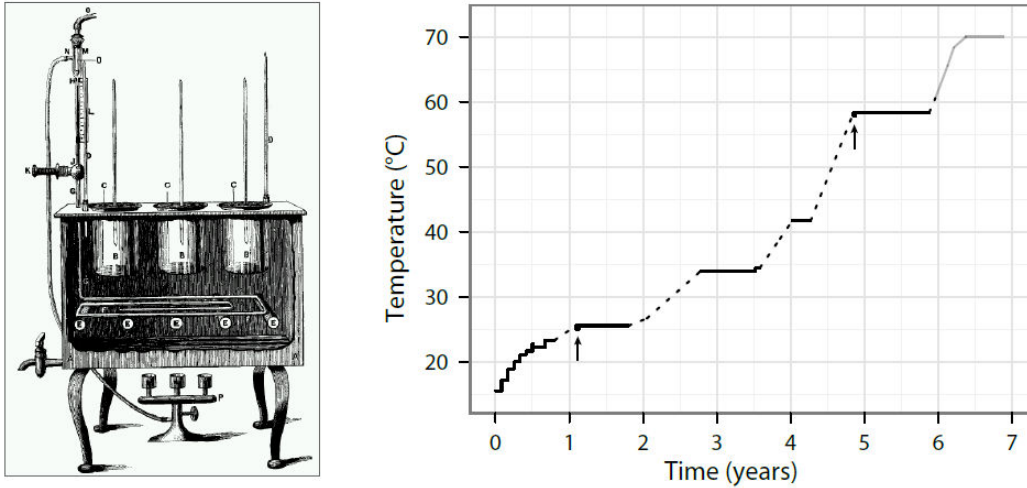


**Figure 1.7: Dallinger experiment** - Experiment conducted by Dallinger [1887] on the three monads *Tetramitus rostratus*, *Monas dallingeri*, *Dallingeria drysdali* (adapted from Julou [2011]).

with temperature. Finally, evolution could only affect  $T_{opt}$  and then lead to asymmetric changes only (asymmetric hypothesis).

## 1.4 Objectives of the thesis

In the present thesis, the objectives can be listed as follow: i)What are the effects of temperature on marine phytoplankton physiology? ii)What are the mechanistic processes that underlie the thermal growth curve? iii)How do phytoplankton adapt to temperature? To answer these questions, we first reviewed the existing models representing the thermal growth curve and the thermally driven physiological mechanisms (section 3). We then compiled thermal growth curves for hundreds of species to determine universal and specific links and try to interpret it in light of a mechanistic model (section 4, 5, 6). We finally constructed evolutionary models (section 7), later confronted to a selection experiment (section 8) and simulated at global ocean scale (section 9).

## 1. INTRODUCTION

---

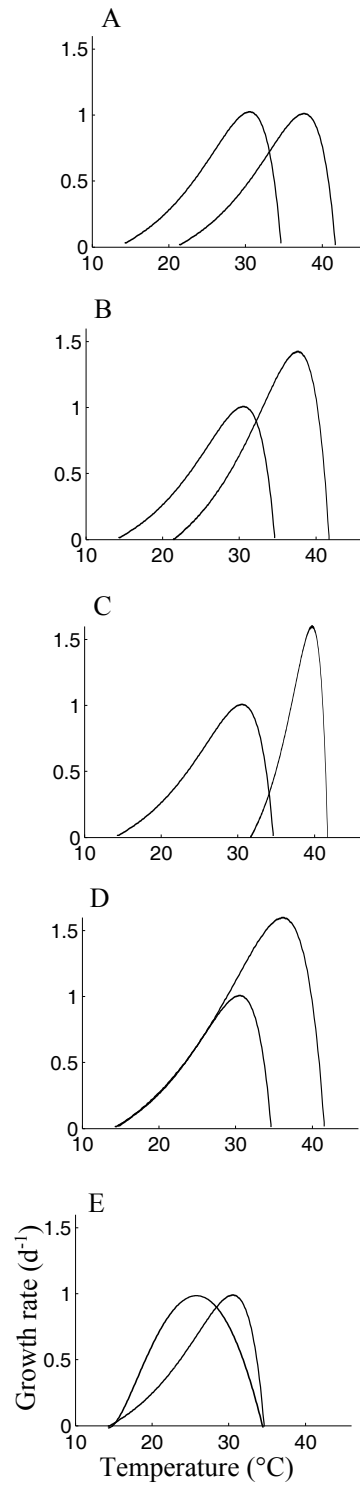


**Figure 1.8: Adaptation of the thermal growth curve** - Different hypotheses for the deformation of the thermal growth curve during thermal adaptation. A, horizontal-shift, B, hotter is better, C, specialist-generalist trade-off, D, hotter is broader and better, E, asymmetric adaptation. Adapted from Knies et al. [2009].

## 2

# Material and methods

**Note:** the first section of this material and methods chapter is extracted and adapted from Bonnefond [2015] with the kind authorization of Dr. Hubert Bonnefond.

## 2.1 Culture device and selection procedure

### 2.1.1 The selectiostats

A selection experiment based on temperature stress has been performed at the Observatoire de Villefranche-sur-Mer (see section 8). In this selection experiment, our culture system, a 1.9 L plane photobioreactor named ‘selectiostat’ (fig. 2.1), was specifically designed to impose an increasing selection pressure on long-term continuous cultures of microalgae. Cultures were continuously and gently homogenized by a magnetic stirrer and a slight air bubbling. Photobioreactors were continuously illuminated with white LED (Nichia NVSL219BT 2 700K) at  $250 \mu\text{mol photons.m}^{-2}.\text{s}^{-1}$ , and light intensity was continuously measured with a plane probe (SKY, SKL2620) placed on the opposite side of the LED. The enrichment sterile medium was prepared in 20 L tanks (Nalgen) filled with 3 weeks matured natural seawater filtered on  $0.1 \mu\text{m}$ , and autoclaved at  $120^\circ\text{C}$  for 40 minutes. After cooling, f/2 medium was added [Guillard, 1975].

Selectiostats were automatically controlled: pH was regulated at 8.2 by computer-controlled micro-addition of  $\text{CO}_2$ . The temperature was controlled by a double water jacket using a programmable cryostat. The inertia system was 30 minutes to change the temperature from  $10^\circ\text{C}$  to  $40^\circ\text{C}$  in the culturing system. Light, pH, temperature, turbidity, dilution rate were continuously recorded by ODIN<sup>®</sup> software developed by INRIA.

Cell concentration, size distribution and biovolume were monitored once or twice a day by optical particle counter (HIAC - Royco, Pacific Scientific Instruments). The first sampling was performed at the beginning of the low temperature period, the second at the beginning of the high temperature period. The variability between triplicate

## 2. MATERIAL AND METHODS

---

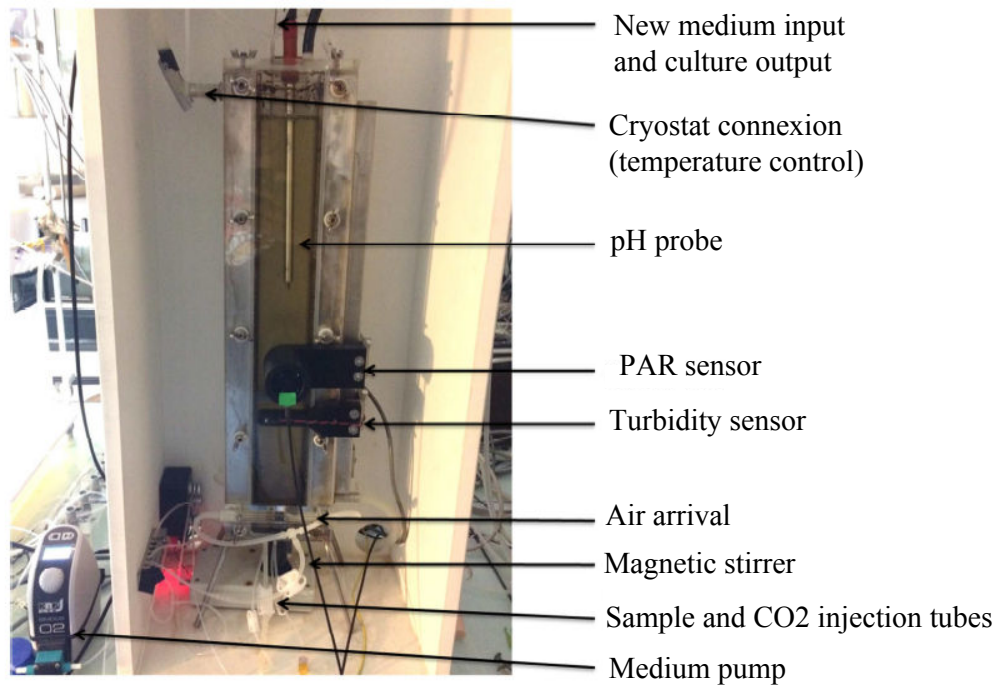


**Figure 2.1:** Selectiostat culture device - Culture of *Tisochrysis lutea* in the 'selectiostat' device. Adapted from Bonnefond [2015].

## 2.1 Culture device and selection procedure

---

measurements was routinely lower than 5 %. The mean cell diameter of the population and the biovolume were calculated from size distribution.

### 2.1.2 Cultivation mode for selection experiments

In the turbidostat culture, turbidity was continuously measured at 800 nm and kept constant (at a turbidity roughly corresponding to  $9.10^5$  cells.mL<sup>-1</sup>) by dynamically adjusting the dilution rate with ODIN<sup>®</sup> software. The set point of biomass was sufficiently high to optimize selection (because of the sufficient number of generations related by a sufficient growth rate) and to allow accurate biochemical analyses on small volume samples, and sufficiently low to prevent nutrient limitation and light shading. The fed-batch culture was diluted with fresh sterile medium every 7 days. Only 5 to 10% of the initial volume was kept, in order to restart cultures with an initial cell density of  $5.10^5$  cells.mL<sup>-1</sup>. Since selection experiments lasted more than 150 days in stressing conditions, a procedure to prevent biofilm formation was required. The selectiostats were restarted monthly: they were cleaned and re-filled with the preserved culture complemented with a sterile medium.

For the feed-batch mode, the growth rate was calculated on the linear part of the logarithm of cell biovolume using the following equation:

$$\mu_{SFb_{exp}} = \frac{\ln(BV_1/BV_2)}{t_2 - t_1} \quad (2.1)$$

where  $BV_1$  and  $BV_2$  are the biovolume ( $\mu\text{m}^3.\text{mL}^{-1}$ ) at time  $t_1$  and  $t_2$  (with  $t_2 - t_1 = 4$  or 5 days). For the turbidostat mode, equilibrium was reached after 1 day. Afterwards, the growth rate was directly equal to the average dilution rate (D) recorded by ODIN on the resting days of the cycle (6 days).

The selection by temperature was processed by modifying the so-called ratchet protocol proposed by Reboud et al. [2007] and later modified by Huertas et al. [2011]. Square wave temperature variations were daily applied. The temperature pattern was identical along a cycle which lasted 7 days. The daily pattern of a cycle consisted in the application of a low temperature ( $T_{low}$ ) during 8 hours and a high temperature ( $T_{high}$ ) during 16 hours, with a daily constant average temperature (28°C). If a stabilized growth rate was observed at the end of each cycle, then the next selection cycle was started. It consisted in reducing  $T_{low}$  by 2°C and increasing  $T_{high}$  by 1°C so as to keep a constant average temperature. The same selection cycle could also be repeated if no positive average growth was observed. For the two last cycles, in highly stressing conditions inducing high mortality,  $T_{high}$  was increased by only 0.5°C and  $T_{low}$  was decreased by only 1°C.

### 2.1.3 The TIP device

The TIP (Temperature, Irradiance, pH) setup developed by Marchetti et al. [2012] was used to measure the temperature response in acclimated conditions before and after



## 2. MATERIAL AND METHODS

---

the selection process (fig. 2.2). This device can assess the effect of pH and irradiance, but here we focused on the temperature response. The exponential growth rates at 8 temperatures ranging from 12°C to 35.5°C, at constant irradiance ( $250 \mu\text{mol.m}^{-2}.\text{s}^{-1}$ ) and pH (7.9) were measured after a lag time of 1 day on the linear part of the logarithm of the optical density measured at 680 nm (DO680).



**Figure 2.2:** TIP device - Cultures of *Tisochrysis lutea* in the multifactorial TIP device designed at IFREMER Nantes.

## 2.2 Data compilation, parameters identification and models calibration

### 2.2.1 Thermal growth curves compilation

We compiled 464 specific growth rate versus temperature data sets (*i.e.* the thermal growth curve) from the literature (including the previously compiled data of Corkrey et al. [2014] Thomas et al. [2012]) for unicellular organism (UO) strains belonging to the 3 domains of life (5728 data points). We later incorporated part of the compiled data of Thomas et al. [2015] for phytoplankton. We only selected data sets obtained in temperature-acclimated batch cultures and in non-limited <sup>1</sup>conditions. For autotrophic organisms, experiments not carried in autotrophic mode were eliminated. The specific

---

<sup>1</sup>We cannot guaranty that the light conditions for photoautotrophic organisms were optimal.

## 2.2 Data compilation, parameters identification and models calibration

growth rate in the exponential phase is defined as:

$$\mu(T) = \frac{1}{X} \frac{dX}{dt} = \frac{\ln(2)}{G(T)} \quad (2.2)$$

where  $T$  is the (constant) temperature,  $X$  is the biomass concentration (assumed to be expressed here in cells.L<sup>-1</sup>),  $G(T)$  is the generation time (*i.e.* the time it takes to double the population size). The organisms are assumed to be in balanced growth conditions as defined by Campbell [1957] (*i.e.* every extensive property of the growing system increases by the same factor). Because data were compiled and therefore come from different authors and experimental protocols, the acclimation time at a given temperature is not the same for all the datasets. The method used to calculate the growth rate also differs between authors. Most of the growth rates were obtained from cell counts, but optical density monitoring using a spectrophotometer was also employed. For photosynthetic organisms, chl  $a$  fluorescence is sometimes used as a proxy of biomass. We assumed that these three different proxies of biomass used to calculate the growth rate give the same cardinal parameters estimation and only affects the maximum growth rate.

### 2.2.2 Species biovolume

We calculated the average cell biovolume for each species/strain mentioned above. To do so, we either directly found the information in the literature or we found informations on cell shape and on the average cell length and width. In the second case, cell biovolume was computed according to their shape, *i.e.* we used the formula of the sphere volume or the ellipsoid volume. For more complicated shapes, we referred to the cell biovolume formula summarized in Olenina [2006].

### 2.2.3 CTMI parameters determination

We estimated the cardinal parameters  $T_{min}$ ,  $T_{opt}$ ,  $T_{max}$  and the maximum growth rate  $\mu_{opt}$  for each data set using the CTMI model (see eq.3.11).

$$\begin{cases} \mu(T) = 0 & \text{if } T < T_{min} \\ \mu(T) = \mu_{opt}\phi(T) & \text{if } T_{min} \leq T \leq T_{max} \\ \mu(T) = 0 & \text{if } T > T_{max} \end{cases} \quad (2.3)$$

with

$$\phi(T) = \frac{\overbrace{(T - T_{max})(T - T_{min})^2}^{\lambda(T)}}{\underbrace{(T_{opt} - T_{min}) \left[ (T_{opt} - T_{min})(T - T_{opt}) - (T_{opt} - T_{max})(T_{opt} + T_{min} - 2T) \right]}_{\beta(T)}} \quad (2.4)$$

under the condition:

$$T_{opt} > \frac{T_{min} + T_{max}}{2} \quad (2.5)$$

## 2. MATERIAL AND METHODS

---

We used a dedicated algorithm developed by Bernard and Rémond [2012] and based on the Quasi-Newton with Broyden-Fletcher-Goldfarb-Shanno method to find the cardinal parameters. For each parameter, the confidence interval was also computed using a Jackknife method developed by Bernard and Rémond [2012]. The estimation of  $T_{min}$  is tricky mainly because the growth is very slow in the lower part of the thermal growth curve and can lead to experimental errors (*i.e.* growth rates artificially equal to zero). Moreover, authors tend to avoid experiments at low temperature and model calibration on this kind of incomplete data sets artificially gives very low  $T_{min}$  with high degrees of uncertainty. Conversely, data are generally lacking in the decreasing upper part of the thermal growth curve and can twist  $T_{max}$  estimation.

### 2.2.4 Data sets selection

After calibration, we eliminated data sets with less than 5 data points, and with less than two data points in the upper part of the thermal growth curve (*i.e.* data points for which  $T \geq T_{opt}$ ). We also did not consider data sets for which the model calibration does not give coherent results, *i.e.* if  $T_{max} - T_{min} > 60^\circ\text{C}$  (the largest known thermal niche width) and if  $\mu_{opt} > 4 \text{ h}^{-1}$  (the highest growth rate known).

### 2.2.5 Hinshelwood model calibration

We calibrated the Hinshelwood model (eq. 3.22) on each selected data set  $\mu_{exp}(T)$  using a dedicated method. Indeed, calibration of this model is made difficult without a precise determination of the initial parameter vector because, for example,  $A_1$  can varies of several order of magnitude. Previous studies used an empirical trial and error method to do so [Valik et al., 2013, Zwietering et al., 1991]. Firstly, we made a first estimate of  $A_1$  and  $E_1$  (written  $\hat{A}_1$  and  $\hat{E}_1$ ) by calibrating the function  $f_1(T)$  (see eq. 3.22) on the lower part of the thermal growth curve (*i.e.* the data points for which  $T < T_{opt}$ ) using an Arrhenius plot (see section 3.2.3). Because the resulting function is a first estimate, we called it  $\hat{f}_1(T)$ . Then, we deduced the semi-experimental death curve  $f_d(T)$  by subtracting  $\hat{f}_1(T)$  to the experimental data points belonging to the upper part of the thermal growth curve ( $T \geq T_{opt}$ ):

$$f_d(T) = \hat{f}_1(T) - \mu_{exp}(T_{>}) \quad (2.6)$$

where  $T_{>}$  is the vector of data temperatures higher than or equal to  $T_{opt}$ . We then obtained the first estimates of parameters  $A_2$  and  $E_2$  (*i.e.*  $\hat{A}_2$  and  $\hat{E}_2$ ) by calibrating function  $f_2(T)$  (see eq.3.22) on  $f_d(T)$ . Again, the estimated function is  $\hat{f}_2(T)$ , and we obtained  $\hat{A}_2$  and  $\hat{E}_2$  using an Arrhenius plot. Secondly, we calibrated the Hinshelwood model on the whole data set using the Matlab<sup>®</sup> function `fminsearch` with  $\hat{A}_1$ ,  $\hat{E}_1$ ,  $\hat{A}_2$  and  $\hat{E}_2$  as initial parameters. The ordinary least-squares criterion was used to fit the model, and the parameter set minimising the sum of the squared residuals was chosen:

$$SSR(\theta) = \sum_{i=1}^n (\mu_{exp}(T_i) - \mu(T_i, \theta))^2 \quad (2.7)$$

where  $\theta$  is the parameter vector.

### 2.2.6 Data analysis

#### 2.2.6.1 Linear relationships between the cardinal temperatures

We described the linear relationships between the cardinal temperatures obtained with the CTMI model using a simple statistical descriptor, the correlation coefficient  $\rho$  between each cardinal temperatures. We tested for the hypothesis of no correlation using the student t-test defined as:

$$t = \frac{\rho}{\sqrt{(1 - \rho)^2 / (n - 2)}} \quad (2.8)$$

where  $n$  is the data set size. The resulting p-value corresponds to the probability of getting a correlation as large as observed by random chance (see table 4.1).

We applied a linear regression between the cardinal temperatures and tested for its goodness using the coefficient of determination  $R^2$  defined as the square of the correlation coefficient between the variable to explain and the linear regression, and the adjusted  $R^2$  (called  $\omega^2$ ) expressed as:

$$\omega^2 = R^2 - (1 - R^2) \frac{p}{n - p - 1} \quad (2.9)$$

where  $p$  is the number of explanatory variables. We then calculated the 95% confidence interval using the Matlab<sup>®</sup> function `polyconf` (see fig. 4.1).

We compared the linear regression between groups obtained by subdividing data sets, and we used the Chow-test combined to a Fisher F-test. This test allows to determine if the coefficient of different linear regressions obtained for two different groups are the same. The Chow-test  $F$  statistic is:

$$F = \frac{(S_{tot} - (S_1 + S_2)) / k}{(S_1 + S_2) / (n_1 + n_2 - 2k)} \quad (2.10)$$

where  $S_{tot}$  is the total sum of squared residuals,  $S_1$  and  $S_2$  are the sum of squared residuals for the two groups,  $n_1$  and  $n_2$  are the groups size,  $k$  is the number of parameters.  $F$  follows the Fisher distribution with  $k$  and  $n_1 + n_2 - 2k$  degrees of freedom.

#### 2.2.6.2 Non-linear relationships between $T_{opt}$ and $\mu_{opt}$

In chapter 5, and on the contrary to Bissinger et al. [2008], we used non-linear quantile regression to describe the non-linear relationship between  $T_{opt}$  and  $\mu_{opt}$  for the whole data set and for each sub-group (defined in chapter 5). Non-linear quantile regression is based on the least absolute deviations regression (LAD) which uses the median rather than the mean, and is therefore less sensitive to extreme outlying values than ordinary least squares (OLS) regression. The quantile  $q$  of interest (here  $q$  is the 99<sup>th</sup> quantile) is estimated using an optimization function that minimizes the sum of weighted absolute

## 2. MATERIAL AND METHODS

---

deviations [Koenker and d'Orey, 1987] (see also the review of Cade and Noon [2003] for biological applications of quantile regression). A linear quantile regression would give, for example:

$$Q(\beta_q) = \sum_{i:y_i \geq x'_i \beta} q |y_i - x'_i \beta_q| + \sum_{i:y_i < x'_i \beta} (1 - q) |y_i - x'_i \beta_q| \quad (2.11)$$

where  $Q(\beta_q)$  is the quantile regression estimator to be minimized,  $x$  and  $y$  are two data vectors (*e.g.*  $T_{opt}$  and  $\mu_{opt}$ ),  $N$  is the size of these vectors,  $\beta$  and  $\beta_q$  are parameters to estimate. The solution to the minimization problem is achieved using an algorithm such as the Nelder-Mead method [Nelder and Mead, 1965]. In our non-linear case, the functions used were polynomial functions (3rd and 4th order degree) as well as the Bernard&Rémond equation. We described the quality of the fit using pseudo- $R^2$ , defined as [Koenker and Machado, 1999]:

$$\text{pseudo-}R^2(q) = 1 - \frac{\sum_{y_i \geq \hat{y}_i} q |y_i - \hat{y}_i| + \sum_{y_i < \hat{y}_i} (1 - q) |y_i - \hat{y}_i|}{\sum_{y_i \geq \bar{y}} q |y_i - \bar{y}| + \sum_{y_i < \bar{y}} (1 - q) |y_i - \bar{y}|} \quad (2.12)$$

where  $\hat{y}_i$  is the predicted value and  $\bar{y}$  is the mean of  $y$ .

### 2.2.6.3 Statistical tools for models comparison

In chapter 6, we used several criterion to compare different models with different number of parameters. First, we used the Akaike Information Critetion (AIC) defined as [Akaike, 1998]:

$$AIC = -2\ln(MSE) + 2k \quad (2.13)$$

where  $k$  is the number of parameters,  $MSE$  is the mean squared error. We also used the corrected AIC called AICc taking sample size into account:

$$AIC_c = AIC \frac{2k(k+1)}{n-k-1} \quad (2.14)$$

where  $n$  is the sample size. Finally, we used the Bayesian Information Criterion (BIC), where the number of parameters has more influence:

$$BIC = -2\ln(MSE) + k\ln(n) \quad (2.15)$$

## 3

# Modelling the temperature effect on unicellular organisms from heterotrophic bacteria to autotrophic eukaryotes: a review

Contributors: Mairet, F., Sciandra, A., Bernard, O.



The Deutsch physical chemist Jacobus Henricus Van't Hoff.

### 3.1 Introduction

The growth of unicellular organisms (UO), from bacteria to heterotrophic unicellular eukaryotes and phytoplankton, is highly impacted by temperature, as pointed out by a recent study at global ocean scale [Sunagawa et al., 2015]. For photosynthetic organisms, temperature is the second most influencing factor after light. It is therefore crucial to understand how temperature affects UO as well as correctly model these effects.

### 3. MODELLING THE TEMPERATURE EFFECT ON UNICELLULAR ORGANISMS FROM HETEROTROPHIC BACTERIA TO AUTOTROPHIC EUKARYOTES: A REVIEW

---

Because of their wide repartition and use, UO have been studied in different scientific domains, ranging from ecological modellers to microbiologists specialized in the food security preservative. A variety of intrinsically different models have been developed for different uses.

The aim of this study is to summarize the existing deterministic temperature growth models in the light of the underlying biological processes (see table 3.1 for a summary). Firstly, models in non-limiting and balanced growth conditions are described. The key processes are presented through a mechanistic approach. Secondly, the specific case of unicellular photosynthetic organisms is addressed. Finally, we present the existing dynamical models, such as the thermal death models.

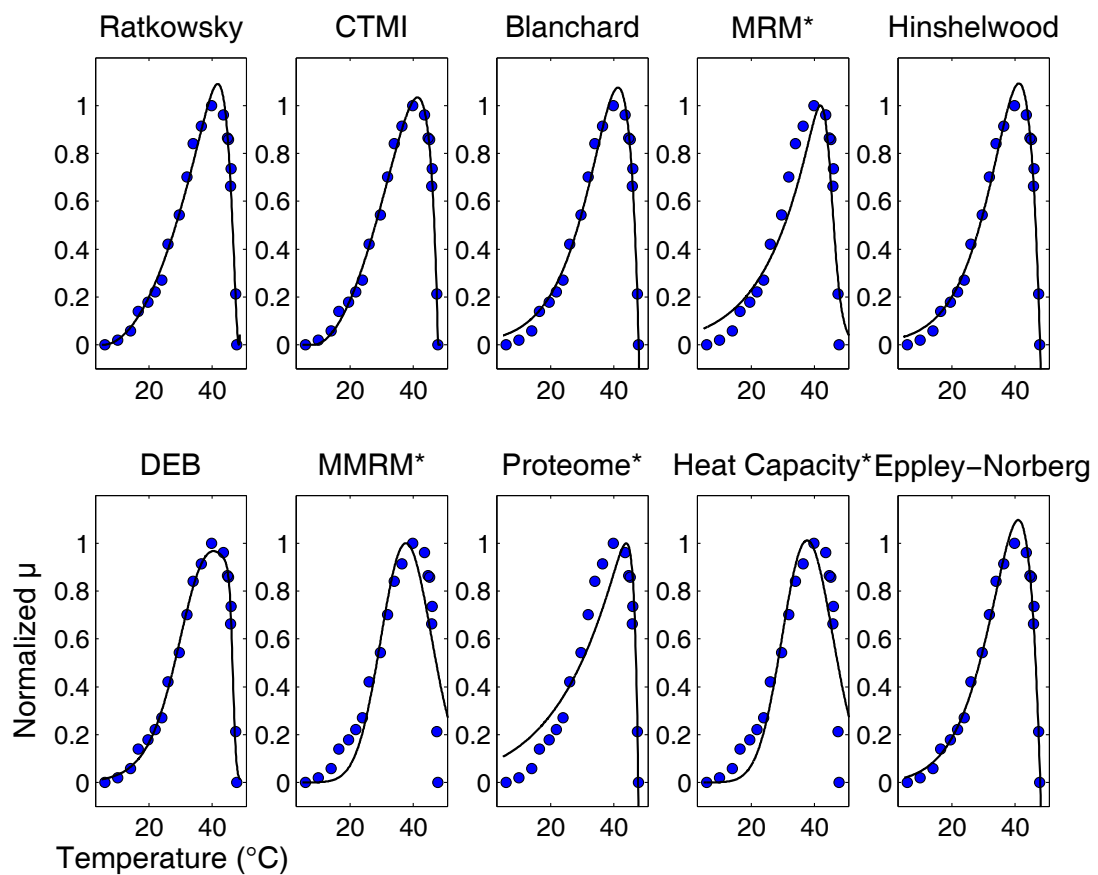


**Figure 3.1: Model fit** - Fit of the 10 described models on the normalized thermal growth curve of *Escherichia coli* (strain code 62 from Corkrey et al. [2014]). Models denoted with a ‘\*’ are normalized.

Model	Type	# Parameters	Validation (data sets)	Cardinal temperatures
Square-root model	E	4	29, bacteria [Ratkowsky et al., 1983]	$T_{min}$ and $T_{max}$ are explicit $T_{opt}$ is found by numerical optimization
CTMI	E	4	47, bacteria & yeast [Rosso et al., 1993]	Explicit
Blanchard model	E	4	2, benthic phytoplankton [Blanchard et al., 1996]	$T_{opt}$ and $T_{max}$ are explicit $T_{min}$ is not defined
<b>Mechanistic models</b>				
Master reaction model (for eq. 3.21)	M	4	1, normalized, bacteria [Johnson and Lewin, 1946] and then yeast [Van Uden, 1985]	$T_{opt} = \frac{\Delta H^\ddagger/R}{\ln\left(\frac{-\Delta H^\ddagger e^{\Delta S} - \Delta H e^{\Delta S}}{\Delta H}\right)}$ $T_{min}$ and $T_{max}$ are not defined
Hinshelwood model	M	4	No	$T_{opt} = \frac{E_1 - E_2}{R \ln\left(\frac{A_1 E_1}{A_2 E_2}\right)}$ $T_{max} = \frac{E_1 - E_2}{R \ln\left(\frac{A_1}{A_2}\right)}$ $T_{min} = T_{opt} \left(\frac{-E_1/\gamma}{T_{opt} - E_2/\gamma}\right)$ with $\gamma = R \ln(A_2/A_1 \epsilon(E_2 - E_1)/E_1)$
DEB theory model	M	6	Yes (DEB theory literature)	$T_{min}$ and $T_{max}$ are not defined $T_{opt}$ is found numerically
<b>Protein-stability based models</b>				
Modified Master reaction model	M	4	230, normalized, all UO types [Corkrey et al., 2014]	$T_{opt} = \frac{\Delta C_p T_0 + \Delta H}{\Delta C_p + R}$ $T_{min}$ and $T_{max}$ are not defined
The proteome model	M	2	12, normalized, bacteria [Dill et al., 2011]	$T_{min}$ and $T_{max}$ are not defined $T_{opt}$ is found numerically
The heat capacity model	M	4	12, soil processes [Schipper et al., 2014]	$T_{min}, T_{opt}, T_{max}$ are found numerically
<b>Phytoplankton dedicated models</b>				
Eppley-Norberg model	E	4	5, phytoplankton [Norberg, 2004]	$T_{opt} = \frac{bz - 1 + \sqrt{(w/2)^2 b^2 + 1}}{b}$ $\text{abs}(T_{max} - T_{min}) = w$
Bernard&Rémond model	E	4	15, phytoplankton [Bernard and Rémond, 2012]	Explicit

Table 3.1: Synthesis of the main models for growth rate as a function of temperature. E, empirical models. M, mechanistic models.



## **3.2 Modelling the specific growth rate of unicellular organisms as a function of temperature**

In this section, we detail the existing models representing the effect of temperature on the specific growth rate of a UO in non-limiting conditions.

### **3.2.1 Methodological clarification**

The specific growth rate is defined, in batch acclimated cultures, as the growth rate during the exponential phase:

$$\mu(T) = \frac{1}{X} \frac{dX}{dt} = \frac{\ln(2)}{G(T)} \quad (3.1)$$

where  $T$  is a fixed temperature,  $X$  is the biomass concentration (assumed to be expressed here in  $\text{cells.L}^{-1}$ ),  $G(T)$  is the generation time (*i.e.* the time it takes to double the population size). The organisms are assumed to be in balanced growth conditions as defined by Campbell [1957] (*i.e.* every extensive property of the growing system increases by the same factor).  $\mu(T)$  is commonly called the thermal growth curve.

It is important to note that the thermal growth curve is dependent on the way biomass is measured. Firstly, some authors use optical density to quantify the cell concentration, or, for the photosynthetic organisms, the chlorophyll  $a$  concentration. These methods are not accurate since pigment content is temperature depend, and an acclimation phase should be needed for pigment acclimation to the new temperature. Moreover, for heterotrophic UO, the results obtained highly depend on the physiological state of the organisms [Monod, 2012]. Secondly, other biomass descriptors are commonly used, such as the particulate organic carbon (POC) concentration. The dynamics of this descriptor is likely to be differently affected by temperature (see section 3.4). Even though the use of the descriptor depends on the processes studied, it should be homogeneous and an ideal biomass estimate should be proportional to the carbon mass with a constant independent of temperature. Thirdly, the experimental acclimation time at a given temperature is of major importance for the consistency of the thermal growth curve; the acclimation time can vary from one day to several weeks. For example, some protocols consist in gradually increasing the temperature and measuring the growth rate. Such approach has the advantage of providing a rapid evaluation of the temperature response. However, the cell acclimation state is unclear and probably provides a less exploitable response curve. For all these reasons, Boyd et al. [2013] have, for example, developed a standard protocol to construct the thermal growth curve for phytoplankton: the population must be acclimated to the experimental temperature for at least 4 generations, the population must be kept at an exponential growth phase using semi-continuous cultures, multiple biomass descriptors must be used and compared to obtain growth rates (cell counts, chlorophyll  $a$  fluorescence, etc.), a minimum of 6 experimental growth rates at 6 different temperatures must be obtained, the cultures must be carried on with three replicates, all the other parameters must be kept constant and if possible at optimal

## 3.2 Modelling the specific growth rate of unicellular organisms as a function of temperature

---

levels, the experiments with temperatures at which the cells do not grow or grow very slowly must be repeated several times, and finally several strains of the same species should be compared.

### 3.2.2 The Arrhenius model from Van't-Hoff to Eyring:

Since the XIX<sup>e</sup> century, chemists are aware of the prodigious effect of temperature change on chemical reaction rates. As early as 1850, Ludwig Ferdinand Wilhelmy published an article dealing with *'The law by which the action of acids on cane sugar occurs'* and its temperature dependence [Wilhelmy, 1850]. At that time, Maxwell's law of distribution of molecular velocities already established that the proportion of molecules having energies greater than the average at ordinary temperatures were very small, but increased with temperature. In 1867, Leopold Pfaundler von Hadermur applied Maxwell's law to chemical equilibrium [Pfaundler, 1867]. Because at chemical equilibrium, reverse and forwards reactions occur at the same rate, he assumed, using Maxwell's law, that only a fraction of molecules having energy greater than a critical parameter  $E$  could undergo chemical-changes. Moreover, this fraction would exponentially change with temperature. In 1884, the famous physical chemist Jacobus van't Hoff contemplated a thermodynamical version of Pfaundler thought [van't Hoff, 1889]. Consider the following chemical equilibrium between two species  $B$  and  $C$ :



with  $k_1$  and  $k_2$  the forward and reverse reaction rate, respectively. Then, van't Hoff assumed that the equilibrium constant defined as  $K = k_1/k_2$  satisfied the following relation for a fixed pressure:

$$\frac{d\ln(K)}{dT} = \frac{\Delta H^0}{RT^2} \quad (3.3)$$

where  $\Delta H^0$  is the standard enthalpy change (corresponding approximately to the internal energy change),  $R$  is the ideal gas constant. To understand the funding principles of this equation, we have to introduce some thermodynamical concepts. Firstly, the definition of change in Gibbs free energy  $\Delta G^0$  is:

$$\Delta G^0 = \Delta H^0 - T\Delta S^0 \quad (3.4)$$

where  $\Delta S^0$  is the system entropy change. Secondly, the link between Gibbs free energy and the equilibrium constant  $K$  is:

$$\Delta G^0 = -RT\ln(K) \quad (3.5)$$

It is possible to find eq.3.3 by combining eq.3.4 and eq.3.5. eq.3.4 results directly from the second law of thermodynamics stipulating that every chemical transformation generates entropy. Eq.3.5 is trickier to detail. However, the natural logarithm 'appears' in this equation and is responsible for the exponential temperature dependence of chemical

### 3. MODELLING THE TEMPERATURE EFFECT ON UNICELLULAR ORGANISMS FROM HETEROTROPHIC BACTERIA TO AUTOTROPHIC EUKARYOTES: A REVIEW

---

reactions described next. Briefly, eq.3.5 comes from the mass action law. Despite van't Hoff approach, the fact remained that eq. 3.3 only related temperature to equilibrium constant and not to reaction rates. In 1889, the Swedish chemist Svante Arrhenius, a former van't Hoff's student, published a study about the temperature effect on cane sugar inversion based on Wilhelmy work [Arrhenius, 1889]. Using eq.3.3, Arrhenius proposed a semi-empirical model which was later applied to bacteria by replacing the rate constant by the species growth rate [Arrhenius, 1889, Ratkowsky et al., 1982]:

$$\mu(T) = Ae^{-E/(RT)} \quad (3.6)$$

where  $R$  is the gas constant,  $A$  is called the 'collision factor' or the pre-exponential part and  $E$  is said to be the activation energy, determined empirically. The Arrhenius model parameters are easy to estimate using an Arrhenius plot, by expressing  $\ln(\mu(T))$  as a function of  $1/T$ , which gives a linear relationship; parameters can thus be obtained with a linear regression. The Arrhenius model allows good representations of growth rates at low temperatures, but some Arrhenius plot does not give straight lines, indicating for example that  $E$  can vary with  $T$ . Moreover, the Arrhenius model cannot represent the decreasing part of the thermal growth curve, *e.g.* when temperature might cause cell death. Arrhenius equation can be reformulated as:

$$\mu(T) = k_1 e^{T_A/T_1 - T_A/T} \quad (3.7)$$

where  $T_1$  is a reference temperature,  $T_A$  is the Arrhenius temperature (*i.e.* slope of the straight line of the Arrhenius plot) and  $k_1$  is the reaction rate at  $T_1$ .

Arrhenius model is said semi-empirical because the parameter meanings were not clear. However, this model worked perfectly in many cases (for a detailed story of the Arrhenius equation, see Laidler [1984]). In 1935, Henry Eyring and two colleagues used a new theory to develop the 'Eyring equation', bringing a mechanistic justification to the Arrhenius equation. This theory, called the Transition State Theory, stipulates that there exists an intermediate form between the reactants and the products (the native and denatured protein and enzyme, for example) which is in rapid equilibrium with the reactants:



where, in this example,  $P_f$  and  $P_u$  are the fraction of native and denatured proteins, respectively. The Eyring equation reads:

$$k(T) = \frac{K_B T}{h} e^{\Delta S^\ddagger/(R)} e^{-\Delta H^\ddagger/(RT)} \quad (3.9)$$

where  $K_B$  is the Boltzmann constant,  $h$  is the Planck's constant. The parameters  $\Delta S^\ddagger$  and  $\Delta H^\ddagger$  correspond to the entropy and enthalpy of activation. The Eyring equation is also used in bacteria growth models nowadays.

## 3.2 Modelling the specific growth rate of unicellular organisms as a function of temperature

---

### 3.2.3 Empirical approach

Historically, empirical models of unicellular organisms specific growth rate as a function of temperature have been developed, mostly for food-processing industry and medical applications. Various empirical models have been proposed since the 1960's, but only three are still commonly used.

**The Square-Root model:** The Square-Root model was initially proposed by David Ratkowsky as an alternative to the Arrhenius model [Ratkowsky et al., 1982] and then extended to the whole biokinetic range [Ratkowsky et al., 1983]:

$$\mu(T) = \left[ b \left( T - T_{min} \right) \left( 1 - e^{c(T - T_{max})} \right) \right]^2 \quad (3.10)$$

where  $T_{min}$  and  $T_{max}$  are the minimal and maximal temperatures for growth,  $b$  is the regression coefficient of the squared root growth rate plotted against temperature below the optimal temperature, and  $c$  is an additional parameter to represent growth rate decrease above the optimal temperature.

**The CTMI model:** The CTMI (Cardinal Temperature Model with Inflexion) was developed by Lobry et al. [1991] and later popularized by Rosso et al. [1993]:

$$\begin{cases} \mu(T) = 0 & \text{if } T < T_{min} \\ \mu(T) = \mu_{opt}\phi(T) & \text{if } T_{min} \leq T \leq T_{max} \\ \mu(T) = 0 & \text{if } T > T_{max} \end{cases} \quad (3.11)$$

with

$$\phi(T) = \frac{\overbrace{(T - T_{max})(T - T_{min})}^{\lambda(T)}}{\underbrace{(T_{opt} - T_{min}) \left[ (T_{opt} - T_{min})(T - T_{opt}) - (T_{opt} - T_{max})(T_{opt} + T_{min} - 2T) \right]}_{\beta(T)}} \quad (3.12)$$

under the condition:

$$T_{opt} > \frac{T_{min} + T_{max}}{2} \quad (3.13)$$

$T_{min}$ ,  $T_{opt}$ ,  $T_{max}$  are the minimal, optimal and maximal temperatures for growth and  $\mu_{opt}$  is the growth rate at  $T_{opt}$ . The model parameters have a direct biological interpretation. The model was built for its easy calibration on experimental data.

**The Blanchard model:** The Blanchard model was developed by Blanchard et al. [1996] to model the photosynthetic response of benthic phytoplankton to temperature. This model can be used to represent the thermal growth curve:

$$\mu(T) = \mu_{max} \left( \frac{T_{max} - T}{T_{max} - T_{opt}} \right)^\beta e^{-\beta(T_{opt} - T)/(T_{max} - T_{opt})} \quad (3.14)$$

### 3. MODELLING THE TEMPERATURE EFFECT ON UNICELLULAR ORGANISMS FROM HETEROTROPHIC BACTERIA TO AUTOTROPHIC EUKARYOTES: A REVIEW

---

with  $T \leq T_{max}$  and  $T_{opt} < T_{max}$ . Parameters  $T_{opt}$  and  $T_{max}$  correspond to the cardinal temperatures,  $\mu_{max}$  is the growth rate at  $T = T_{opt}$  and  $\beta$  is a dimensionless parameter.

**Model comparison:** A comparison between the Square-Root model and the CTMI was made by Rosso et al. [1993] and more recently by Valik et al. [2013]. According to these studies, the two models fit equally well the data. Both models were validated by Valik et al. [2013] using an F-test. However, the  $b$  and  $c$  parameters of the Square-root model are correlated, whereas the CTMI parameters are not, which allows easier parameter identification. CTMI proves useful for cardinal temperatures identification.

#### 3.2.4 Mechanistic approach

The former model types allow to identify the main characteristics of the thermal growth curve. However, the mechanistic approach aims to represent the thermal growth curve as a result of inherent physiological processes. These models are mostly based on the Arrhenius formulation (see 3.2.3).

**The master reaction model:** In 1946, Johnson and Lewin [1946] noticed that cultures of *Escherichia coli* exposed to 45°C during a long time ceased to grow, but grew exponentially again when replaced at 37°C. The longer the cultures were exposed to the high temperature, the lower was the growth rate at 37°C. However, there was no sign of viability loss. They concluded that cells endured reversible damage, particularly protein denaturation. They considered a simple case where a single reaction controlled by one master enzyme  $E_n$  limits growth (with no substrate limitation):

$$\mu(T) = cTE_n e^{-\Delta H_A^\ddagger/(RT)} e^{\Delta S_A^\ddagger/R} \quad (3.15)$$

where  $c$  is a constant given by the Eyring formulation (see 3.8),  $\Delta H_A^\ddagger$  is the enthalpy of activation (enthalpy difference between the transition complex and the active form) and  $\Delta S_A^\ddagger$  is the entropy of activation. The enzyme goes from a native, active form  $E_n$  to a reversibly denatured, inactive form  $E_d$ :



The chemical equilibrium is defined as:

$$K = k_1/k_2 = E_n/E_d = e^{-\Delta H/(RT) - \Delta S/R} \quad (3.17)$$

where  $\Delta H$  is the enthalpy difference between the active form and the inactive form,  $\Delta S$  is the entropy difference. If  $E_0$  is the total amount of enzyme,  $E_0 = E_n + E_d$ . It follows that:

$$E_n = \frac{E_0}{1 + K} = \frac{E_0}{1 + e^{-\Delta H/(RT) - \Delta S/R}} \quad (3.18)$$

Then, by posing  $C = ce^{\Delta S_A^\ddagger/R} E_0$  and replacing  $E_n$  by Eq.3.18 in Eq.3.15, Johnson and

### 3.2 Modelling the specific growth rate of unicellular organisms as a function of temperature

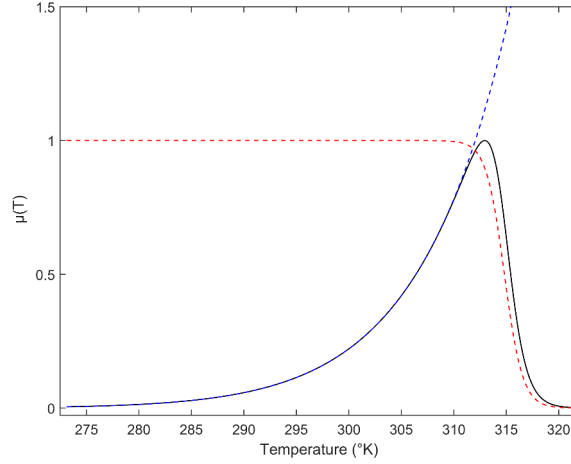


**Figure 3.2: Master reaction model (eq. 3.19)** - Illustration of the master reaction model. The black line corresponds to  $\mu(T)$ , the blue dashed line corresponds to  $CTe^{-\Delta H^\ddagger/(RT)}$ , the red dashed line corresponds to  $P(T)$ .

Lewin obtained the master reaction model (see fig. 3.2):

$$\mu(T) = CT e^{-\Delta H^\ddagger/(RT)} \cdot \underbrace{\frac{1}{1 + e^{-\Delta G(T)/(RT)}}}_{P(T)} \quad (3.19)$$

where  $P(T)$  is the probability that the enzyme is in its native state and  $\Delta G(T)$  is the Gibbs free energy change:

$$\Delta G(T) = \Delta H - T\Delta S \quad (3.20)$$

An other version of eq.3.19 exists, where the exponential part does not follow an Eyring formulation but rather an Arrhenius one, which is relevant in the case of reactions with high activation energy like protein denaturation Bischof and He [2005]:

$$\mu(T) = C e^{-\Delta H^\ddagger/(RT)} \cdot \frac{1}{1 + e^{-\Delta G(T)/(RT)}} \quad (3.21)$$

It is worth noting that this simplified equation here does not have any influence on the model fit and behaviour, and simplifies the calculation of the cardinal temperature  $T_{opt}$  (see table 3.1).

**The Hinshelwood model:** In 1945, Sir Norman Hinshelwood proposed a rather simple model in which the temperature-dependent growth rate is just the difference between a synthesis rate  $f_1(T)$  and a degenerative rate  $f_2(T)$  [Hinshelwood, 1945] (see fig. 3.3):

$$\mu(T) = \underbrace{A_1 e^{-E_1/(RT)}}_{f_1(T)} - \underbrace{A_2 e^{-E_2/(RT)}}_{f_2(T)} \quad (3.22)$$

### 3. MODELLING THE TEMPERATURE EFFECT ON UNICELLULAR ORGANISMS FROM HETEROTROPHIC BACTERIA TO AUTOTROPHIC EUKARYOTES: A REVIEW

---

where  $A_1$  and  $A_2$  are related to entropy and  $E_1$  and  $E_2$  are related to enthalpy. Hinshelwood believed that the function  $f_2(T)$ , which causes the ‘catastrophic decline to zero’, represents protein denaturation. He argued that the model only works if  $E_2$  is higher than  $E_1$ , because the degenerative process represented by  $f_2(T)$  must be sudden. Since protein denaturation possesses a high activation energy, it is a good candidate for driving the process. Moreover,  $A_2$  (corresponding to entropy) also has to be quite high. Thus, the ‘activated state must be highly disordered compared with the initial state’ which ‘results in an easy transition to the activated state in spite of the large amount of energy which has to be taken up to reach it’. Precisely, protein denaturation leads from a highly ordered state to an highly disordered state and is therefore associated with a large entropy increase. From the Hinshelwood model, after some mathematical manipulations, it is

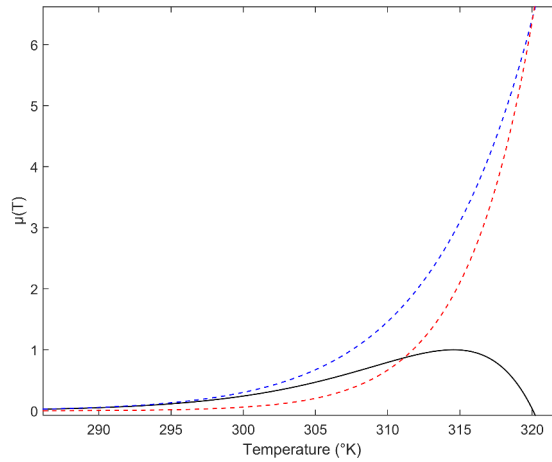


**Figure 3.3: Hinshelwood model** - Illustration of the Hinshelwood model. The black line corresponds to  $\mu(T)$ , the blue dashed line corresponds to  $f_1(T)$ , the red dashed line corresponds to  $f_2(T)$ .

possible to express  $T_{opt}$ ,  $T_{max}$ ,  $\mu_{opt}$  (see section 10.3):

$$T_{opt} = \frac{E_1 - E_2}{R \ln \left( \frac{A_1 E_1}{A_2 E_2} \right)} \quad (3.23)$$

$$T_{max} = \frac{E_1 - E_2}{R \ln \left( \frac{A_1}{A_2} \right)} \quad (3.24)$$

$$\mu_{opt} = \theta A_2 \left( \frac{A_1}{(1 + \theta) A_2} \right)^{(1 + \theta)/\theta} = \frac{E_2 - E_1}{E_1} A_2 e^{-E_2/(RT_{opt})} \quad (3.25)$$

with  $\theta = (E_2 - E_1)/E_1$ . Given that  $\mu(T)$  does not cancel for low temperature,  $T_{min}$  is defined in this case by  $\mu(T_{min}) = \epsilon \mu_{opt}$  and arbitrarily fixing  $\epsilon = 0.05$  (see proof in

## 3.2 Modelling the specific growth rate of unicellular organisms as a function of temperature

---

section 10.3):

$$T_{min} \simeq \frac{-T_{opt}E_1/\gamma}{T_{opt} - E_2/\gamma} \quad (3.26)$$

where:

$$\gamma = R \ln \left( \frac{E_2 - E_1}{E_1} \frac{A_2}{A_1} \epsilon \right) \quad (3.27)$$

**The DEB theory approach:** In the Dynamics Budget Theory, the effect of temperature on population growth is taken into account using a modified Master Reaction model [Kooijman, 2010], where all the temperature-dependent functions are Arrhenius modified equations (eq. 3.7):

$$\mu(T) = \frac{k_1 e^{T_A/T_1 - T_A/T}}{\underbrace{1 + e^{T_{AL}/T - T_{AL}/T_L} + e^{T_{AH}/T_H - T_{AH}/T}}_{f_D}} \quad (3.28)$$

where  $T_L$  and  $T_H$  are related to cold and hot denaturation (lower and upper boundaries),  $T_{AL}$  and  $T_{AH}$  are the Arrhenius temperatures at low and high temperature respectively (see eq.3.7). The ratio  $f_D^{-1}$  corresponds to the fraction of enzyme in its native state, modelling also cold denaturation contrary to the Master Reaction model.

### 3.2.5 The protein thermal stability challenge

Protein thermal stability plays a key role in the UO thermal growth curve [Johnson and Lewin, 1946, Pena et al., 2010, Rosenberg et al., 1971, Zeldovich et al., 2007] (see section 5.1 and 6). In line with the master reaction model, some publications went further in the comprehension of protein thermal stability and its consequences on UO growth.

**The modified master reaction model:** The master reaction model assumes that  $\Delta G$ , the Gibbs free energy difference between the native and denatured protein, is temperature independent. Based on Murphy et al. [1990] work, Ross [1993] and then Ratkowsky et al. [2005] remarked that  $\Delta G$  should vary with  $T$  in eq.3.19 following eq. 3.20. Moreover, [Murphy et al., 1990] showed that globular proteins (including enzymes) share common thermodynamic properties. For any protein, the denaturation enthalpy change  $\Delta H$  and the denaturation entropy change  $\Delta S$ , normalized to the number of amino-acids residues of this protein, both converge to a fixed value  $\Delta H^*$  and  $\Delta S^*$  at  $T_H^*$  and  $T_S^*$  respectively [Privalov, 1979]. The reason for such a temperature convergence is still unclear. Nonetheless, it has been shown that at  $T_H^*$  and  $T_S^*$ , the hydrophobic contribution to  $\Delta H$  and  $\Delta S$  approaches zero [Robertson and Murphy, 1997]. At that stage, we have to introduce a novel thermodynamics parameter, the heat capacity  $C_p$ . According to [Murphy et al., 1990],  $\Delta H$  and  $\Delta S$  can be expressed as a function of the heat capacity change:

$$\Delta H = \Delta H^* + \Delta C_p(T - T_H^*) \quad (3.29)$$

$$\Delta S = \Delta S^* + \Delta C_p \ln(T/T_S^*) \quad (3.30)$$



### 3. MODELLING THE TEMPERATURE EFFECT ON UNICELLULAR ORGANISMS FROM HETEROTROPHIC BACTERIA TO AUTOTROPHIC EUKARYOTES: A REVIEW

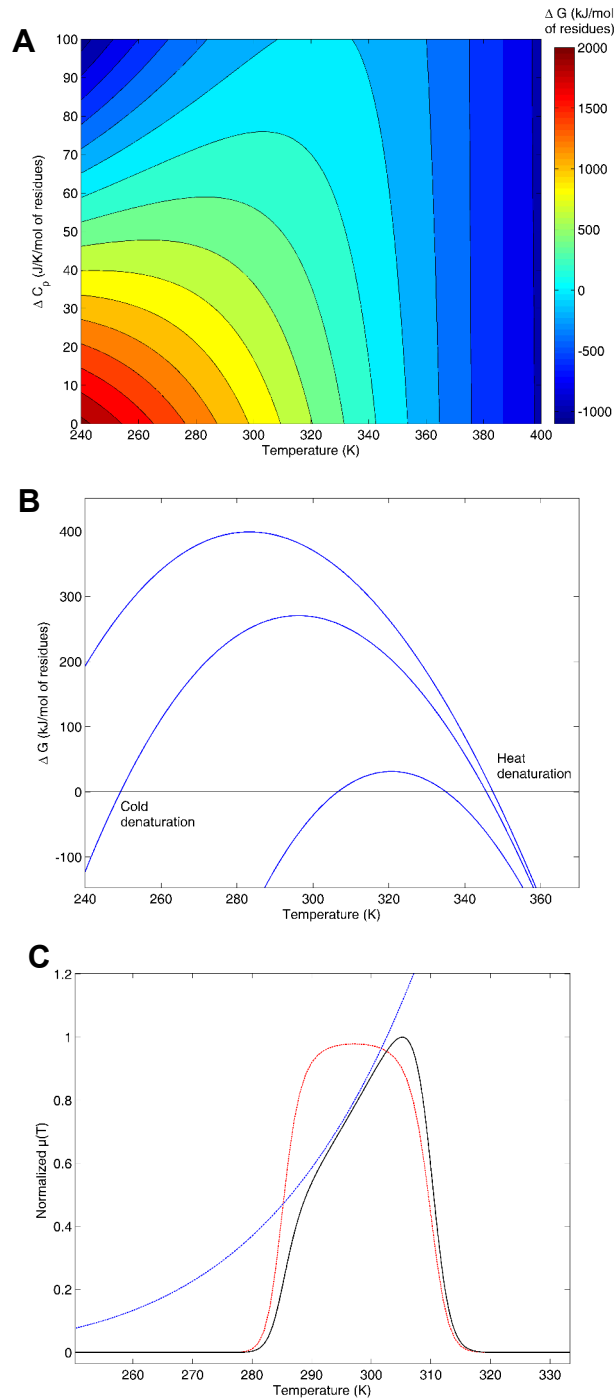


**Figure 3.4: Modified master reaction model** - Illustration of the modified master reaction model. A, the Gibbs free energy change as a function of heat capacity change and temperature. B, Gibbs free energy change as a function of temperature only for different fixed heat capacity change (and thus for a given protein). C, the modified master reaction model plot for a UO (black line) with activation function (blue dashed line) and protein denaturation probability  $P(T)$  (red dashed line).

### 3.2 Modelling the specific growth rate of unicellular organisms as a function of temperature

---

where  $\Delta H^*$  is the enthalpy change per mol of amino-acid residue of the enzyme at  $T_H^*$ ,  $\Delta S^*$  is the entropy change per mol of amino-acid residue of the enzyme at  $T_S^*$ ,  $\Delta C_p$  is the heat capacity difference between the native and denatured protein,  $T_H^*$  is the temperature at which the contribution of  $\Delta C_p$  to enthalpy is zero and  $T_S^*$  is the temperature at which the contribution of  $\Delta C_p$  to entropy is zero. The heat capacity change  $\Delta C_p$  is constant for a given protein [Privalov and Khechinashvili, 1974]. Using Eq.3.29 and 3.30, the Gibbs free energy of protein denaturation (*i.e.* the protein thermal stability) is (Fig. 3.4A and B):

$$\Delta G(T) = n[\Delta H^* - T\Delta S^* + \overbrace{\Delta C_p[(T - T_H^*) - T\ln(T/T_S^*)]}^{\Delta G_{hydro}}] \quad (3.31)$$

where  $n$  is the number of amino-acid residues in the master enzyme and  $\Delta G_{hydro}$  is the hydrophobic contribution to the free energy change. Eq.3.31 describes protein thermal stability in terms of hydrophobic contribution of apolar compounds.

Ross [1993] and Ratkowsky et al. [2005] proposed to replace  $\Delta G$  by Eq.3.31 in Eq.3.19 (forming the modified master reaction model). Because  $T_H^*$ ,  $T_S^*$  and  $\Delta S^*$  are considered as universal constant for globular proteins [Murphy and Gill, 1991], the modified master reaction model has 5 parameters (Fig. 3.4C). As a validation, Ratkowsky et al. [2005] fitted the model on 35 bacterial strains normalized data sets obtained in non-limiting conditions. Their main conclusion points towards the crucial role played by a single master enzyme whose thermal sensitivity is driven by hydrophobic interactions.

Recently, Corkrey et al. [2014] extended the modified master reaction model to unicellular and multicellular eukaryotes. They considered  $\Delta H^*$  as a universal constant as well, reducing the model parameters to 4. They fitted the model on 230 strains normalized data sets covering a range of 124°C. Their principal conclusion states that the model is able to find coherent protein thermodynamics parameters with only growth data (*i.e.* growth rate versus temperature). Hyperthermophiles proteins seem to be more widely robust. Moreover, they found several link between thermodynamic parameters, for example between  $T_{opt}$  and  $\Delta C_p$  (enzyme stability), and between  $T_{opt}$  and  $\Delta H^\ddagger$  (enzyme activity). However, they did not provide further explanations. They finally speculate on the nature of the single limiting reaction. They assume that if a single reaction (and not several) is rate limiting, then it should be linked to the protein unfolding and re-folding process. They particularly focus on the role of chaperones proteins responsible for *de novo* folding.

**The proteome approach:** In 2007, Zeldovich et al. [2007] proposed that the whole proteome plays a role in UO thermal sensitivity. Resuming this idea, Chen and Shakhnovich [2010] considered that each important protein  $i$  has its own Gibbs free energy of denaturation  $\Delta G_i$ . The growth rate of an UO becomes dependent of the stability of each protein, and the thermal denaturation of several proteins causes a bottleneck effect on growth:

$$\mu(T) = CT e^{-\Delta H^\ddagger/(RT)} \cdot \frac{1}{\prod_i^{N_p} 1 + e^{-\Delta G_i(T)/(RT)}} \quad (3.32)$$

### 3. MODELLING THE TEMPERATURE EFFECT ON UNICELLULAR ORGANISMS FROM HETEROTROPHIC BACTERIA TO AUTOTROPHIC EUKARYOTES: A REVIEW

---

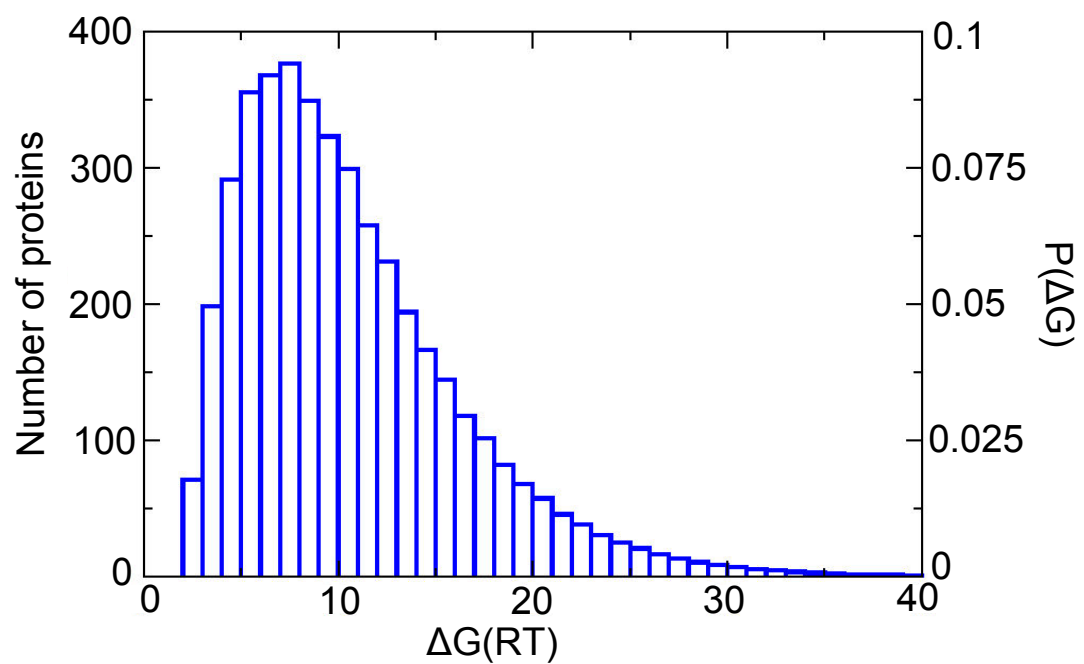


**Figure 3.5: Free energy distribution** - Gibbs free energy distribution of *Escherichia coli* proteome at 37°C (adapted from Ghosh and Dill [2010]).

### 3.2 Modelling the specific growth rate of unicellular organisms as a function of temperature

---

where  $N_p$  is the number of proteins. According to Zeldovich et al. [2007], the proteome can be described in protein stability distribution thanks to a dedicated probability function of the Gibbs free energy,  $P(\Delta G)$  (see fig.3.5). By taking the natural logarithm of eq.3.32 and by integrating the resulting equation over the whole  $P(\Delta G)$  distribution range, Chen and Shakhnovich [2010] expressed the growth rate as:

$$\ln(\mu(T)) = \ln(CT) - \Delta H^\ddagger/(RT) - \sum_{i=1}^{N_p} \ln\left(1 + e^{-\Delta G_i/(RT)}\right) \quad (3.33)$$

that is, by averaging over the proteome:

$$\boxed{\ln(\mu(T)) \simeq \ln(CT) - \Delta H^\ddagger/(RT) - N_p \int_0^L \ln\left(1 + e^{-\Delta G/(RT)}\right) P(\Delta G) d\Delta G} \quad (3.34)$$

where  $L$  is the maximum value of  $\Delta G$  (for example  $L = 40$  in fig. 3.5).  $N_p$  can be reduced to the number of the only important proteins. According to Sawle and Ghosh [2011] and Ghosh and Dill [2010],  $\Delta G$  can be expressed as a function of  $\Delta H$ ,  $\Delta S$  and  $\Delta C_p$  (using eq. 3.29 and eq. 3.30), itself depending on the protein chain length denoted  $N$ :

$$\Delta G = \Delta H(N) + \Delta C_p(N)(T - T_h) - T\Delta S(N) - T\Delta C_p(N)\ln(T/T_s) \quad (3.35)$$

with

$$\begin{aligned} \Delta H(N) &= aN + b \\ \Delta S(N) &= cN + d \\ \Delta C_p(N) &= lN + m \end{aligned} \quad (3.36)$$

where  $a, b, c, d, l, m$  are empirical parameters constant defined for mesophilic and for thermophilic organisms. The distribution of chain length over the proteome  $P(N)$  can be known [Zhang, 2000] and is used to estimate  $P(\Delta G)$ . It can be modelled by a gamma distribution:

$$P(N) = \frac{N^{\alpha-1} e^{-N/\theta}}{\Gamma(\alpha)\theta^\alpha} \quad (3.37)$$

where  $\theta$  and  $\alpha$  are the parameters of the gamma distribution corresponding to:

$$\begin{aligned} \langle N \rangle &= \alpha\theta \\ \langle (\Delta N)^2 \rangle &= \alpha\theta^2 \end{aligned} \quad (3.38)$$

The brackets represent the mean over all the proteins.  $\Gamma(\alpha)$  is the gamma function evaluated at  $\alpha$ . The model (eq. 3.34), presented as universal, has thus only two parameters,  $N_p$  and  $\Delta H^\ddagger$ . It has been validated on 12 normalized data sets of prokaryotes.

**The heat capacity hypothesis:** Recently, Hobbs et al. [2013] and Schipper et al. [2014] proposed a model called the Macromolecular Rate Theory (MMRT) in which the thermal growth curve is driven by the heat capacity change of activation  $\Delta C_p^\ddagger$  (*i.e.*

### 3. MODELLING THE TEMPERATURE EFFECT ON UNICELLULAR ORGANISMS FROM HETEROTROPHIC BACTERIA TO AUTOTROPHIC EUKARYOTES: A REVIEW

---

the heat capacity difference between the ground state and the transition state). More precisely, the growth rate is expressed as:

$$\mu(T) = \frac{k_B}{h} T e^{\Delta G^\ddagger(T)/(RT)} \quad (3.39)$$

where  $k_B$  and  $h$  are the Boltzmann and Planck's constants,  $\Delta G^\ddagger$  is the Gibbs free energy difference between the ground state and the transition state of a possible rate-limiting enzyme. Contrary to the master reaction model, the MMRT considers that enzymes do not denature easily and are in rapid equilibrium with a folded, inactive intermediate (*i.e.* the transition state). The Gibbs free energy difference can be here written as:

$$\Delta G^\ddagger(T) = \Delta H_{T_0}^\ddagger + \Delta C_p^\ddagger(T - T_0) + T(\Delta S_{T_0}^\ddagger + \Delta C_p^\ddagger \ln(T/T_0)) \quad (3.40)$$

If  $\Delta C_p^\ddagger > 0$ , then the heat capacity difference between the ground state and the transition state (*i.e.* the inactive folded enzyme) itself is sufficient to explain the decrease of growth rate above  $T_{opt}$ . Schipper et al. [2014] validated the MMRT model on microbial soil processes data sets.

### 3.3 The special case of unicellular photosynthetic organisms

Unicellular photosynthetic organisms perform oxygenic photosynthesis. This metabolic particularity is ensured by special structures and enzymes, such as the rubisco enzyme involved in CO<sub>2</sub> fixation, and the photosystems protein complexes which harvest photons. The thermal sensitivity of unicellular photosynthetic organisms is thus expected to be distinct and will be discussed in this section.

#### 3.3.1 The Eppley point of view for phytoplankton

In 1972, Richard Eppley published a review dealing with the effect of temperature on phytoplankton growth in the sea [Eppley, 1972]. Comparing different thermal growth curves for a variety of phytoplankton species in non-limiting conditions (nearly 200 data points), Eppley determined that the maximal growth rate  $\mu_{opt}$  for each species is constrained by a virtual envelope along the optimal temperature trait  $T_{opt}$ , the so-called 'Eppley curve' (see Fig.3.6). Eppley stated that for any phytoplankton species growing under 40°C, 'hotter is faster'.

In 2004, Jon Norberg used Eppley's hypothesis to develop a temperature-growth model, the 'Eppley-Norberg' model [Norberg, 2004]:

$$\mu(T) = \left[ 1 - \left( \frac{T - z}{w} \right)^2 \right] a e^{bT} \quad (3.41)$$

### 3.3 The special case of unicellular photosynthetic organisms

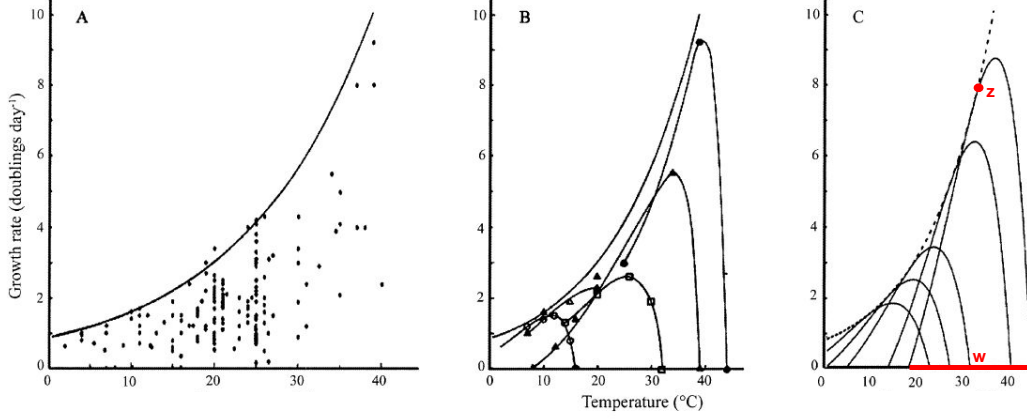


**Figure 3.6: Eppley curve** - A, Eppley envelope function with the original data points. B, 5 data sets for eukaryotic phytoplankton species. C, Eppley-Norberg plot for the 5 species (redrawn from Norberg [2004]).

where  $w$  is the thermal niche width,  $z$  is the temperature at which the growth rate is equal to the Eppley function and is a proxy of  $T_{opt}$ ,  $a$  and  $b$  are parameters of the Eppley function. The Eppley-Norberg model is widely used by the scientific community working on phytoplankton (see for example the recent paper of Taucher et al. [2015]). The Eppley envelope is designed for phytoplankton but is likely to be modified for bacteria (see section 5).

Follows et al. [2007] proposed a slightly different version of the Eppley-Norberg model to take into account photosynthesis:

$$\mu(T, I) = \mu_{max} \cdot \underbrace{\frac{1}{\tau_1} \left( A^T e^{-B(T-T_0)^c} - \tau_2 \right)}_{\gamma^T} \cdot \underbrace{\frac{1}{\gamma_{max}^I} \left( 1 - e^{-k_p I} \right) e^{-k_i I}}_{\gamma^I} \quad (3.42)$$

where  $\mu_{max}$  is the species maximum growth rate,  $\gamma^T$  and  $\gamma^I$  are respectively the normalized temperature photosynthesis functions. The parameters  $\tau_1$  and  $\tau_2$  ensure the normalization of  $\gamma^T$ , while parameters  $A$ ,  $B$ ,  $T_0$  and  $c$  modify its shape by taking into account the Eppley hypothesis (see fig.3.7). Similarly,  $\gamma_{max}^I$  ensures the normalization of  $\gamma^I$ ,  $k_p$  represents the increase of growth with light at low irradiance and  $k_i$  represents photo-inhibition.

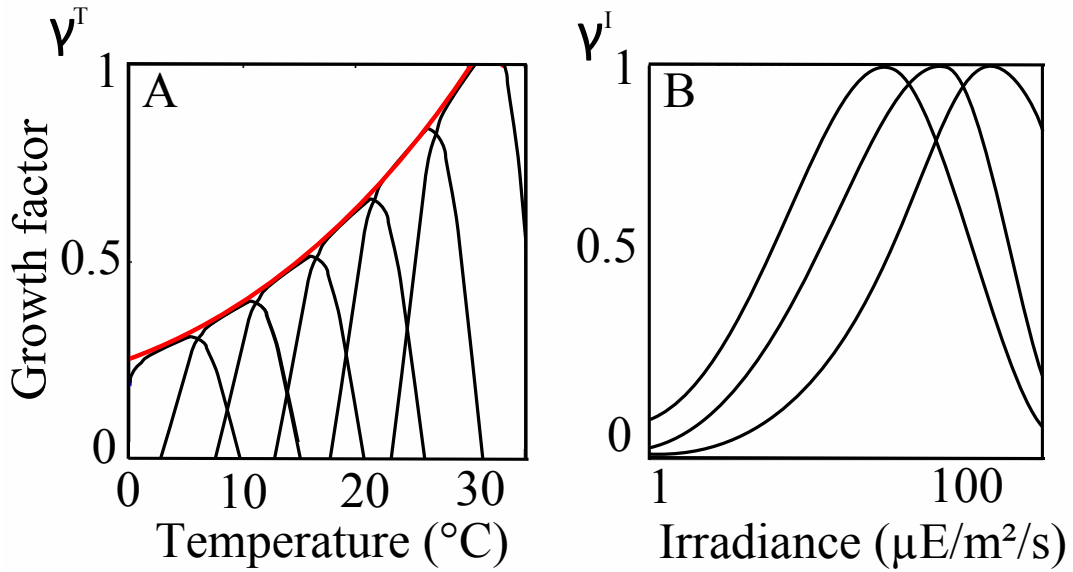


**Figure 3.7: Modified Eppley model** - A, Eppley curve normalized at 30 $^{\circ}\text{C}$ . B, photosynthesis as represented in eq. 3.42. The figure is redrawn after Follows et al. [2007].

### 3.3.2 The link between photosynthesis and temperature in the models

Photosynthesis involves two distinct parts with different sensitivities to temperature (the dark phase and the light phase, see section 10.1.2). The light phase is virtually not affected by temperature, leading to a possible disequilibrium between the photons harvested and their conversion into chemical energy whenever the dark phase is affected by temperature (see for example the review by Ras et al. [2013]). The model supported by data related to the light phase of photosynthesis ( $\text{O}_2$  production of Pulse Amplitude-Modulated (PAM) fluorescence) therefore includes a moderated temperature effect [Béchet et al., 2013].

**Photosynthesis and temperature uncoupled:** These models assume that temperature and light are independent factors. For example, the model developed by Bernard and Rémond [2012] assumes that the growth rate is expressed as:

$$\mu(T, I) = f(I) \cdot \phi(T) \quad (3.43)$$

where  $\phi(T)$  corresponds to the CTMI (eq.3.12) and:

$$f(I) = \mu_{max} \frac{I}{I + \frac{\mu_{max}}{\alpha} \left( \frac{I}{I_{opt}} - 1 \right)^2} \quad (3.44)$$

$\mu_{max}$  is the maximum growth rate at optimal light intensity  $I_{opt}$  and optimal temperature  $T_{opt}$ ,  $\alpha$  is the initial slope of the light response curve.  $f(I)$  was built in line with the

### 3.4 The dynamical effect of temperature on unicellular organisms

Peeters and Eilers [1978] model with photoinhibition, but reparametrized for a better parameter identification. Bernard and Rémond [2012] developed an algorithm to obtain the cardinal temperatures from data sets with different light conditions. This model was validated on 15 phytoplankton species. The uncoupled hypothesis is, however, no longer valid at high light intensities (*i.e.* when photoinhibition occurs) as temperature is known to play a role in photoinhibition [Jensen and Knutsen, 1993a]. For example, low temperature induces an imbalance between the light harvesting and the carbon fixation which is enzyme-dependent (carboxylase) and thus generates light saturating conditions (see 10.1.2 and Young et al. [2015]).

**Photosynthesis and temperature coupled:** Some models consider the coupling between temperature and photosynthesis, such as the model developed by Dermoun et al. [1992] for the unicellular Rhodophyta *Porphyridium cruentum*:

$$\mu(T, I) = 2\mu_m(T)(1 + \beta_1) \frac{I/I_{opt}(T)}{1 + 2\beta_1 I/I_{opt}(T) + (I/I_{opt}(T))^2} \quad (3.45)$$

where  $\mu_m(T)$  is the maximum specific growth rate at a given temperature  $T$ ,  $I_{opt}$  is the optimal irradiance at a given temperature  $T$  and  $\beta_1$  is the shape factor for limiting irradiance.  $\mu_m(T)$  and  $I_{opt}(T)$  are functions similar to eq. 3.45 (see Dermoun et al. [1992]). It is worth noting that the tight coupling between light and temperature in this model leads to identifiability problems partially due to excessive number of parameters (9 here). Furthermore, when light is limiting, it is not essential to take into account the coupling between light and temperature. For all these reasons, we avoid the use of such models. An other example [Carvalho and Malcata, 2003] is detailed in Béchet et al. [2013].

## 3.4 The dynamical effect of temperature on unicellular organisms

Previously, we exposed the different effects of temperature on acclimated cells, using static growth models. However, temperature can have a short-term effect on growth. Internal metabolites such as starch or lipid can accumulate at a rate which can be driven differently by temperature. Moreover, in the natural environment or in outdoor cultures, temperature is varying with time. Dynamical models are thus essential to capture the resulting effects of these varying temperature conditions on growth.

### 3.4.1 The metabolic response to temperature acclimation

Most of the models representing the growth of an UO when the temperature  $T(t)$  is time-varying include a function  $\phi(T(t))$  directly in each reaction kinetic, which has the same mathematical formulation as  $\mu(T)$  described in section 3.2, assuming that the specific growth rate defined by temperature is adopted instantaneously (see for example Baranyi et al. [1995], Baranyi and Roberts [1995]). However, this approach is not always



### 3. MODELLING THE TEMPERATURE EFFECT ON UNICELLULAR ORGANISMS FROM HETEROTROPHIC BACTERIA TO AUTOTROPHIC EUKARYOTES: A REVIEW

---

satisfactory given that temperature-driven metabolite accumulation, temperature-driven respiration and acclimation processes can take place. In the following, we introduce the existing models dealing with temperature variations.

For heterotrophic UO, dynamical models developed by microbiologists mostly take into account a slowly changing temperature (see for example Baranyi et al. [1995] and Kovarova et al. [1996]). Dougherty et al. [2002] developed a model for the bacteria *Lactococcus lactis* under more rapid temperature fluctuations. The model considers the total amount of energy per cell as a state variable, and its distribution for different biosynthesis pathways (here malic acid and lactic acid) have different temperature sensitivities.

Richard Geider was one of the first to develop a dynamical model accounting for temperature effect on phytoplankton growth. Firstly, he took into account the fact that phytoplankton cells are able to adapt their pigment content to temperature changes. The chlorophyll concentration is adjusted to the photon flux and to the cell capacity of converting it into chemical energy. It has been clearly shown that the carbon to chlorophyll ratio ( $C/Chla$ ) decreases exponentially with temperature, and Geider [1987] modelled it:

$$\boxed{\frac{C}{Chla} = a - bT + cIe^{-kT}} \quad (3.46)$$

where  $a$ ,  $b$ ,  $c$ ,  $k$  are constants and  $I$  is the light intensity. However, eq. 3.46 isn't valid anymore when the temperature is higher than the species  $T_{opt}$  [Geider, 1987]. This model has thus to be included into a dynamical model where carbon or chlorophyll are state variables.

Later, Geider et al. [1998] developed a dynamical model for the whole phytoplankton growth. The model deals with the co-limitation by nutrient, light and temperature on growth. The state variables and biomass descriptors are the bulk nitrogen, carbon and chlorophyll concentrations. Using an Arrhenius equation, they consider that temperature acts equally on respiration, chlorophyll synthesis and nitrogen assimilation so that different metabolic processes have the same temperature dependence. However, the model considers that temperature affects the light-saturated photosynthesis whereas it does not affect the initial slope of the photosynthesis versus light intensity curve. The Geider et al. [1998] model was later modified by Quinn et al. [2011] for phytoplankton biotechnological applications assuming that temperature does not affect respiration.

For marine biogeochemical applications, Thomas et al. [2012] have developed a model for phytoplankton in which the substrate uptake follows an Eppley formulation (eq. 3.41). The temperature-induced losses are arbitrary set to 5% of the Eppley curve regardless of the species thermal trait.

More recently, Muñoz-Tamayo et al. [2013] constructed a model based on Mairet et al. [2010] itself based on the Droop model [Droop, 1968] to account for the temperature fluctuations effects in outdoor phytoplankton cultures. The model assumes again that temperature has the same effect on all kinetic reactions by incorporating the CTMI model (eq. 3.12) in the ODE system. Yet, it considers chlorophyll acclimation to temperature by including eq.3.46 in the chlorophyll state variable dynamics.

#### 3.4.2 The thermally-induced death

UO cells submitted to cooling or warming can die because of protein denaturation, membranes injuries or an imbalance between the needed and produced ATP. Several question related to lethal temperatures are still open: i) What is the effect of the time-duration of cooling or heating on mortality? ii) What happens for temperature lower or higher than the physiological  $T_{min}$  and  $T_{max}$ ? iii) Does death rate already increase for temperatures lower than the  $T_{opt}$ ?

**The survival curve:** Thermal mortality was first investigated, once again, by microbiologists dealing with bacterial disinfection in food industry. They particularly focused their study on the survival curve, *i.e.* the natural logarithm of the remaining alive cells plotted against time. Applying a fixed temperature above the species  $T_{max}$ , Moats [1971] describes 4 types of survival curve (fig. 3.8). Numerous empirical models exist to represent the survival curves within isothermal conditions (see the recent review Smelt and Brul [2014]); they are called primary model, because they don't take into account the temperature time variation effect. The Weibull model [Mafart et al., 2002] is one of the most widely used:

$$\ln(N(t)) = -\ln(N_0) - \left( \frac{t}{\delta(T)} \right)^{p(T)} \quad (3.47)$$

where  $t$  is the time of heating,  $\delta(T)$  is the temperature-dependent scale parameter and  $p(T)$  is the temperature-dependent shape parameter. The Weibull model accounts for the upward or downward concavity that the survival curve can take shape. If  $p(T) = 1$ , then the mortality rate is exponential. Because the survival curve is the combination of several processes, including cell damages and repairs, mechanistic models have also been developed [Smelt et al., 2002]. Nonetheless, primary models can't be used in dynamical conditions.

Secondary death models associate a temperature-dependent function to the parameters of primary models (*i.e.* isothermal models). They allow to consider temperature as a time-varying variable. The simpler and mechanistic use of secondary model is constructed on an Arrhenius equation. Qin et al. [2014], for example, used such a secondary model for eukaryote cells. Because the irreversible cell denaturation rate regarding temperature follows an Arrhenius equation, the denatured cell fraction  $F_D$  during an heating process can be written as:

$$F_D = 1 - \exp \left( -1/B \int_{T_0}^{T_{end}} k(T) dT \right) \quad (3.48)$$

where  $k(T)$  is the cell denaturation rate,  $B$  is the rate of temperature change (temperature is linearly varying here),  $T_0$  and  $T_{end}$  are the temperature at the beginning and at the end of the heating process. It is worth noting that other mechanistic approaches exist, such as proposed by Valdramidis et al. [2007] who developed a model for *Escherichia coli* taking into account heat resistance (and thus repair mechanisms) of cells. Empirical

### 3. MODELLING THE TEMPERATURE EFFECT ON UNICELLULAR ORGANISMS FROM HETEROTROPHIC BACTERIA TO AUTOTROPHIC EUKARYOTES: A REVIEW

---

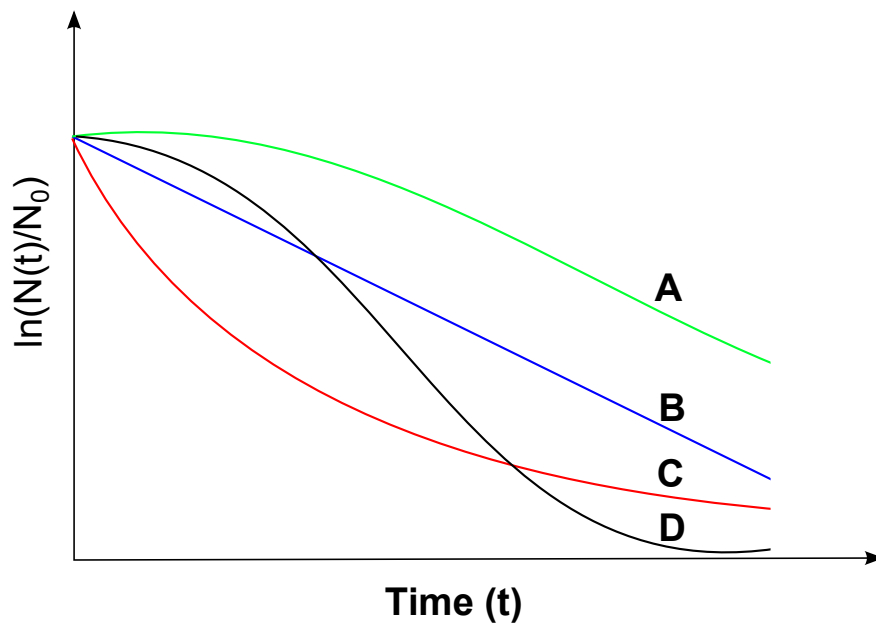


**Figure 3.8: Survival curves** - Cell survival curves in batch conditions (here expressed as the concentration of alive cells  $N(t)$  on initial cells concentration  $N_0$ .) when exposed to temperature higher than  $T_{max}$  (redrawn from Moats [1971]). A, initial lag in death followed by a log-linear death rate, B, log-linear death rate, C, heterogeneous population with different death rates, D, death rate with inflexion.

secondary-based models are also common; Corradini and Peleg [2007] constructed an empirical model for bacteria based on the Weibull model (eq. 3.47) where  $\delta(T(t))$  and  $p(T(t))$  are explicit temperature-dependent functions.

**Coupling growth and death models:** In variable conditions, cells can be submitted to lethal and non-lethal temperatures. For this reason, microbiologists have sought to couple growth models with mortality models (fig. 3.9). Van Uden [1985], for example, combines a master reaction growth model with an exponential mortality model (*i.e.* a primary model) for yeast. For bacteria, this kind of models has been reviewed by Corradini and Peleg [2006]. Some authors have coupled growth models and secondary death models in order to also take into account the effect of the time duration of heating and cooling (see for example Baranyi et al. [1996]).

## 3.5 Conclusion

In this chapter, we have pictured out the different types of existing temperature-growth models for UO. In non-limiting conditions and balanced growth, the empirical temperature models better fit the data than mechanistic models (see fig. 3.1).

However, the limiting steps in the thermal growth curve, as depicted by the mechanistic models, are not clearly understood. Despite the recent development of a universal unicellular growth model [Corkrey et al., 2014], the ‘proteome paradigm’ should be further investigated. The proteome implication in thermal adaptation should be considered.

Modelling of the temperature effect on photosynthetic organisms still has shortcomings. The temperature coupling with light has not clearly been investigated at high light intensity. The Eppley hypothesis has only been applied to phytoplankton and could be adapted for other groups. Also, this hypothesis may depend on the phytoplankton group considered.

The effect of temporal temperature variations on the cell metabolic reactions are not well described by the models [Ras et al., 2013]. Data are clearly lacking to understand and model how internal metabolites such as starch or lipid react to temperature variations. Because temperature is naturally varying in the environment, its fluctuations may drive temperature acclimation and its effects have to be determined.

Finally, the thermally-induced death still has to be investigated. Few studies exist for unicellular eukaryotes, especially for phytoplankton. It is not clear if death rate increases under theoretically sublethal temperatures. Moreover, the capacity of cell to repair its damages and regrow after an heat or cold shock is not clearly understood and modelled, as well as the acclimation and adaptation to temperature. The molecular mechanisms leading to or protecting against death are not clearly understood, and should be closely related to the proteome thermal sensitivity.

### 3. MODELLING THE TEMPERATURE EFFECT ON UNICELLULAR ORGANISMS FROM HETEROTROPHIC BACTERIA TO AUTOTROPHIC EUKARYOTES: A REVIEW

---

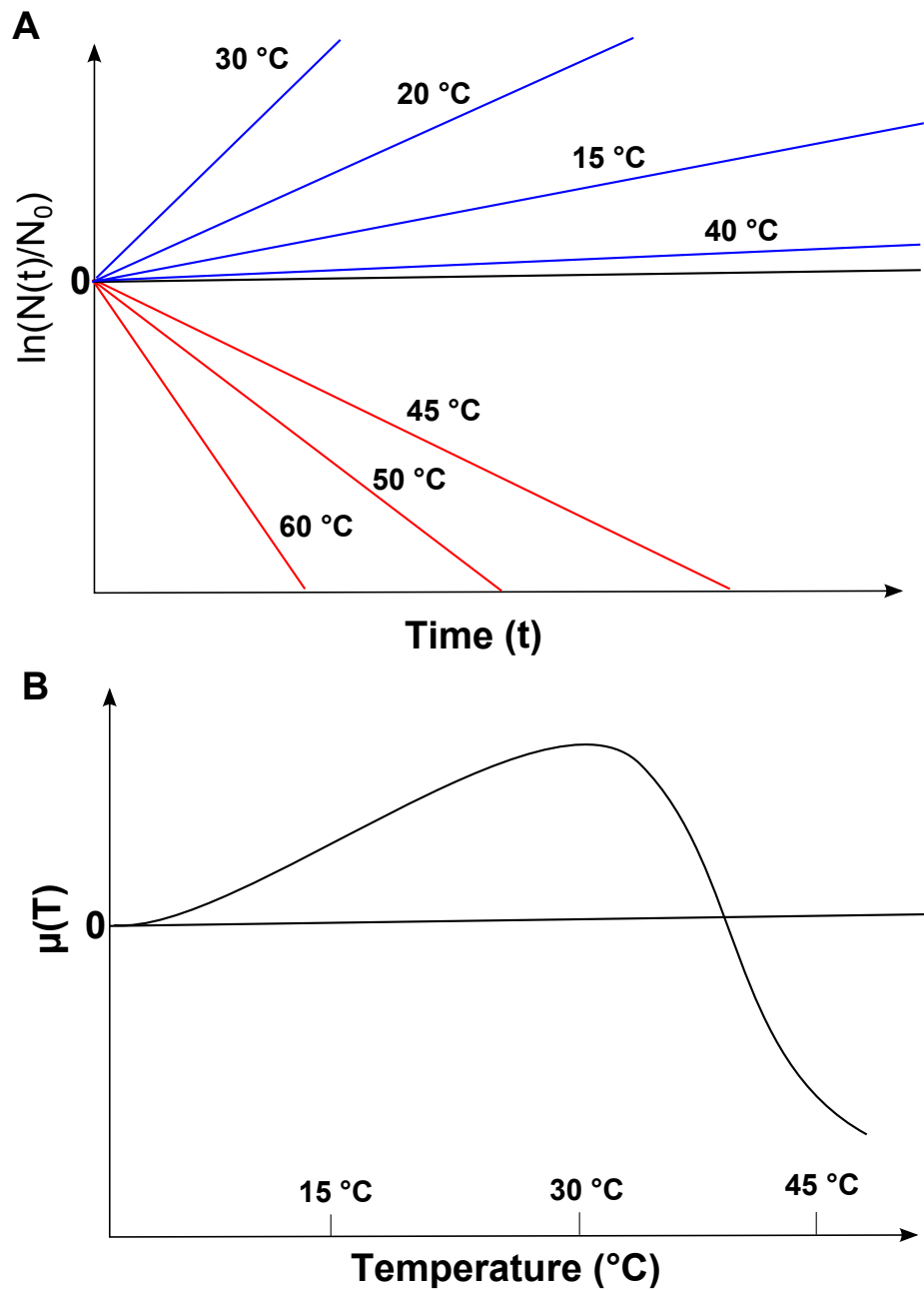


**Figure 3.9: Coupled growth and death models - A, first-order reaction kinetic (blue, growth, red, death) for a fictive UO when the time spent at each temperature is sufficiently long. B, resulting growth rate versus temperature curve. Redrawn from Corradini and Peleg [2006]**

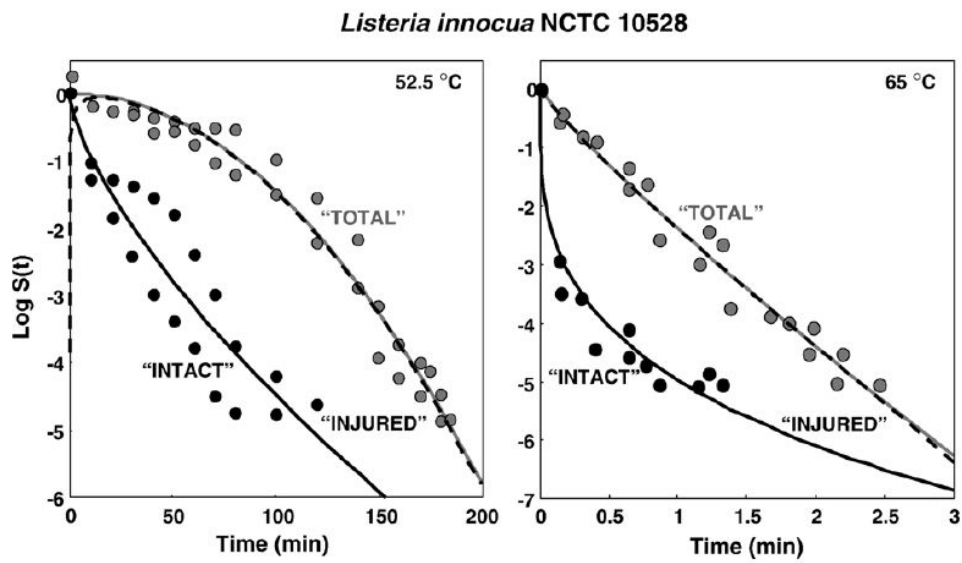


**Figure 3.10:** Survival curves obtained at different temperatures - Temporal dynamics of temperature injury on *Listeria innocua* at two different temperatures (adapted from Corradini and Peleg [2007]).

### 3. MODELLING THE TEMPERATURE EFFECT ON UNICELLULAR ORGANISMS FROM HETEROTROPHIC BACTERIA TO AUTOTROPHIC EUKARYOTES: A REVIEW

---

#### Summary of section 3:

- Empirical models better describe the thermal growth curve than mechanistic ones
- The effect of temperature on physiology are not well understood, especially when temperature is fluctuating
- The coupled effects of temperature and light have to be further investigated
- The thermally-induced death is only modelled by empirical models

## 4

# Correlation between the cardinal temperatures: insight into thermal adaptation

Contributors: Bernard, O., Mairet, F., Sciandra, A.

*Ærarissima nostro simplicitas*

---

### 4.1 Introduction

Unicellular organisms (UO) are poikilotherms, which means that their internal temperature is at equilibrium with the environmental temperature, thus constraining their metabolic rate. However, these microorganisms have colonized most of the thermal windows, ranging from psychrophilic (temperature < 15°C) to hyperthermophilic (temperature > 90°C) niches Rothschild and Rocco [2001]. The underlying adaptation mechanisms have been extensively studied over the past decade Chen and Shakhnovich [2010], Cooper et al. [2001], Kingsolver [2009], but are still in debate. The adaptation capability is strongly dependent on the different phylogenetic groups. For example, the two phytoplankton groups of diatoms and dinophytes do not adapt in the same way despite their close ecological role [Huertas et al., 2011]. In a warming world, two questions are critical: i) What controls thermal adaptation? ii) Is thermal adaptation driven by some universal mechanisms?

Temperature controls the rate of metabolic activity Gillooly et al. [2001a], but also induces enzyme denaturation Zeldovich et al. [2007]. These antagonistic effects are responsible for the asymmetry of the thermal growth curve, which links growth rate to temperature for a given species Angilletta [2009]. Each species can be characterized



## 4. CORRELATION BETWEEN THE CARDINAL TEMPERATURES: INSIGHT INTO THERMAL ADAPTATION

---

by three thermal parameters called cardinal temperatures: its minimal ( $T_{min}$ ), optimal ( $T_{opt}$ ) and maximal ( $T_{max}$ ) temperatures for growth. It has been previously shown that there exists a linear relationship between  $T_{min}$ ,  $T_{opt}$  and  $T_{max}$ , in bacteria Rosso et al. [1993], but this has not been explained yet.

We investigated the correlation between cardinal temperatures in the three domains of life (Archaea, Bacteria, and unicellular Eukaryota). To this end, we modelled the thermal growth curve using an empirical model, the Cardinal Temperature Model with Inflexion (CTMI) Rosso et al. [1993] (see eq. 3.11). CTMI allows to identify the cardinal temperatures from experimental data using a method developed by Bernard and Rémond [2012]. We analysed 464 growth rates versus temperature curves (representing more than 5780 points) from the literature for species belonging to the three domains of life and ranging from psychrophiles to hyperthermophiles (see section 2.2). We determined the associated cardinal temperatures for each curve. We validated our approach by comparing experimental data points to model predictions.

We show that there exists linear correlations between  $T_{min}$  and  $T_{opt}$  and between  $T_{max}$  and  $T_{opt}$  valid for all UO, with a marked difference between prokaryotes and eukaryotes.

### 4.2 Relation between the cardinal temperatures

#### 4.2.1 Linear relationships

Using the CTMI model, Rosso et al. [1993] have previously shown that the cardinal temperatures are linearly correlated for psychrophiles, mesophiles and thermophiles bacteria. We tested if such a linear relationship holds for all the UO and we calculated a linear regression between the cardinal temperatures obtained for our data set (see fig 4.1 and table 4.1). It turns out that a similar relationship holds for the whole data set, including groups for which this relation has never been tested before, *i.e.* phytoplankton, yeasts, archae, cyanobacteria ( $\rho = 0.981$  for the relationship ( $T_{opt}, T_{max}$ ),  $\rho = 0.871$  for the relationship ( $T_{opt}, T_{min}$ ), and  $\rho = 0.867$  for the relationship ( $T_{min}, T_{max}$ ),  $p < 0.01$  (T-test); see table 4.1), with the best linear fit obtained for the linear regression between  $T_{opt}$  and  $T_{max}$  ( $r^2 = 0.962$ ). The thermal profile of a UO can thus be expressed as:

$$\begin{aligned} T_{max} &= a_1 T_{opt} + b_1 \\ T_{min} &= a_2 T_{opt} + b_2 \end{aligned} \tag{4.1}$$

with  $a_1 = 1.035$ ,  $b_1 = 7.367^\circ\text{C}$ ,  $a_2 = 0.819$ ,  $b_2 = -19.006^\circ\text{C}$ . The results are in accordance with Rosso et al. [1993] ( $p < 0.05$ , Chow-test) (see table 4.1). The slope  $a_1$  of the linear regression between  $T_{opt}$  and  $T_{max}$  is nearly equal to one, indicating that the difference between  $T_{max}$  and  $T_{opt}$  is fairly constant and equal to the intercept of the linear regression ( $b_1 = 7.367$ ). This is not the case for the linear regression between ( $T_{opt}, T_{min}$ ) and ( $T_{min}, T_{max}$ ) ( $a_2 = 0.819$  and  $a_3 = 0.773$  respectively) meaning that the thermal niche width  $w = |T_{max} - T_{min}|$  theoretically increases with  $T_{max}$  ( $w$  increases by  $0.216^\circ\text{C}$  as  $T_{max}$  increases by  $1^\circ\text{C}$ ).

## 4.2 Relation between the cardinal temperatures

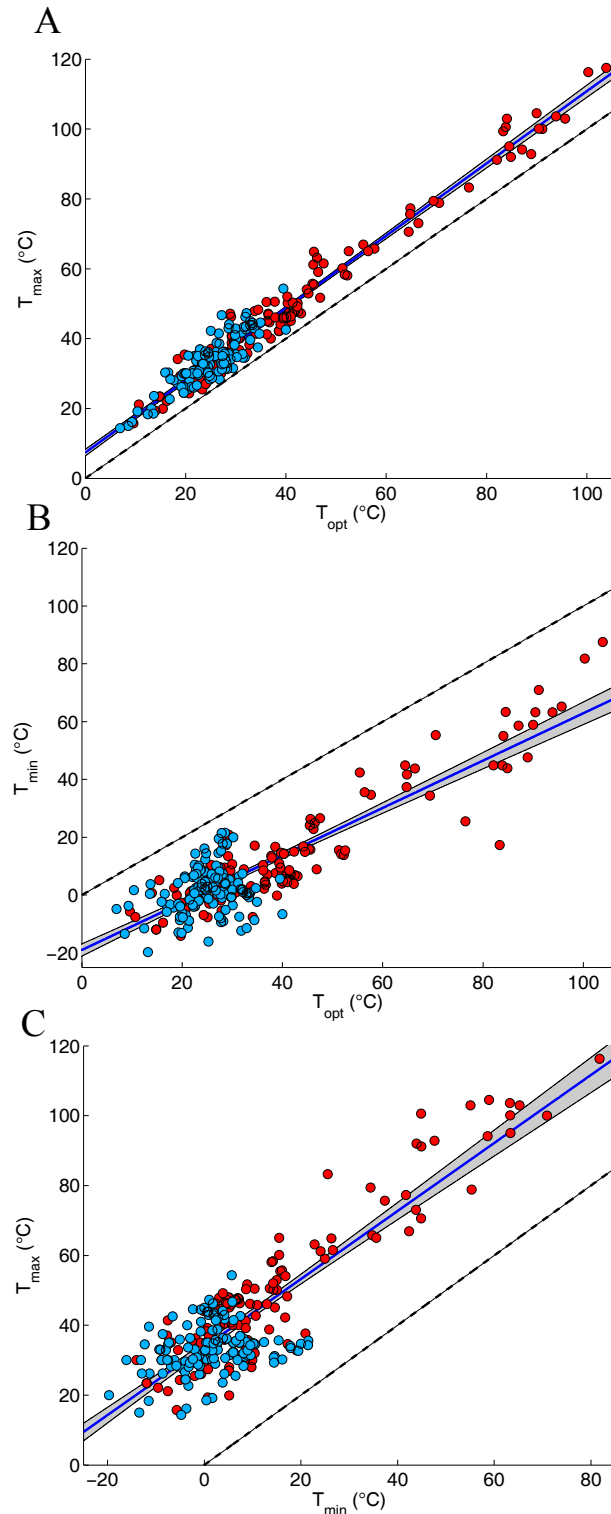


**Figure 4.1: Linear regression between the cardinal temperatures.** - A,  $T_{opt}, T_{max}$ , B,  $T_{opt}, T_{min}$ , C,  $T_{min}, T_{max}$ . The blue line corresponds to the linear regression, the grey areas are the 95% prediction intervals. The dashed line is the  $y = x$  function. Prokaryotes and Eukaryotes are indicated by red and blue points respectively.

## 4. CORRELATION BETWEEN THE CARDINAL TEMPERATURES: INSIGHT INTO THERMAL ADAPTATION

---

### 4.2.2 Differences among the phylogenetic groups

To challenge the universality of these linear relationships, we divided the data set into two groups, prokaryotes and eukaryotes, and 5 subgroups according to phylogenetic and metabolic criteria: bacteria (heterotrophic prokaryotes), archae (heterotrophic prokaryotes), cyanobacteria (photosynthetic prokaryotes), microalgae (photosynthetic eukaryotes), yeast (heterotrophic eukaryotes).

For the couple  $(T_{opt}, T_{max})$ , the linear regression is better for prokaryotes than for eukaryotes, the significance of the linear relationship being verified for both ( $\rho = 0.986$  and  $\rho = 0.851$  respectively,  $p < 0.01$ ). Moreover, the slope and the intercept are comparable ( $p < 0.05$ , Chow-test; see table 4.1) and significantly close to that found by Rosso et al. [1993] ( $p < 0.05$ , Chow-test). However, for the couple  $(T_{opt}, T_{min})$ , the linear correlation is only significant for prokaryotes, and the linear regression gives a satisfactory result only for this group ( $\rho = 0.916$ ,  $R^2 = 0.839$ ,  $p < 0.01$  (T-test) for prokaryotes and  $\rho = 0.238$ ,  $R^2 = 0.056$  for eukaryotes). The linear regression only gives values significantly close to that of Rosso et al. [1993] for prokaryote ( $p < 0.05$ , Chow-test). The same differences prokaryotes/eukaryotes are observed for the couple  $(T_{max}, T_{min})$  ( $\rho = 0.911$ ,  $p < 0.01$  (T-test) for prokaryotes and  $\rho = 0.260$  for eukaryotes). From these data analysis, it results that Rosso et al. [1993] observations only hold for prokaryotes. Eukaryotes, on the other way, solely follow the linear rule between  $T_{opt}$  and  $T_{max}$ .

The three prokaryote subgroups archae, bacteria and cyanobacteria all verify the linear correlations between cardinal temperatures and have the same linear regressions for the cardinal temperatures, without subgroup specificities ( $p < 0.05$ , Chow-test) (see fig. 4.2, 4.3, 4.4 A,B,C). The eukaryote subgroups of microalgae and yeasts also show a significant linear correlation between  $T_{opt}$  and  $T_{max}$  (see table 4.1). The linear regression coefficients obtained for microalgae are comparable to the ones obtained for prokaryotes, but differ from those of yeasts (see fig. 4.2, 4.3, 4.4 D,E).

The metabolism type (heterotrophic or autotrophic) does not seem to affect the linear link between the cardinal temperatures (but see section 5.3). However, microalgae and cyanobacteria have a lower average thermal niche width ( $29.535 \pm 8.579$  and  $29.640 \pm 7.949$  respectively) than heterotrophic UO (fig. 4.6). It is worth noting that most of the autotrophic organisms can change their metabolism to an heterotrophic mode under particular environmental conditions. Here, all the phytoplankton data sets are obtained in autotrophic conditions.

## 4.2 Relation between the cardinal temperatures

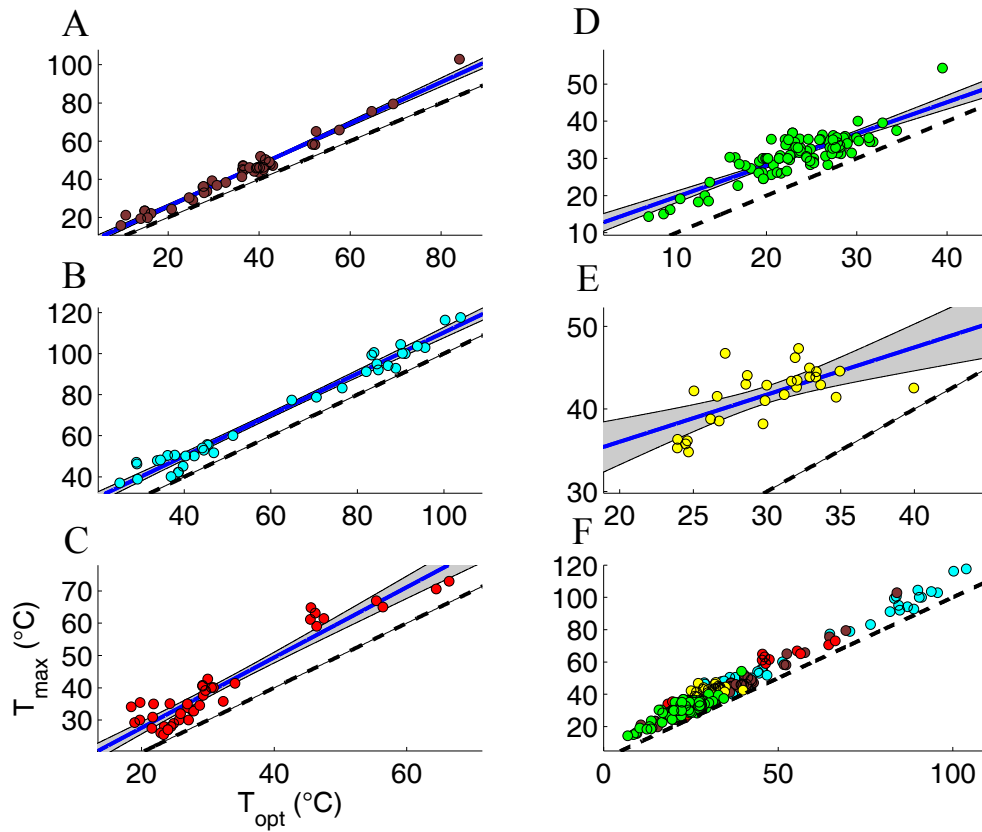


**Figure 4.2: Linear regression between  $T_{opt}$  and  $T_{max}$  - A, bacteria, B, archae, C, cyanobacteria, D, microalgae, E, yeasts, F, whole data set. The blue line corresponds to the linear regression, the grey areas are the 95% prediction intervals. The dashed line is the  $y = x$  line.**

#### 4. CORRELATION BETWEEN THE CARDINAL TEMPERATURES: INSIGHT INTO THERMAL ADAPTATION

---

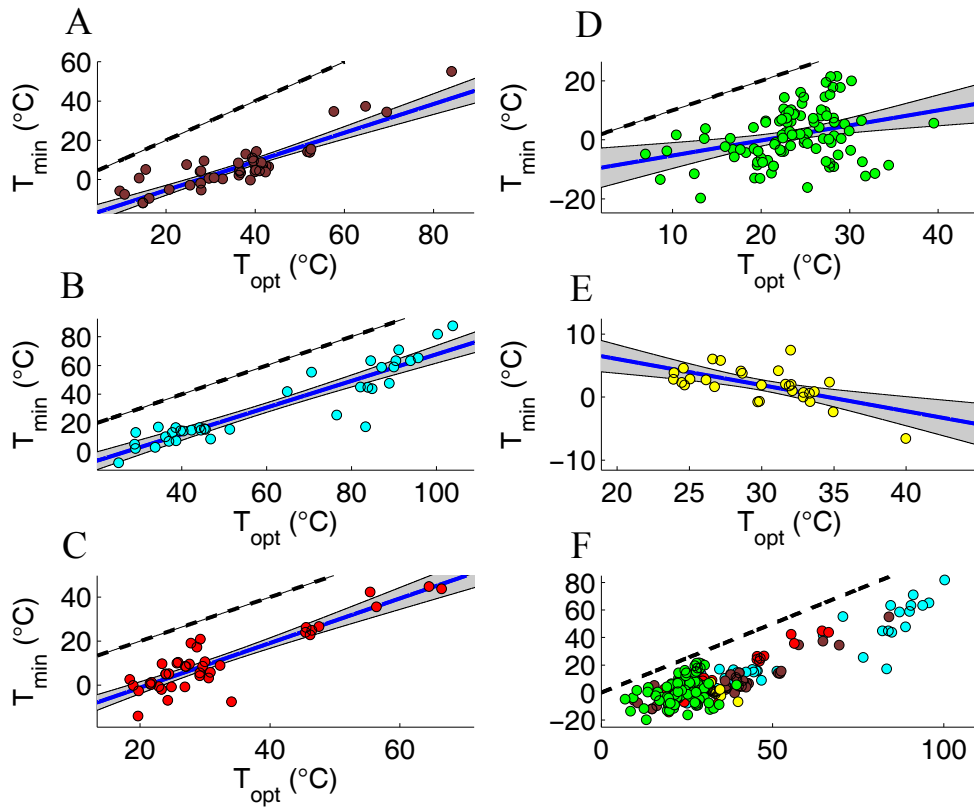


**Figure 4.3:** Linear regression between  $T_{opt}$  and  $T_{min}$  - A, bacteria, B, archae, C, cyanobacteria, D, microalgae, E, yeasts, F, whole data set. The blue line corresponds to the linear regression, the grey areas are the 95% prediction intervals. The dashed line is the  $y = x$  line.

## 4.2 Relation between the cardinal temperatures

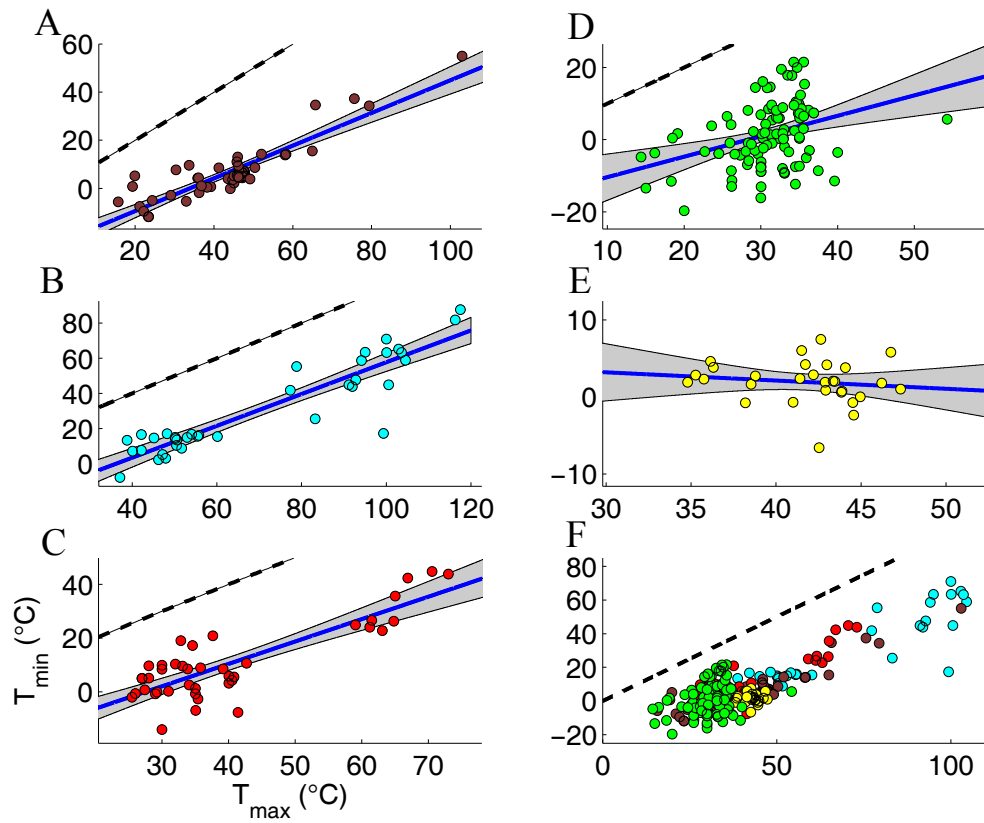


**Figure 4.4: Linear regression between  $T_{max}$  and  $T_{min}$**  - A, bacteria, B, archae, C, cyanobacteria, D, microalgae, E, yeasts, F, whole data set. The blue line corresponds to the linear regression, the grey areas are the 95% prediction intervals. The dashed line is the  $y = x$  line.

**Table 4.1:** Parameters of the linear regression between cardinal temperatures and statistical descriptors.  $\hat{a}$  and  $\hat{b}$  correspond to the slope and to the intercept of the linear regression  $y = \hat{a}x + \hat{b}$ .

Group	Linear regression	$\hat{a}$	$\hat{b}$	$\rho$	$R^2$	Adjusted $R^2$	$p < 0.01$ (T-test)
Microalgae (autotrophic eukaryotes)	$T_{min} = \hat{a}T_{opt} + \hat{b}$	0.510	-10.437	0.316	0.1	0.091	no
	$T_{max} = \hat{a}T_{opt} + \hat{b}$	0.849	11.148	0.842	0.709	0.706	yes
	$T_{min} = \hat{a}T_{max} + \hat{b}$	0.566	-16.057	0.354	0.125	0.117	yes
Yeast (heterotrophic eukaryotes)	$T_{min} = \hat{a}T_{opt} + \hat{b}$	-0.4136	14.313	-0.609	0.370	0.347	no
	$T_{max} = \hat{a}T_{opt} + \hat{b}$	0.572	24.570	0.654	0.428	0.407	yes
	$T_{min} = \hat{a}T_{max} + \hat{b}$	-0.106	6.393	-0.137	0.018	-0.017	no
Cyanobacteria (autotrophic bacteria)	$T_{min} = \hat{a}T_{opt} + \hat{b}$	1.015	-21.482	0.898	0.806	0.801	yes
	$T_{max} = \hat{a}T_{opt} + \hat{b}$	1.087	5.871	0.953	0.908	0.905	yes
	$T_{min} = \hat{a}T_{max} + \hat{b}$	0.832	-22.9	0.841	0.707	0.699	yes
Heterotrophic bacteria	$T_{min} = \hat{a}T_{opt} + \hat{b}$	0.732	-20.062	0.878	0.772	0.767	yes
	$T_{max} = \hat{a}T_{opt} + \hat{b}$	1.084	4.168	0.988	0.976	0.975	yes
	$T_{min} = \hat{a}T_{max} + \hat{b}$	0.680	-23.077	0.896	0.803	0.799	yes
Archae	$T_{min} = \hat{a}T_{opt} + \hat{b}$	0.924	-24.739	0.925	0.856	0.852	yes
	$T_{max} = \hat{a}T_{opt} + \hat{b}$	1.002	10.001	0.988	0.975	0.975	yes
	$T_{min} = \hat{a}T_{max} + \hat{b}$	0.904	-32.677	0.918	0.843	0.838	yes
Prokaryotes	$T_{min} = \hat{a}T_{opt} + \hat{b}$	0.867	-21.287	0.916	0.839	0.837	yes
	$T_{max} = \hat{a}T_{opt} + \hat{b}$	1.049	6.455	0.986	0.973	0.973	yes
	$T_{min} = \hat{a}T_{max} + \hat{b}$	0.811	-25.862	0.912	0.831	0.830	yes
Eukaryotes	$T_{min} = \hat{a}T_{opt} + \hat{b}$	0.323	-6.394	0.238	0.056	0.049	no
	$T_{max} = \hat{a}T_{opt} + \hat{b}$	0.989	8.691	0.851	0.724	0.722	yes
	$T_{min} = \hat{a}T_{max} + \hat{b}$	0.304	-8.509	0.260	0.067	0.061	yes
Three kingdoms of life	$T_{min} = \hat{a}T_{opt} + \hat{b}$	0.819	-19.006	0.871	0.759	0.758	yes
	$T_{max} = \hat{a}T_{opt} + \hat{b}$	1.035	7.367	0.981	0.962	0.962	yes
	$T_{min} = \hat{a}T_{max} + \hat{b}$	0.773	-24.055	0.867	0.752	0.751	yes
Rosso et al. [1993]	$T_{min} = \hat{a}T_{opt} + \hat{b}$	<b>0.953</b>	<b>-28.913</b>	-	-	-	-
	$T_{max} = \hat{a}T_{opt} + \hat{b}$	<b>1.101</b>	<b>3.203</b>	-	-	-	-
	$T_{min} = \hat{a}T_{max} + \hat{b}$	<b>0.866</b>	<b>-31.687</b>	-	-	-	-

## 4.2 Relation between the cardinal temperatures

---

Finally, to test whether the differences previously observed could be related to the range of temperature growth, we divided the data set into 3 groups according to their thermal preferences: psychrophiles ( $T_{opt} < 15^{\circ}\text{C}$ ), mesophiles ( $15^{\circ}\text{C} \leq T_{opt} < 45^{\circ}\text{C}$ ), thermophiles ( $T_{opt} \geq 45^{\circ}\text{C}$ ) [Willey, 2008]. No significant differences were found between these groups. This indicates that the species thermal preferendum does not play a role in the correlation between the cardinal temperatures.

### 4.2.3 A closer look at microalgae

To validate the linear correlations found between the cardinal temperatures, we analysed a data set recently compiled by Thomas et al. [2015] for eukaryotic phytoplankton. We divided this data set into 4 phylogenetic groups: Dinophyta, Ochrophyta (diatoms and related), Haptophyta and Chlorophyta. We applied the same linear regression as for the other groups, with the same data set selection criteria (see section 2.2.4). Results (fig. 4.5 and table 4.2) confirmed the correlations observed for  $(T_{opt}, T_{max})$  for eukaryotes, with no significant differences between the linear regressions for Dinophyta, Ochrophyta and Chlorophyta ( $p < 0.05$ , Chow-test). Nevertheless, for Haptophyta, the linear regression gave significantly different results; because there is only 12 data points for this group, it was not possible to conclude that Haptophyta are particularly different.

The link between  $T_{min}$  and the other cardinal temperatures found here nuances the results obtained for the microalgae data set compiled in section 4.2.2. Indeed, among the 4 microalgae groups considered here, Dinophyta have a significant linear correlation between  $T_{opt}$  and  $T_{min}$ . At that stage, it is not possible to determine if it is a specificity of Dinophyta, or if this correlation could apply to the other microalgae groups using a better protocole to determine  $T_{min}$ .



#### 4. CORRELATION BETWEEN THE CARDINAL TEMPERATURES: INSIGHT INTO THERMAL ADAPTATION

**Table 4.2:** Parameters of the linear regression between cardinal temperatures and statistical descriptors for Thomas et al. [2015] data set (microalgae).  $\hat{a}$  and  $\hat{b}$  correspond to the slope and to the intercept of the linear regression  $y = \hat{a}x + \hat{b}$ .

Group	Linear regression	$\hat{a}$	$\hat{b}$	$\rho$	$R^2$	Adjusted $R^2$	$p < 0.01$ (T-test)
Dinophyta	$T_{min} = \hat{a}T_{opt} + \hat{b}$	0.94393	-19.652	0.4961	0.246	0.233	yes
	$T_{max} = \hat{a}T_{opt} + \hat{b}$	1.1676	3.323	0.695	0.482	0.473	yes
	$T_{min} = \hat{a}T_{max} + \hat{b}$	0.7087	-19.079	0.626	0.392	0.381	yes
Ochromphyta	$T_{min} = \hat{a}T_{opt} + \hat{b}$	0.201	-9.231	0.0971	0.00943	0.00131	no
	$T_{max} = \hat{a}T_{opt} + \hat{b}$	0.836	12.445	0.6871	0.472	0.468	yes
	$T_{min} = \hat{a}T_{max} + \hat{b}$	0.182	32.739	0.3089	0.0954	0.088	no
Haptophyta	$T_{min} = \hat{a}T_{opt} + \hat{b}$	0.924	-22.342	0.204	0.0414	-0.0544	no
	$T_{max} = \hat{a}T_{opt} + \hat{b}$	0.649	14.953	0.475	0.226	0.148	yes
	$T_{min} = \hat{a}T_{max} + \hat{b}$	0.095	29.13	0.316	0.099	0.0099	no
Chlorophyta	$T_{min} = \hat{a}T_{opt} + \hat{b}$	0.202	-7.326	0.116	0.014	0.003	no
	$T_{max} = \hat{a}T_{opt} + \hat{b}$	1.061	8.461	0.719	0.517	0.512	yes
	$T_{min} = \hat{a}T_{max} + \hat{b}$	0.267	37.014	0.315	0.099	0.09	no
All groups	$T_{min} = \hat{a}T_{opt} + \hat{b}$	0.355	-10.619	0.177	0.031	0.028	no
	$T_{max} = \hat{a}T_{opt} + \hat{b}$	0.999	8.861	0.718	0.515	0.514	yes
	$T_{min} = \hat{a}T_{max} + \hat{b}$	0.222	33.898	0.319	0.102	0.099	yes

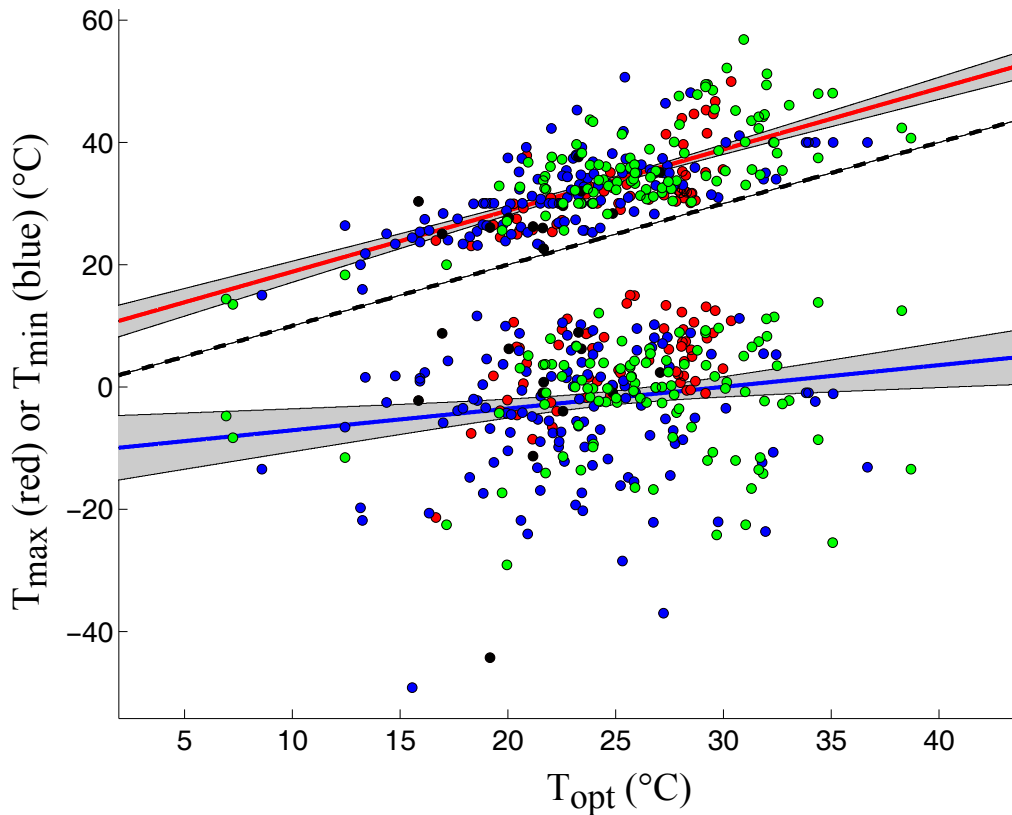


**Figure 4.5:** Linear regression between  $T_{opt}$  and  $T_{min}$ ,  $T_{opt}$  and  $T_{max}$  for phytoplankton (data from Thomas et al. [2015]) - Red, Dinophyta, blue, Ochrophyta, black, Haptophyta, green, Chlorophyta. The blue and red lines correspond to the linear regressions between  $T_{opt}$  and  $T_{min}$ ,  $T_{opt}$  and  $T_{max}$  respectively. The grey areas are the 95% prediction intervals. The dashed line is the  $y = x$  line.

### 4.3 Thermal adaptation and the thermal niche width

The unveiled linear relationships between the cardinal temperatures, universal for  $T_{opt}$  and  $T_{max}$ , specific to prokaryotes for  $T_{opt}$  and  $T_{min}$ , let us assume that thermal adaptation, at least within the prokaryote group, proceeds by translation of the thermal growth curve. This result corresponds to the ‘horizontal-shift’ hypothesis of Huey and Kingsolver [1989] (see also Kingsolver [2009]). This translation is not strict, because, as previously found for the whole data set, the thermal niche width of prokaryotes is supposed to slightly increase with  $T_{opt}$  (see eq. 4.1). Eukaryotes seem to follow a different pattern with a possible absence of linear link between  $T_{min}$  and  $T_{max}$ , and thus eukaryotes could

## 4. CORRELATION BETWEEN THE CARDINAL TEMPERATURES: INSIGHT INTO THERMAL ADAPTATION

---

have a more flexible thermal niche width and a special ability to adapt to cold temperatures. Nevertheless, eukaryotes and prokaryotes (fig. 4.6 and fig. 4.7) have similar average thermal niche widths ( $31.757^{\circ}\text{C} \pm 8.947$  and  $35.016^{\circ}\text{C} \pm 8.500$  respectively), even within the phytoplankton eukaryotic group (fig. 4.7). The thermal adaptation mechanisms are maybe different (explaining the possible uncoupling between  $T_{min}$  and  $T_{max}$  for eukaryotes) but the same physical constrains apply for the two groups. For example, some authors have highlighted the crucial role played by membrane structures during thermal adaptation [Arthur and Watson, 1976, Caspeta et al., 2014, Daniel et al., 2004, Liberles et al., 2012, Los et al., 2013]. Because eukaryotes possess complex membranes compared to prokaryotes, this could be a key concept for explaining the eukaryote  $T_{min}$  flexibility. Recently, Caspeta et al. [2014] have enhanced the thermal tolerance of the yeast *Saccharomyces cerevisiae* by continuously selecting more thermal tolerant strains. The resulting strains had a different sterol composition, a key component of membrane fluidity. Lipids composition of membranes is also highly modified during thermal adaptation of microalgae, as recently shown by Bonnefond et al. [subm.]. Additionally, some microalgae are able to regulate their ribosome cell concentration as an adaptation to cold temperatures [Toseland et al., 2013].

### 4.4 Conclusion

The linear correlations between the cardinal temperatures unveiled by Rosso et al. [1993] have been confirmed for all the UO. However, eukaryotes seem to have a more flexible  $T_{min}$  and have a higher capability to adapt to cold temperatures. The thermal niche width is highly constrained by these linear links, but is not constant. This study supports the hypothesis that thermal adaptation proceeds by horizontal shifts of the thermal growth curve, with possible small fluctuations of its skewness.

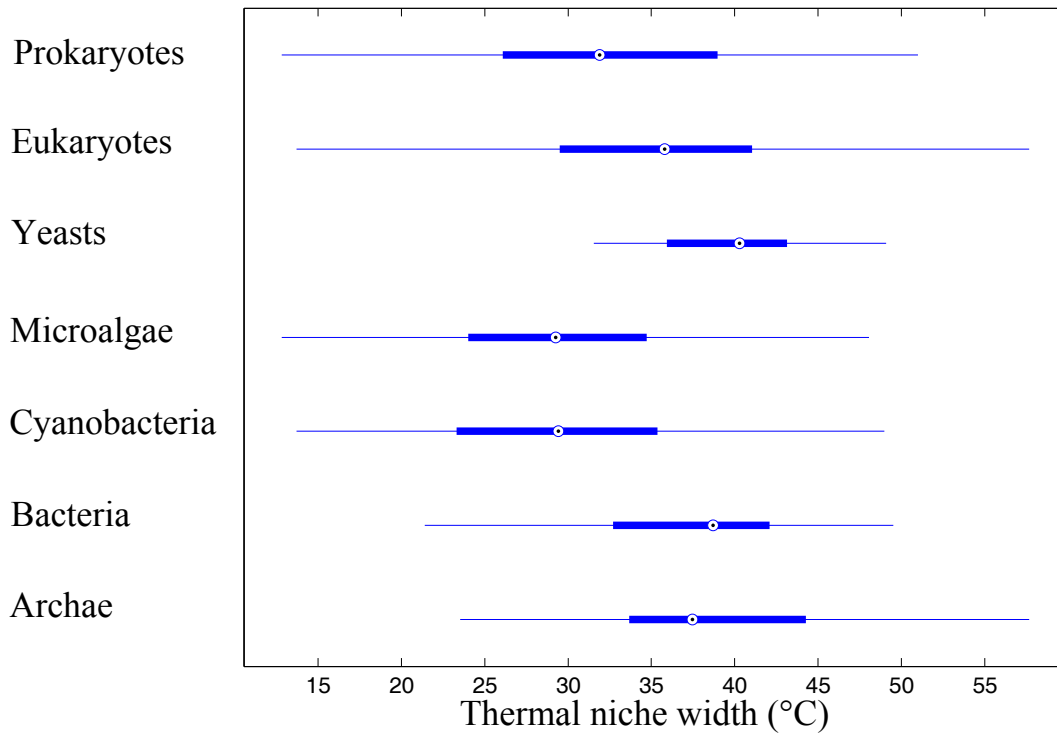


**Figure 4.6: Thermal niche width box plot** - Boxplot of the thermal niche width  $T_{max} - T_{min}$  of the different groups. The bold whiskers correspond to the 25<sup>th</sup> and 75<sup>th</sup> percentiles, the points correspond to the median. The thin whiskers are the 5<sup>th</sup> and 95<sup>th</sup> percentiles.

#### 4. CORRELATION BETWEEN THE CARDINAL TEMPERATURES: INSIGHT INTO THERMAL ADAPTATION

---

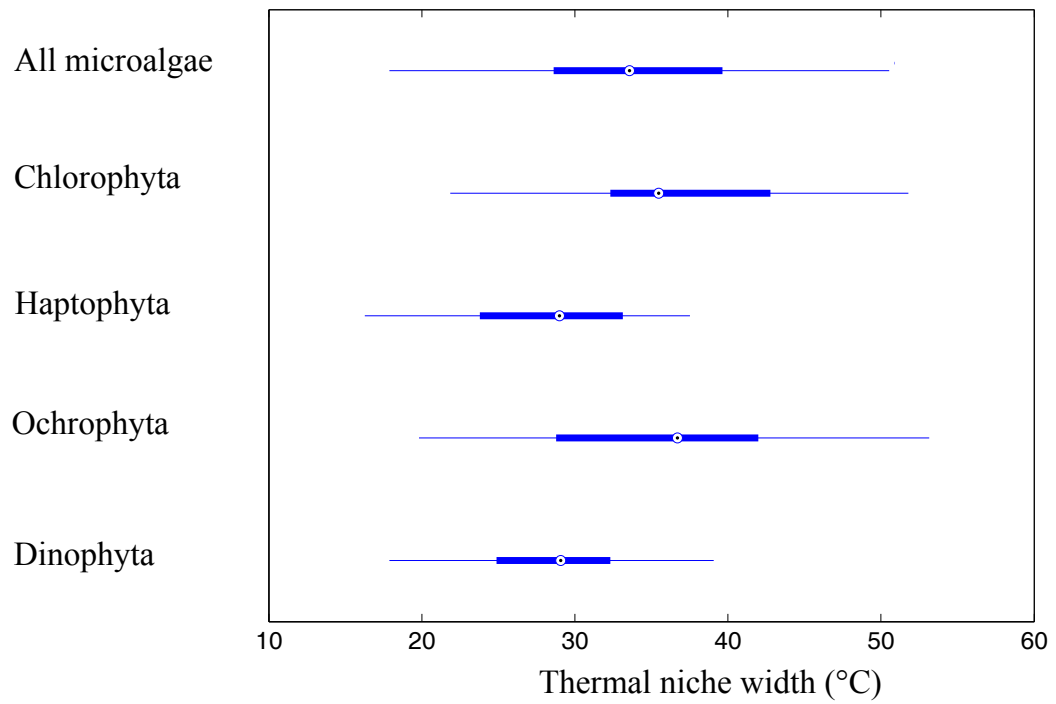


**Figure 4.7: Thermal niche width box plot for Thomas et al. [2015] data set** - Boxplot of the thermal niche width  $T_{max} - T_{min}$  of the different microalgae groups. The bold whiskers correspond to the 25<sup>th</sup> and 75<sup>th</sup> percentiles, the points correspond to the median. The thin whiskers are the 5<sup>th</sup> and 95<sup>th</sup> percentiles.

### Summary of section 4:

- The cardinal temperatures of all UO are linearly linked.
- The relationship between  $T_{min}$  and  $T_{opt}$  is not verified in eukaryotes, which have more adaptive properties at cold temperatures. It is verified in eukaryotic phytoplankton.
- The thermal growth curve may evolve by horizontal shifting, with potential fluctuations of its skewness during adaptation.

#### **4. CORRELATION BETWEEN THE CARDINAL TEMPERATURES: INSIGHT INTO THERMAL ADAPTATION**

---

# 5

## Revisiting the Eppley hypothesis

Contributors: Mairet, F., Sciandra, A., Bernard, O.

*A common fallacy in much of the adverse criticism to which science is subjected today is that it claims certainty, infallibility and complete emotional objectivity. It would be more nearly true to say that it is based on wonder, adventure and hope.*

---

*Sir Norman Hinshelwood*

### 5.1 Introduction

In 1973, Richard Eppley established a relationship between the maximal growth rate of phytoplankton and their living temperature, formalized by an exponential envelop function Eppley [1972]. Since Eppley, the ‘hotter is faster hypothesis’ prevails. Relieved and modelled by Norberg [2004], Eppley’s hypothesis is based on the classical Arrhenius formulation and seduced the scientific community who applied it for every UO. In addition to temperature, the cell biovolume is known to influence the maximal growth rate. In this way, the results obtained by Eppley and since then by many others [Bissinger et al., 2008, Chollet, 2011] highly depend on this link. Despite several works [Brown et al., 2004, Nielsen, 2006, Rose and Caron, 2007, Sal et al., 2015], the clear inter-relation between temperature, biovolume, and maximal growth rate is still unclear.

Here, we challenged Eppley’s hypothesis using only the relation between  $T_{opt}$  and  $\mu_{opt}$  [Bissinger et al., 2008]. We assumed that the maximal measured growth rate is a proxy for  $\mu_{opt}$ . We also normalized the maximal growth rate by the species biovolume. We found that  $\mu_{opt}$  is an increasing function of  $T_{opt}$  until a certain temperature that is



## 5. REVISITING THE EPPLEY HYPOTHESIS

---

group dependent, and thereafter decreases. We then focused on phytoplankton to get further insight into the Eppley hypothesis.

### 5.2 Hotter is not always faster

#### 5.2.1 Describing the relationship between $T_{opt}$ and $\mu_{opt}$ using quantile regression

We compiled the optimal temperature for growth  $T_{opt}$  and the maximal growth rate at  $T_{opt}$  (*i.e.*  $\mu_{opt}$ ), using CTMI model (see section 2.2) for 464 species or strains of UO. We assumed that in non-limited conditions  $\mu_{opt}$  is the maximal growth rate that a species or a strain can reach. However, cultures conditions are rarely perfectly optimized because, for example, growth depends on many different factors. For the same temperature range, the lowest growth rates should not be considered. Therefore, in line with Bissinger et al. [2008], we used quantile regression Koenker and Bassett [1978] to infer relationships between  $T_{opt}$  and  $\mu_{opt}$  from the upper edge of the plot  $\mu_{opt} = f(T_{opt})$  (see section 2.2.6 for a full description of the method used). The quantile regression was calculated on the 99<sup>th</sup> quantile, corresponding to the line below which 99% of the observations are found. The 99<sup>th</sup> quantile was chosen because it is the most reliable way to calculate the edge of the data, with the possibility of calculating interval errors, which would not be possible with the 100<sup>th</sup> quantile [Bissinger et al., 2008]. Unlike Bissinger et al. [2008], we used non-linear quantile regression with third and fourth degree polynomial functions. This choice was motivated by the fact that, as supposed by Eppley [1972], optimal growth rate  $\mu_{opt}$  should increase exponentially with temperature (and thus with  $T_{opt}$ ) until a certain value above which it starts to decrease. Indeed, Eppley [1972] only described the exponential part but hypothesized that such a threshold exists: ‘*There is a gradual and exponential increase of  $\mu$  up to about 40°C. Temperature data above 40°C, obtained with thermophilic, blue-green algae (...) show no further increase in  $\mu$ . (...) Such temperatures are outside the range encountered in the ocean and will not be furthered discussed.*’

Results (fig. 5.1) shows that, indeed, an optimal  $T_{opt}$  equal to 70.6°C and corresponding to  $\mu_{opt} = 2.95\text{h}^{-1}$  seems to exist in UO meaning that hotter is not always faster for all the UO analyzed together. The two polynomial functions fit well the 99<sup>th</sup> quantile, with pseudo- $R^2=0.679$  and pseudo- $R^2=0.748$  respectively. Conversely, if we only take into account data below the optimal  $T_{opt}$ , the function that best describes the link between  $T_{opt}$  and  $\mu_{opt}$  is the exponential function, as described in Eppley [1972] for phytoplankton. It is not possible to find such an increasing trend above the optimal  $T_{opt}$  despite the existence of extreme notorious exceptions in archae not represented here (*e.g.* *Thermococcus celericrescens* growing at 3 h<sup>-1</sup> at 80°C [Kuwabara et al., 2007]).

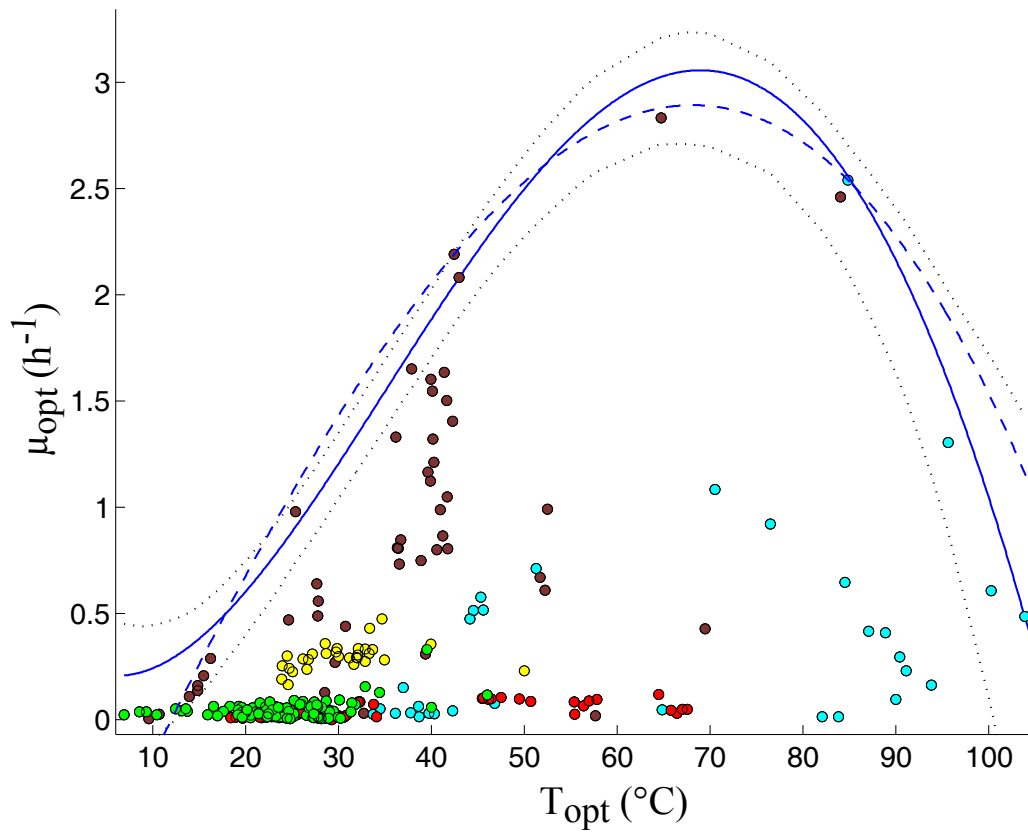


**Figure 5.1:** Maximal growth rate  $\mu_{opt}$  as a function of  $T_{opt} - \mu_{opt}$  plotted against  $T_{opt}$  for the 5 different groups studied (brown, bacteria, green, microalgae, yellow, yeasts, red, cyanobacteria, blue, archae). The bold and dashed blue lines are the 99<sup>th</sup> quantile regression of a fourth and third order polynomial functions respectively, dotted lines are the 95% confidence intervals for the fourth order quantile regression.

## 5. REVISITING THE EPPLEY HYPOTHESIS

**Table 5.1:** Parameters of the fourth order polynomial function  $\mu_{opt}(T) = \sum p_i T^i$  applied to the 5 groups.

Group	p5	p4	p3	p2	p1	Pseudo-R <sup>2</sup>
Archae	3.491.10 <sup>-7</sup>	-1.131.10 <sup>-4</sup>	0.012	-0.462	5.817	0.741
Bacteria	1.277.10 <sup>-6</sup>	-2.205.10 <sup>-4</sup>	0.0127	-0.225	1.589	0.722
Cyanobacteria	2.028.10 <sup>-7</sup>	-3.856.10 <sup>-5</sup>	0.0025	-0.0595	0.5248	0.821
Microalgae	-1.554.10 <sup>-6</sup>	1.750.10 <sup>-4</sup>	-0.0064	0.091	-0.341	0.803
Yeast	-7.318.10 <sup>-6</sup>	0.001	-0.054	1.291	-11.011	0.617
All groups	1.857.10 <sup>-7</sup>	-5.974.10 <sup>-5</sup>	0.0049	-0.075	0.451	0.8003

### 5.2.2 Group specificities

The metabolism efficiency of the different UO considered is probably highly group-dependent, resulting in completely different  $\mu_{opt}$  at least between heterotrophs and autotrophs. We thus divided the data set into the same 5 groups as in section 4.2.2 and calculated the same 99<sup>th</sup> quantile regression. We also calibrated the CTMI model on the 99<sup>th</sup> quantile:

$$\mu_{opt}(T_{opt}) = \phi(T_{opt}) \quad (5.1)$$

with  $\phi(\cdot)$  corresponding to eq. 3.12. Parameters of the CTMI model become:  $T_{opt_{min}}$ ,  $T_{opt_{opt}}$ ,  $T_{opt_{max}}$  the minimal, optimal and maximal  $T_{opt}$  that a given group can reach, and  $\mu_{opt_{opt}}$  the maximal reachable  $\mu_{opt}$ .

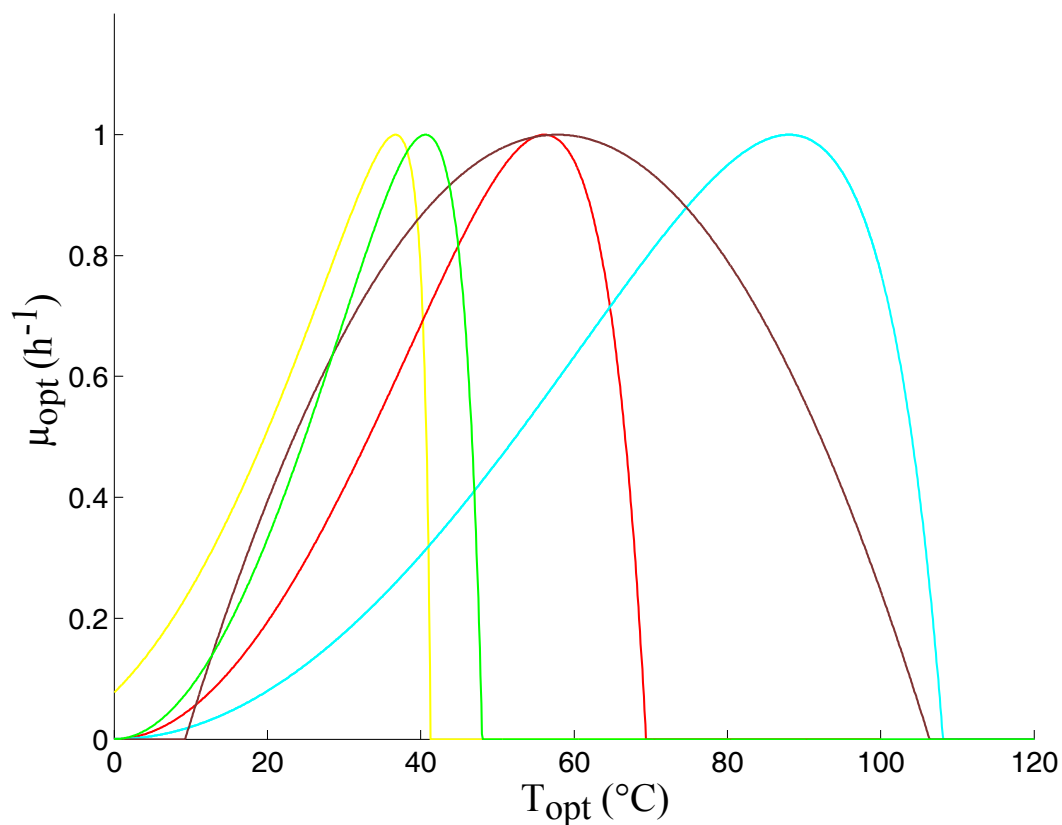
Results (fig. 5.3, table. 5.2 and 5.1) using polynomials functions and CTMI model quantile regressions are different but not contradictory. The repartition of data points is not homogeneous on the thermal range of each group particularly at hotter temperatures, and, as a result,  $T_{max_{opt}}$  parameter is not well estimated. It is worth noting that eukaryotes have a lower  $T_{max_{opt}}$  but also a lower  $T_{min_{opt}}$  than prokaryotes (fig. 5.2). To have a clear comparison between the different group thermal sensitivities, we normalized each group by its maximal growth rate (fig. 5.2). The group succession on the  $T_{opt}$  axis is consistent with Storch et al. [2014], who hypothesized that group thermal sensitivity is related to cell complexity. In this way, archae are more widely tolerant to temperature and especially more resistant to warm than bacteria and then unicellular eukaryotes. Here, we complete this picture by observing the following decreasing thermal tolerance order: archae, bacteria, cyanobacteria, microalgae, yeasts. However, the observed difference between microalgae and yeasts is probably not significant given the lack of points at high temperature for microalgae.

### 5.2.3 Scaling law in the thermal growth curve

The method used in section 5.2.2 is coherent for closely related species. However, for groups as vast and diverse as bacteria, for example, the method is insufficient. It has

**Table 5.2:** Parameters of the CTMI model applied to the 5 groups.

Group	$T_{opt_{min}}$ ( $^{\circ}\text{C}$ )	$T_{opt_{opt}}$ ( $^{\circ}\text{C}$ )	$T_{opt_{max}}$ ( $^{\circ}\text{C}$ )	$\mu_{opt_{opt}}$ ( $\text{h}^{-1}$ )	Pseudo- $R^2$
Archae	1.32	89.4	108.2	1.02	0.572
Bacteria	9.41	57.31	106.42	1.04	0.587
Cyanobacteria	1.21	56.53	69.43	0.101	0.712
Microalgae	0.01	40.61	48.63	0.191	0.736
Yeast	-8.36	36.62	41.34	0.454	0.623

**Figure 5.2:** Normalized thermal envelope of the  $\mu_{opt} = f(T_{opt})$  curve. - Brown: bacteria, green: microalgae, yellow: yeasts, red: cyanobacteria, blue: archae.

## 5. REVISITING THE EPPLEY HYPOTHESIS

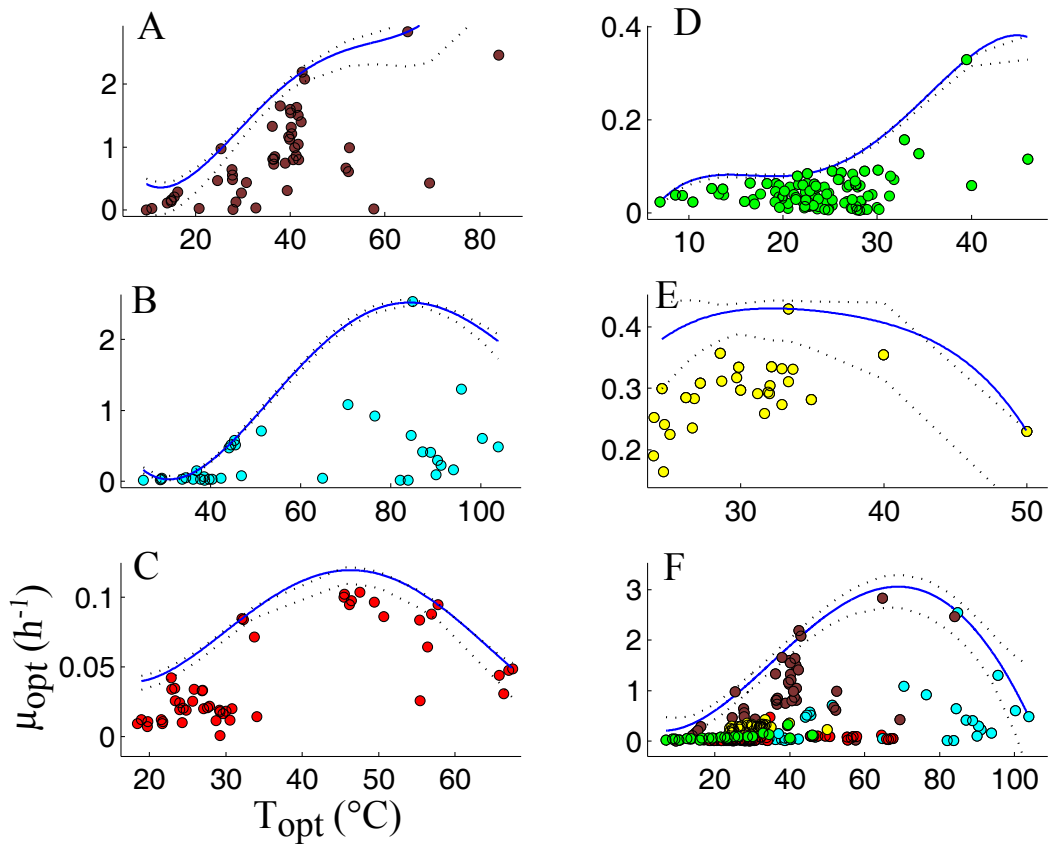
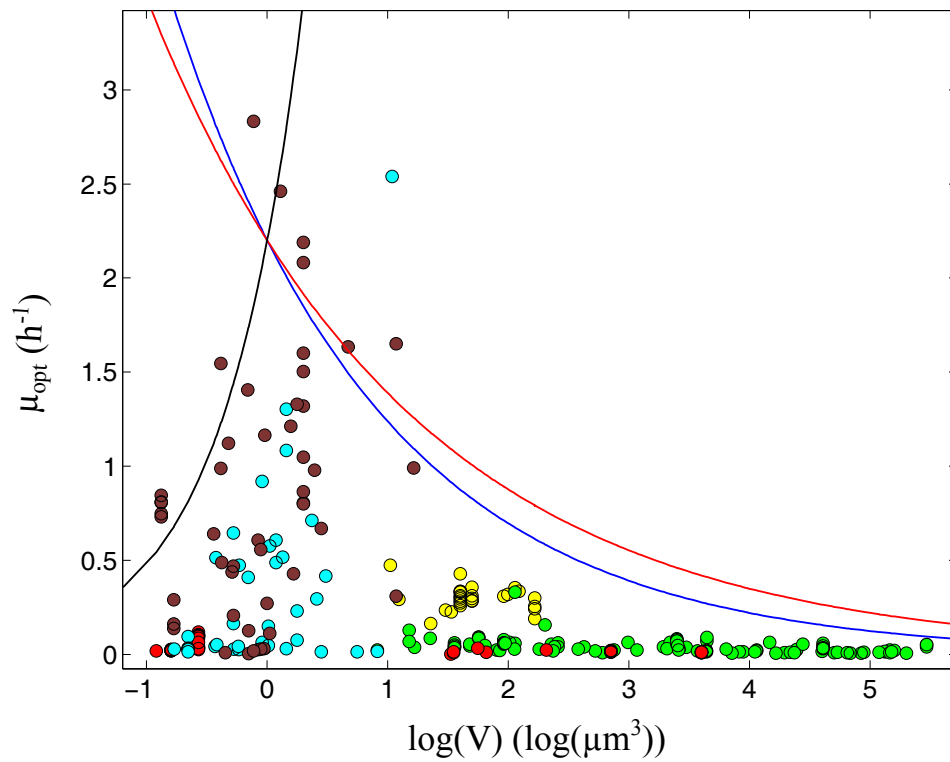


Figure 5.3: Maximal growth rate  $\mu_{opt}$  as a function of  $T_{opt}$  and 99th quantile regression with fourth degrees polynomial for the 5 groups - A, bacteria, B, archae, C, cyanobacteria, D, microalgae, E, yeasts, F, all species.



**Figure 5.4:** Log of cell biovolume  $V$  as a function of  $\mu_{opt}$  - brown, bacteria, green, microalgae, yellow, yeasts, red, cyanobacteria, blue, archae. The blue, red and black lines correspond to eq. 5.2 with  $a_0 = 2.2$  and  $\alpha = -1./4$ ,  $\alpha = -0.2$  and  $\alpha = 0.66$  respectively.

## 5. REVISITING THE EPPLEY HYPOTHESIS

---

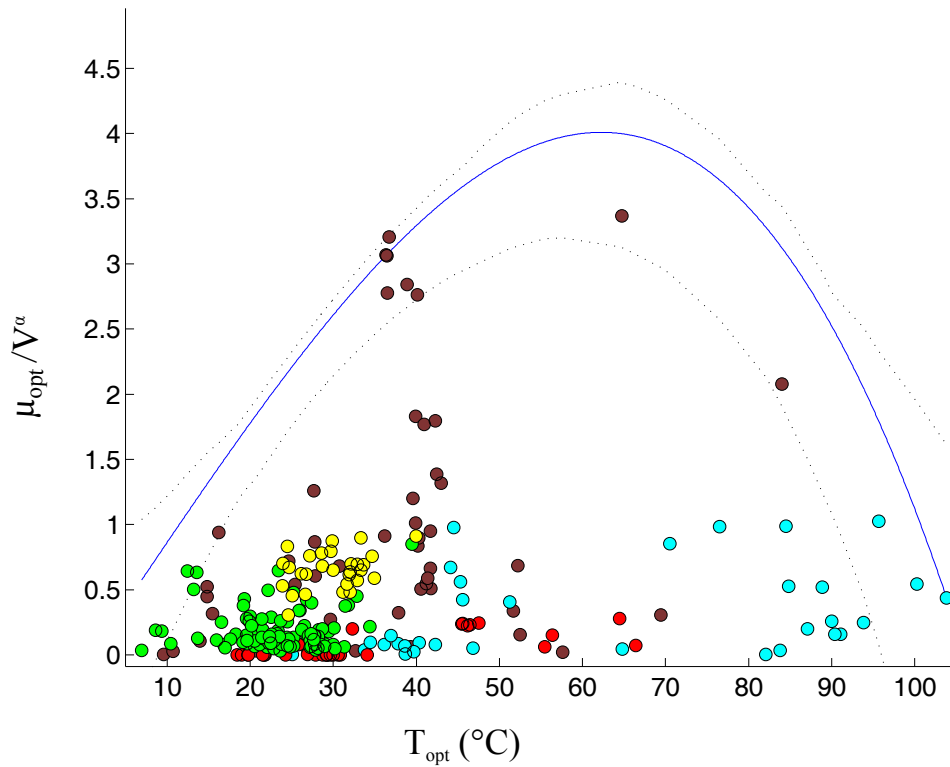


**Figure 5.5:** Maximal growth rate biovolume-adjusted  $\mu_{opt}/V^\alpha$  as a function of  $T_{opt}$  and third polynomial 99th quantile regression for the whole data set - Brown, bacteria, green, microalgae, yellow, yeasts, red, cyanobacteria, blue, archae. The blue line corresponds to the quantile regression.  $\alpha = 0.66$  for prokaryotes and  $\alpha = -0.2$  for eukaryotes.

been shown, indeed, that cell size is strongly related to the maximal growth rate for every UO Brown et al. [2004], Gillooly et al. [2001b], Johnson et al. [2009], Kempes et al. [2012]. This is well summarized by Niklas [2015]: ‘*This aspect of cell growth is treated here in light of studies showing that cell growth, metabolism, and division rates decrease across (and often within) species as cell size increases [...] Explanations for these inverse relationships differ among investigators, but considerations typically involve the size-dependent (scaling) relationships among cell surface area, volume, and dry mass (as measured by carbon or DNA content). The relationship between cell surface area and volume (and its effect on cell growth rates and division rates) has received the most attention because of the dictum that growth requires energy and, regardless of the form of energy garnered by a cell (radiant energy in plants; chemical energy in fungi and animals), the ability to harvest energy is some function of external surface area, whereas the metabolic requirement for energy is some function of volume*’. Various authors have claimed that the following relationship exists between the maximal growth rate and the dry mass or biovolume of any given UO [Banse, 1982, Brown et al., 2004, Gillooly et al., 2001b, Kleiber et al., 1947]:

$$\mu_{opt} = a_0 V^\alpha \quad (5.2)$$

where  $V$  is the biovolume or the dry mass,  $a_0$  is a scaling parameter and  $\alpha = -1/4$ . Eq. 5.2, called the ‘Keibler 3/4 power law’, states that ‘smaller is better’. There is a current debate around the value of  $\alpha$  for UO. DeLong et al. [2010] found that  $\alpha = 0.66$  for prokaryotes and  $\alpha = -0.2$  for unicellular eukaryotes, arguing that prokaryotes metabolic rate is limited by the number of genes whereas unicellular eukaryotes are limited by the number of respiratory complexes (fig. 5.4). Kempes et al. [2012] and Johnson et al. [2009], on the other way, point towards the intra and inter-specific variability of  $\alpha$ , especially for microalgae.

The Keibler power law, as well as the  $\alpha$  values proposed by DeLong et al. [2010] are coherent with the result obtained with our database (fig. 5.4). However, the relation between  $V$  and  $\mu_{opt}$  is not obvious. As explained by Gillooly et al. [2001b] and in section 5.2,  $\mu_{opt}$  critically depends on temperature. To obtain a relation between the biovolume and the maximal growth rate *ceteris paribus*,  $\mu_{opt}$  has to be ‘temperature compensated’. Indeed, Gillooly et al. [2001b] considered the following equation:

$$\mu_{opt} = a_0 V^\alpha f(T_{opt}) \quad (5.3)$$

where  $f(T_{opt})$  is a classical Arrhenius equation of the form  $e^{-E/(RT_{opt})}$ . Then, by taking the natural logarithm of eq. 5.3, it is possible to obtain a ‘biovolume-corrected’ or a ‘temperature-corrected’ expression of the maximal growth rate. However, motivated by fig. 5.3, we claim here that  $f(T_{opt})$  is not a simple Arrhenius equation, and rather:

$$\mu_{opt} = a_0 V^\alpha \left( e^{-E1/(RT_{opt})} - e^{-E2/(RT_{opt})} \right) \quad (5.4)$$

where  $f(T_{opt})$  corresponds to an Hinshelwood equation. To obtain an approximation of  $f(T_{opt})$ , we divided the experimental maximal growth rates by  $V^\alpha$ , with  $\alpha = 0.66$  for prokaryotes and  $\alpha = -0.2$  for eukaryotes, in line with DeLong et al. [2010]. The result,



## 5. REVISITING THE EPPLEY HYPOTHESIS

---

presented in fig. 5.5, tends to validate eq. 5.4. However, since there is no clear consensus on the value of  $\alpha$ , fig. 5.5 has to be analyzed carefully. An experimental way to get further insight into  $f(T_{opt})$  would be to analyse the maximal growth rate of different set of species with the same  $T_{opt}$  or with the same biovolume (see section 5.3.2).

### 5.3 The phytoplankton paradigm

#### 5.3.1 The revisited Eppley curve for phytoplankton

Since the work of Eppley [1972], the exponential Eppley curve setting that ‘hotter is better’ for phytoplankton species living in the ocean *volens nolens* has been massively used, especially for marine biogeochemical models using the formulation proposed by Norberg [2004]. Some works have challenged the validity of this hypothesis, claiming for example that *in situ* phytoplankton growth rates are often underestimated because of the Eppley curve [Bissinger et al., 2008, Brush et al., 2002]. Chollet [2011], for example, showed that despite a clear exponential trend at low temperature, the link between  $T_{opt}$  and  $\mu_{opt}$  differs from that of an Eppley curve for diatoms.

Here, we focused on the result found for microalgae in section 5.2.2 by adding the Thomas et al. [2015] database to our, filtered with the same criteria. We also included the eukaryote extremophile *Cyanidinium caldarium* owing an optimal growth rate at 45°C [Doemel and Brock, 1971]. We applied the same 99<sup>th</sup> quantile regression as in section 5.2.2 with a third polynomial function and the CTMI model. Results (fig. 5.6) suggest that there exists an intrinsic thermal limit for  $T_{opt}$  (comprised between 4.7°C and 47.3°C), proper to microalgae, and that the maximal growth rate is highly constrained by this limit, following the shape of a single species thermal growth curve. We will refer as it as the ‘modified Eppley curve’ all along the manuscript.

This result is highly variable between microalgae groups. We thus split microalgae into the four phylogenetic groups Dinophyta, Ochrophyta, Haptophyta, Chlorophyta and applied again the same method. Fig. 5.7 shows that Chlorophyta is the most thermotolerant group, whereas Haptophyta and Dinophyta are the less ones. Data are probably lacking for Haptophyta, however. The maximal optimal growth rate is also widely different between groups, probably emphasizing different intrinsic physiological limits and photosynthesis yields [Raven et al., 2013].

These groups differences may also be the result of the influence of cell biovolume on maximal growth rates, as seen in section 5.2.3. Marañón et al. [2014], for example, claim that the maximal growth rate of microalgae expressed a function of the biovolume follows an unimodal function. Nevertheless, Marañón et al. [2014] did not take into account the optimal temperature of growth nor thermally compensated their growth data, and their results are in contradiction with Sal et al. [2015]. However, we did not have the biovolume information for the Thomas et al. [2015] database and could not further investigate the question.

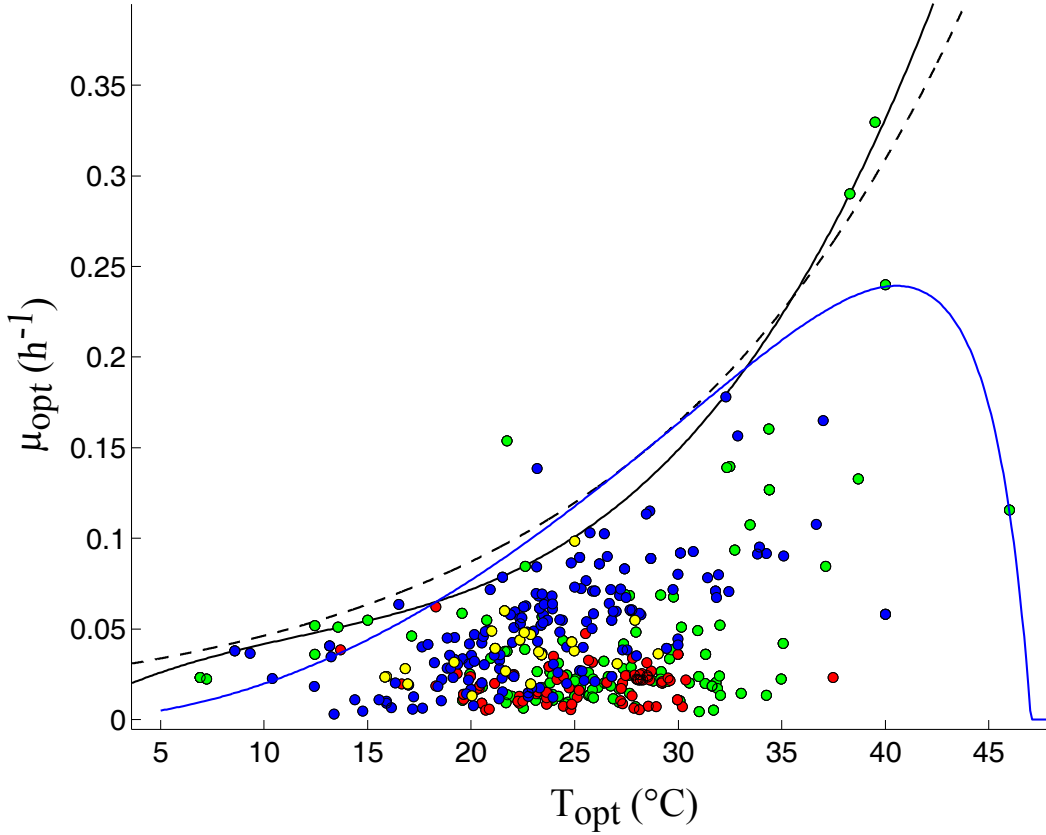


**Figure 5.6:** Maximal growth rate  $\mu_{opt}$  as a function of  $T_{opt}$  and 99th quantile regression for 4 microalgae subgroups - Red, Dinophyceae, blue, Ochrophyta (diatoms), yellow, Haptophyceae, green, Chlorophyceae. The dashed line corresponds to the Eppley curve, the bold line to a third order polynomial function and the blue line to the CTMI model.

**Table 5.3:** Parameters of the CTMI model applied to microalgae groups.

Group	$T_{opt_{min}}$ (°C)	$T_{opt_{opt}}$ (°C)	$T_{opt_{max}}$ (°C)	$\mu_{opt_{opt}}$ (h <sup>-1</sup> )
Dinophyta	8.43	32.34	39.23	0.049
Ochrophyta	4.81	34.43	41.22	0.145
Haptophyta	11.23	25.81	29.72	0.075
Chlorophyta	10.34	42.91	46.63	0.274
Microalgae (with Thomas et al. [2015])	4.7	39.2	47.3	0.248

## 5. REVISITING THE EPPLEY HYPOTHESIS

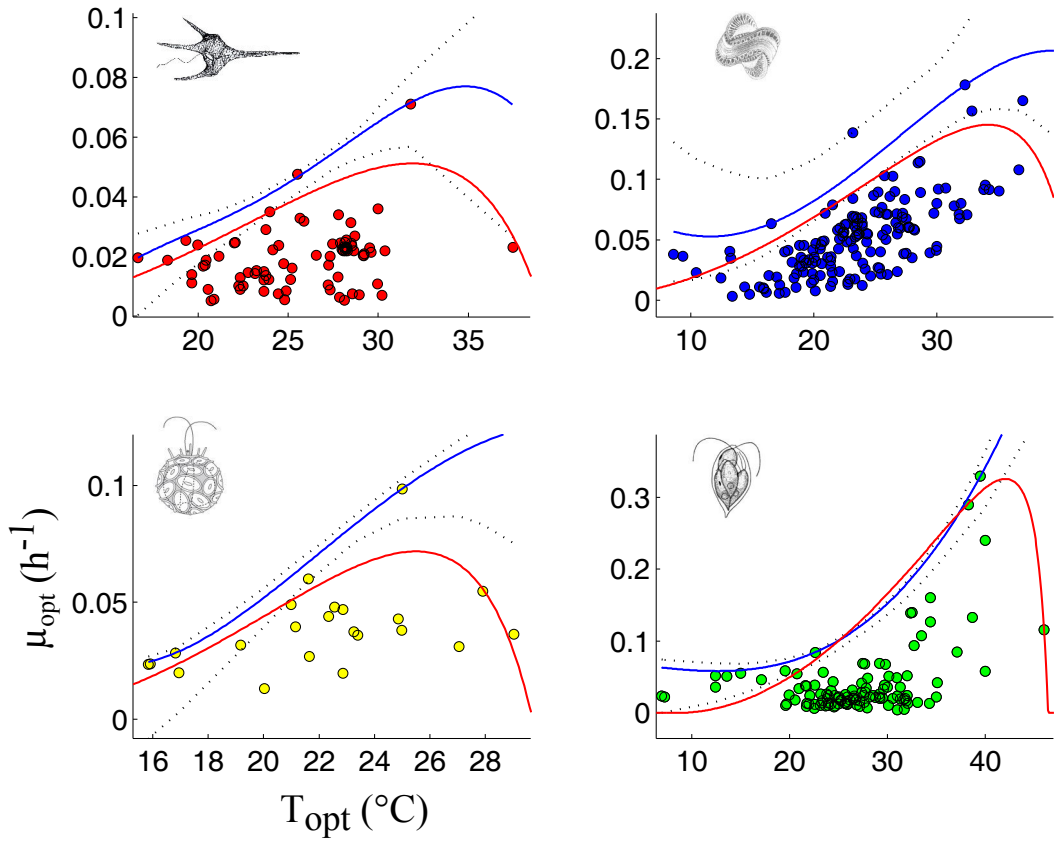


**Figure 5.7:** Maximal growth rate  $\mu_{opt}$  as a function of  $T_{opt}$ , 99th quantile regression and CTMI model calibration for 4 microalgae subgroups - Red, Dinophyta, blue, Ochrophyta (diatoms), yellow, Haptophyta, green, Chlorophyta. The red and blue lines represent the quantile regression and the CTMI model, respectively.

### 5.3.2 A case study: the cyanobacteria *Synechococcus* sp.

Among the unicellular photosynthetic organisms, *Synechococcus* sp. have been particularly studied, especially for its huge capacity to tolerate a wide range of temperature. Some *Synechococcus* sp. strains are for example capable to live above 70°C. In 2000, Miller and Castenholz [2000] analysed the thermal growth curve of several *Synechococcus* sp. strains growing from 25°C to 70°C, and deduced from phylogenetic considerations that these strains evolved from a less thermotolerant ancestor. The same team identified four amino acid substitutions that together increased stability and activity of Calvin cycle enzyme ribulose-1, 5-bisphosphate carboxylase/oxygenase (RuBisCO) at higher temperatures in high temperature adapted strains [Miller et al., 2013, Miller, 2003]. Miller's results highlight the crucial role played by RuBisCO during thermal adaptation.

Later, Pittera et al. [2014] identified several *Synechococcus* sp. thermal ecotypes in the ocean and studied their thermal growth curve. Here, by compiling Pittera et al. [2014] and Miller and Castenholz [2000] data, we show that not only the *Synechococcus* sp. strains have evolved by shifts of the thermal growth curve with conservation of the thermal niche width (see for example fig. 1.8), but also followed a modified Eppley curve for the link between  $\mu_{opt}$  and  $T_{opt}$  (fig. 5.8). At low and high temperatures, strains are less efficient. Since the biovolume is not affected between the different strains, this observation argues towards a clear existence of the modified Eppley hypothesis, as formulated in eq. 5.4.

These results pose different challenging questions: is the RuBisCO enzyme driving the thermal evolution in cyanobacteria and causing the efficiency loss at low and high temperatures? Are these mechanisms also driving adaptation in microalgae? Several studies exist on the effect of temperature on RuBisCO [Galmes et al., 2015] and are a promising trail for unraveling the modified Eppley curve.

## 5.4 Conclusion

We have shown that, contrary to the commonly accepted Eppley hypothesis, 'hotter is not always faster'. Each phylogenetic group might have its own modified Eppley curve, following the exact shape of a single species thermal growth curve. It is, indeed, rather surprising that the modified Eppley curve follows the shape of a CTMI or an Hinshelwood function; further investigations are needed to clarify this fact. In addition to temperature, cell biovolume has a great influence on the maximal growth rate  $\mu_{opt}$ , and it is not easy to separate between these two factors. Following the Gillooly et al. [2001b] expression and the Keibler power law, we showed that the pure effect of temperature on the maximal growth rate is an Hinshelwood-like function rather than an Arrhenius (and thus Eppley) exponential one, confirming our modified Eppley hypothesis.

We then compared our results to the unicellular photosynthetic group, emphasizing the intrinsic thermal limits of microalgae. We highlighted the great sub-groups differences among microalgae. We then showed that the Cyanobacteria *Synechococcus* sp. well follows the rules developed in chapter 4 and in this chapter, and linked it to the

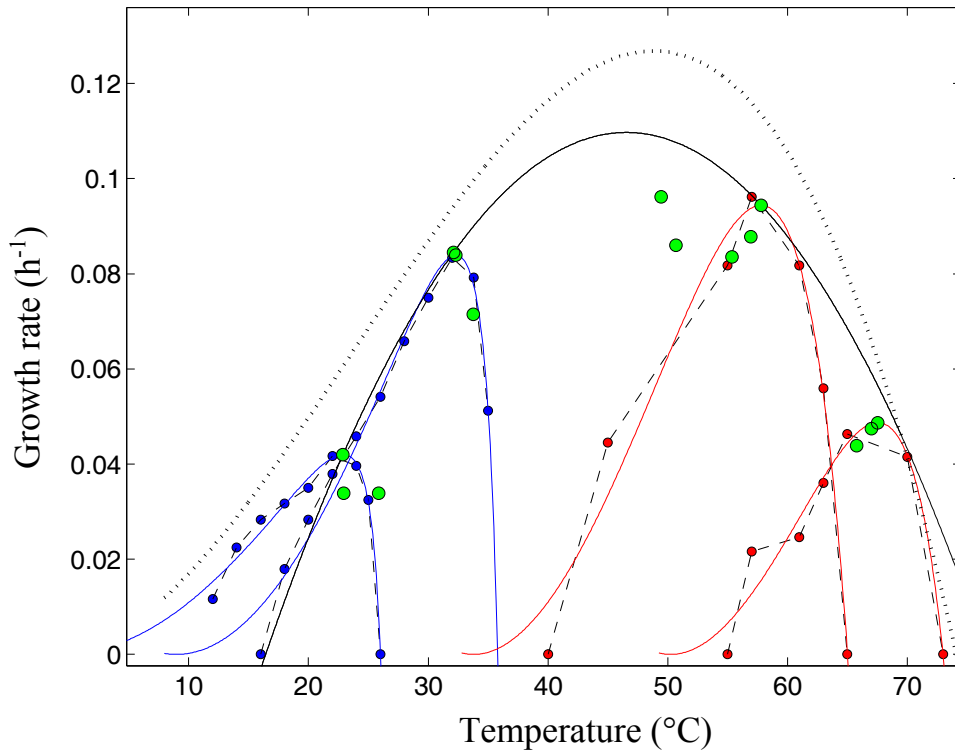


**Figure 5.8: Thermal growth curve of *Synechococcus* sp. strains.** - Growth rate as a function of temperature for different thermal ecotypes of *Synechococcus* sp. In blue, data from two chosen species from Pittera et al. [2014], in red, data from two selected species from Miller and Castenholz [2000]. The green points correspond to  $\mu_{opt}$  as a function of  $T_{opt}$  for the species described in Miller and Castenholz [2000] and Pittera et al. [2014]. The dashed curve corresponds to the theoretical third order polynomial function linking  $\mu_{opt}$  to  $T_{opt}$  described in section 5.2.3. The bold curve corresponds to the second order polynomial function.

thermal sensitivity of the key enzyme RuBisCO.

## 5. REVISITING THE EPPLEY HYPOTHESIS

---

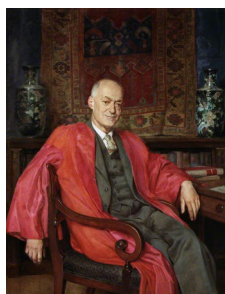
### Summary of section 5:

- ‘Hotter is not always faster’.
- The Eppley curve is group-specific and has to take into account the decrease at hot temperatures.
- Cell biovolume plays a key role in  $\mu_{opt}$  and has to be taken into account to obtain the ‘normalized’ thermal effect.
- Phytoplankton paradigm has to be reconsidered; there exists strong group specificities in the Eppley hypothesis, that we call the ‘modified Eppley hypothesis’.
- This theory is particularly well illustrated with different strains of *Synechococcus* sp.

## 6

# Towards understanding the thermodynamical fundament of the thermal growth curve: a modelling approach

Contributors: Bernard, O., Mairet, F., Sciandra, A.



The English physical chemist Sir Cyril Norman Hinshelwood.

### 6.1 Introduction

In chapter 4 and 5, we have shown that a linear correlation between the cardinal temperatures as well as a specific relationship between  $T_{opt}$  and  $\mu_{opt}$  exist. How to explain these links? To get insight into the mechanisms underlying the thermal growth curve, we developed here a mechanistic model which can be simplified to obtain the Hinshelwood model. We calibrated the Hinshelwood model on the data set used in the



## 6. TOWARDS UNDERSTANDING THE THERMODYNAMICAL FUNDAMENT OF THE THERMAL GROWTH CURVE: A MODELLING APPROACH

---

previous chapters and search for possible links between its parameters. It appears that the entropy-enthalpy compensation during enzyme thermal denaturation as well as the enzyme thermal activity-stability trade-off could play a key role to explain the observed parametric correlations. A simplified model with only two parameters is derived based on these concepts.

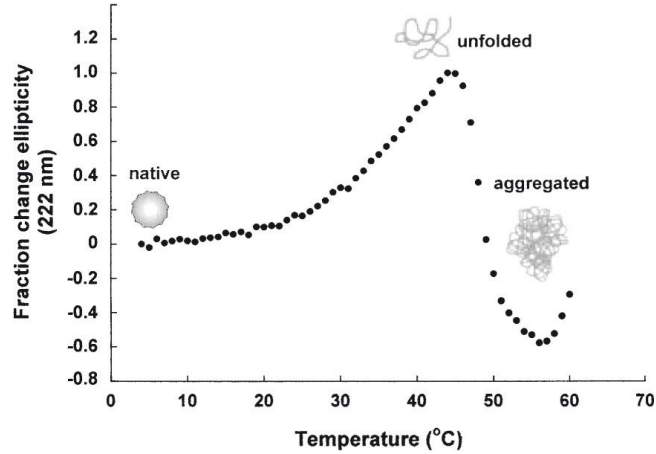


**Figure 6.1:** Thermostability of *Escherichia coli* homoserine transsuccinylase - Unfolding starts at low temperatures, around 20°C. Reproduced after Julou [2011].

## 6.2 The Hinshelwood model as a theoretical framework

### 6.2.1 Metabolism represented as a set of $n$ autocatalytic reactions

In line with Iyer-Biswas et al. [2014], and as first proposed by Hinshelwood [1952], we considered that exponential growth is the result of an autocatalytic cycle of  $n$  reactions where each enzyme  $x_i$  catalyzes the production of the next at a rate  $k_i$ . Moreover, each enzyme denatures or is inactivated at a rate  $d_i$  (illustrated in fig. 6.1). Considering the temperature effect on production and inactivation, the resulting model is:

$$\begin{aligned}
 \dot{x}_1 &= k_1(T)x_n - d_1(T)x_1 \\
 \dot{x}_2 &= k_2(T)x_1 - d_2(T)x_2 \\
 &\vdots \\
 \dot{x}_n &= k_n(T)x_{n-1} - d_n(T)x_n
 \end{aligned} \tag{6.1}$$

where the biomass concentration  $X$  is proportional to the sum of all the  $x_i$  enzymes. Under non-limited conditions, the growth rate  $\mu(T)$  defining the thermal growth curve

## 6.2 The Hinshelwood model as a theoretical framework

---

is:

$$\mu(T) = \frac{\sum_{i=1}^n \dot{x}_i}{\sum_{i=1}^n x_i} \quad (6.2)$$

However, equation (6.2) depends on each enzyme dynamics as they appear in equations (6.1). We approximated these equations in order to propose a simpler expression for  $\mu(T)$ , as proposed by Koch [1970] who used the operator method to compute the growth rate  $\mu$  in a similar but two dimensional autocatalytic system. Assuming that the rates  $d_i$  are significantly lower than the growth rate, we extended the two dimensional Koch [1970] approach, and we deduced the overall growth rate  $\mu(T)$  (see demonstration in section 10.3):

$$\mu(T) = [k_1(T) \dots k_n(T)]^{1/n} - \frac{1}{n} \sum_{i=1}^n d_i(T) \quad (6.3)$$

Each synthesis step is supposed to vary according to an Eyring equation as established by the transition-state theory (see section 3.8), but it can be approximated by using an Arrhenius term. It follows from eq.6.3:

$$\mu(T) = (A_1 \dots A_n)^{1/n} e^{-(E_1 + \dots + E_n)/(RT)} - \frac{1}{n} \sum_{i=1}^n d_i(T) \quad (6.4)$$

where the terms  $A_i$  correspond to the entropy of activation  $e^{\Delta S_i^\ddagger/R}$  and  $E_i$  to the enthalpy of activation  $\Delta H_i^\ddagger$ . We assumed that the rates  $d_i(T)$  correspond to reversible unfolding leading to denaturation with a two state transition (see section 3.8). This assumption has been validated experimentally for globular proteins with more than 100 amino-acids [Feller et al., 1999, Siddiqui and Cavicchioli, 2006]. Then:

$$d_i(T) = e^{-\Delta G_i^\ddagger/(RT)} \quad (6.5)$$

where  $\Delta G_i^\ddagger$  is the activation energy for unfolding. Because of the two state transition,  $\Delta G_i^\ddagger$  does not depend on the temperature  $T$ . Finally:

$$\mu(T) = A e^{-E/(RT)} - \frac{1}{n} \sum_{i=1}^n e^{-\Delta G_i^\ddagger/(RT)} \quad (6.6)$$

with  $A = (A_1 \dots A_n)^{1/n}$  and  $E = \sum_{i=1}^n E_i$ . Because  $e^{-\Delta G_i^\ddagger/(RT)}$  is equal to  $e^{\Delta S_i^\ddagger/R} e^{-\Delta H_i^\ddagger/(RT)}$

which can be written  $\tilde{A}_i e^{-\tilde{E}_i/(RT)}$ , eq.6.6 is similar to the Hinshelwood model (see section 3.2.4) with thermodynamical meanings of the model parameters:

$$\mu(T) = A e^{-E/(RT)} - \langle A_d e^{-E_d/(RT)} \rangle \quad (6.7)$$

where  $\langle . \rangle$  is the arithmetic mean. An important point is that the degradation term in the Hinshelwood model appears here to be related to the average of the denaturation

## 6. TOWARDS UNDERSTANDING THE THERMODYNAMICAL FUNDAMENT OF THE THERMAL GROWTH CURVE: A MODELLING APPROACH

---

of all the enzymes. This approach can be compared to other mechanistic models such as those developed by Corkrey et al. [2014] or Dill et al. [2011] based on the role played by the whole proteome. This formulation seems to invalidate the hypothesis of a single or few limiting enzymes and highlights the cell potential to soften degradation of key components through the auto-catalytic interactions of the whole proteome. This is also a key strategy for adaptation.

The maximal and optimal temperatures predicted by the Hinshelwood model can be derived after simple mathematical computations. The minimal temperature is defined as the temperature for which the growth rate is below  $\epsilon$  ( $\epsilon$  is an arbitrary small number, we took  $\epsilon = 0.05$ ). The cardinal temperatures can then be derived from the Hinshelwood parameters. Simple computations provide the functional link between the cardinal temperatures and the Hinshelwood parameters. (see section 3). Therefore, the Hinshelwood model relates the cardinal temperatures and the maximal growth rate to parameters derived from thermodynamical considerations. For sake of simplicity, in the following, the Hinshelwood parameters are written according to eq. 3.22.

### 6.2.2 Data normalization and calibration of the Hinshelwood model

In chapter 5, we studied the relationship between  $T_{opt}$  and  $\mu_{opt}$  for different phylogenetic groups. However, our data set surely contains many experiments where the optimal growth rate has not been reached. Indeed, especially for phytoplankton, experiments are often carried out far from the optimal growth conditions (for example when light is not saturating). We therefore normalized the growth rate by the estimate of the optimal growth rate as computed from eq. 5.1, on the basis of the knowledge of parameter  $T_{opt}$ . Once the data set has been normalized, we calibrated the Hinshelwood model using the method described in section 2. Typical model fit is shown in Fig. 3.1. The fit turns out to be of equal quality than the CTMI model. Now we explore and explain the correlations between the thermodynamically based Hinshelwood parameters.

## 6.3 Accounting for the enthalpy-entropy compensation

### 6.3.1 Theoretical approach

The negative term in the Hinshelwood model (function  $f_2(T)$ ; see eq. 3.22), can be interpreted as representing the unfolding reaction. The enthalpy  $\Delta H$  and the entropy  $\Delta S$  of the reaction corresponding respectively to  $E_2$  and  $R\ln(A_2)$  are known to compensate each others according to eq.6.8, where  $1/(aR)$  is the compensation temperature at which every unfolding reactions have the same rate  $e^b$ .

$$\ln(A_2) = aE_2 + b \quad (6.8)$$

Eq. 6.8 is called ‘enthalpy-entropy compensation’ (EEC) [Liu and Guoa, 2001, Rosenberg et al., 1971]. EEC has been observed for proteins denaturation but also for a wide range of organisms at their upper temperature limits, from virus to bacteria and even

## 6.4 Accounting for the activity-stability trade-off

drosophila [Bischof and He, 2005, Liu et al., 2000, Qin et al., 2014, Rosenberg et al., 1971]. EEC seems to be a universal characteristic, but has been widely debated due to experimental errors that could possibly lead to artificial EEC [Banks et al., 1972, Harris, 1973]. Moreover, some intrinsic correlations between Arrhenius function parameters are suspected. The current view is that EEC is a real phenomenon in protein denaturation and unfolding, but protein unfolding data analysis have to be carried out carefully on a sufficiently large range of activation enthalpy (*e.g.* from  $10^4\text{J/mol}$  to  $10^6\text{J/mol}$ ) to be significant [Bischof and He, 2005, Liu et al., 2000]. The reason for such a compensation is possibly related to water reorganization during protein denaturation which contributes to enthalpy and entropy but little to free energy [Liu et al., 2000].

### 6.3.2 Calibration

The parameters  $a$  and  $b$  were calibrated using the estimated values of  $A_2$  and  $E_2$  (see fig. 6.2). Different authors, for example Rosenberg et al. [1971] and Qin et al. [2014], found similar values of  $a$  and  $b$ , *i.e.*  $a = 0.00038 \text{ mol}\cdot\text{J}^{-1}$ ,  $b = -9.36$ , with the compensation temperature equal to 316.52 K. We found close values with  $a = 0.0003844 \text{ mol}\cdot\text{J}^{-1}$  and  $b = -0.427$ . We thus considered that  $a$  and  $b$  could be universal, and we replaced  $A_2$  by eq. 6.8 in the Hinshelwood model to take EEC into account. It results that EEC highly constrains  $f_2(T)$  because a high change of enthalpy is compensated by a high change of entropy and a resulting small change of free energy.

## 6.4 Accounting for the activity-stability trade-off

### 6.4.1 Theoretical approach

The activity of an enzyme is described by its maximum number of substrates converted to products per active site and per unit of time. During *in vitro* thermal adaptation, the thermal stability of enzymes is modified to fit the new thermal environment, and, in turn, the enzyme activity on the thermal range is modified. It has been shown that a trade-off exists between stability and activity at low temperature [Arnold et al., 2001, Couñago et al., 2008, Howell et al., 2014]. This effect directly results from the trade-off between rigidity, which confers thermal resistance but low activity at low temperature, and fluidity, which confers the exact opposite [Karshikoff et al., 2015, Siddiqui and Cavicchioli, 2006, Zavodszky et al., 1998]. In the Hinshelwood model, this would be expressed by a link between the synthesis function  $f_1(T)$ , which corresponds to enzyme activity according to eq. 6.6, and the unfolding function  $f_2(T)$  which represents enzyme thermal stability.

After taking EEC into account, it turns out that the enthalpy ratio  $E_1/E_2$  increases with the maximum temperature at which the organism is adapted. We interpreted it as a result of activity-stability trade-off. To express this relation properly, we assumed that  $E_1$  is zero when  $T_{max}$  is near the compensation temperature. By definition, parameter  $E_2$  is higher than  $E_1$ , but both converge at high temperature. We proposed a simple

## 6. TOWARDS UNDERSTANDING THE THERMODYNAMICAL FUNDAMENT OF THE THERMAL GROWTH CURVE: A MODELLING APPROACH

---

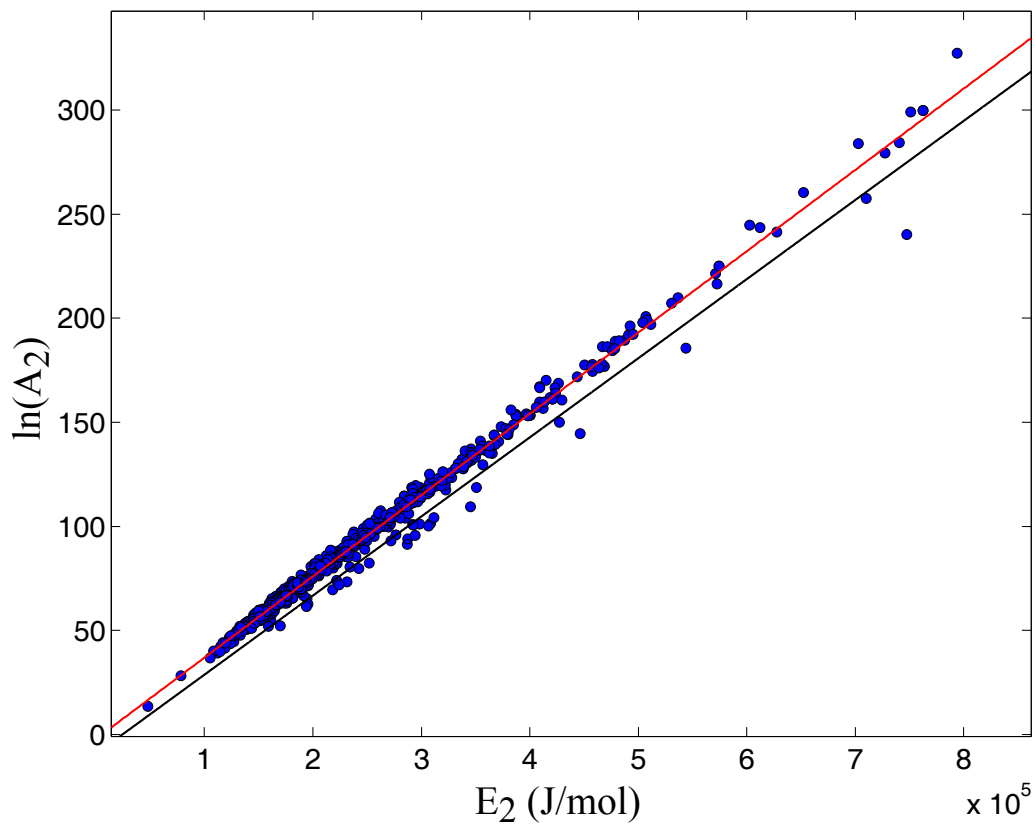


**Figure 6.2: Log-linear relation between  $A_2$  and  $E_2$**  - Log-linear plot with  $\ln(A_2)$  as a function of  $E_2$ . The log-linear regression appears in red. The black line corresponds to the log-linear regression found by Rosenberg et al. [1971].

## 6.5 The two parameters Hinshelwood model

**Table 6.1:** Parameters of the activity/stability trade-off function

Group	$T_s$ (K)	$T_c$ (K)
Archae and Bacteria	326.668	311.938
Cyanobacteria	310.547	300.142
Yeast	315.079	312.842
Dinophyta	309.452	307.135
Ochrophyta	320.175	301.254
Haptophyta	304.342	302.145
Chlorophyta	313.218	302.341

Michaelis-Menten type equation to represent the enthalpy ratio:

$$E_1/E_2 = \frac{T_{max} - T_o}{T_{max} - 2T_o + T_s} \quad (6.9)$$

This non-linear relation includes parameter  $T_s$  (see fig. 6.3), for which  $E_2 = 2E_1$  and  $T_o$ , which is supposed to be close to the compensation temperature.

### 6.4.2 Calibration

Relationship 6.9 was tested and calibrated on different groups with the set of available data. It turns out that this relationship is satisfied, with values specific to each group (see table 6.1). Archae and bacteria were grouped together because the results obtained were very close.

## 6.5 The two parameters Hinshelwood model

### 6.5.1 Reducing the parameter number of the Hinshelwood model down to 2

We introduced eq. 6.9 and eq. 6.8 in eq. 3.22 to reduce the Hinshelwood model to two parameters,  $A_1$  and  $E_2$  (we will refer at it as the 2P-Hinshelwood model). Parameters  $E_1$  and  $A_2$  are derived as follows:

$$E_1(E_2) = \frac{T_{max} - T_o}{T_{max} - 2T_o + T_s} E_2 \quad (6.10)$$

and

$$A_2(E_2) = A_c e^{E_2/(RT_c)} \quad (6.11)$$

with  $A_c = e^b$ . Moreover, it is possible to express  $A_1$  as a function of  $T_{max}$  and  $E_2$ :

$$A_1 = f(T_{max}, E_2) = A_c e^{E_2/(RT_c)} e^{(E_1(E_2) - E_2)/(RT_{max})} \quad (6.12)$$

## 6. TOWARDS UNDERSTANDING THE THERMODYNAMICAL FUNDAMENT OF THE THERMAL GROWTH CURVE: A MODELLING APPROACH

---

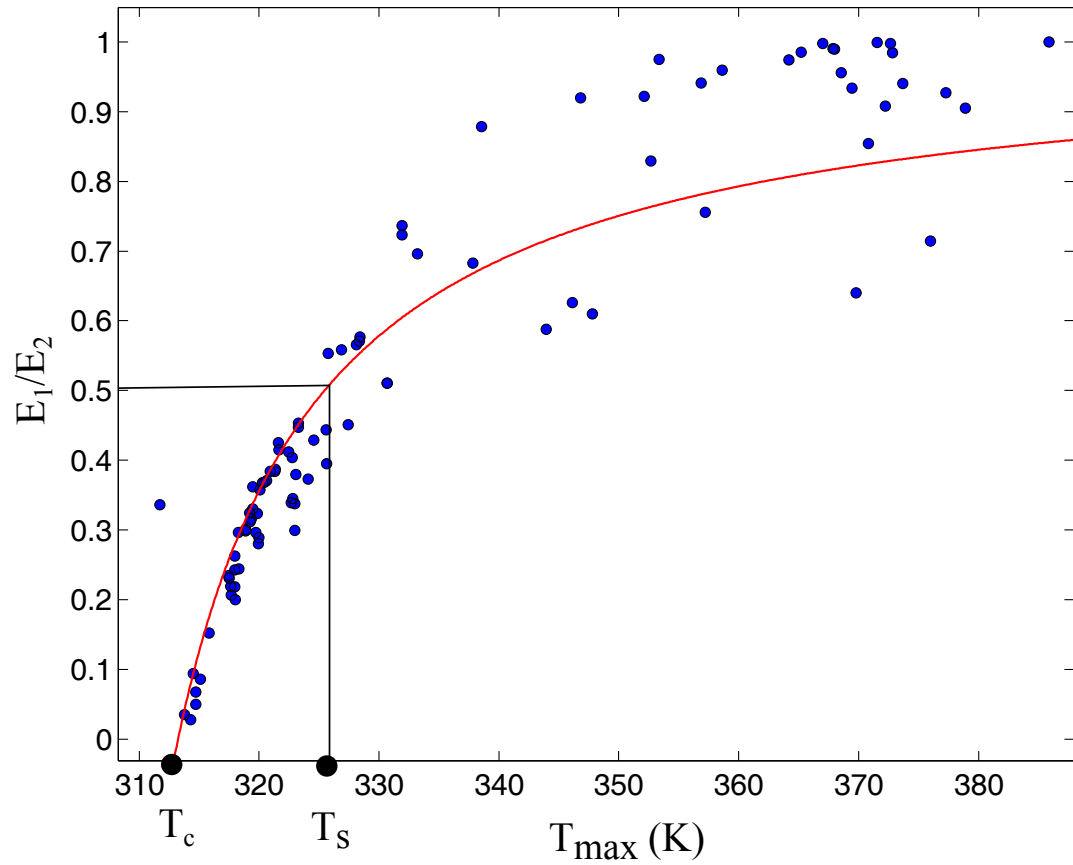


**Figure 6.3:**  $E_1/E_2$  as a function of  $T_{max}$  for bacteria and archaea - Non-linear relationship between the enthalpy ratio and  $T_{max}$ . The red line corresponds to eq. 6.9.

## 6.5 The two parameters Hinshelwood model

**Table 6.2:** Models comparison on normalised data sets

Group	$R^2$	Adjusted- $R^2$	AIC	AICc	BIC
Hinshelwood 4p	0.815	0.771	-32.301	-9.736	17.648
Hinshelwood 2p	0.754	0.707	-30.712	-13.857	16.643
Bernard&Remond3p	0.947	0.935	-44.057	-25.606	20.709
Bernard&Remond2p	0.890	0.864	-40.176	-36.90	14.477

The Hinshelwood model can therefore be expressed as:

$$\mu(T) = A_c e^{E_2/(RT_c)} e^{-\frac{T_{max} - T_o}{T_{max} - 2T_o + T_s} (1 - E_2/(RT_{max}) - 1/(RT))} - A_c e^{E_2(1/(RT_c) - 1/(RT))} \quad (6.13)$$

where  $T_o$  and  $T_s$  are given for each group (see table 6.1), while  $A_c$  and  $T_c$  are universal constants:  $A_c = 0.652$  and  $T_c = 312.901$  K. Only the two parameters  $T_{max}$  (or  $A_1$ ) and  $E_2$  need to be determined for each species. This reduced parametrization turns out to accurately reproduce the available data sets, as it can be seen on fig. 6.4 with normalized data sets.

### 6.5.2 Comparison between the reduced Hinshelwood and the reduced CTMI models

To validate our approach, we compared the normalized 2P-Hinshelwood model to the normalised CTMI model as well as to the normalized four parameters Hinshelwood model. We also compared it to the normalized two parameters CTMI model (2P-CTMI model) with:

$$T_{min} = \alpha_1 T_{opt} + \alpha_2 T_{max} \quad (6.14)$$

where  $\alpha_1$  and  $\alpha_2$  are constants, equal to 0.152 and 0.091 respectively, that we formerly found using the whole data set. Comparison results on normalized data set (fig. 6.4, 6.6 and 6.7; table 6.2) shows that 2P-Hinshelwood and 2P-CTMI models are satisfyingly fitting the data. The 2P-CTMI model has the best trade-off between parameter numbers and fitting quality because it has the lowest Bayesian information criterion (BIC) and the lowest Akaike criterion (AIC) (see table 6.2). However, the 2P-Hinshelwood model comes just after it, also combining a low number of parameters and a high accuracy for predicting thermal growth curve. Moreover, the 2P-Hinshelwood model, when not normalized, can also predict the  $mvu_{opt}$ , contrary to the two parameters CTMI (fig. 6.5).

### 6.5.3 Correlation between the cardinal temperatures

Does the two parameters of the Hinshelwood model shed light on the linear correlations found between cardinal temperatures in chapter 4? To evaluate it, we simulated thermal growth curves for different couples of parameters ( $A_1, E_2$ ) on coherent values ranges



## 6. TOWARDS UNDERSTANDING THE THERMODYNAMICAL FUNDAMENT OF THE THERMAL GROWTH CURVE: A MODELLING APPROACH

---

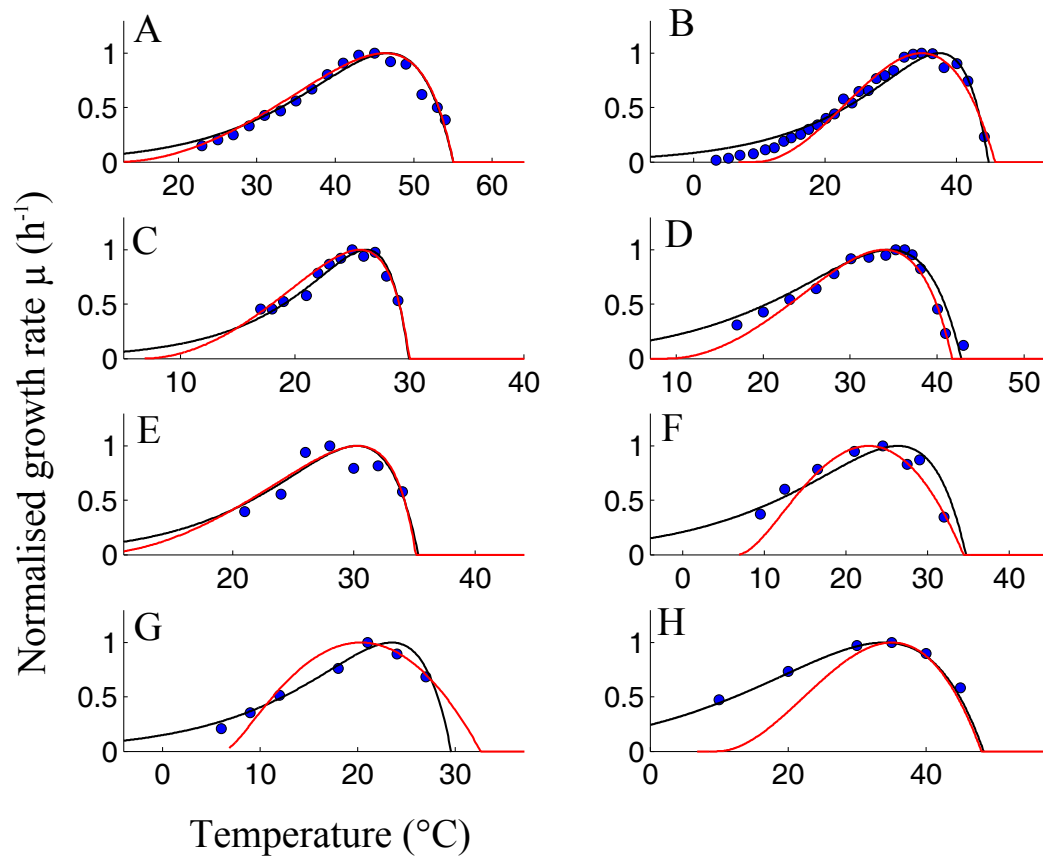


**Figure 6.4: Normalised model validation** - Two parameters Hinshelwood model (black) and two parameters CTMI (red) fitted on normalized data sets. A, Archae, B, Bacteria, C, Cyanobacteria, D, Yeasts, E, Dinophyta, F, Ochrophyta, G, Haptophyta, H, Chlorophyta.

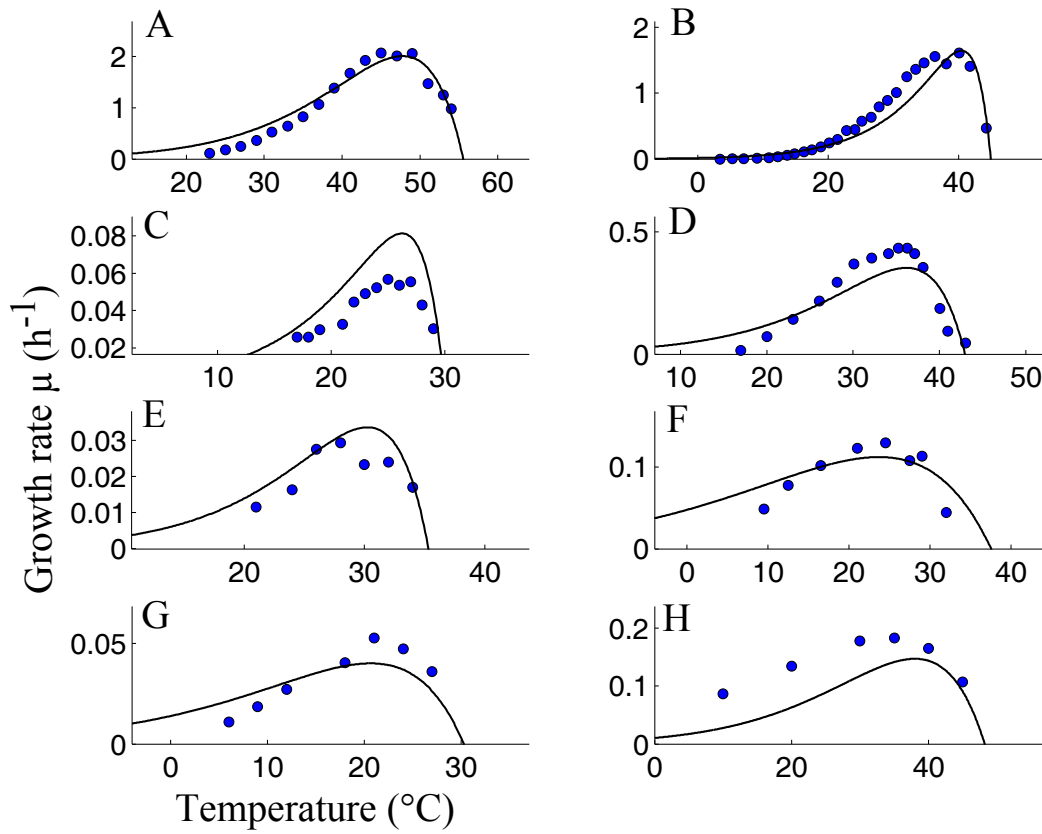


**Figure 6.5: Model validation** - Two parameters Hinshelwood model (black) fitted on original data sets. A, Archae, B, Bacteria, C, Cyanobacteria, D, Yeasts, E, Dinophyta, F, Ochrophyta, G, Haptophyta, H, Chlorophyta. Species are the same as fig. 6.4.

## 6. TOWARDS UNDERSTANDING THE THERMODYNAMICAL FUNDAMENT OF THE THERMAL GROWTH CURVE: A MODELLING APPROACH

---

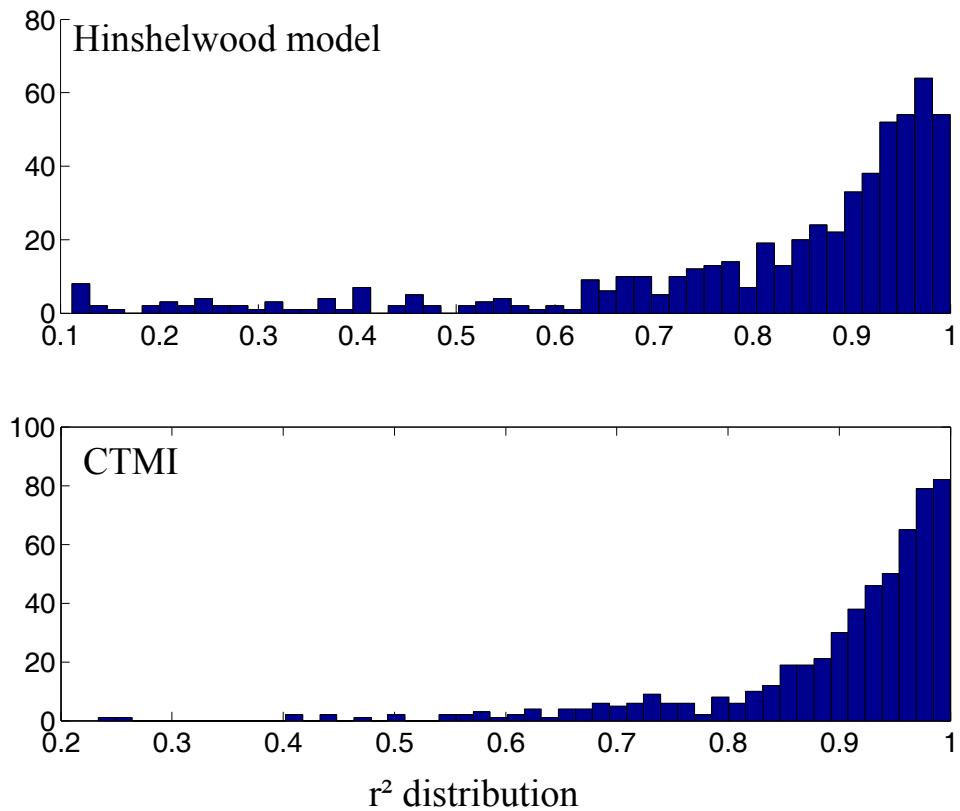


**Figure 6.6: Histogram of  $r^2$  distribution** - Histogram of the  $r^2$  distribution for the 2P-Hinshelwood model and CTMI.

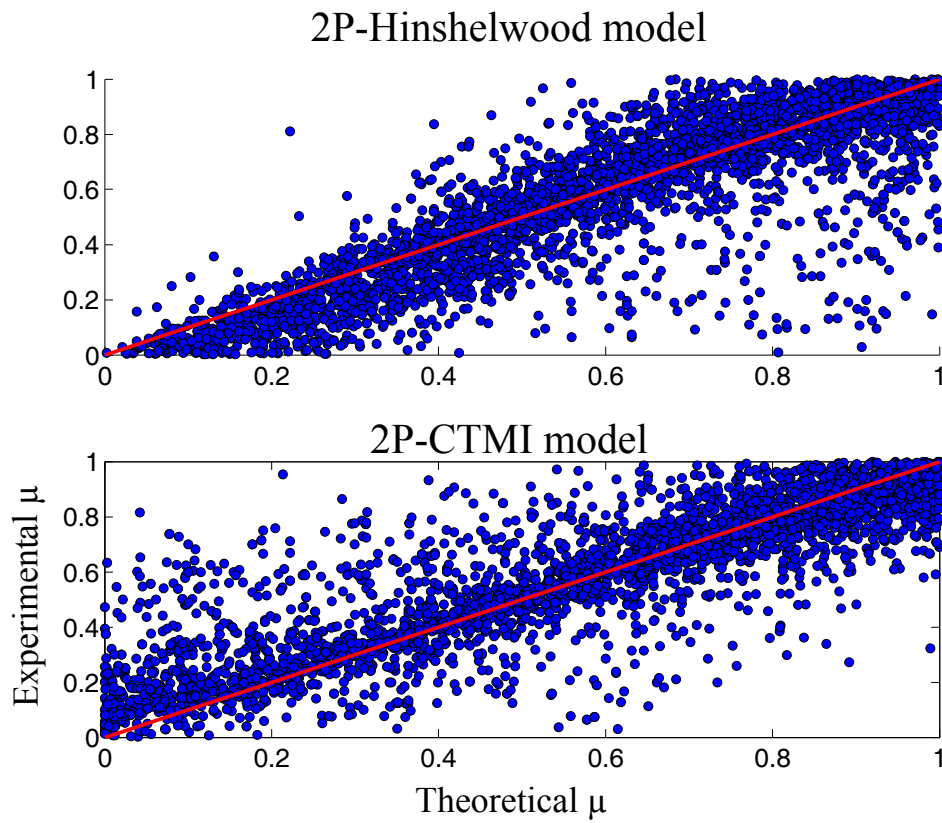


**Figure 6.7:** Predicted versus experimental growth rate - Predicted growth rate compared to experimental growth rate for normalized data set. The red lines correspond to  $y = x$ .

## 6. TOWARDS UNDERSTANDING THE THERMODYNAMICAL FUNDAMENT OF THE THERMAL GROWTH CURVE: A MODELLING APPROACH

---

(*i.e.*  $\ln(A_1)$  is comprised between 1 and 200, and  $E_2$  is comprised between  $10^4$  and  $10^6$  J.mol<sup>-1</sup> with criteria ensuring that the thermal growth curve is possible for each  $(A_1, E_2)$  combination. This gives small ranges of predicted  $T_{max} - T_{opt}$  and  $|T_{opt} - T_{min}|$  variations (fig. 6.8). Particularly, for each fixed  $A_1$ , the predicted cardinal temperatures are linearly correlated (fig. 6.8).

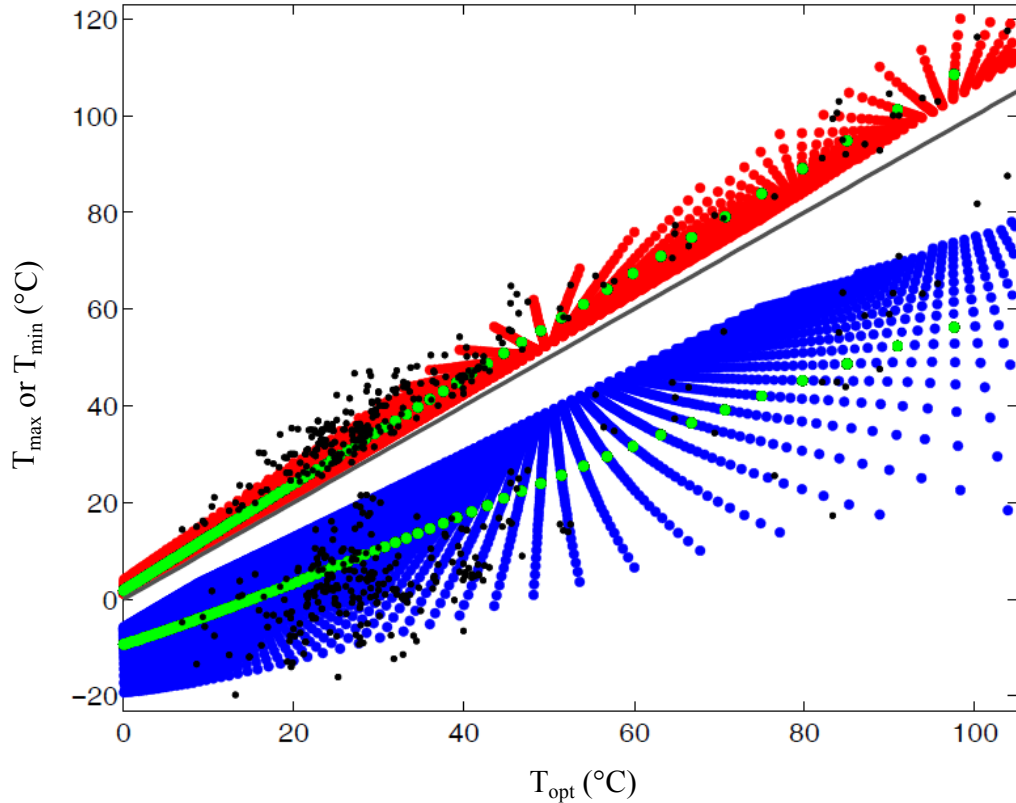


**Figure 6.8:** Cardinal temperatures predicted by the Hinshelwood model -  $T_{min}$  (blue) and  $T_{max}$  (red) as a function of  $T_{opt}$  according to the Hinshelwood model with two parameters for coherent values of  $A_1$  and  $E_2$ . The linear relationships appear when  $A_1$  is fixed (represented by green points).

### 6.6 Conclusion

We have proposed a mechanistic view of the Hinshelwood formula from an autocatalytic model of cell exponential growth with parameters based on thermodynamic considerations. This model has been calibrated on a large thermal growth curve data set.

We found two correlations between its parameters. Firstly, the enthalpy-entropy compensation of protein denaturation (or desactivation through unfolding), which highly constrains the enzyme stability regarding temperature. Secondly, the activity-stability trade-off characteristic of enzymes. The model, taking these phenomena into account, was reduced to two parameters, and compared to the two parameters CTMI. It results that it almost equally fits the normalized data, while it can also predict maximal growth rates. The two parameters Hinshelwood model also partially explains the linear links between the cardinal temperatures as well as the relations between  $\mu_{opt}$  and  $T_{opt}$ .

## 6. TOWARDS UNDERSTANDING THE THERMODYNAMICAL FUNDAMENT OF THE THERMAL GROWTH CURVE: A MODELLING APPROACH

---

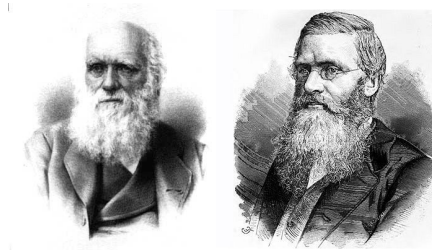
### Summary of section 6:

- The Hinshelwood model can be derived from an autocatalytic view of cell growth.
- In this scheme, thermal sensitivity appears to result from the average sensitivity of all the enzymes rather than some specific enzymes.
- The physical phenomenon of entropy-enthalpy compensation as well as the activity-stability trade-off of enzymes play a key role in the thermal growth curve, partially explaining the linear correlations between the cardinal temperatures.
- A two parameters mechanistic model can be obtained with these hypotheses.

# 7

## Modelling thermal adaptation in microalgae: an adaptive dynamics point of view

Contributors: Mairet, F., Sciandra, A., Bernard, O.



The two fathers of the theory of evolution, Charles Darwin and Alfred Russel Wallace.

### 7.1 Introduction

In chapters 4, 5 and 6 we have shown that temperature has a crucial effect on microalgae growth, and we have determined the potential links existing between the different thermal parameters. We now study how temperature shapes microalgae evolution. Because of their high division rate, microalgae are able to rapidly adapt to their environment through a process of selection-mutation. To date, there is only one model which predicts microalgae adaptation to temperature [Thomas et al., 2012], by simulations based on the Adaptive Dynamics theory. However, this model implies several assumptions that have been discussed [Boyd et al., 2013].



## 7. MODELLING THERMAL ADAPTATION IN MICROALGAE: AN ADAPTIVE DYNAMICS POINT OF VIEW

---

Adaptive dynamics is a theoretical framework developed during the last decade aiming to understand the long-term consequences of small mutations on adaptive traits visible through the phenotype [Dieckmann and Law, 1996, Geritz et al., 1998, Metz et al., 1992, 1996]. On the contrary to other evolutionary modelling such as the quantitative genetics theory [Falconer et al., 1996], the adaptive dynamics theory does not focus on genetic changes during evolution but rather combines ecology and evolution, taking into account the density-dependent effects inherited from game theory [Smith, 1982].

Here, we propose firstly a simple Monod-like model that represents the effect of a constant temperature on growth and extend it to model microalgae adaptation to temperature. In line with Thomas et al. [2012], we use the Adaptive Dynamics theory. We keep the model as simple as possible to study it analytically. In a second part, we use the model under periodic temperature to account for more realistic conditions. Finally, we simulate strain separation through evolutionary branching under fluctuating temperature.

### 7.2 Simple dynamical model describing the temperature effect on microalgae in chemostat

#### 7.2.1 The Monod model in chemostat

The dynamical effect of temperature on UO growth can be represented using a Monod-type growth model in chemostat, including for example the CTMI statical model:

$$M : \begin{cases} \dot{S} &= D(S_{in} - S) - \mu(T)\rho(S)X \\ \dot{X} &= \mu(T)\rho(S)X - DX \end{cases} \quad (7.1)$$

where  $\mu(T)$  is the CTMI model (eq. 3.11),  $S$  is the nutrient concentration in the chemostat,  $X$  is the algal biomass concentration,  $D$  is the dilution rate and with:

$$\rho(S) = \frac{S}{K + S} \quad (7.2)$$

$K$  is a half-saturation coefficient. It is possible to calculate the non zero equilibrium  $(S^*, X^*)$  of system  $(M)$ :

$$\begin{aligned} S^* &= \frac{KD}{\mu(T) - D} \\ X^* &= (S_{in} - S^*) \end{aligned} \quad (7.3)$$

with the hypothesis  $\mu(T)\rho(S_{in}) - D > 0$ . In the following, we use a Lyapunov function taken from Harisson [1979] to prove that (7.3) is globally asymptotically stable.

## 7.2 Simple dynamical model describing the temperature effect on microalgae in chemostat

---

**Lemma 7.2.1** *The Lyapunov candidate function is given:*

$$V(S, X) = \int_{S^*}^S \frac{\mu(T)\rho(w) - \mu(T)\rho(S^*)}{\mu(T)\rho(w)} dw + \int_{X^*}^X \frac{w - X^*}{w} dw \quad (7.4)$$

with  $V : B \rightarrow \mathbb{R}^2$  where  $B$  is an open containing  $(S^*, X^*)$ .  $V(S, X)$  is zero at  $(S^*, X^*)$ , positive at all other points  $(S, X)$ , defined and monotone increasing when  $|X - X^*|$  or  $|S - S^*|$  increases. The time derivative of  $V$  is:

$$\dot{V}(S, X) = \frac{1}{\mu(T)\rho(S)} (D - \mu(T)\rho(S)) [\mu(T)\rho(S)(S_{in} - S^*) - D(S_{in} - S)] \quad (7.5)$$

**Proof:** It is obvious that  $V(S^*, X^*) = 0$ . Moreover, since the integrands are of the same sign as  $X - X^*$  and  $S - S^*$ , the integrals are positive and increasing as  $|X - X^*|$  and  $|S - S^*|$  increase.

**Proposition 7.2.2** *If  $D < \mu(T)\rho(S_{in})$ , System (M) admits one non-zero equilibrium which is globally asymptotically stable.*

**Proof:** It is sufficient to prove that (7.5)  $< 0 \forall (S, X) \in B$ ,  $(S, X) \neq (S^*, X^*)$ . If  $S > S^*$  (resp.  $S < S^*$ ), then  $D - \mu(T)\rho(S) < 0$  (resp.  $> 0$ ) because  $\mu(T)\rho(S^*) = D$ , and  $[\mu(T)\rho(S)(S_{in} - S^*) - D(S_{in} - S)] > 0$  (resp.  $< 0$ ) because  $S_{in} - S < S_{in} - S^*$  (resp.  $S_{in} - S > S_{in} - S^*$ ). Thus, (7.5)  $< 0$  is verified, and  $(S^*, X^*)$  is globally asymptotically stable.

### 7.2.2 The specific case of the Droop model in chemostat

The Monod-type models assume a ‘constant yield’, *i.e.* the biomass produced is proportional to the nutrients that are consumed. For microalgae, this hypothesis is unsatisfying with poor fit on experimental data. In 1968, Michael Droop introduced a new model [Droop, 1968] considering an additional state variable, the nutrient cell quota, defined as the concentration of internal nutrient<sup>1</sup> per unit of biomass. Growth then depends on stored intra-cellular nutrients. The Droop model is currently preferred to the Monod-like models for describing growth, notably in chemostat [Sommer, 1991]. It is possible to introduce the temperature effect on growth in the Droop model:

$$M_{Droop} \begin{cases} \dot{S} &= D(S_{in} - S) - \mu_1(T)\rho(S)X \\ \dot{q} &= \mu_1(T)\rho(S) - \mu_2(T)(q - Q_0) \\ \dot{X} &= \mu_2(T) \left(1 - \frac{Q_0}{q}\right) X - DX \end{cases} \quad (7.6)$$

where  $q$  is the cell nutrient quota,  $Q_0$  is the minimal cell quota that sustains growth,  $\mu_1(T)$  and  $\mu_2(T)$  are Bernard&Rémond equations (eq. 3.11) with different parameters.

---

<sup>1</sup>Transformed into stored material or not, depending on the nature of the nutrient

## 7. MODELLING THERMAL ADAPTATION IN MICROALGAE: AN ADAPTIVE DYNAMICS POINT OF VIEW

---

We thus assume that the nutrient uptake and the growth on internal nutrients have different thermal sensitivities. In this particular case, it is not immediate to deduce the global growth rate of the population, *i.e.* for example reconstructing the thermal growth curve using the growth rate at each temperature.

Under balanced growth, we set that  $\dot{q} = 0$ . Then:

$$q^* = \frac{\mu_1(T)}{\mu_2(T)}\rho(S) + Q_0 \quad (7.7)$$

and so:

$$\frac{\dot{X}}{X} = \mu_2(T) \frac{\mu_1(T)\rho(S)}{\mu_1(T)\rho(S) + \mu_2(T)Q_0} - D \quad (7.8)$$

If nutrient is not limited (*i.e.*  $\rho(S) \simeq 1$ ) and  $\mu_1(T)\rho(S) > \mu_2(T)Q_0$ , then, the thermal growth curve of the microalgae species is mainly the result of  $\mu_2(T) - D$ . However, if nutrient is limited ( $\rho(S) < 1$ ) then the  $T_{opt}$  of the thermal growth curve is modified by  $\mu_1(T)$  and  $\mu_{opt}$  is affected too (fig. 7.1). This is an important result for the study of the Droop model in an evolutionary perspective, as well as for the comprehension of the coupled effects of nutrient and temperature on growth.

### 7.3 Evolutionary Model

#### 7.3.1 General case

Now that the global stability of the positive equilibrium of system ( $M$ ) has been shown, we study system ( $M$ ) in the context of adaptive dynamics, introducing a mutant  $X_{mut}$  with an adaptive trait  $a_{mut}$  (*i.e.* a quantifiable trait that is likely to evolve) different from the resident trait  $a$ , with  $\mu_{mut}(a_{mut}, T)$  and  $\mu(a, T)$  [Dieckmann and Law, 1996]. For further introduction to adaptive dynamics, see Dieckmann [2004]. To define the canonical equation of adaptive dynamics, *i.e.* the equation of the evolution of trait  $a$  [Dieckmann and Law, 1996], we need to find the mutant growth rate (*per capita*) in the resident population at equilibrium, called invasion fitness  $f(a_{mut}, a)$  (see eq. 2.4 for the complete expression of  $\beta(T)$  and  $\lambda(T)$ ).

**Proposition 7.3.1** *The invasion fitness for System (7.1) is given by:*

$$f(a_{mut}, a) = D \left( \frac{\lambda_{mut}}{\lambda} \frac{\beta}{\beta_{mut}} - 1 \right) \quad (7.9)$$

**Proof:** This results from the steady-state condition of the resident system, and from the hypothesis that the mutant is initially rare. We can thus replace  $S$  by its equilibrium value  $S^*$ :

$$f(a_{mut}, a) = \mu_{mut}(a_{mut}, T)\rho(S^*) - D \quad (7.10)$$

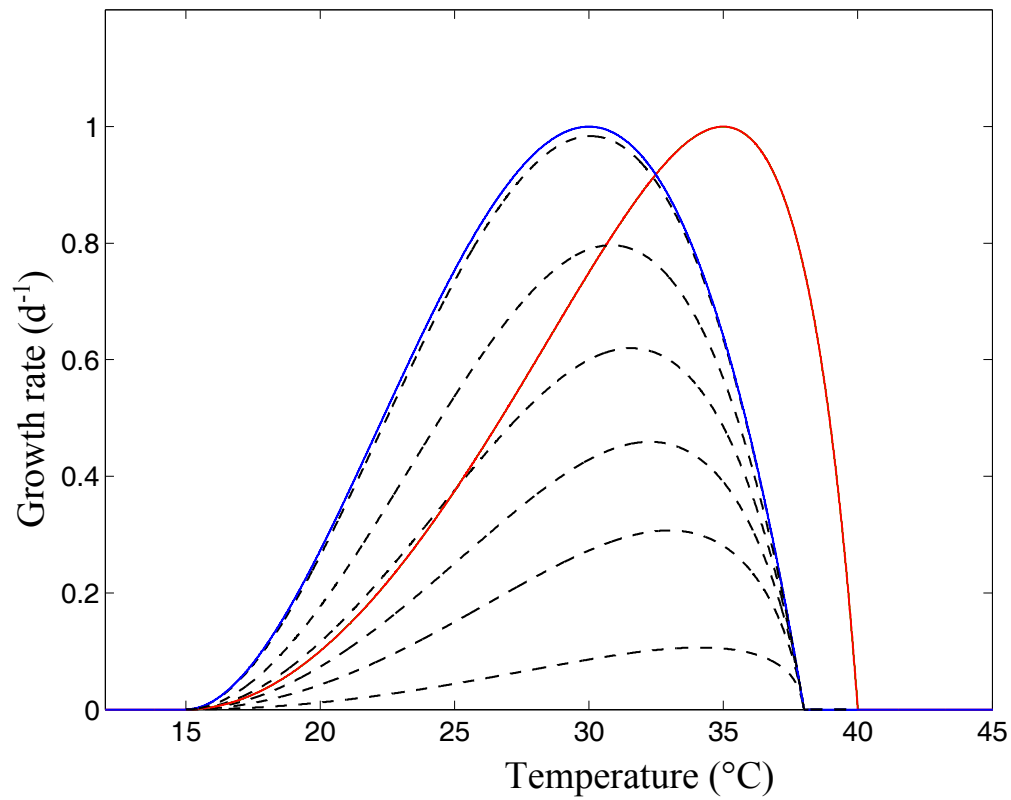


**Figure 7.1: Thermal growth curve obtained with the Droop model** - The blue line corresponds to  $\mu_2(T)$ , the red line to  $\mu_1(T)$  and the dashed lines are the resulting growth rates  $\dot{X}/X$  obtained by increasing  $\rho(S)$  or  $Q_0$ .

## 7. MODELLING THERMAL ADAPTATION IN MICROALGAE: AN ADAPTIVE DYNAMICS POINT OF VIEW

---

### 7.3.2 Modelling the evolution of the optimal temperature trait

We choose to study the adaptive trait  $a = T_{opt}$ , assuming that temperature will mainly affect the optimal conditions for growth. Because of the constraint (3.13) on  $T_{opt}$ , we choose to study the case:

$$T > \frac{T_{min} + T_{max}}{2} \quad (7.11)$$

We calculate the selection gradient, which gives the direction of the selection, using (7.9):

$$\left. \frac{\partial f(a_{mut}, a)}{\partial a_{mut}} \right|_{a_{mut}=a} = -\frac{\beta'(a)}{\beta(a)} D \quad (7.12)$$

with

$$\beta'(a) = -6a^2 + (6T + 2T_{max} + 4T_{min})a + (-2T_{max} - 4T_{min})T \quad (7.13)$$

We can deduce the canonical equation of the adaptive trait, that describes the evolution of  $T_{opt}$  at the evolutionary time scale  $\theta$ :

$$\frac{da}{d\theta} = -M_p \sigma^2 X^* D \frac{\beta'(a)}{\beta(a)} \quad (7.14)$$

where  $M_p$  is the probability to be a mutant at each apparition, and  $\sigma$  is the mutation step.

We then search for the evolutionary singular strategy. We find that  $da/d\theta = 0$  for  $a^* = T$ , which means that the optimal temperature trait tends to equal the environment temperature (Fig. 7.2 B). Note that the same results can be obtained with the Droop model presented in section 7.2.2 (not presented here for sake of brevity). We investigate the stability of the singular strategy examining the sign of the fitness invasion second order derivative.

**Proposition 7.3.2**  $a^*$  is a *Convergent Stable Strategy (CSS)*, which means that the singular strategy is attractive, and an *Evolutionary Stable Strategy (ESS)*, which means that the resident  $a^*$  cannot be invaded by another mutant.

**Proof:** The following conditions are respected:

$$\mathbf{H1.} \quad \left. \frac{\partial^2 f(a_{mut}, a)}{\partial a_{mut}^2} \right|_{a_{mut}=a=a^*} < \left. \frac{\partial^2 f(a_{mut}, a)}{\partial a^2} \right|_{a_{mut}=a=a^*}$$

$$\mathbf{H2.} \quad \left. \frac{\partial^2 f(a_{mut}, a)}{\partial a_{mut}^2} \right|_{a_{mut}=a=a^*} < 0$$

Indeed, we have:

$$\begin{aligned} \left. \frac{\partial^2 f(a_{mut}, a)}{\partial a_{mut}^2} \right|_{a_{mut}=a=a^*} &= -D \frac{\beta''\beta - 2\beta'^2}{\beta^2} \\ \left. \frac{\partial^2 f(a_{mut}, a)}{\partial a^2} \right|_{a_{mut}=a=a^*} &= D \frac{\beta''}{\beta} \end{aligned} \quad (7.15)$$

$\beta'(a^*) = 0$ , and so it is sufficient to prove:

$$-D \frac{\beta''(a^*)}{\beta(a^*)} < 0 \quad (7.16)$$

Yet, we have  $\beta(a^*) = -(T - T_{min})(T - T_{max})(T_{min} - T) < 0$  because  $T_{min} < T < T_{max}$ . Also,  $\beta''(a^*) = 2T_{max} + 4T_{min} - 6T$ .  $\beta''(a^*) < 0$  is equivalent to  $T > (2T_{min} + T_{max})/3$  which is true because of (7.11). Thus, (7.16) is true. H1 and H2 are verified.

### 7.3.3 Structural link between adaptive traits

In nature, it is possible that several adaptive traits evolve concurrently. By taking the adaptive trait  $a = T_{opt}$  and considering that  $T_{min}$ ,  $T_{max}$  and  $\mu_{opt}$  can evolve with  $a$ , the selection gradient becomes:

$$\left. \frac{\partial f(a_{mut}, a)}{\partial a_{mut}} \right|_{a_{mut}=a} = D \frac{\lambda'(a)\beta(a) - \beta'(a)\lambda(a)}{\lambda(a)\beta(a)} \quad (7.17)$$

Then, different cases can be assumed.

**Case 1:  $T_{opt}$  and  $T_{max}$  are linearly linked.** We have previously pointed out (section 4) that the strongest linear links between the cardinal temperatures are those existing between these two parameters:

$$T_{max} = a_1 T_{opt} + b_1 \quad (7.18)$$

In expression (7.9), we replace  $T_{max}$  by (7.18). Thus:

$$\beta'(a) = T_{opt}^2(3a_1 - 6) + T_{opt}(6T + 4T_{min} + 2b_1 - 4Ta_1) - 4TT_{min} - 2Tb_1 - T_{min}^2 a_1 + 2TT_{min}a_1 \quad (7.19)$$

and:

$$\lambda'(a) = -a_1(T - T_{min})^2 \quad (7.20)$$

We search for the evolutionary singular strategy by setting eq.(7.23) equal to zero. As for (7.14), we find that  $a^* = T$ , and thus  $T_{max}^* = a_1 T + b_1$  (fig. 7.2 C). This is an important

## 7. MODELLING THERMAL ADAPTATION IN MICROALGAE: AN ADAPTIVE DYNAMICS POINT OF VIEW

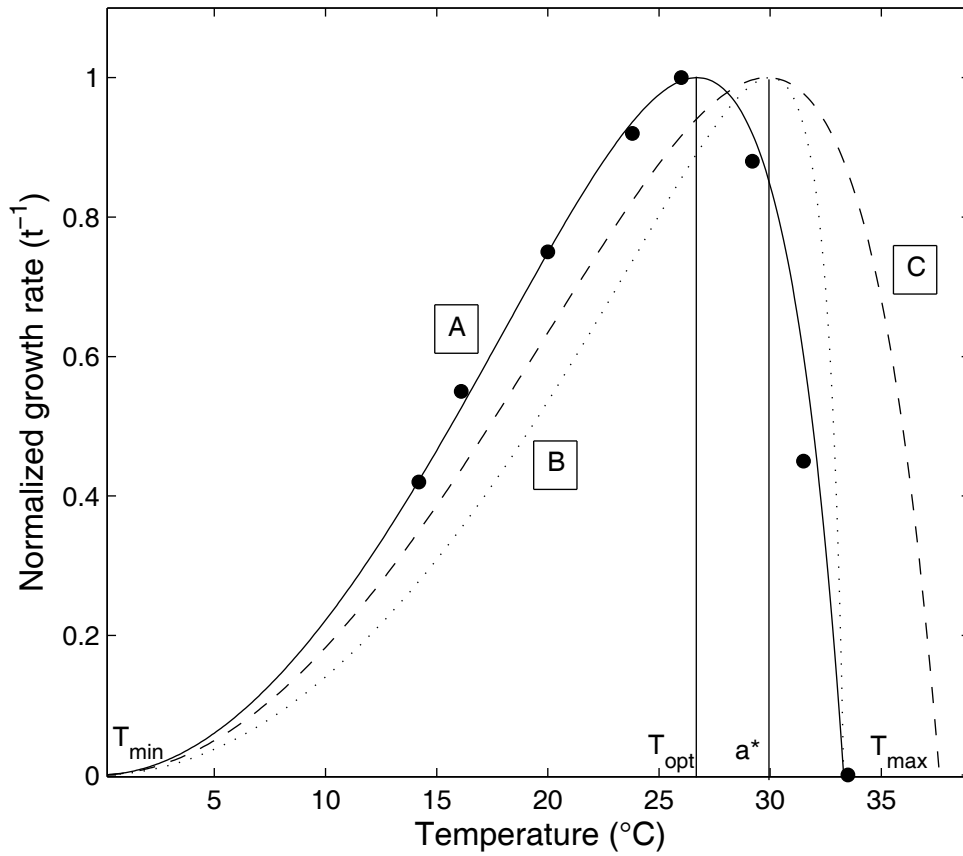


**Figure 7.2:** Thermal growth curve of *Nannochloropsis oceanica* - A, Initial thermal growth curve *Nannochloropsis oceanica*. B and C are the evolutionary cases for  $T = 30^{\circ}\text{C}$  with  $a^* = T$ ,  $T_{min}$  and  $T_{max}$  are fixed, and with  $T_{max} = a_1 a^* + b_1$ , respectively. The black circles are data from Sandnes et al. [2005] for *N. oceanica*.

result in the context of co-evolving species, because whether  $T_{max}$  evolve or not, the thermal growth curve will differently affect the species fitness in its environment, and so its competition with other species or stains.

**Case 2: accounting for all the linear links between cardinal temperatures.**

If  $T_{min}$  is also linked to  $T_{opt}$  according to eq. 4.1, then:

$$\beta'(a) = [(T - T_{opt})(T_{opt}(-1 + a_2)b_2) - (T_{opt}T(-1 + a_1)b_1)(T_{opt} - 2T + b_2 + a_2T_{opt})](a_2 - 1) - (b_2 + T_{opt}(a_2 - 1))(T_{opt}(-4 + 2a_1 + 2a_1a_2) + 3T + b_1 - 2Ta_1 - Ta_2 + a_1b_2 + a_2b_1) \quad (7.21)$$

and

$$\lambda'(a) = -a_1(b_2 - T + a_2T_{opt})^2 - 2a_2(b_1 - T + a_1T_{opt})(b_2 - T + a_2T_{opt}) \quad (7.22)$$

At the evolutionary equilibrium, we found again  $a^* = T$ . Note that in this particular case, the thermal niche width can be kept constant.

**Case 3:  $\mu_{opt}$  is linked to  $T_{opt}$  (Eppley hypothesis and modified-Eppley hypothesis).** In this case, on top of the linear links between cardinal temperatures,  $\mu_{opt}$  is linked to  $T_{opt}$  according to a function  $g(T_{opt})$ , *i.e.*  $\mu_{opt} = g(a)$  (which can represent one of the hypotheses developed in section 5). Then:

$$\left. \frac{\partial f(a_{mut}, a)}{\partial a_{mut}} \right|_{a_{mut}=a} = D \frac{g(a)(\lambda'(a)\beta(a) - \beta'(a)\lambda(a)) + g'(a)\lambda(a)\beta(a)}{\lambda(a)\beta(a)} \quad (7.23)$$

Surprisingly, the evolutionary equilibrium is different from  $T$  for the Eppley and modified Eppley equations; it was found numerically for the both hypotheses. This means that, even at constant temperature,  $T_{opt}$  tends to be higher than  $T$  if the hotter is better hypothesis prevails. This could be a key result to explain why *Cyanobacteria* of the genus *Synechococcus* sp. grown by Pittera et al. [2014] have experimental  $T_{opt}$  much higher than the temperature at which they have been maintained during several years.

## 7.4 Fluctuating temperature

### 7.4.1 Ecological timescale

We now study the system ( $M$ ) in the context of fluctuating temperature:

$$\begin{cases} T(t) = T_{inf} & \text{if } t \bmod \tau \in [\epsilon; \tau_1 - \epsilon[ \\ T(t) = T_{supp} & \text{if } t \bmod \tau \in [\tau_1 + \epsilon; \tau - \epsilon] \end{cases} \quad (7.24)$$

with  $T_{inf} < T_{supp}$ . By applying the conservation principle assuming that the sum  $S + X$  has reached its asymptotic value  $S_{in}$ , we have the equality  $S = S_{in} - X$ . Thus, the system ( $M$ ) can be reduced to a one dimension differential equation:

$$\dot{X} = [\mu(T(t))\rho(S_{in} - X) - D]X \quad (7.25)$$



## 7. MODELLING THERMAL ADAPTATION IN MICROALGAE: AN ADAPTIVE DYNAMICS POINT OF VIEW

---

where  $T(t)$  is given by Eq. (7.24). We define  $g(t, X) \stackrel{\text{def}}{=} \mu(T(t))\rho(S_{in} - X) - D$ .

We follow the same reasoning as Butler et al. [1985] and Butler and Freedman [1981] who studied a similar Monod-type model, but with a time varying dilution rate  $D(t)$  instead, and a predator-prey system with periodic coefficients, respectively.

**Theorem 7.4.1** *For  $D < \min(\mu(T)\rho(S_{in}))$ , equation (7.25) has a unique nontrivial positive periodic solution  $\psi(t)$  which is globally orbitally asymptotically stable. Moreover, we have  $\min_{s \in [0, \tau]} A(s) \leq \psi(t) \leq \max_{s \in [0, \tau]} A(s)$  with*

$$A(t) := [D(S_{in} + K) - \mu(T(t))S_{in}]/(D - \mu(T(t)))$$

(which corresponds to the steady state biomass concentration for constant  $T$ ).

**Proof:**  $\partial g/\partial X$  exists and is continuous for  $(t, X) \in R^1 \times R_+^1$  with  $R_+^1 = \{X \in R^1 : X \geq 0\}$ .

Moreover,  $\exists A(t) > 0 \ni [X - A(t)]g(t, X) < 0 \quad \forall X > 0, X \neq A(t)$ . Indeed, given  $D < \min(\mu(T)\rho(S_{in}))$ , we have:

$$[X - A(t)]g(t, X) < 0 \quad \forall X > 0, X \neq A(t) \quad (7.26)$$

Thus, Massera's theorem [Massera, 1950] easily implies the existence of a periodic solution  $\psi(t)$  of (7.25) satisfying  $\min_{s \in [0, \tau]} A(s) \leq \psi(t) \leq \max_{s \in [0, \tau]} A(s)$ .  $\psi(t)$  is the unique solution of (7.25), given that  $X\partial g(t, X)/\partial X < 0$  for all  $(t, X) \in R^1 \times R_+^1$ . Indeed, we have:

$$X \frac{\partial g(t, X)}{\partial X} = \mu(T)X \frac{-K}{(S_{in} - X + K)^2} \quad (7.27)$$

Because  $X > 0, K > 0, X\partial g(t, X)/\partial X < 0$  is always verified. Following the same reasoning as Butler and Freedman [1981],  $X\partial g(t, X)/\partial X < 0$  implies that  $g(t, X)$  is strictly decreasing as a function of  $X$ , for  $X > 0$ , for all  $t$ . So, if two solutions  $\psi(t)$  and  $\psi_2(t)$  exist, with  $\psi(t) < \psi_2(t)$ , it implies that  $\psi'(t)/\psi(t) = g(t, \psi(t)) > g(t, \psi_2(t)) = \psi_2'(t)/\psi_2(t)$  for all  $t$ . Integrating this inequality over  $[0, \tau]$  leads to a contradiction which prove the uniqueness of  $\psi(t)$ .

Using theorem 7.4.1, we have the following inequality with the periodic temperature (7.24):

$$\frac{D(S_{in} + K) - \mu(T_{inf})S_{in}}{D - \mu(T_{inf})} \leq X(t) \leq \frac{D(S_{in} + K) - \mu(T_{supp})S_{in}}{D - \mu(T_{supp})} \quad (7.28)$$

which means that

$$\frac{DK}{\mu(T_{inf}) - D} \leq S(t) \leq \frac{DK}{\mu(T_{supp}) - D} \quad (7.29)$$

If the time spent at each temperature is sufficiently long, then, when  $T = T_{inf}$  (resp.  $T = T_{supp}$ ), the substrate concentration converges towards its equilibrium  $S_{inf}^* = DK/(\mu(T_{inf}) - D)$  (resp.  $S_{supp}^* = DK/(\mu(T_{supp}) - D)$ ). We assume that the state transition between  $S_{inf}^*$  and  $S_{supp}^*$  is negligible. From a biological point of view, this assumption implies that the growth rates at both temperatures are quite similar.

## 7.4.2 Evolutionary timescale

### 7.4.2.1 Case 1: $T_{opt}$ is varying only

As explained previously, we assume that the resident population reaches rapidly its equilibrium for each temperature. In the case with the adaptive trait  $a = T_{opt}$  and considering constant  $T_{min}$  and  $T_{max}$ , we obtain:

$$\begin{cases} f(a_{mut}, a) = D \left( \frac{\beta(T_{inf})}{\beta_{mut}(T_{inf})} - 1 \right) & \text{if } T = T_{inf} \\ f(a_{mut}, a) = D \left( \frac{\beta(T_{supp})}{\beta_{mut}(T_{supp})} - 1 \right) & \text{if } T = T_{supp} \end{cases} \quad (7.30)$$

It is possible to use the average mutant growth rate in the resident population at steady-state [Ripa and Dieckmann, 2013]:

$$\bar{f}(a_{mut}, a) = \frac{1}{\tau} \int_0^\tau f(a_{mut}, a; t) dt \quad (7.31)$$

which is equivalent to:

$$\begin{aligned} \bar{f}(a_{mut}, a) = D & \left[ \frac{\beta(a, T_{inf})}{\beta(a_{mut}, T_{inf})} \frac{\tau_1}{\tau} \right. \\ & \left. + \frac{\beta(a, T_{supp})}{\beta(a_{mut}, T_{supp})} \frac{\tau - \tau_1}{\tau} - 1 \right] \end{aligned} \quad (7.32)$$

We thus deduce the selection gradient:

$$\left. \frac{\partial \bar{f}(a_{mut}, a)}{\partial a_{mut}} \right|_{a_{mut}=a} = D \left[ - \frac{\tau_1}{\tau} \frac{\beta'(T_{inf})}{\beta(T_{inf})} - \frac{\tau - \tau_1}{\tau} \frac{\beta'(T_{supp})}{\beta(T_{supp})} \right] \quad (7.33)$$

and so the canonical equation of the adaptive trait with fluctuating temperature is:

$$\frac{da}{d\theta} = M_p \sigma \bar{X}^* \left. \frac{\partial \bar{f}(a_{mut}, a)}{\partial a_{mut}} \right|_{a_{mut}=a} \quad (7.34)$$

Equation (7.34) is not analytically tractable. We perform simulations of (7.34) to search for the evolutionary singular strategy. Result (Fig. 7.3 C) shows that, at steady,  $T_{opt}$  does not converge to the average temperature  $T_{mean}$ . This result still holds if we replace  $T_{max}$  by a linear function of  $T_{opt}$  (Fig. 7.3 B), even if  $a^*$  is different. The asymmetric property of the thermal growth curve is probably the reason for such outcome.

## 7. MODELLING THERMAL ADAPTATION IN MICROALGAE: AN ADAPTIVE DYNAMICS POINT OF VIEW

---

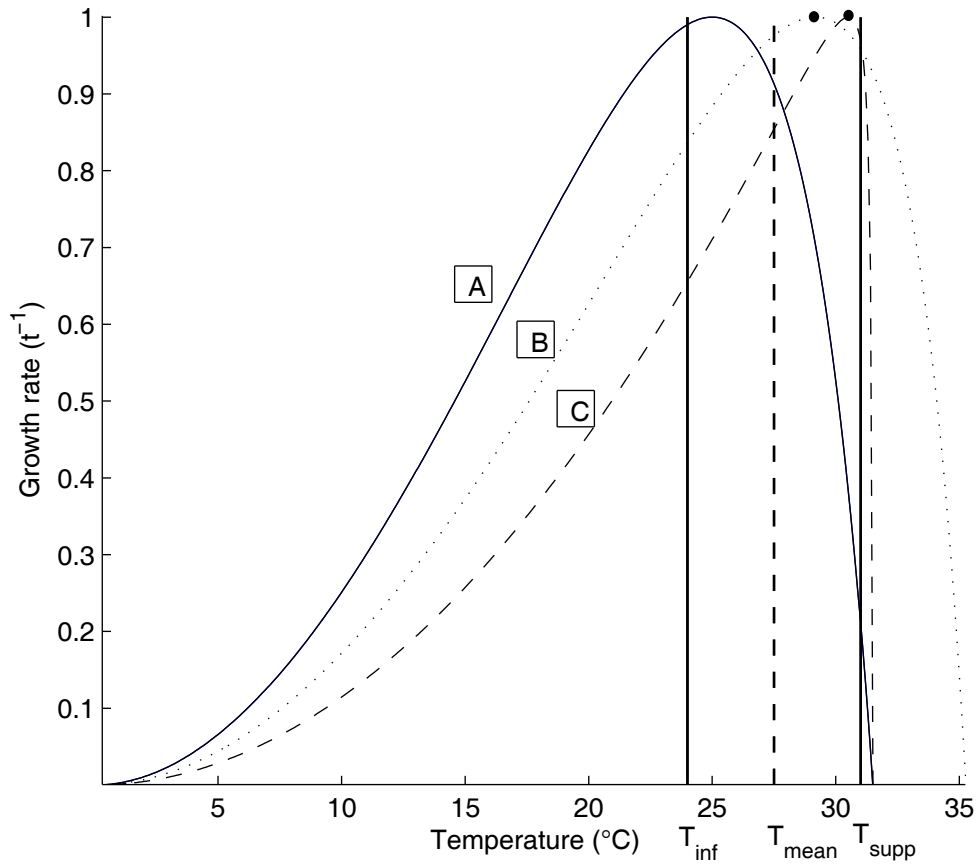


**Figure 7.3: Evolution of the thermal growth curve** - Evolution of the thermal growth curve for  $T_{inf} = 24^{\circ}\text{C}$ ,  $T_{supp} = 31^{\circ}\text{C}$ . (A) is the initial thermal growth curve, (B) is the evolutionary thermal growth curve for  $a = T_{opt}$  and  $T_{max} = mT_{opt} + p$  at steady-state, and (C) is the evolutionary thermal growth curve for  $a = T_{opt}$  and  $T_{max} = 31.5^{\circ}\text{C}$  at steady state. The singular strategies are represented by black points.

### 7.4.2.2 Case 2: the thermal niche width is kept constant

If the thermal niche width is kept constant and  $\mu_{opt} = 1$ , it is possible to demonstrate that  $T_{opt}^* \geq T_{mean}$ .

**Proposition 7.4.2** *Suppose that  $T$  is periodically varying as in eq. 7.24 with  $\tau_1 = \tau$  to simplify. Consider  $\psi(T_{opt}) = [\phi(T_1, T_{opt}) + \phi(T_2, T_{opt})]/2$ . Consider the following hypotheses:*

**H1.**  $T_{min} = T_{opt} - b_2$  et  $T_{max} = T_{opt} + b_1$  (all the curve is shifting horizontally on  $T$ ) and  $\mu_{opt} = 1$

**H2.**  $\left| \frac{\partial \phi(T, T_{opt})}{\partial T} \Big|_{T=T_{opt}-x} \right| < \left| \frac{\partial \phi(T, T_{opt})}{\partial T} \Big|_{T=T_{opt}+x} \right|$  for all  $x > 0$  ( $\phi(T)$  is asymmetrical)

**H3.**  $\left| \frac{\partial \phi(T, T_{opt})}{\partial T} \Big|_{T=T_{opt}+x} \right| < \left| \frac{\partial \phi(T, T_{opt})}{\partial T} \Big|_{T=T_{opt}+x+y} \right|$  with  $y > x \geq 0$  ( $\phi(T)$  is concave on the interval  $[T_{opt}, T_{max}]$ ).

Then, under H1-H3:

$$\frac{d\psi(T_{opt})}{dT_{opt}} = 0 \Rightarrow T_{opt}^* \geq T_{mean} \quad (7.35)$$

with  $T_{mean} = (T_1 + T_2)/2$ .

**Proof:** We start with hypotheses H1-H3. Suppose now that:

$$T_{opt}^* < (T_1 + T_2)/2 \quad (7.36)$$

Consider that:

$$\Delta_1 = \phi(T_{opt}^*, T_1) - \phi(T_{opt}^* + \epsilon, T_1) \quad (7.37)$$

$$\Delta_2 = \phi(T_{opt}^* + \epsilon, T_2) - \phi(T_{opt}^*, T_2) \quad (7.38)$$

with  $\epsilon > 0$ . According to H1,

$$\Delta_1 \simeq \epsilon \frac{d\phi(T_{opt}^*, T)}{dT} \Big|_{T=T_1} \quad (7.39)$$

and

$$\Delta_2 \simeq \epsilon \frac{d\phi(T_{opt}^*, T)}{dT} \Big|_{T=T_2} \quad (7.40)$$

## 7. MODELLING THERMAL ADAPTATION IN MICROALGAE: AN ADAPTIVE DYNAMICS POINT OF VIEW

---

One can easily show that  $T_1 < T_{opt} < T_2$  and so it is possible to write  $T_1 = T_{opt} - \alpha$  with  $\alpha > 0$ .

According to eq. 7.36,  $T_2 = T_{opt} + \alpha + \theta$ ,  $\theta > 0$ .

According to H2:

$$|\Delta_1| = \left| \epsilon \frac{d\phi(T_{opt}^*, T)}{dT} \Big|_{T=T_{opt}-\alpha} \right| < \left| \epsilon \frac{d\phi(T_{opt}^*, T)}{dT} \Big|_{T=T_{opt}+\alpha} \right| \quad (7.41)$$

According to H3,

$$\left| \epsilon \frac{d\phi(T_{opt}^*, T)}{dT} \Big|_{T=T_{opt}+\alpha} \right| < \left| \epsilon \frac{d\phi(T_{opt}^*, T)}{dT} \Big|_{T=T_{opt}+\alpha+\theta} \right| = |\Delta_2| \quad (7.42)$$

We thus have:

$$|\Delta_1| < |\Delta_2| \quad (7.43)$$

It is possible to show that  $\Delta_1 > 0$  and  $\Delta_2 > 0$ . In that case, after eq. 7.43:

$$\phi(T_{opt}^*, T_1) - \phi(T_{opt}^* + \epsilon, T_1) < \phi(T_{opt}^* + \epsilon, T_2) - \phi(T_{opt}^*, T_2) \quad (7.44)$$

And therefore:

$$\phi(T_{opt}^*, T_1) + \phi(T_{opt}^*, T_2) < \phi(T_{opt}^* + \epsilon, T_2) + \phi(T_{opt}^* + \epsilon, T_1) \quad (7.45)$$

Eq. 7.45 imply that  $T_{opt}^*$  is not the value for which  $\psi(T_{opt})$  is maximum, and thus eq 7.36 is wrong. Thus,  $T_{opt}^* > (T_1 + T_2)/2$  and prop. 7.4.2 is verified (see fig. 7.4).

This is an important result for applying adaptive dynamics to asymmetrical growth curve. This result would no longer be available for pH variations for example, given that the effect of pH on growth is a symmetrical function [Rosso et al., 1995]. It also implicitly implies that the more the curve is asymmetrical, the more  $T_{opt}^*$  is higher than  $T_{mean}$ .

### 7.4.3 Evolutionary Branching conditions

Under particular conditions, Adaptive Dynamics predicts that evolution can converge to a specific singular strategy called ‘branching point’ where selection becomes disruptive, so that two strains move apart [Metz et al., 1992]. The mutant can invade the resident and reciprocally, and both stably coexist.

We investigate the evolutionary dynamics of (7.3) by using a pairwise invasibility plot (PIP) (Fig. 7.5)[Geritz et al., 1998]. This allows us to determine the stability of the singular strategy, studying graphically the sign of the mutant invasion fitness. For temperatures comprised between  $T_{inf} = 20^\circ\text{C}$  and  $T_{supp} = 36^\circ\text{C}$ , and with  $T_{min} = 4^\circ\text{C}$ ,

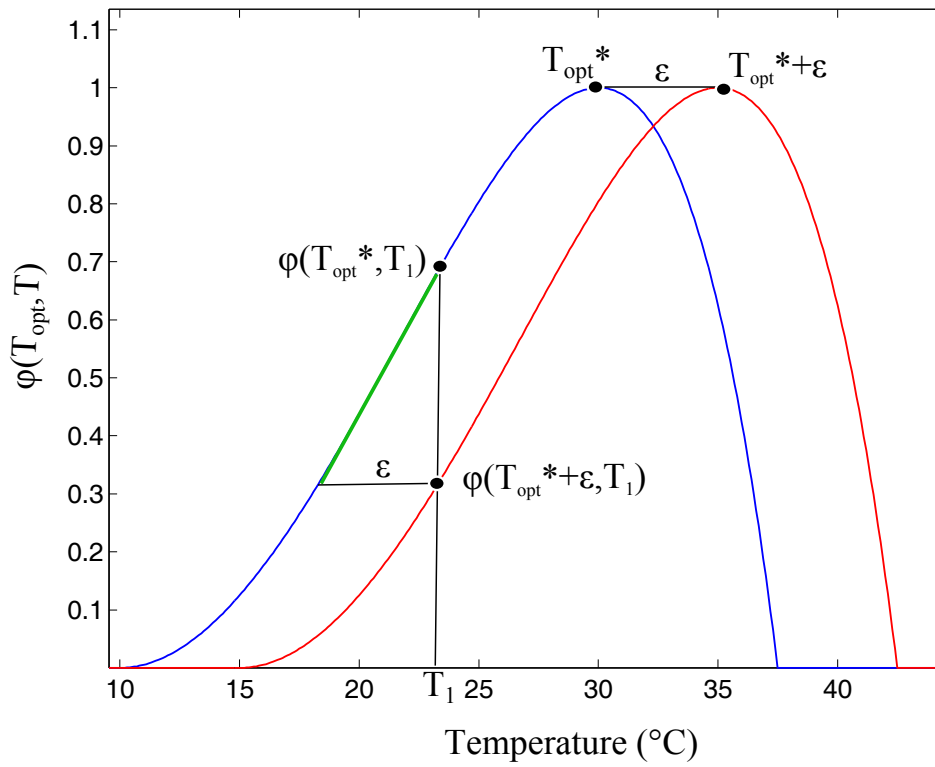


**Figure 7.4:** Evolution of  $T_{opt}$  if the niche width is kept constant - If  $\epsilon$  is sufficiently small, then the green segment corresponds to  $d\varphi(T_{opt}^*, T)/dT$  evaluated at  $T = T_1$ .

## 7. MODELLING THERMAL ADAPTATION IN MICROALGAE: AN ADAPTIVE DYNAMICS POINT OF VIEW

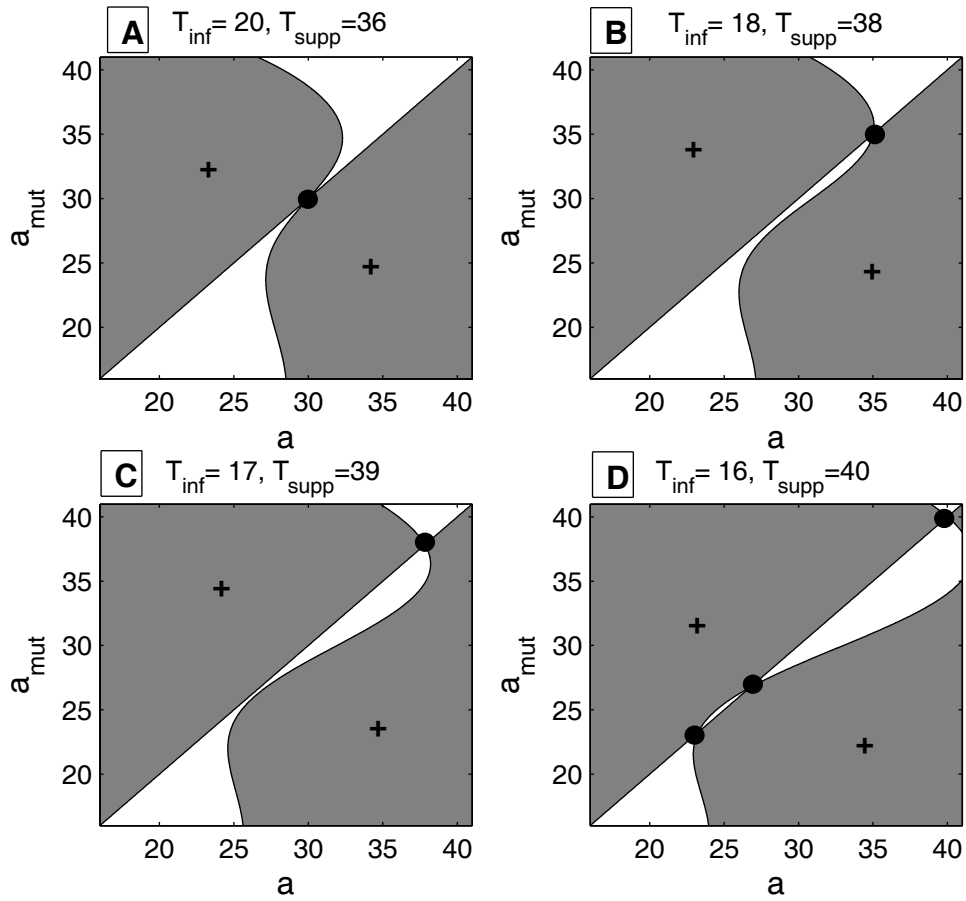


**Figure 7.5: Pairwise Invasibility Plots** - Pairwise Invasibility Plots across a range of values of  $T_{inf}$  and  $T_{supp}$  (expressed in  $^{\circ}\text{C}$ ). The other parameters are listed in Table 7.1. Grey and white represent positive and negative invasion fitness, respectively. Evolutionary singular strategy are represented by a black circle.

$T_{max} = 40^\circ\text{C}$ , we find that there exists a branching point (fig. 7.5 A). Indeed, at this point, mutant and resident can mutually invade in such a way that two strains separate. For a range of values around the previous ones, we observe that the singular strategy bifurcates in three singular strategies (fig. 7.5 B, C, D). In fig. 7.5 D, there is still a branching point, which seems to allow a strong separation between strains because of the large area of positive invasion fitness.

Parameters	Unit
$T_{min}$ , minimal temperature for growth	$4^\circ\text{C}$
$T_{max}$ , maximal temperature for growth	$40^\circ\text{C}$
$T_{inf}$ , inferior temperature applied	$20^\circ\text{C}$
$T_{supp}$ , superior temperature applied	$36^\circ\text{C}$
$\tau_1$ , time during which $T_{inf}$ is applied	12 h
$\tau$ , period of temperature fluctuation	24 h

**Table 7.1: Model parameters for evolutionary branching.**

To confirm the results found previously, we perform a simulation of an evolutionary branching. In line with Mirrahimi et al. [2011], we consider a model where the adaptive trait  $a$  becomes a continuous trait:

$$\begin{cases} \partial_t X(a, t) = X(a, t)[\mu(a, T)S(t) - D] + \epsilon \Delta X(a, t) \\ S(t) = \frac{DS_{in}}{D + \int \mu(a, T)X(a, t) da} \end{cases} \quad (7.46)$$

where  $X(a, t)$  is the species density with trait  $a = T_{opt}$ ,  $S(t)$  is the quasi-static approximation of resource dynamics,  $\epsilon$  is the mutation rate. We use the parameters listed in Table 7.1. Fig. 7.6 shows that an evolutionary branching really occurs. Two general morphs with two distinct  $T_{opt}$  appear and stabilize.

## 7.5 Conclusion

We have proposed a simple model of temperature effect on microalgae growth based on the model developed by Bernard and Rémond [2012]. We used it in an evolutionary perspective thanks to the adaptive dynamics. We found that, under constant temperature, the optimal temperature tends to equal the environmental temperature in different scenarios, if  $T_{min}$  and  $T_{max}$  are fixed or if they are linearly linked to  $T_{opt}$ . However, as soon as  $\mu_{opt}$  is linked to  $T_{opt}$ , then the hotter is better hypothesis (at least on a given interval) induced that  $T_{opt}^* > T$ .

We then studied the model under a simple fluctuating temperature signal. We showed that a stable periodic solution exists. The evolutionary study reveals that  $T_{opt}^*$  is always



## 7. MODELLING THERMAL ADAPTATION IN MICROALGAE: AN ADAPTIVE DYNAMICS POINT OF VIEW

---

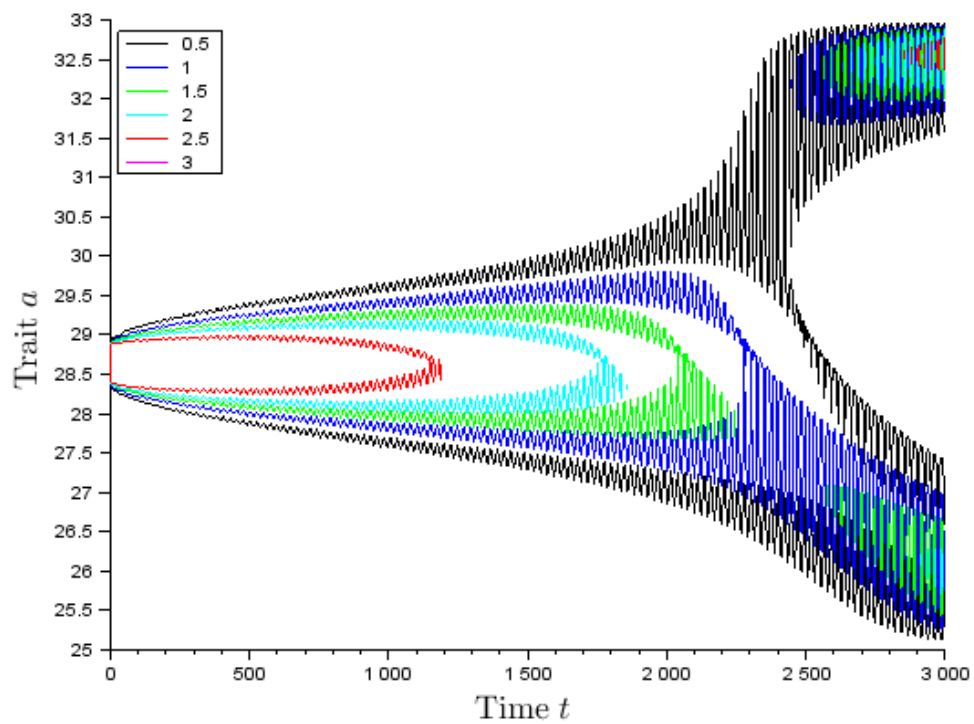


**Figure 7.6: Evolutionary branching of trait  $a$ .** - Evolutionary branching of trait  $a$  for the parameters of Table 7.1. The trait  $a$  is expressed in  $^{\circ}\text{C}$ ,  $t$  is arbitrarily expressed in hours. The colored lines correspond to a population size for each trait value.

higher than or equal to the average temperature  $T_{mean}$ . At evolutionary time scale, the fluctuating temperature allows strains to separate if  $T_{min}$ ,  $T_{max}$  and  $\mu_{opt}$  are fixed, and evolutionary branching occurs. We simulated the strain separation and found results consistent with our theoretical approach. This may be a first step to understand how species coexist under fluctuating temperature. It could serve to find a criterion for selecting species with the highest growth rate under particular temperature conditions, which is of key interest for microalgae outdoor production.

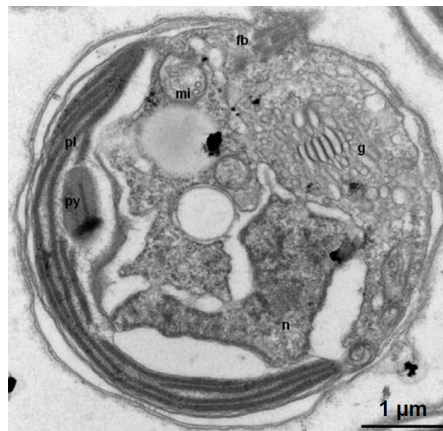
Summary of section 7:

- At constant temperature, the optimal temperature  $T_{opt}$  tends to equal the ambient temperature regardless of the underlying hypotheses on the cardinal temperatures.
- If  $\mu_{opt}$  is linked to  $T_{opt}$  (Eppley hypothesis and modified Eppley hypothesis), then the evolutionary equilibrium  $T_{opt}^*$  is always higher than the ambient temperature  $T$ .
- Under fluctuating temperatures,  $T_{opt}$  is always higher than or equal to the average temperature. This is enhanced by the modified Eppley hypothesis.
- Finally, if  $T_{min}$  and  $T_{max}$  are fixed and temperature is varying, strain separation through evolutionary branching can occur.

8

# Selecting thermal tolerant strains of the Haptophyceae *Tisochrysis* *lutea*

Contributors: Bonnefond, H., Mairet, F., Pruvost, E., Sciandra, A.,  
Bernard, O.



Picture of *Tisochrysis lutea* from a Transmission Electron Microscope

## 8.1 Introduction

In the 1990's, Bennett and Lenski [1993] carried several thermal adaptation experiments on *Escherichia coli* during several years for more than 2000 generations and obtained

## 8. SELECTING THERMAL TOLERANT STRAINS OF THE HAPTOPHYCEAE *TISOCHRYSIS LUTEA*

---

strains with enhanced thermal niche width. Since then, similar evolutionary experiments where temperature was driving the selective pressure have been carried out with UO. Most of the studies took place at a constant temperature to test the adaptation capability in a warmer world [Guyot et al., 2014, Julou, 2011]. Authors were searching for the key physiological mechanisms leading to temperature adaptation [Caspeta et al., 2014] and ways to infer a general theory of thermal adaptation [Kingsolver, 2009, Knies et al., 2009] (see section 1). These approaches were also used in biotechnology to enhance the productivity of some strains of industrial interest [Guyot et al., 2015, Wei et al., 2015].

In phytoplankton, thermal adaptation experiments are recent and mostly dedicated to the study of the global warming effect [Huertas et al., 2011, Reusch and Boyd, 2012]. Using ratchet protocols, these experiments proved that microalgae and cyanobacteria can indeed adapt in several months to (constant) temperatures which were initially lethal [Costas et al., 2014a,b, Huertas et al., 2011]. They also highlighted that this adaptation is preceded by phases of physiological acclimation and selection of pre-adapted individuals.

Here, we present the results of the selection experiment carried out with fluctuating temperatures by Bonnefond et al. [subm.]. Realized in chemostat, either in fed-batch mode or in turbidostat, the experimental conditions insure that nutrients were not limiting and that individuals with the highest average growth rate were selected in stressing conditions [Masci et al., 2008]. We analyze the result by re-constructing the competition and the adaptation story and try to represent the thermal evolution using the adaptive dynamics theory.

### 8.2 Selection experiment in controlled systems

#### 8.2.1 Summary of the experiment

The selection experiment was performed in two controlled systems, a chemostat in fed-batch mode (*i.e.* with periodical washout rate) and a turbidostat called ‘selectiostat’ (see section Material and Methods 2.1 and Bonnefond et al. [subm.] for more details). The phytoplankton strain used was derived from the Haptophyceae *Tisochrysis lutea* (CCAP 927/14) previously named *Isochrysis galbana* clone Tahiti [Bendif et al., 2013]. This strain (CCAP 927/17, called **W2X** here) resulted from a mutation/selection procedure, Bougaran et al. [2012] which enhanced its capability to store lipids. Indeed, it produced two times more neutral lipids under nitrogen starvation, without significant modification of the maximum growth rate in nitrogen replete conditions.

In the two cultures, a daily temperature cycle was applied consisting in 8 hours at low temperature and 16 hours at high temperature while the average temperature was maintained at 28°C. Each cycle was repeated at least for one week, and the cycles were elaborated to be progressively more selective (see fig. 8.2). If the growth rate was positive, the next cycle was started. If not, cultures stayed in the same cycle. The experiment was carried for 293 days with 10 cycles. In the last cycle, temperature varied between 12°C and 36°C.

### 8.2.2 Main results

The final strains were called **S-Turb** and **S-Fb** for the turbidostat and the fed-batch cultures, respectively. Strains' final thermal tolerance called  $\theta_{Turb}$  and  $\theta_{Fb}$  was determined using the TIP calibration device developed by Marchetti et al. [2012] (fig. 8.1) and the Bernard&Rémond model. Results showed that S-Turb and S-Fb have broader thermal niche width (11% and 22% more, respectively), a higher  $T_{opt}$  (1.4°C and 2.4°C higher) and a higher  $\mu_{opt}$  (10 % higher) than the initial strains W2X [Bonnefond et al., subm.] (fig. 8.1 and table 8.1). Bonnefond et al. [subm.] insisted on the stronger effect of cold temperatures on adaptation/selection.

**Table 8.1:** Bernard & Rémond model parameters for strains W2X, S-Turb and S-Fb. The error interval correspond to the mean  $\pm$  standard deviation determined by a jackknife analysis as in Bernard and Rémond [2012].

Strain	$T_{min}$ (°C)	$T_{opt}$ (°C)	$T_{max}$ (°C)	$\mu_{opt}$ (d <sup>-1</sup> )
W2X ( $\theta_{W2X}$ )	14.8 $\pm$ 1	26.3 $\pm$ 0.5	35.0 $\pm$ 0.5	1.1 $\pm$ 0.1
S-Turb ( $\theta_{Turb}$ )	12.4 $\pm$ 1	27.7 $\pm$ 0.5	34.9 $\pm$ 0.2	1.2 $\pm$ 0.1
S-Fb ( $\theta_{Fb}$ )	11.6 $\pm$ 2.5	28.8 $\pm$ 1	36.2 $\pm$ 2	1.2 $\pm$ 0.1

Bonnefond et al. [subm.] inferred that the experiment was split into three parts (fig. 8.2): first, from cycle 1 to cycle 5, *T. lutea* physiologically acclimated to the temperatures applied. For example, growth rate in turbidostat was higher than expected during these cycles because microalgae are synchronized by the temperature temporal periodicity [Bonnefond et al., 2016]. Second, from cycle 6 to cycle 8, individuals with pre-adaptive mutations were selected. This was considered to be pure selection, only based on competition. Third, from cycle 8 to cycle 10, adaptation was supposed to occur, resulting from apparition of new mutants (fig. 8.2). The different points in cycle 9, for example, corresponded to a gradual increase of the growth rate, possibly corresponding to adaptation.

We compared the theoretical thermal tolerance of strains S-Turb and S-Fb (using the Bernard&Rémond model parameters obtained by Bonnefond et al. [subm.]) to the growth rates measured during each cycle in each culture. We used the cardinal temperature values provided by the TIP experiment, performed several months after the end of the selection experiment. We neglected acclimation to temperature and assumed that growth instantaneously acclimated to a new temperature. We therefore simply computed the growth rate as follows, assuming that the transition phase between  $T_{low}$  and  $T_{high}$  was equivalent to one hour at average temperature:

$$\bar{\mu}_{th} = \frac{\tau_1}{24}\mu(T_{low}) + \frac{\tau_2}{24}\mu(T_{high}) + \frac{1}{24}\mu(T_{average}) \quad (8.1)$$

where  $T_{average}$  is equal to 28°C and with  $\tau_1 = 7.5$ h and  $\tau_2 = 15.5$ h. The model for strain S-Fb seems coherent ( $R^2 = 0.714$ , average error equal to 28.63%) even if gradual

## 8. SELECTING THERMAL TOLERANT STRAINS OF THE HAPTOPHYCEAE *TISOCHRYSIS LUTEA*

---

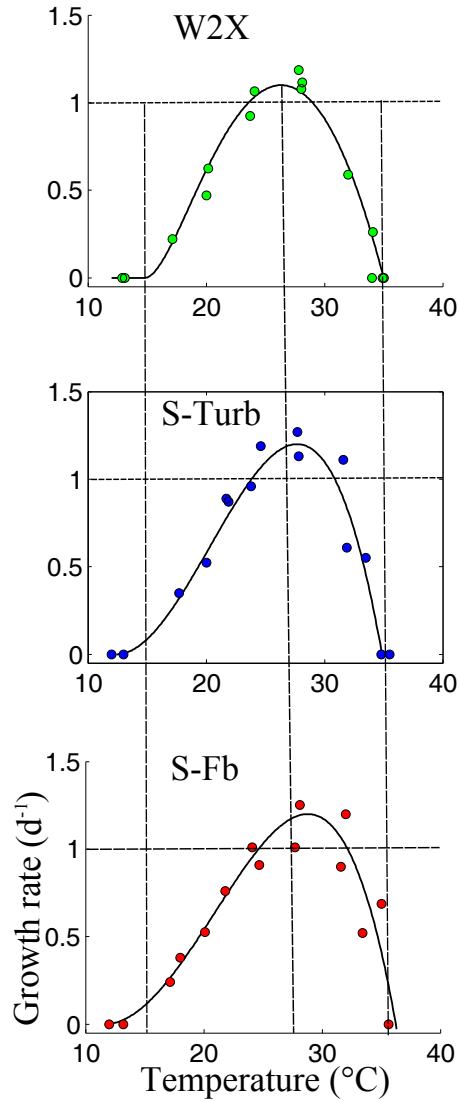


**Figure 8.1:** Thermal growth curves of the initial and adapted strains of *Tisochrysis lutea* - The data points result from the TIP calibration experiment. The black lines correspond to the Bernard&Rémond model with the parameters estimated in Bonnefond et al. [subm.].

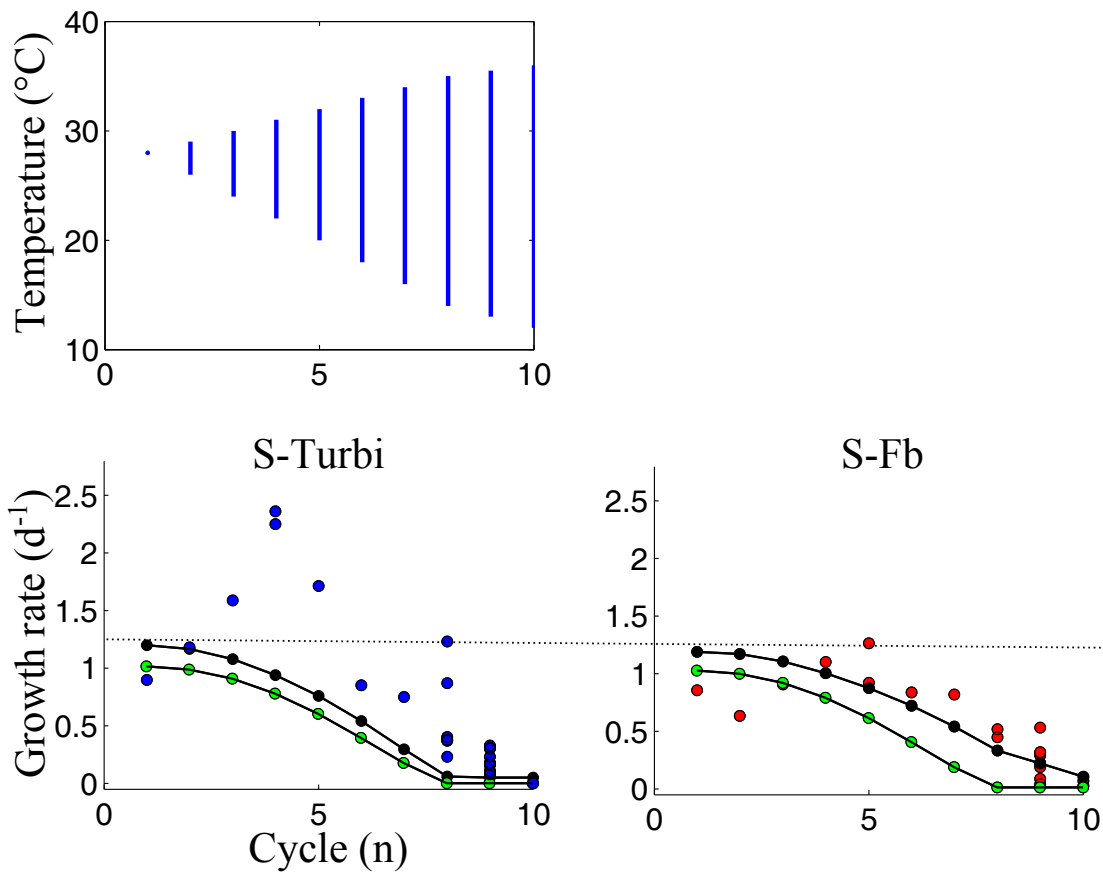


**Figure 8.2: Growth rates of the different strains during each cycle of the experiment** - Data points appear in blue and red for the turbidostat and the fed-batch cultures respectively. The black points correspond to the average theoretical growth rates for S-Turbi and S-Fb (corresponding to  $\bar{\mu}_{th}$ ). The green points correspond to the theoretical growth rate of the initial strain W2X. The blue lines on the top figure represent the temperatures daily applied to the cultures [Bonfond et al., *subm.*].



## 8. SELECTING THERMAL TOLERANT STRAINS OF THE HAPTOPHYCEAE *TISOCHRYSIS LUTEA*

---

adaptation of the growth rate appears inside each cycle, starting from cycle 8, which is not matched by the theoretical curve (fig. 8.2). For strain S-Turb, however, the difference between the simplistic model and the growth rates ( $R^2 = 0.62$ , average error equal to 63.27%) suggests that S-Turb thermal tolerance does not correspond to the effective thermal tolerance of the strain at the end of the experiment. This probably reflects the progressive modification of the strain phenotype. It may also result from the delay between the end of the selection experiment and the TIP. It is likely that, during this period, the strain maintained at 23°C have drifted. Two different hypotheses will then be tested in the following to represent the progressive adaptation of the strains in this fluctuating environment.

### 8.3 Modelling selection during the experiment

#### 8.3.1 Re-identification of the final thermal tolerance parameters

The thermal parameters derived from the TIP device for S-Turb and S-Fb cannot explain the dynamics observed during the selection experiment. Especially, the final strains obtained at the very end of the experiment seem more widely thermoresistant than the performance recorded 6 months later in the TIP. We thus re-identified parameters ( $T_{min}, T_{opt}, T_{max}, \mu_{opt}$ ) for S-Turb and S-Fb using different methods and considering that only selection occurred. Indeed, at the beginning of the experiment, and contrary to Huertas et al. [2011], Bonnefond et al. [subm.] chose to start with a polymorphic population. This imply that, first, the observed growth rate was a population average growth rate with potentially different individuals harvesting different phenotypes and, second, that pre-adapted individuals must exist. We successively used two methods for the parameters re-identification: i) Identification of the average population thermal parameters, ii) Identification considering two sub-populations.

##### 8.3.1.1 Identification at the population scale

At the population scale, the growth rate is averaged over the existing phenotypes and the population is considered as a single strain. We adjusted parameters ( $T_{min}, T_{opt}, T_{max}, \mu_{opt}$ ), that we called  $\hat{\theta}_{Turb}$  and  $\hat{\theta}_{Fb}$  for strains S-Turb and S-Fb, in order to match  $\bar{\mu}_{th}(\hat{\theta}_{Turb})$  and  $\bar{\mu}_{th}(\hat{\theta}_{Fb})$  (see eq. 8.1) to the maximal experimental growth rate for each cycle starting from cycle 5. In line with Bonnefond et al. [subm.], we considered that selection starts occurring during this cycle. The optimization consisted in searching for a parameter vector  $\theta$  minimizing the weighted ordinary least-squares criterion SSR using the matlab `fminsearch` function:

$$SSR(\theta) = \frac{1}{n} \sum_{i=1} w(i) [\mu_{exp}(cycle_i) - \bar{\mu}(T(cycle_i), \theta)]^2 \quad (8.2)$$

where  $\mu_{exp}(cycle_i)$  is the maximum experimental growth rate for cycle  $i$ ,  $n$  is the total number of cycles,  $T(cycle_i)$  corresponds to the temperatures applied at cycle  $i$  and  $w(i)$

### 8.3 Modelling selection during the experiment

---

is the weight associated to cycle  $i$ . The choice of a weighted SSR is motivated by the fact that we want to characterize the final strains, which have progressively emerged ( $w(i)$  is increasing from 0 to 1).

It is worth noting that the practical identifiability of eq. 8.2 is not guaranteed because  $\theta$  is a vector of 4 parameters while the experimental data set is scarce. The optimization was thus successively done by fixing three parameters and allowing only one to change. We then did the same for the cardinal temperatures taken two by two and we used each identified cardinal temperature set to initiate the 3 parameters  $\theta$  where only  $\mu_{opt}$  is fixed (see table 8.2). Finally, we identified the two parameters  $\theta$  under different possible assumptions: i) The thermal niche width is kept constant and  $\mu_{opt}$  and  $T_{opt}$  can change, ii) The thermal niche width is kept constant and  $\mu_{opt}$  is linked to  $T_{opt}$  according to eq. 5.1 (corresponding to the modified Eppley curve) for Haptophyta and Ochrophyta grouped together, iii) The thermal niche width is kept constant and  $\mu_{opt}$  is linked to  $T_{opt}$  according to the Eppley equation. For the two last approaches, the link between  $\mu_{opt}$  and  $T_{opt}$  is adapted to the value of  $\mu_{opt}$  at  $T_{opt}$  for the strain W2X (using a proportionality factor equal to 0.765%), assuming that the growth conditions are not perfectly optimal.

Results (table 8.2 and fig. 8.3, 8.4, 8.5, 8.6) show that, firstly, the identification with only 1 parameter is poor compared to the other identifications (fig. 8.3 and 8.4). This simple observation points towards the evidence that during the selection experiment, individuals with at least modification of two thermal parameters have been selected. When the three cardinal temperatures can simultaneously change,  $T_{min}$  tends to be very small. This is consistent with the experimental observations that the physiology of the microalgae (lipid structure) indicates an acclimation to low temperatures. The results obtained with the 3 cardinal temperatures are close to that obtained when calibrating only  $T_{min}$  and  $T_{max}$  (fig. 8.5). This may indicate that these two cardinal temperatures are the most important in the thermal selection process if  $\mu_{opt}$  is fixed. Finally, the result obtained with the modified Eppley hypothesis (method 7) gave the best results, comforting the idea that the hypothesized links between the thermal parameters makes sense. However, method 8 (Eppley curve) gives the nearest results, with higher  $\mu_{opt}$ .

A possible justification for the difference between  $\hat{\theta}_{T_{urb}}$ ,  $\hat{\theta}_{F_b}$  and  $\theta_{T_{urb}}$ ,  $\theta_{F_b}$  is that the strains continued to drift during their 6 months at 23°C before the TIP experiment. We conjecture that the thermal performance of the enhanced strains has been altered during this period. Moreover, this method with constant thermal parameters fails to represent the gradual modification of the growth rates along each cycle. To get further into selection, we considered a simple competition model.

**Table 8.2:** Re-identified parameters for strains S-Turb and S-Fb. The initial parameters which do not change appear in gray.

Parameter(s) identified	Strain	$T_{min}$ (°C)	$T_{opt}$ (°C)	$T_{max}$ (°C)	$\mu_{opt}$ (d <sup>-1</sup> )	R <sup>2</sup>	Method number
$T_{min}$	$\theta_{Turb}$	-3.4e+16	26.3	35.0	1.1	0.667	1
	$\theta_{Fb}$	-133.7	26.3	35.0	1.1	0.767	
$T_{opt}$	$\theta_{Turb}$	14.8	35.0	35.0	1.1	0.593	2
	$\theta_{Fb}$	14.8	34.6	35.0	1.1	0.588	
$T_{max}$	$\theta_{Turb}$	14.8	26.3	37.9	1.1	0.58	3
	$\theta_{Fb}$	14.8	26.3	38.0	1.1	0.857	
$\mu_{opt}$	$\theta_{Turb}$	14.8	26.3	35.0	1.3	0.502	4
	$\theta_{Fb}$	14.8	26.3	35.0	2.6	0.777	
$T_{min}, T_{opt}, T_{max}$ $\mu_{opt}$ fixed	$\theta_{Turb}$	-2.8	31.8	36.0	1.1	0.685	5
	$\theta_{Fb}$	12.0	26.3	40.6	1.1	0.872	
$\mu_{opt}$ and $T_{opt}$ ( $T_{max} - T_{min}$ ) fixed	$\theta_{Turb}$	16.1	27.7	36.4	2.5	0.658	6
	$\theta_{Fb}$	16.3	27.9	36.5	2.0	0.899	
$T_{min}$ and $T_{opt}$ ( $T_{max}$ and $\mu_{opt}$ linked to $T_{opt}$ , Ochrophyta and Haptophyta)	$\theta_{Turb}$	18.0	27.6	36.3	2.7	0.68	7
	$\theta_{Fb}$	15.8	28.1	36.8	1.3	0.915	
$T_{min}$ and $T_{opt}$ ( $T_{max}$ and $\mu_{opt}$ linked to $T_{opt}$ , Eppley curve)	$\theta_{Turb}$	17.0	28.6	37.4	1.6	0.632	8
	$\theta_{Fb}$	18.1	29.7	38.6	1.6	0.861	

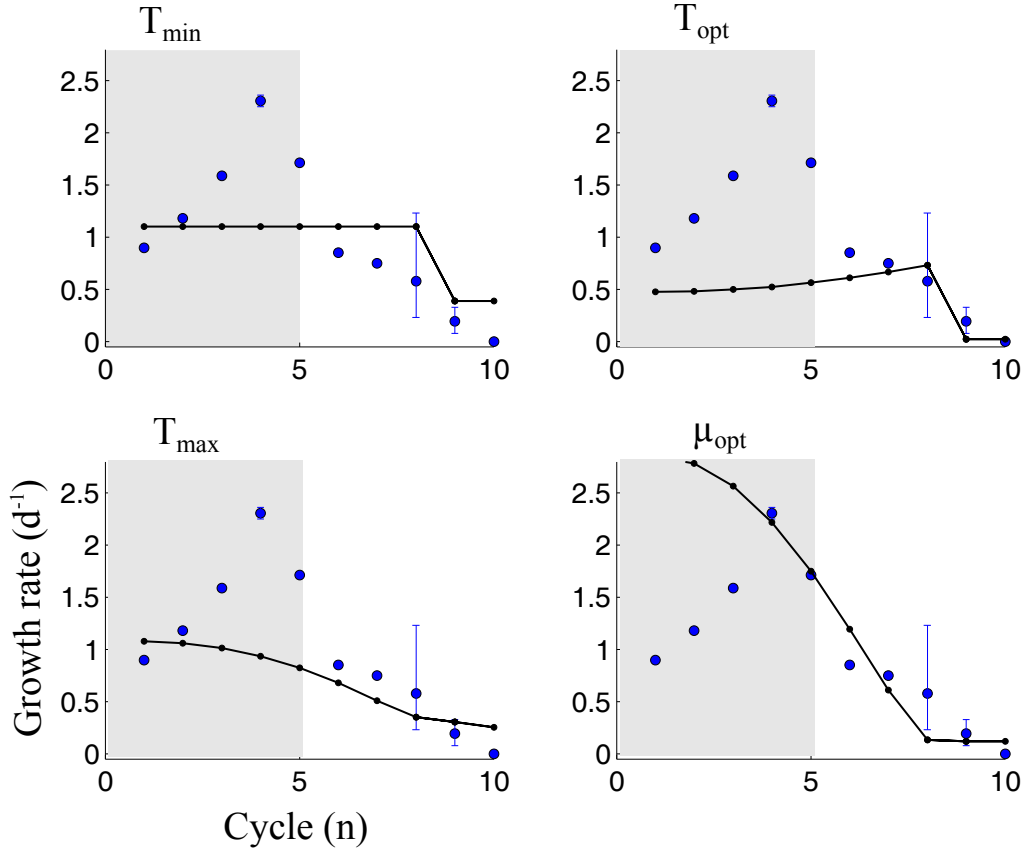


**Figure 8.3: Re-identified strains with one parameter for Turbidostat** - Data points appear in blue. The black points correspond to the average theoretical growth rates for  $\hat{\theta}_{Turb}$  and  $\hat{\theta}_{Fb}$ . Identification is done after the grey part. Bars represent minimal and maximal growth rate in each cycles.

### 8.3.1.2 Competition between two thermal phenotypes

The microalgal population variability can be described by a sum of polymorphic sub-populations competing cycles after cycles. As a first approach, we studied the competition between two sub-populations with two different phenotypes denoted  $x_1$  and  $x_2$  associated to growth rates  $\mu_1(T)$  and  $\mu_2(T)$ , respectively. We considered the following dynamical system:

$$\begin{aligned}\dot{x}_1 &= [\mu_1(T) - D(t)]x_1 \\ \dot{x}_2 &= [\mu_2(T) - D(t)]x_2\end{aligned}\tag{8.3}$$

where  $D(t)$  is the dilution rate. Starting from the first TIP of strain W2X, the competition between these populations has been simulated with the temperature profile

## 8. SELECTING THERMAL TOLERANT STRAINS OF THE HAPTOPHYCEAE *TISOCHRYSIS LUTEA*

---

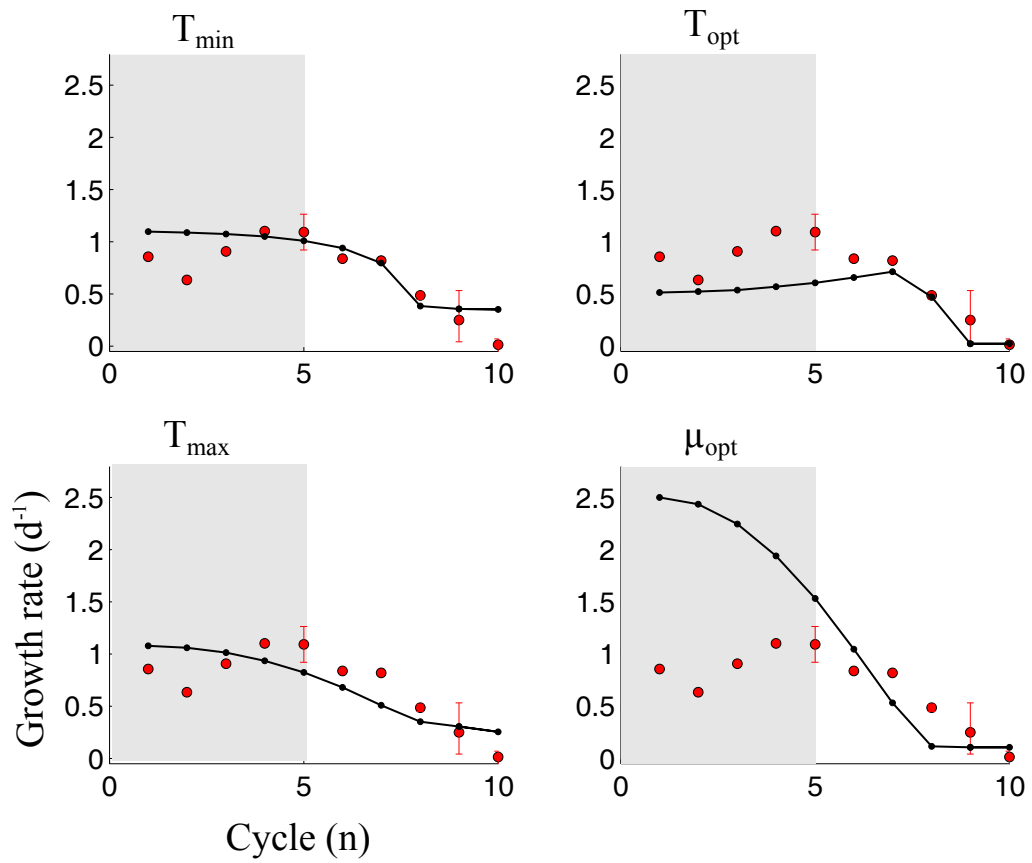


**Figure 8.4: Re-identified strains with one parameter for Fed-batch** - Data points appear in red. The black points correspond to the average theoretical growth rates for  $\hat{\theta}_{T_{urb}}$  and  $\hat{\theta}_{Fb}$ . Identification is done after the grey part. Bars represent minimal and maximal growth rate in each cycles.

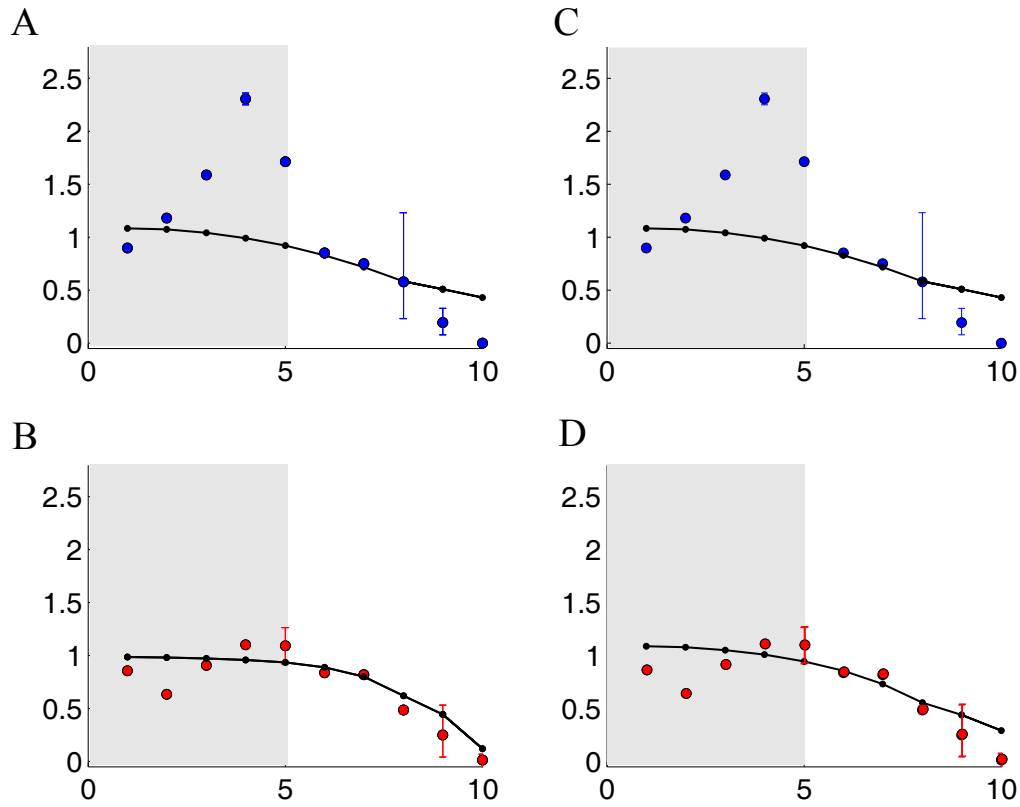


**Figure 8.5: Re-identified strains using method 5** - Data points appear in blue and red for the turbidostat and the fed-batch cultures respectively. The black points correspond to the average theoretical growth rates for  $\hat{\theta}_{Turb}$  (A) and  $\hat{\theta}_{Fb}$  (B) with method 5 (see table 8.2). C and D correspond to the same identification but with parameters  $T_{min}$ ,  $T_{max}$ . Identification is done after the grey part. Bars represent minimal and maximal growth rate in each cycles.

## 8. SELECTING THERMAL TOLERANT STRAINS OF THE HAPTOPHYCEAE *TISOCHRYSIS LUTEA*

---

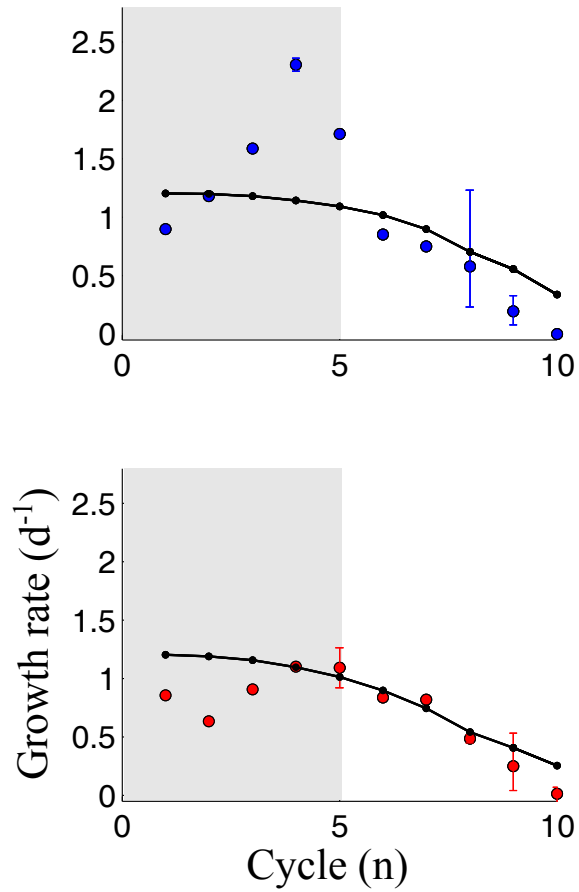


**Figure 8.6: Re-identified strains using method 7** - Data points appear in blue and red for the turbidostat and the fed-batch cultures respectively. The black points correspond to the average theoretical growth rates for  $\hat{\theta}_{Turb}$  (A) and  $\hat{\theta}_{Fb}$  (B) with method 7 (see table 8.2). Identification is done after the grey part. Bars represent minimal and maximal growth rate in each cycles.

### 8.3 Modelling selection during the experiment

---

experienced during the selection experiment and, after that, the temperature of 23°C experienced during 6 months before the TIP. We finally took into account this final TIP (see fig. 8.7). Set  $z = x_2/x_1$  in Equations (8.3). Then:

$$\dot{z} = [\mu_2(T) - \mu_1(T)]z = \Delta\mu z \quad (8.4)$$

and so:

$$z(t) = z(0)e^{\Delta\mu(T)t} \quad (8.5)$$

We computed  $\Delta\mu(T)$  from the daily average difference between competitors,  $\Delta\bar{\mu}(T)$ . Contrary to section 8.3.1.1, we account for the detailed temperature history. To avoid practical identification problems, we reduced the parameter numbers from 9 to 3 by considering that the thermal niche width is constant, that  $T_{max}$  is linearly linked to  $T_{opt}$  and that  $\mu_{opt}$  follows a modified Eppley curve (in the same way as section 8.3.1.1). To ensure that none of the competitors are never extinct, we saturated the minimum value of  $z$  to  $10^{-10}$ .

Results (table 8.3 and fig. 8.8) show that, for both cultures, an initial strain (corresponding here to  $x_1$ ) is solely responsible for the W2X TIP response and that a final strain (corresponding here to  $x_2$ ) is also, in the same way, only responsible for the final TIP response. The invasion of the final strain is rapid (40.5 days and 32.5 days for turbidostat and fed-batch cultures, respectively to reach  $z = 10^2$ ). It takes place during the first cycle of the selection experiment (constant temperature of 28°C). Experimentally, we observe an increase of growth rate during cycle reiterations (cycle 8 and 9), which is probably due to the emergence of a new strain. From the simulation, we can infer that the final strain was not present initially (otherwise, it would have emerged before the last cycles). During the storage period carried after the selection experiment with a constant temperature applied for 6 months, the  $z$  ratio  $x_1/x_2$  tends to increase again, but the  $\Delta\mu(T)$  is too low to insure that the initial strain  $x_1$  can replace the strain  $x_2$ . Additional simulations indicate that, in these constant conditions, it would take 253 days and 287 days for  $x_1$  in the turbidostat and fed-batch cultures respectively to overcome  $x_2$  (starting from  $z = 10^{-10}$  and with parameters as specified in table 8.3).

The two competitors method has clear limitations since it cannot take into account a wide initial diversity and thus poorly represents the gradual selection assumed to take place in the cultures. A competition model with  $n$  competitors would be more accurate, but its calibration would be very tricky. Moreover, to represent adaptation, we must take into account mutants apparition. In this perspective, we used the adaptive dynamics theory.





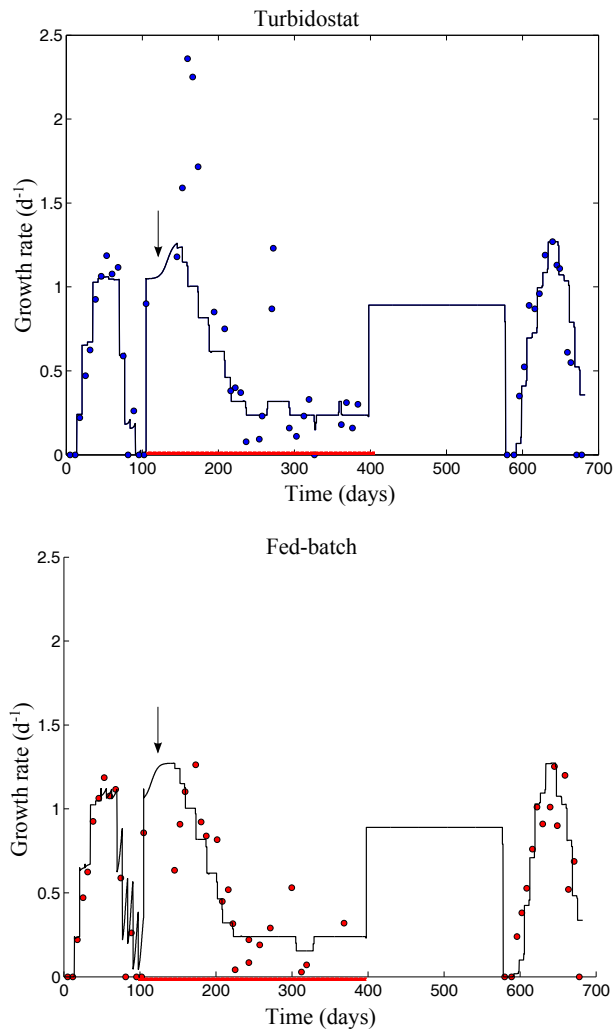


**Figure 8.8: Competition dynamics for the Fed-batch culture** - Growth rate data points appear in blue and red. The black line corresponds to the modelled population overall growth rate. The arrow shows the invasion time. The red line corresponds to the selection experiment period.

## 8.4 Modelling thermal adaptation during the experiment

### 8.4.1 Determining the invasion fitness

In section 7, we have shown that it is possible to use the adaptive dynamics theory with a simple chemostat model when the temperature applied is periodical and piecewise constant. Here, we have to show the same in a turbidostat and in a fed-batch mode. We

## 8. SELECTING THERMAL TOLERANT STRAINS OF THE HAPTOPHYCEAE *TISOCHRYSIS LUTEA*

---

therefore modelled the population dynamics in each culture mode.

### 8.4.1.1 Population dynamics, invasion fitness and selection gradient in a turbidostat growth model

Consider the following system:

$$M_{Turb} : \begin{cases} \dot{S} &= D(t)(S_{in} - S) - \mu(T(t))\rho(S)X \\ \dot{X} &= \mu(T(t))\rho(S)X - D(t)X \end{cases} \quad (8.6)$$

In the turbidostat mode,  $D$  is automatically adjusted to the growth rate to maintain a constant biomass:

$$D(t) = \mu(T(t))\rho(S) \quad (8.7)$$

where  $T(t)$  is time varying according to eq. 7.24. In the turbidostat mode, the microalgae biomass  $X$  is supposed to reach the consign biomass  $X_{co}$ . Eq. 8.7 insures that  $\dot{X} = 0$ . It is thus possible to find the following positive equilibrium:

$$\begin{aligned} S^* &= S_{in} - X_{co} \\ X^* &= X_{co} \end{aligned} \quad (8.8)$$

This equilibrium is stable thanks to a dedicated control approach to satisfy equation (8.7). Thus, we can use system ( $M_{Turb}$ ) in an evolutionary perspective using the adaptive dynamics theory. Based on the same method as in section 7.4.2, we can define the invasion fitness of a mutant with trait  $a_{mut}$  in the resident population with trait  $a$  at equilibrium, averaged over a temperature cycle:

$$\bar{f}_{Turb}(a_{mut}, a) = 1/\tau \int_{t_0}^{t_0+\tau} \bar{\mu}_m(T(t))\rho(S^*) - \bar{\mu}(T(t))\rho(S^*) dt \quad (8.9)$$

We can deduce the average selection gradient:

$$\begin{aligned} \left. \frac{\partial \bar{f}_{Turb}(a_{mut}, a)}{\partial a_{mut}} \right|_{a_{mut}=a} &= 1/\tau \int_{t_0}^{t_0+\tau} \frac{\lambda'(a_{mut}, T(t))\beta(a_{mut}, T(t)) - \beta'(a_{mut}, T(t))\lambda(a_{mut}, T(t))}{\beta(a_{mut}, T(t))^2} \\ &\cdot g(a_{mut}) + g'(a_{mut}) \frac{\lambda(a_{mut}, T(t))}{\beta(a_{mut}, T(t))} dt \end{aligned} \quad (8.10)$$

where  $g(a_{mut})$  represents the link between  $\mu_{opt}$  and  $a_{mut}$  (*i.e.*  $T_{opt}$ ).

### 8.4.1.2 Population dynamics, invasion fitness and selection gradient in a fed-batch growth model

Similarly, consider the following system:

$$M_{Fb} : \begin{cases} \dot{S} &= D(t)(S_{in} - S) - \mu(T(t))\rho(S)X \\ \dot{X} &= \mu(T(t))\rho(S)X - D(t)X \end{cases} \quad (8.11)$$

We assume that the invasion fitness is the same as in the turbidostat culture.

### 8.4.2 Evolutionary dynamics

Eq. 8.10 can be used to study the evolutionary dynamics of the considered adaptive trait, here  $a = T_{opt}$ . Here, we assume a constant thermal niche width equal to that of the W2X strain;  $T_{min}$  and  $T_{max}$  are thus linearly linked to  $T_{opt}$  as in eq. 4.1 but with  $a_1 = 1$ ,  $a_2 = 1$ ,  $b_1 = 8.68$ ,  $b_2 = 11.53$ . Moreover,  $\mu_{opt}$  is linked to  $T_{opt}$  as in section 8.3.1.1 with the same proportionality factor. We obtained the two following canonical equations:

$$\dot{a}_{mut_{Turb}} = M_{p_{Turb}} \sigma_{Turb} X_{Turb}^* \left. \frac{\partial \bar{f}_{Turb}(a_{mut}, a)}{\partial a_{mut}} \right|_{a_{mut}=a} \quad (8.12)$$

$$\dot{a}_{mut_{Fb}} = M_{p_{Fb}} \sigma_{Fb} X_{Fb}^* \left. \frac{\partial \bar{f}_{Fb}(a_{mut}, a)}{\partial a_{mut}} \right|_{a_{mut}=a} \quad (8.13)$$

where  $M_p$  is the probability to be a mutant at each apparition, and  $\sigma$  is the mutation step. We simulated eq. 8.12 and 8.13 in the real temperature conditions of the selection experiment. We calibrated the value of the product  $M_p \sigma$  on experimental data using the Sum of Squared Residual criterion and the matlab function `fminsearch`. Results (fig. 8.9 and 8.10) show that the evolutionary model correctly matches the growth rate dynamics (mean error equal to 10.94% and 14.32% respectively, including the TIP experimental points). With this model, the gradual increase within a selection cycle is represented (fig. 8.9 B and 8.10 B). Taking into account the slide effect related to the 6 months of storage at 23°C, we are able to reproduce the final results of the TIP for both strains  $S_{Turb}$  and  $S_{Fb}$  (fig. 8.9 C and 8.10 C). Interestingly, at the end of the selection experiment (*i.e.* day 292), the strains obtained for the turbidostat and fed-batch modes were apparently more thermoresistant at high temperatures and had a higher  $\mu_{opt}$  than S-Turb and S-Fb, equal to 1.327 d<sup>-1</sup> and 1.325 d<sup>-1</sup> respectively ( $T_{opt}=28.98^\circ\text{C}$  and  $T_{opt}=28.97^\circ\text{C}$ ) (fig. 8.9 C and 8.10 C). But this feature was lost during the conservation period.

The hypothesis of a constant thermal niche width during adaptation is not fully coherent with the thermal parameters obtained for S-Turb and S-Fb. This is especially related to the poor knowledge we have of how  $T_{min}$  evolution is affected by temperature in microalgae. To better represent the evolutionary dynamics of *T. lutea*, we replaced  $a_2$  and  $b_2$  by the interpolation between the results found for W2X, S-Turb and S-Fb, *i.e.*  $a_2 = -1.310$ ,  $b_2 = 49.021$ . Simulations give a mean error equal to 1.53% and 3.81% for the turbidostat and the fed-batch, respectively, arguing towards a global increase of the thermal niche width during the experiment.

It is worth noting that adaptive dynamics assumes that the mutant invasion is fast enough to be negligible. In section 8.3.1.2, we have shown that a strain  $x_2$  can rapidly replaces another resident strain  $x_1$  if the ratio  $x_1/x_2$  is not too low, *i.e.*  $x_1/x_2 < 10^3$ . Additional calculations show that a mutant  $x_2$  with a thermal parameter set equal to  $\theta_{Fb}$  would totally replace a resident  $x_1$  with a thermal parameter set equal to  $\theta_{W2X}$  in 73 days during cycle 8 if initially  $x_1/x_2 = 10^8$  (*i.e.* total replacement is considered up to  $x_1/x_2 < 10^{-2}$ ). Such timescale represents 25% of the selection experiment duration and is not negligible. Moreover, adaptive dynamics only considers mutation/selection

## 8. SELECTING THERMAL TOLERANT STRAINS OF THE HAPTOPHYCEAE *TISOCHRYSIS LUTEA*

---

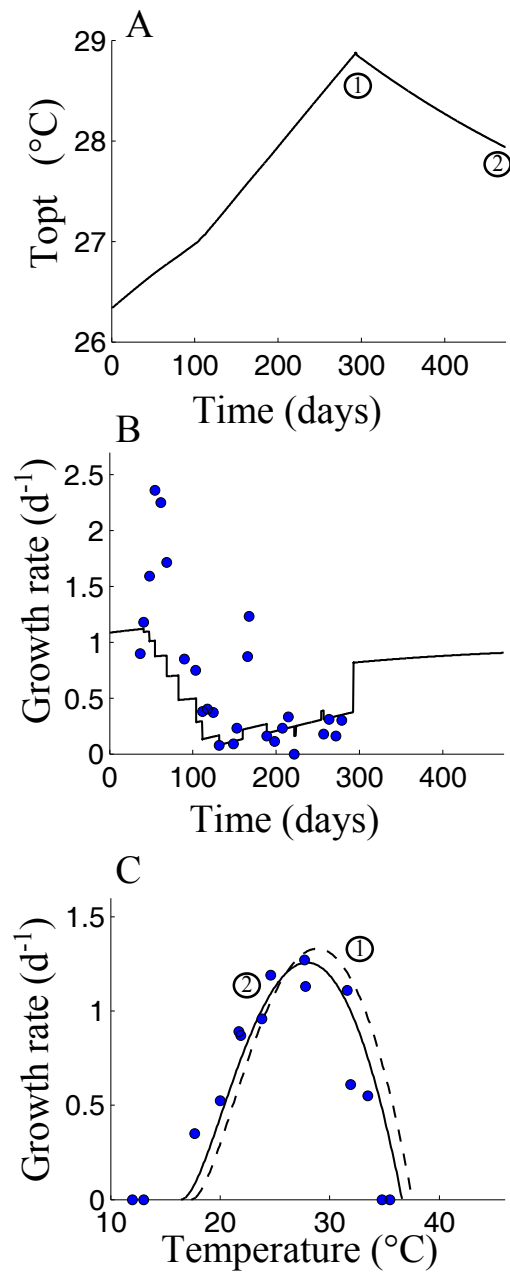


**Figure 8.9: Adaptation during the selection experiment in turbidostat** - Experimental growth rates appear in blue. The black line represents the modelled growth rate. A, evolution of  $T_{opt}$  during the selection experiment and the storage period. B, evolution of the population growth rate. C, strain thermal growth curve obtained at the end of the selection experiment (2) and at the end of the storage period (1).

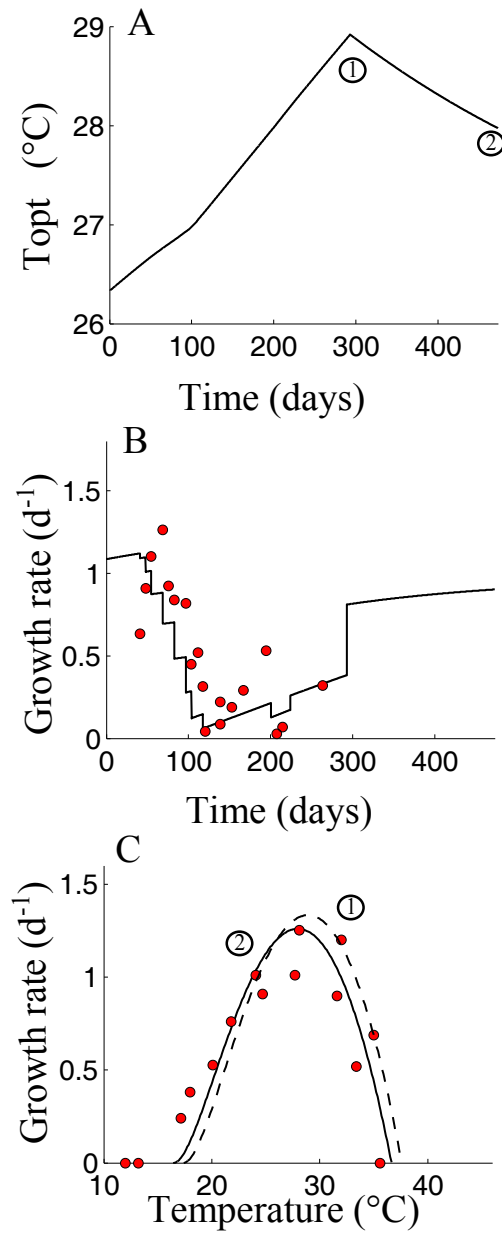


**Figure 8.10: Adaptation during the selection experiment in fed-batch** - Experimental growth rates appear in blue. The black line represents the modelled growth rate. A, evolution of  $T_{opt}$  during the selection experiment and the storage period. B, evolution of the population growth rate. C, strain thermal growth curve obtained at the end of the selection experiment (2) and at the end of the storage period (1).

## 8. SELECTING THERMAL TOLERANT STRAINS OF THE HAPTOPHYCEAE *TISOCHRYSIS LUTEA*

with small steps, which is not necessarily the case in this example. Even if an evolutionary framework gives coherent results here and shows adaptation inside a temperature cycle, it is thus tricky to differentiate selection from adaptation at that stage. Costas et al. [2014b] and Costas et al. [2014a] carried evolution experiments by gradually increasing the temperature medium of several microalgae, including *Isochrysis galbana*. To differentiate between acclimation, selection and adaptation, they separated the initial population into clones of the different thermal genotypes. If all genotypes survived, they considered that acclimation occurred; if only several genotypes survived, it was selection. If they all initially experienced massive mortality, then it was adaptation, either due to mutation or still possibly due to selection of rare pre-adapted individuals. Interestingly, they observed that 75 days of adaptation at 35°C were necessary for *Isochrysis galbana* to detect a growth in the population.

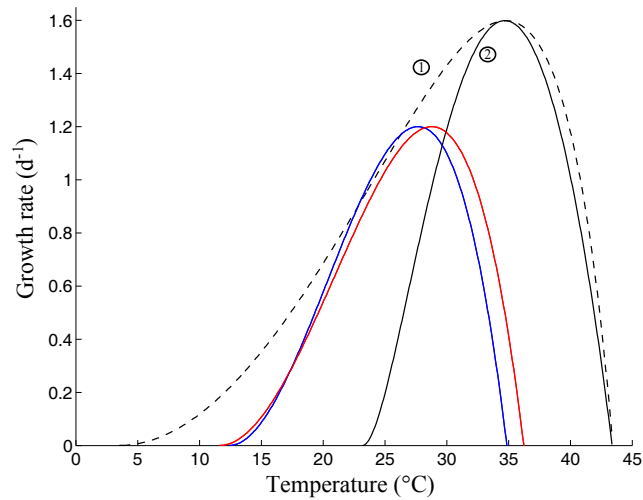


**Figure 8.11: Thermal growth curve at the evolutionary equilibrium** - The black line (1) corresponds to the evolutionary equilibrium for the fixed thermal niched width hypothesis, the black dashed line (2) to the  $T_{min}$  linearly linked to  $T_{opt}$  hypothesis according to the W2X, S-Turb and S-Fb parameters link. S-Turb and S-Fb are represented in blue and red respectively.

### 8.4.3 Evolutionary equilibrium

It is very likely that microalgae did not reach the evolutionary equilibrium even at the end of the selection experiment. We looked at the evolutionary equilibrium that microalgae would have reached if we had waited for a sufficient time in the condition of cycle 9. Results (fig. 8.11) show that starting from W2X and using parameters  $M_p$  and  $\sigma$  found in section 8.4.2, it would have taken 2128 days and 2122 days (with turbidostat and fed-batch parameters respectively) to reach the equilibrium, with  $T_{opt}^* = 34.772^\circ\text{C}$  and  $\mu_{opt}^* = 1.598\text{d}^{-1}$ . Linking  $T_{min}$  to  $T_{opt}$  according to strains W2X, S-Turb and S-Fb, the

model predicted a drastic increase in the thermal niche up to  $40.95^{\circ}\text{C}$  ( $T_{min}^* = 4.97^{\circ}\text{C}$ ). This prediction is probably overestimated, but highlights a potential gain for a longer experiment.

## 8.5 Conclusion

We proved that the selection experiment did produce thermally enhanced strains. We showed that it resulted from a combination of competition of pre-adapted individuals and adaptations. Separating clearly these two phases is however very tricky. Moreover, the permanent acclimation of the cells to the fluctuating temperature makes the picture more complex, and an additional model to quantify this effect would help to decipher the effect of these three mechanisms. The analysis of the experimental results reveals that the relationship between the thermal parameters stated in this thesis seems to be valid in *Tisochrysis lutea*. However,  $T_{min}$  appears to be more flexible from an evolutionary point of view. A more accurate protocol to determine  $T_{min}$  would be required to explore more extensively the consequence of adaptation on the response at low temperatures.



## 8. SELECTING THERMAL TOLERANT STRAINS OF THE HAPTOPHYCEAE *TISOCHRYSIS LUTEA*

---

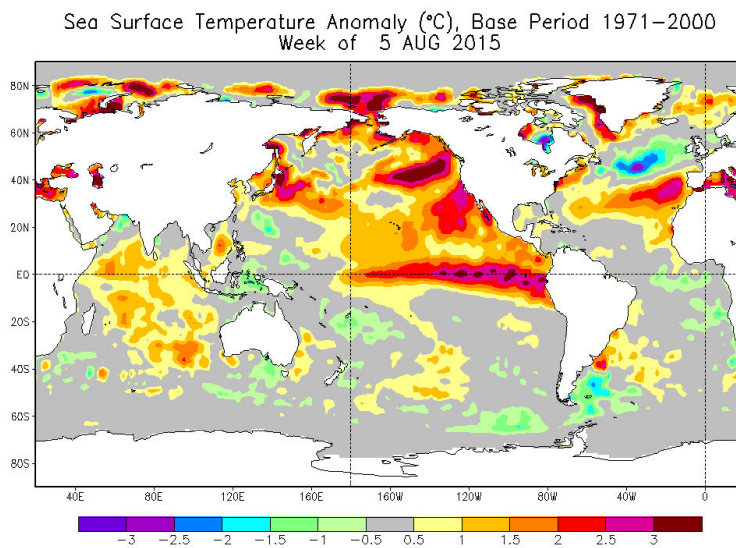
### Summary of section 8:

- We carried a selection experiment with fluctuating temperatures and obtained thermally enhanced strains
- We were not able to distinguish between competition/selection *stricto sensu* and evolution
- However, evolution did occur and the adaptive dynamics model well captures the evolutionary trajectories
- The link between the thermal parameters are coherent, but we failed to represent the ‘autonomous’ evolution of  $T_{min}$
- This is a first step for designing optimal experiment for directed evolution

9

# Modelling the effect of temperature on phytoplankton growth across the global ocean

Contributors: Ayata, S. D., Mairet, F., LeGuennec, V., Sciandra, A., Bernard, O.



Sea Surface Temperature anomaly.

## 9. MODELLING THE EFFECT OF TEMPERATURE ON PHYTOPLANKTON GROWTH ACROSS THE GLOBAL OCEAN

---

### 9.1 Introduction

In the oceans, phytoplankton are the input point of inorganic carbon in the trophic net thanks to photosynthesis and form the base of marine food web. They play a key role in biogeochemical cycles at global scale [Falkowski et al., 1998]. Their activity depends on many factors, primarily light, nutrient availability and temperature [Falkowski and Raven, 2007]. In the context of global warming, predicting how the ocean temperature increase will affect marine phytoplankton is a challenging issue.

Since the past decade, scientists have tried to figure out how phytoplankton would deal with a warmer world. First of all, Huertas et al. [2011] (and later Costas et al. [2014b] and Costas et al. [2014a]) carried warming experiments in batch cultures of 12 phytoplankton species belonging to 4 major phytoplankton groups. Their results highlight phytoplankton capacity to adapt to constant warm temperatures, particularly for species living in areas with high temperatures fluctuations. The need for experimental evolution became an evidence [Reusch and Boyd, 2012]. Later, Thomas et al. [2012] analysed a vast database of phytoplankton thermal growth curves, comparing their thermal tolerance to their extraction site in the ocean. They showed that variation in phytoplankton temperature optima over latitude is linked to a gradient in mean ocean temperature. They tried to reconstruct the observed thermal repartition using the adaptive dynamic theory based on a competition model between phytoplankton species. The main result of this study is the supposed high sensitivity of tropical and polar strains to warming because of their close maximal temperature tolerance to ambient temperature.

The race to phytoplankton study in a warming world was then launched. Toseland et al. [2013] and [Yvon-Durocher et al., 2015] tried to predict how warming would modify phytoplankton stoichiometry, particularly the N:P ratio, and how it would affect biogeochemical cycles. [Dutkiewicz et al., 2013] modelled future ‘*winners and losers*’, mostly resulting from the effect of temperature on nutrient availability. Padfield et al. [2015b] got insight into phytoplankton thermal adaptation by submitting the well known *Chlorella vulgaris* Chlorophyceae species to a 2°C warming above its basic upper thermal limit. They emphasized the role of carbon-use efficiency during adaptation and the high speed of adaptation (less than 100 generations). Finally, a community-wide publication aimed to standardise phytoplankton thermal study in the laboratory for future modelling and prediction of eco-regional phytoplankton changes [Boyd et al., 2013]. In line with Boyd et al. [2013], a thermal evolution experiments was carried by Listmann et al. [2016] on the key phytoplankton species *Emiliana huxleyi*.

In 2014, Marañón et al. [2014] were still rather sceptical and claimed that ‘*Biogeographic patterns in phytoplankton size structure and growth rate are independent of temperature and driven mainly by changes in resource supply*’. However, the methods leading to this conclusion are controversial (see section 5.2.3). Moreover, these results are in contradiction with [Reuman et al., 2014] who modelled competition for nutrient in concordance with temperature and cell size in phytoplankton. Chen [2015] deeply confirmed the effect of temperature on phytoplankton repartition at global ocean scale and the implication of warming, extending the Thomas et al. [2012] database.

[Thomas et al., 2015] then enhanced again this database, finding that ‘*functional groups differ strongly in their patterns of adaptation: traits are similar in hot tropical environments, but diverge at temperate latitudes*’.

We focus here on temperature as an evolutionary driver in phytoplankton at global scale with a modelling point of view. Evolution of phytoplankton facing realistic temperature conditions has already been modeled by Thomas et al. [2012] using Norberg [2004] model and by Grimaud et al. [2014a] using Bernard and Rémond [2012] model (see chapter 7). In line with Thomas et al. [2012] and Grimaud et al. [2014a], we used the adaptive dynamics theory to study a given temperature-dependent growth model in an evolutionary perspective. Nevertheless, we proposed an original approach showing that the study of evolutionary equilibrium can be reduce to a function optimization problem. By doing so, we drastically decreased the computational time required to compute the evolutionary equilibrium and we were able to predict the evolutionary outcomes at the global ocean scale. We validated our approach on a data set of 194 observations (extracted from Thomas et al. [2012]) of the temperature response for different species for which isolation sites are known. We compared different hypotheses, and we addressed the questions of how phytoplankton adapts to *in situ* temperature variations, investigating the implications at global scale.

## 9.2 Evolutionary model for thermal adaptation

### 9.2.1 Slow-fast dynamical system

First, we consider a simplified chemostat model to focus on the adaptation mechanisms driven by temperature. We tested two different models to represent the impact of temperature on phytoplankton growth rate:

$$\mu_B(T(t)) = \phi(T(t)) \quad (\text{horizontal – shift hypothesis}) \quad (9.1)$$

$$\mu_E(T(t)) = Ep(T_{opt})\phi(T(t)) \quad (\text{Eppley hypothesis}) \quad (9.2)$$

where  $\phi(T(t))$  is the CTMI model and  $Ep(T_{opt})$  is the Eppley curve linking  $T_{opt}$  to  $\mu_{opt}$ .

In line with Grimaud et al. [2014a], we included eq.(9.1), eq.(9.2) in a simple chemostat model of phytoplankton growth with varying temperature:

$$M^\epsilon : \begin{cases} \dot{S} &= f_S(S, X, T(t)) = D(S_{in} - S) - \mu(T(t))\rho(S)X \\ \dot{X} &= f_X(S, X, T(t)) = [\mu(T(t))\rho(S) - D]X \\ \dot{T} &= \epsilon f_T(t) = \epsilon \cos(\omega t) \end{cases} \quad (9.3)$$

$S$  is the nutrient concentration in the chemostat,  $S_{in}$  is the inflow substrate concentration,  $X$  is the algal biomass concentration,  $\mu(T(t))$  is either  $\mu_B(T(t))$  or  $\mu_E(T(t))$  or  $\mu_{ME}(T(t))$ ,  $f_T(t)$  is a periodic function (reflecting seasonality),  $D$  is the dilution rate with  $D < \mu(T(t))\rho(S_{in}) \forall t$ , and  $\rho(S)$  is the substrate uptake defined as:

$$\rho(S) = \frac{S}{K + S} \quad (9.4)$$

## 9. MODELLING THE EFFECT OF TEMPERATURE ON PHYTOPLANKTON GROWTH ACROSS THE GLOBAL OCEAN

---

where  $K$  is a half-saturation coefficient. We consider that growth, in term of carbon fixation, is fast compared to temperature fluctuations, *i.e.*  $\epsilon$  is a small positive parameter. It is possible to analyze system  $(M^\epsilon)$  using the Singular Perturbation Theory [Tikhonov, 1952]. The fast dynamics, where  $T(t) = T(0)$ , corresponds to the classical chemostat model:

$$\begin{cases} \dot{S} &= f_S(S, X, T(t)) \\ \dot{X} &= f_X(S, X, T(t)) \end{cases} \quad (9.5)$$

System (9.5) has a unique positive globally asymptotically stable equilibrium  $(S^*(T(t)), X^*(T(t))) \in \mathbb{R}_+^2$  (see e.g. Grimaud et al. [2014a]), where:

$$S^*(T(t)) = \frac{KD}{\mu(T(t)) - D} \quad (9.6)$$

$$X^*(T(t)) = (S_{in} - S^*(T(t)))$$

The slow dynamics is given by:

$$M^0 : \begin{cases} S^*(T(t)) &= \frac{KD}{\mu(T(t)) - D} \\ X^*(T(t)) &= (S_{in} - S^*(T(t))) \\ \dot{T} &= \epsilon f_T(t), \quad T(0) = T_0 \end{cases} \quad (9.7)$$

The reduced system  $(M^0)$  admits a unique solution  $T^*(t)$ :

$$T^*(t) = T_0 + \frac{\epsilon}{\omega} \sin(\omega t) \quad (9.8)$$

Tikhonov's theorem [Tikhonov, 1952] allows us to conclude:

**Proposition 9.2.1** *For sufficiently small values of  $\epsilon > 0$ , system  $(M^\epsilon)$  admits a unique positive solution  $(X^\epsilon(t); S^\epsilon(t); T^\epsilon(t))$  on  $[0; \tau]$ , where  $0 < \tau < +\infty$ . Moreover:*

$$\begin{aligned} \lim_{\epsilon \rightarrow 0} S^\epsilon(t) &= S^*(t) \\ \lim_{\epsilon \rightarrow 0} X^\epsilon(t) &= X^*(t) \end{aligned} \quad (9.9)$$

From a biological point of view, prop 9.2.1 shows that phytoplankton populations are always at equilibrium because growth is faster than long-term temperature variations. Assuming small annual temperature fluctuations of amplitude  $\delta$ , we obtain  $\epsilon = \delta\omega \ll 1$ . The long-term (*i. e.* annual) dynamics of the algal biomass can thus be approximated by:

$$\begin{aligned} S^*(T(t)) &= \frac{KD}{\mu(T(t)) - D} \\ X^*(T(t)) &= (S_{in} - S^*(T(t))) \\ T(t) &= T_0 + \delta \sin(\omega t) \end{aligned} \quad (9.10)$$

### 9.2.2 Evolutionary model using Adaptive Dynamics theory

We now study system  $(M^\epsilon)$  in an evolutionary perspective using the adaptive dynamics theory [Dieckmann and Law, 1996]. To do so we allow one parameter to evolve, called the adaptive trait, here  $T_{opt}$ . One mutant  $X_{mut}$  appears in the resident population at equilibrium with a different value of  $T_{opt}$ ,  $T_{opt}^{mut}$ :

$$M_{mut}^\epsilon : \begin{cases} \dot{S} &= S^*(T(t), T_{opt}) \\ \dot{X} &= X^*(T(t), T_{opt}) \\ \dot{X}_{mut} &= f_{X_{mut}}(T(t), T_{opt}, T_{opt}^{mut})X_{mut} \\ &= [\mu_{mut}(T(t))\rho(S) - D]X_{mut} \\ \dot{T} &= \epsilon f_T(t) \end{cases} \quad (9.11)$$

Assuming that the mutant is initially rare, we compute the mutant growth rate in the resident population,  $f_{X_{mut}}(T(t), T_{opt}, T_{opt}^{mut})$ . Depending on the sign of  $f_{X_{mut}}(T(t), T_{opt}, T_{opt}^{mut})$ , the mutant can invade and replace the resident or not. Prop 9.2.1 insures that resident population is actually at equilibrium during mutant invasion. Here, because  $T$  is a periodically time varying variable of period  $\tau$ , we use the time average mutant growth rate [Ripa and Dieckmann, 2013]:

$$\langle f_{X_{mut}}(T_{opt}, T_{opt}^{mut}) \rangle = \frac{1}{\tau} \int_0^\tau f_{X_{mut}}(T(t), T_{opt}, T_{opt}^{mut}) dt \quad (9.12)$$

We then compute the selection gradient  $g(T_{opt}, T_{opt}^{mut})$  which gives the selection direction (*e.g.* growing or decreasing values of  $T_{opt}$  are selected through evolution). The selection gradient is defined as the partial derivative of the time average mutant growth rate with respect to  $T_{opt}^{mut}$  evaluated in  $T_{opt}^{mut} = T_{opt}$ :

$$g(T_{opt}, T_{opt}^{mut}) = \left. \frac{\partial \langle f_{X_{mut}}(T_{opt}, T_{opt}^{mut}) \rangle}{\partial T_{opt}^{mut}} \right|_{T_{opt}^{mut}=T_{opt}} \quad (9.13)$$

At the evolutionary equilibrium, the selection gradient is equal to zero:

$$\left. \frac{\partial \langle f_{X_{mut}}(T_{opt}, T_{opt}^{mut}) \rangle}{\partial T_{opt}^{mut}} \right|_{T_{opt}^{mut}=T_{opt}=T_{opt}^*} = 0 \quad (9.14)$$

The evolutionary outcome of the model is thus given by the selection gradient. However, it is possible to simplify the way to find  $T_{opt}^*$  in order to decrease the numerical computation time:

**Proposition 9.2.2** *The evolutionary equilibrium  $T_{opt}^*$  is given by:*

$$T_{opt}^* = \arg \max_{T_{opt}} \langle \ln(\mu(T(t), T_{opt})) \rangle \quad (9.15)$$

## 9. MODELLING THE EFFECT OF TEMPERATURE ON PHYTOPLANKTON GROWTH ACROSS THE GLOBAL OCEAN

---

**Proof.** According to Grimaud et al. [2014a]:

$$\left. \frac{\partial \langle f_{X_{mut}}(T_{opt}, T_{opt}^{mut}) \rangle}{\partial T_{opt}^{mut}} \right|_{T_{opt}^{mut}=T_{opt}} = \frac{D}{\tau} \cdot \int_0^\tau \frac{\mu'(T(t), T_{opt})}{\mu(T(t), T_{opt})} dt \quad (9.16)$$

Moreover:

$$\frac{\partial \langle \ln(\mu(T(t), T_{opt})) \rangle}{\partial T_{opt}} = \frac{1}{\tau} \int_0^\tau \frac{\mu'(T(t), T_{opt})}{\mu(T(t), T_{opt})} dt \quad (9.17)$$

If  $T_{opt} = T_{opt}^*$  (evolutionary equilibrium), eq.(9.16)=0. Thus:

$$\frac{\partial \langle \ln(\mu(T(t), T_{opt}^*)) \rangle}{\partial T_{opt}} = 0$$

which is equivalent to say that:

$$T_{opt}^* = \arg \max_{T_{opt}} \langle \ln(\mu(T(t), T_{opt})) \rangle$$

We formally show that finding the evolutionary equilibrium is equivalent here to a simple optimization problem. This result revoices the question addressed by Metz et al. [2008] in the adaptive dynamics framework: ‘*when does evolution optimize ?*’. In particular, Metz et al. [2008] showed that ‘*a pure optimization approach holds water only when the eco-evolutionary feedbacks are of a particularly simple kind*’, and we do believe that this is the case here.

### 9.3 Global ocean scale simulations

#### 9.3.1 Evolutionary model with realistic temperature signal

We now study phytoplankton thermal evolution at global ocean scale. Let us consider an ubiquitous phytoplankton species which has evolved locally at each sea surface location  $(i, j)$  in response to environmental pressure. In a first assumption, each point of latitude/longitude  $(i, j)$  can be viewed as a chemostat with growth equations given by eq. (9.3). Assuming that the sea surface temperature is a proxy of the temperature experienced by the phytoplankton cells, we use a realistic temperature signal  $T(t, i, j)$  from *in situ* observations. The sea surface temperature data for the global ocean have been downloaded from the European short term meteorological forecasting website (<http://apps.ecmwf.int>). The data cover the years 2010 to 2012 and the spatial resolution is  $1^\circ$  in latitude and longitude with a temporal resolution of 3 hours.

We calculate for each time step (3 hours) at a given location, the value of the function  $\phi(T(t, i, j), T_{opt})$ , depending on the perceived *in situ* temperature  $T(t, i, j)$  and the optimum growth temperature  $T_{opt}$ . We then calculate the average of the integrated function over  $3\tau = 3$  years (2010, 2011, 2012):

$$\psi(T_{opt}) = \frac{1}{3\tau} \cdot \int_0^{3\tau} \ln(\mu(T(t, i, j), T_{opt})) dt \quad (9.18)$$

Using prop 9.2.2, we search for the evolutionary optimum temperature  $T_{opt}^*$  achieving the maximum of eq. (9.18).

#### 9.3.2 Global scale simulations

Global scale simulations for eq. 9.1 (fig. 9.1 A) show that for any range of temperature experienced by phytoplankton, the evolutionary temperature  $T_{opt}^*$  at a given place  $(i, j)$  is always higher or equal to the average temperature  $\bar{T}(i, j)$ . In the tropical zone, where the average temperature is high (near 26°C),  $T_{opt}^*(i, j) \simeq \bar{T}(i, j)$ . In temperate and coastal zones, where the average temperature is between 10 and 20°C,  $T_{opt}^*(i, j) > \bar{T}(i, j)$ .

This corresponds to areas where the temperature range  $\max(T(t)) - \min(T(t))$  is higher than 10°C (Fig. 9.1 C). We suppose that due to the thermal growth curve asymmetrical shape, it is more suitable to have higher  $T_{opt}$  when temperature fluctuates. This assumption is in good agreement with Kimura et al. [2013] observations for Archaea; these organisms live near their maximum temperature, with a  $T_{opt}$  much higher than the environmental  $\bar{T}$ .

Simulations with eq. 9.2 (Eppley hypothesis) (fig. 9.1 B) show similar results, however the evolutionary temperature is always higher than the average temperature (for about 6°C).

#### 9.3.3 Comparison with experimental data

Using model (9.1), we determined the cardinal temperatures ( $\hat{T}_{min}$ ,  $\hat{T}_{opt}$ ,  $\hat{T}_{max}$ ) for the 194 phytoplankton strains studied by Thomas et al. [2012] thanks to growth rate versus temperature data sets as detailed in chapter 2. The calibration was coupled to a Jack-kniffe statistical test evaluating the confidence interval of the parameters as in Bernard and Rémond [2012]. We then only considered strains associated with data sets providing a confidence interval smaller than 5°C for the estimated  $\hat{T}_{opt}$ , *i. e.* 57 strains.

Since the geographical coordinates of the isolation of the 194 stains are known, it is possible to compare  $\hat{T}_{opt}$  to *in situ*  $\bar{T}(i, j)$  (fig. 9.2 A). Results support the fact that  $T_{opt}$  is much higher than  $\bar{T}$  (here the maximum difference is 10°C) in temperate areas and almost the same as  $\bar{T}$  in tropical and polar areas. We simulate the eq. 9.1 and eq. 9.2 at the isolation coordinates of the 57 selected strains (fig. 9.2 B, green points). Simulations with eq. 9.1 give the same non-linear trend previously stated (fig. 9.2 B, blue points) whereas simulations with the Eppley hypothesis mostly capture a more flattened relationship between  $T_{opt}^*$  and  $\bar{T}$  (fig. 9.2 B, red points).

We define  $\Delta = T_{opt}^* - \bar{T}$ . For simulations with eq. 9.1 representing the horizontal-shift hypothesis, we obtain  $\Delta \geq 0$ . Here, it is worth noting that  $\Delta$  can be equal to zero due to the assumption that  $\mu_{opt}$  does not depend on  $T_{opt}$ . This is particularly true in tropical zones, which is in accordance to experimental data. Quite the opposite,  $\Delta$  is always higher than 6° C for simulations with the Eppley hypothesis and does not allow to match the points situated in tropical zones. Moreover, the Eppley simulation gives a rather linear relationship between  $T_{opt}^*$  and  $\bar{T}(t)$ . Results obtained with eq. 9.1 (horizontal-shift hypothesis) are therefore more coherent with



## 9. MODELLING THE EFFECT OF TEMPERATURE ON PHYTOPLANKTON GROWTH ACROSS THE GLOBAL OCEAN

---

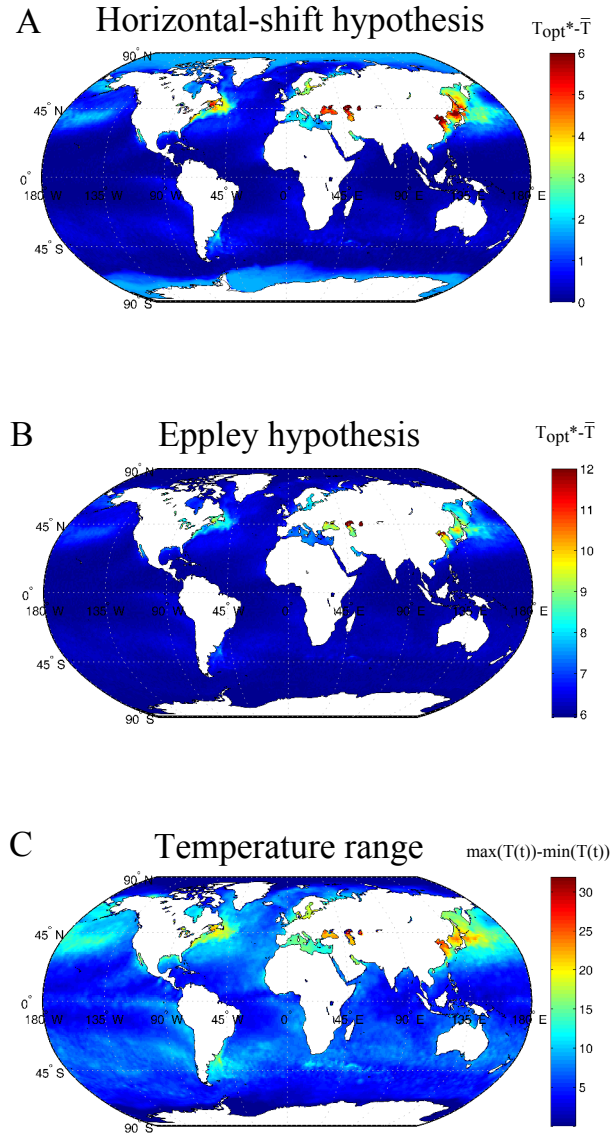


**Figure 9.1: Global ocean scale simulations** - World map of the difference between the optimal temperature for growth and the mean temperature  $\Delta = T_{opt}^* - \bar{T}$  for the horizontal-shift hypothesis simulation (A) and Eppley hypothesis simulation (B) (red correspond to areas where  $\Delta \geq 6^\circ\text{C}$  for (A) and  $\Delta \geq 12^\circ\text{C}$  for (B)), and temperature range  $\max(T(t)) - \min(T(t))$  for the three years 2010, 2011, 2012 (C).

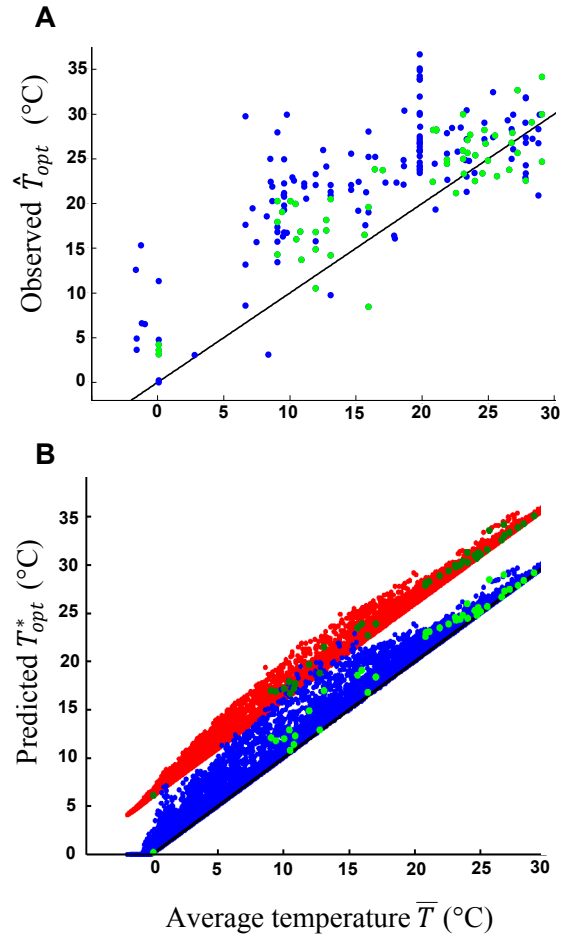


**Figure 9.2: Model predictions** - (A) Observed  $\hat{T}_{opt}$  for 194 phytoplankton strains as a function of  $\bar{T}$ . The 57 selected strains are indicated in green points. (B) Predicted  $T_{opt}^*$  as a function of  $\bar{T}$  for eq. 9.1 simulations (horizontal shift hypothesis) (blue points) and Eppley hypothesis simulations (red points). The  $y = x$  curve is indicated in black. The green points correspond to the predicted  $T_{opt}^*$  for the 57 selected strains (light green for eq. 9.1 simulations, dark green for Eppley hypothesis simulations).

## 9. MODELLING THE EFFECT OF TEMPERATURE ON PHYTOPLANKTON GROWTH ACROSS THE GLOBAL OCEAN

---

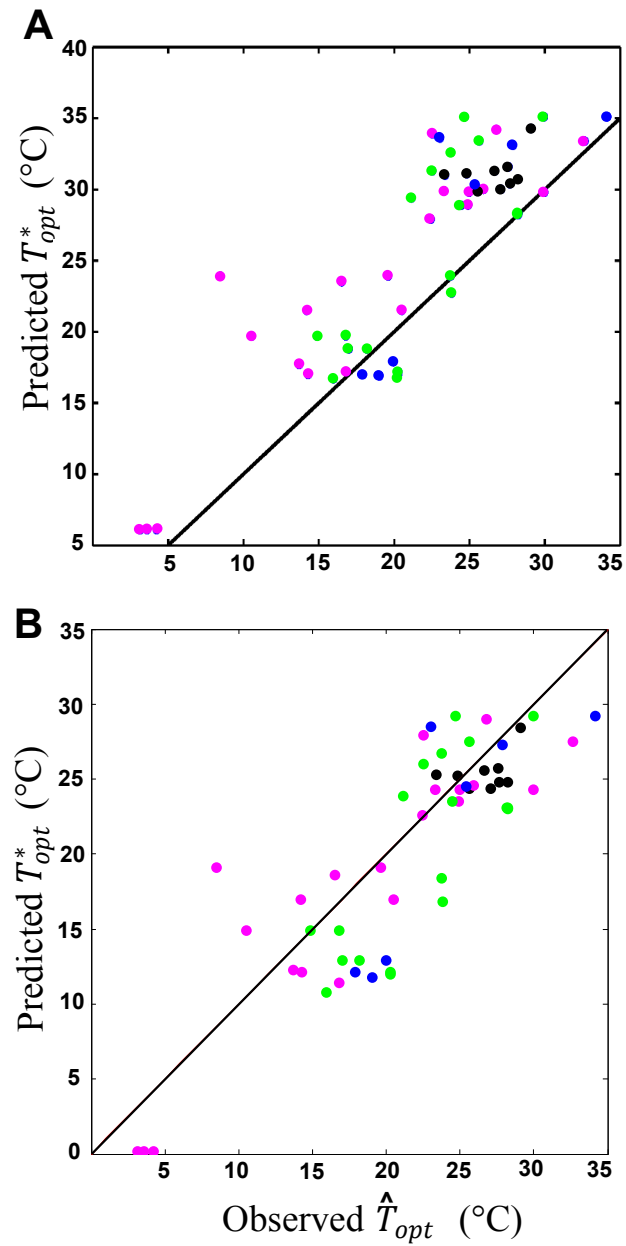


**Figure 9.3: Comparison to experimental data** - Predicted  $T_{opt}^*$  compared to experimental  $\hat{T}_{opt}$  for Eppley hypothesis (A) and eq. 9.1 simulations (B). Phytoplankton phylogenetic groups are indicated in color in (B): green: Dinoflagellates, pink: Diatoms, black: Cyanobacteria, blue: others.

[Chen, 2015, Thomas et al., 2015] and illustrate perfectly Boersma et al. [2016]: ‘*Projecting effects of climate change on marine systems is the mean all that matters ?*’

We then compare predicted  $T_{opt}^*$  to observed  $\hat{T}_{opt}$  (fig. 9.3). For simulations with the horizontal-shift hypothesis, mean error calculated as  $|T_{opt}^* - \hat{T}_{opt}|/\hat{T}_{opt}$  is 21.7% whereas for Eppley hypothesis simulation, mean error is 25.5%. Error is thus quite similar for the two models, but the Eppley simulation overestimates  $T_{opt}^*$ . The accuracy of the model predictions, despite the model simplicity, is really surprising. Thus, direct temperature effect must drive evolution at global scale, contrary to what is claimed by Marañón et al. [2014].

There are some unavoidable biases in our approach. The first one is due to the age of the microalgae cultures which have been used to provide the data. In general, the measurements were not performed right after *in situ* isolation. It results that the strains may have evolved, due to the temperature where the strains are stored in the culture collection. Second, we only consider the effect of temperature. Effects of light and nutrients which also strongly drive  $\mu_{opt}$  are not taken into account. Finally, we use sea surface temperature. Phytoplankton can migrate and are advected along the water column, and experience temperatures different from the surface.

Despite these biases, we estimated with a certain accuracy the  $T_{opt}^*$ , *e.g.* for the cyanobacteria group, which lives in areas where the average temperature is high. It is thus possible that the sea surface temperature, where light is available, is actually a good proxy to predict thermal adaptation.

#### 9.3.4 The warming scenario

In our method, the cardinal temperatures are linearly linked. We can thus obtain the upper thermal limit at evolutionary equilibrium,  $T_{max}^*$ , from  $T_{opt}^*$ . We compared  $T_{max}^*$  to the annual maximal temperature experienced *in situ*, defined as  $\Delta_m = T_{max}^* - \max(T(t))$ . The results (fig. 9.4) show that for the horizontal-shift hypothesis as for the Eppley hypothesis simulations, temperate areas with annual high temperature fluctuations have the low  $\Delta_m$ . For the horizontal-shift hypothesis,  $\Delta_m$  is even slightly negative in several places such as the Japan sea. We infer that in case of warming, even for the most optimistic scenario with only 1°C of annual average temperature increase before the end of the century, thermal extreme events (such as El niño) will drastically increase the maximal temperature experienced and thus challenge phytoplankton survival in temperate areas. This result is counter-intuitive and in contradiction with that of Thomas et al. [2012], who claim that tropical and polar areas where the  $T_{opt}^*$  is the closest to the experienced (and stable) temperature are the more sensitive to warming. We rather show here that even if, in temperate areas, simulations give  $T_{opt}^*$  higher than the annual average temperature compared to tropical areas, this difference is low compared to the high difference between the maximal temperature  $\max(T(t))$  and the annual average temperature  $\bar{T}(t)$  in temperate areas.

Huertas et al. [2011] challenged this hypothesis with experimental evolution and have highlighted the following trade-off: in temperate areas,  $T_{max}^*$  is closed to  $\max(T(t))$  and

## 9. MODELLING THE EFFECT OF TEMPERATURE ON PHYTOPLANKTON GROWTH ACROSS THE GLOBAL OCEAN

---

a potential warming would directly affect phytoplankton if the speed of adaptation is not high enough. However, Huertas et al. [2011] showed that temperate phytoplankton species have higher genetic capabilities to adapt to thermal changes.

### 9.4 Conclusion

We have presented a new method based on adaptive dynamics theory to study the outcome of phytoplankton adaptation at global ocean scale. We defined a standard ubiquitous phytoplankton species and we compared at first two different thermal growth models, the horizontal-shift hypothesis and the Eppley hypothesis, describing it in the context of evolution. We found, in agreement with chapter 7, that the evolutionary optimal temperature  $T_{opt}^*$  is always equal or higher than the average temperature experienced by the phytoplankton  $\bar{T}$ . Moreover, the area with high difference between  $T_{opt}^*$  and  $\bar{T}$  characterizes large temperature fluctuations. When based on the horizontal-shift hypothesis, our model successfully fits the data, contrary to the Eppley hypothesis which linearly links  $T_{opt}^*$  and  $\bar{T}$ , and overestimates  $T_{opt}^*$ . We inferred that direct temperature effect strongly drives evolution at the scale of the global ocean. It is worth noting that the modified Eppley hypothesis is still to be tested in this evolutionary model.

In contradiction with Thomas et al. [2012] and Ward [2015], we showed that temperate areas are more sensitive to global warming because of the small difference between  $T_{max}^*$  and  $\max(T(t))$  there. However, this could be compensated by the perhaps higher evolutionary capabilities of phytoplankton in these areas [Huertas et al., 2011].

The evolutionary effect of temperature on phytoplankton should now be investigated concomitantly to other factors (which has been partially done by [Sauterey et al., 2014]), such as irradiance, nutrient [Irwin et al., 2015] or pH and CO<sub>2</sub> concentrations [Coello-Camba et al., 2014]. The phytoplankton species *Emiliana huxleyi* is known to be acid-sensitive, but its adaptation capability to co-variation of temperature and pH are not clearly understood [Fielding, 2014, Gibbs et al., 2016, Schlüter et al., 2014].

Finally, as co-evolution is a powerful driver, co-evolutionary models taking into account the predators sensitivity to temperature should be developed [Amarasekare, 2015, Chen et al., 2012, Rose and Caron, 2007]

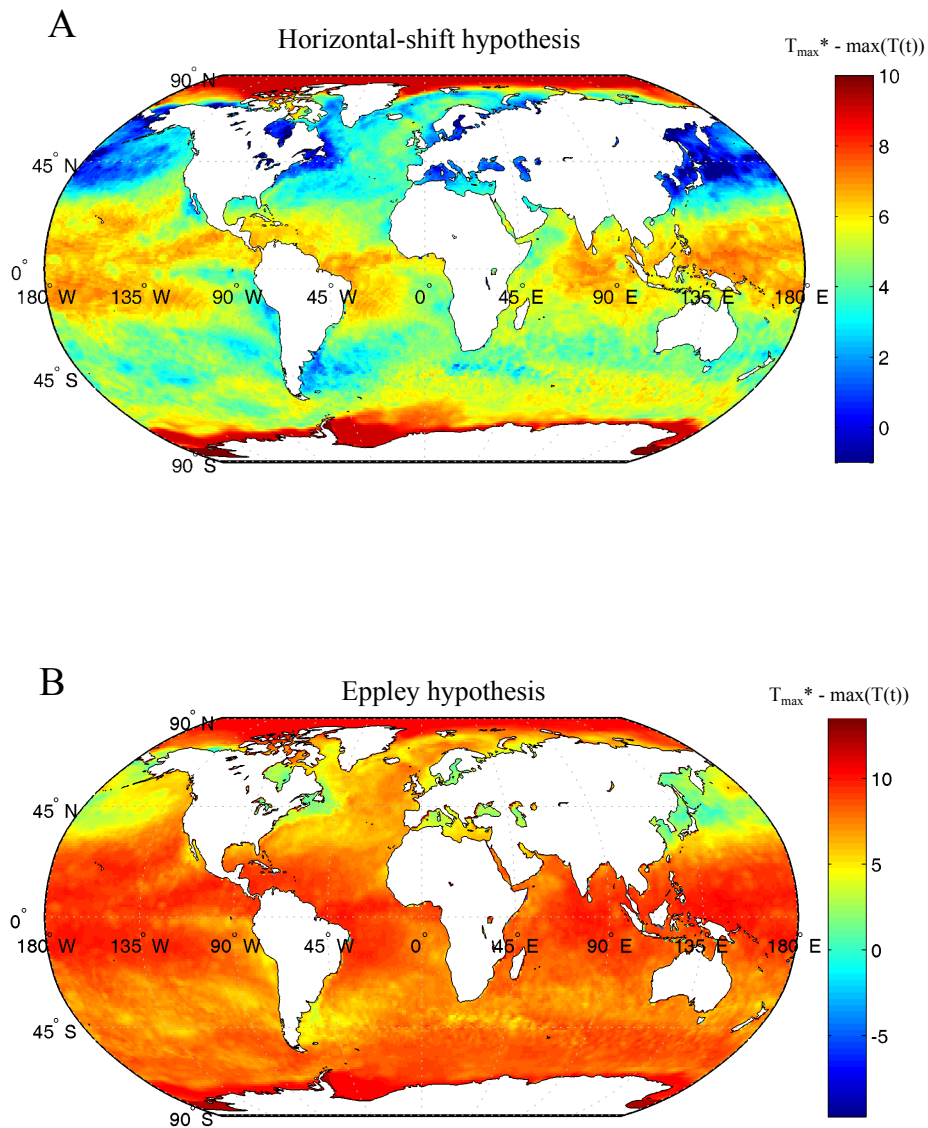


**Figure 9.4: Global ocean scale simulations of  $T_{max}^*$ .** - World map of the difference between the maximal temperature for growth and the maximal annual temperature *in situ*,  $T_{max}^* - \max(T)$  for the horizontal-shift hypothesis simulation (A) and Eppley hypothesis simulation (B). The blue areas correspond to potentially sensitive zones.

## 9. MODELLING THE EFFECT OF TEMPERATURE ON PHYTOPLANKTON GROWTH ACROSS THE GLOBAL OCEAN

---

### Summary of section 9:

- We reduced a thermal evolutionary model to a simple optimization problem, allowing to compute  $T_{opt}^*$  at the global ocean scale
- *In situ* simulations are coherent with experimental results
- *In situ* simulations show that in temperate areas,  $T_{opt}^* > \bar{T}(t)$ , which is correlated to the annual thermal range
- In these temperate areas,  $T_{max}^*$  is close to  $\max(T(t))$ . Temperate areas are thus probably sensitive to ocean warming

# Conclusion & Perspectives

## 10.1 The physiological impacts of temperature on phytoplankton

### 10.1.1 From empirical models to thermodynamical insights

In chapter 3, we have reviewed the different models representing the effect of temperature on UO growth, classifying them into empirical and mechanistic categories. We have shown that empirical models, and most particularly the Bernard and Rémond [2012] model, are the most reliable for dealing with the low number of points which characterize, in practice, these data sets. Mechanistic models, contribute to explain and highlight the thermally induced physiological effects. If we compare to the broad literature dedicated to understanding the effect of light on growth, the poor knowledge of the mechanisms balancing or favoring growth is very surprising. The current consensus is that temperature affects enzyme conformational stability. Despite the recent development of a unicellular growth model said to be universal [Corkrey et al., 2014], we have shown that the ‘proteome paradigm’ should be further investigated. Some authors, for example, claim that physiological mechanisms compensating each others, particularly the respiration rate, are the basis of the thermal growth curve [Poertner, 2012, Ruoff et al., 2007, Zakhartsev et al., 2015] (this is called the metabolic hypothesis). The process of temperature acclimation did not receive much attention, and should definitely be more extensively studied and integrated into the models.

In the same way, cell mortality at low or high temperatures still has to be investigated. Few studies exist for unicellular eukaryotes, especially for phytoplankton. It is not clear if death rate increases under theoretically sub-lethal temperatures (*i.e.* below  $T_{opt}$ ). The molecular mechanisms leading to death are not definitely unveiled and definitely need further investigations. Moreover, the capacity of cell to repair its damages and regrow after an heat or cold shock is not clearly understood and modelled.

In chapter 4 and chapter 5, an opportunity to clarify the situation is given by the exploration of universal links between the cardinal temperatures, on one hand, and be-



## 10. CONCLUSION & PERSPECTIVES

---

tween the optimal growth rates and the optimal temperature for growth on the other hand. Since Rosso et al. [1993], it has been noticed that an unexpected linear link between the cardinal temperatures exists for bacteria. We have extended this observation to a large range of UO, including unicellular eukaryotes, and discovered that not only a linear relationship is observed too, but that this relation is exactly the same. It is also valid for different phytoplankton sub-groups such as Chlorophyta. Nonetheless, the relation between  $T_{min}$  and the other cardinal temperatures is more confused for eukaryotes, perhaps because of the difficulty to study these organisms at low temperature (probably because of the specificity of their membrane fluidity [Caspeta et al., 2014]). Our results do not tend to support, for example, a tough constant thermal niche width for all the organisms. The asymmetry of the thermal growth curve is also subject to variations [Thompson et al., 1992]. Yet, we have shown that these linear relations are highly significant, and that there is a clear trade-off between the cardinal temperatures for every UO despite the large variety of metabolisms. On top of that, we also unveiled group-specific links between the theoretical optimal growth rate and the optimal temperature for growth, and thus we proposed a correction of the Eppley law [Eppley, 1972] for the highest temperatures. Although depending on many factors including cell biovolume and scaling laws, we have shown that growth is intrinsically limited by an upper and a lower bound that seems to be rather constant for a given group. More experiments in the framework of Boyd et al. [2013] are necessary using agreed and standardized protocols.

In chapter 6, we revisited these universal features using a mechanistic model, the Hinshelwood model. We firstly showed that the Hinshelwood model arises from considering an autocatalytic model with  $n$  enzymes in interactions that are thermally unfolded. This model shows that the average unfolded proteome, rather than a specific unfolding enzyme, matters at high temperature (on the contrary to what is claimed by Corkrey et al. [2014]). This theory has deep implications for thermal adaptation. We then included two thermodynamically-motivated links in the model: the entropy-enthalpy compensation (EEC) and the activity-stability trade-off. When proteins unfold, EEC stipulates that enthalpy always compensates entropy such that the Gibbs free energy difference of unfolding cannot widely vary. The activity-stability trade-off accounts for the loss of enzyme activity linked to its stability when it unfolds. With these hypotheses, we were able to satisfactorily represent the thermal growth curves with only two parameters. Finally, we explained the links between thermal parameters previously highlighted. Further work is needed to explore the underlying thermodynamical principles of the thermal growth curve beyond its Arrhenius type response. The use of metabolic models under non-balanced growth, while explicitly accounting for the thermal sensitivity of each single metabolic reaction could be used to challenge this problematic [Baroukh, 2014].

### 10.1.2 The submerged iceberg of unknown: future works

In chapter 7, we have exploited an experiment where phytoplankton was grown in dynamical conditions under periodically varying temperatures. We have developed a dynamical model, and we have shown that a periodical solution theoretically exists. Using the

Droop model [Droop, 1968], we have challenged the duality of both growth and nutrient uptake thermal sensitivities. However, as soon as temperature is varying, our knowledge concerning cell metabolic reactions becomes limited [Ras et al., 2013]. Data are clearly lacking to understand how internal metabolites such as starch or lipid respond to temperature variations. Again, the use of metabolic models under non-balanced growth [Baroukh, 2014] could deeply help to decipher between the different impacts of temperature, and finally understand the unclear observations. Additionally, Bonnefond et al. [2016] have shown that temperature variations contribute to synchronize the cell cycle and can strongly favor growth by reducing the loss of carbon by respiration during the night.

Temperature is a central parameter for phytoplankton, but as it acts on the whole metabolism, it is linked to several other factors, making the understanding of its effect in a real environment very challenging. First of all, the coupling between temperature and photosynthesis is still to be explored. The temperature coupling with light has not clearly been investigated at high light intensity [Bernard and Rémond, 2012, Jensen and Knutsen, 1993b, Ras et al., 2013], where it seems to lead to nonlinear effects. The development of cell-scaled models representing the different states of the reaction centers involved in the photon harvesting process (see for example Han [2001]) and their temperature sensitivity (as done by Duarte [1995]) could help to better understand and model the temperature and light coupling in conditions of photosaturation and photoinhibition. Moreover, the process by which low temperatures induce photoinhibition has not been modelled yet.

Temperature also influences the oxygen concentration in the medium. It therefore indirectly affects the respiration rate, but can also more deeply impact the metabolism, at high biomass density, when oxygen stimulates photorespiration or mortality due to oxygen free radicals. Some authors have pointed out the importance of this coupling for unicellular diazotrophic cyanobacteria (UCYN) owning the nitrogenase, the enzyme responsible of the  $N_2$  fixation, which is highly inhibited by oxygen [Brauer et al., 2013, Stal, 2009]. For now on, no model exists to take this phenomenon into account but the Grimaud et al. [2014b] model could be a starting point.

## 10.2 Capturing the evolutionary trajectories

### 10.2.1 Selection experiments and evolutionary modelling

In chapters 7, we have modelled phytoplankton temperature adaptation using the adaptive dynamics theory applied to a simple Monod model in constant and varying thermal conditions. We have taken into account the links described in the previous chapters, incorporating them into the Bernard&Rémond model. We depicted several possibilities among these links and their potential effects on adaptation. The main results show that, firstly, the optimal growth temperature tends to equal the applied temperature if the temperature is kept constant and the optimal growth rate does not change. This is an important result for long-term conservation conditions of phytoplankton in labo-

## 10. CONCLUSION & PERSPECTIVES

---

ratory cultures [Garrido et al., 2013]. As a consequence, the thermal response of the strains which have been for decades maintained at 20°C may strongly diverge from the response of the strain still in the natural environment. On top of that, under Eppley or modified-Eppley hypotheses, the optimal growth temperature tends to be higher than the applied temperature. Secondly, we showed and demonstrated that  $T_{opt}$  tends to be always higher than the average temperature in fluctuating regimes. This phenomenon is highly amplified when considering the modified Eppley hypothesis. Finally, we showed that if  $T_{min}$  and  $T_{max}$  are fixed, evolutionary branching can occur meaning that two new strains can coexist and separate.

In chapter 8, we compared our model to a selection experiment carried by Bonnefond et al. [subm.] for the Facteur 4 ANR project in controlled conditions with piece-wise linear fluctuating temperatures. We designed the canonical equation of the adaptive dynamics in line with Kremer and Klausmeier [2013] for fluctuating conditions. We calibrated the evolution model using the experimentally measured growth rates. This model was able to nicely reproduce the evolutionary dynamics. However, it was not possible to distinguish between the acclimation, selection and adaptation phases. In this kind of evolutionary experiments, competitions models as well as evolutionary models should be built together to better understand and estimate the time-scale of the different phenomenons. A future step would be to deduce optimal experimental conditions to select a particular adaptive trait using the adaptive dynamics theory. This was partially done here by extrapolating the theoretical evolution of  $T_{opt}$  for a long lasting experiment. We also estimated the derivation of  $T_{opt}$  during the strain conservation period.

The adaptive dynamics theory gave us insight into thermal adaptation here, but suffers from structural limitations. First of all, it is only possible to represent the evolution of a single adaptive trait. We overcame this limitation thanks to the links existing between some parameters, but these links are not always clear or universal. Some authors are currently searching for a way to fix this limitation and model multi-dimensional traits space [Champagnat et al., 2002], notably by using the new notion of function valued adaptive dynamics [Parvinen et al., 2006]. Moreover, multi-dimensional phenotypic traits cannot be taken into account most of the time [Ispolatov et al., 2016], which constitute a big gap with  $n$  species competition models. The mutant invasion time could also be a limitation. In the adaptive dynamics theory, it is assumed to be instantaneous. In the same way, the mutation rates cannot be easily deduced from the canonical equation.

### 10.2.2 Evolution in the ocean

In chapter 9, we have tried to extend our evolutionary modelling approach to the global ocean for phytoplankton. Firstly, we have reduced the model exposed in chapter 7 to an optimization problem. In this simple formulation, it was possible to simulate phytoplankton evolution at the global ocean scale using 3 years Sea Surface Temperatures data. The main result suggests that the higher is the temperature annual fluctuation, the higher will be the difference between  $T_{opt}$  and the annual average temperature, and this was particularly linked to the modified Eppley hypothesis, specific for each

phytoplankton group. Surprisingly, it was possible to compare the experimental data relating a strain phenotype to its geographical original. Indeed, we were able to predict optimal temperatures for phytoplankton species at a given location in the world. A close view to the corresponding  $T_{max}$  showed that species located in areas with wider range of annual temperature fluctuations had  $T_{max}$  closer to the maximal temperatures recorded there and could thus be more sensitive to a potential increase of sea water temperature as well as extreme thermal events. Moreover, it is worth noting that each phytoplankton group has its own intrinsic thermal limits.

These results have to be cautiously considered because of the huge variability encountered at global scale. Some other authors are currently trying to represent thermal evolution in the ocean using similar methods. Thomas et al. [2012] and [Padfield et al., 2015a, Yvon-Durocher et al., 2015] use similar adaptive dynamics model whereas David Claessen with the ANR Phytback project is constructing a large scale multi-dimensional adaptive dynamics model considering several varying environmental factors. It is obvious that many factors impact evolution in the ocean. For example, temperature increase is associated to ocean acidification by an increase in dissolved  $\text{CO}_2$ .

Moreover, temperature affects all the organisms, unicellular or not. The eco-regional repartition of copepods is highly influenced by temperature, for example [Benedetti et al., 2016]. Co-evolution should thus be considered even in a thermal problematic, and even community-thermal response could be studied [Brauer et al., 2009].

## 10.3 Conclusion

This PhD thesis has tried to figure out how phytoplankton adapt to temperature. The overall picture is still very incomplete, but the developed approaches can be extended to the whole microbial world. In a warming context, it becomes crucial to understand and estimate the evolutionary capacity of this invisible microscopic world, and anticipate its adaptation capability. Our new results characterizing the short and long term responses to temperature are expected to challenge biogeochemical models as well as scientific minds.



# Annexes

Contributors: Mairet, F. & Bernard, O.

## Determining $T_{min}$ in the Hinshelwood model

The Hinshelwood model (eq. 3.22) considers that growth rate tends to zero when temperature tends to minus infinity, and it is thus not possible to define an exact minimum temperature for growth  $T_{min}$ . We considered that  $T_{min}$  can also be defined as the temperature at which the growth rate is equal to a small fraction  $\epsilon$  of the optimal growth rate:

$$\mu(T_{min}) = \epsilon\mu_{opt} \quad (10.1)$$

We assumed that, at  $T_{min}$ , the function  $f_2(T)$  corresponding to thermal deactivation/denaturation is negligible regarding  $f_1(T)$  (see eq. 3.22 and eq. 3.25):

$$A_1 e^{-E_1/(RT_{min})} \simeq \epsilon \frac{E_2 - E_1}{E_1} A_2 e^{-E_2/(RT_{opt})} \quad (10.2)$$

and thus:

$$\boxed{T_{min} \simeq \frac{-T_{opt}E_1/\gamma}{T_{opt} - E_2/\gamma}} \quad (10.3)$$

where:

$$\gamma = R \ln \left( \frac{E_2 - E_1}{E_1} \frac{A_2}{A_1} \epsilon \right) \quad (10.4)$$

We arbitrarily fixed  $\epsilon = 0.05$ .

## Autocatalytic view of the Hinshelwood model

The autocatalytic system described in section 6.2.1 is written:

$$\begin{aligned} \dot{x}_1 &= k_1(T)x_n - d_1(T)x_1 \\ \dot{x}_2 &= k_2(T)x_1 - d_2(T)x_2 \\ &\vdots \\ \dot{x}_n &= k_n(T)x_{n-1} - d_n(T)x_n \end{aligned} \quad (10.5)$$

During balanced growth, every reactions can be expressed as a function of the growth rate  $\mu$  [Hinshelwood, 1952]:

$$\begin{aligned} \dot{x}_1 &= \mu x_1 \\ \dot{x}_2 &= \mu x_2 \\ &\vdots \\ \dot{x}_n &= \mu x_n \end{aligned} \tag{10.6}$$

Each reaction  $i$  can be written:

$$\frac{\dot{x}_i}{x_i} = k_i \frac{x_{i-1}}{x_i} - d_i = \mu \tag{10.7}$$

Moreover, because:

$$\prod_{i=1}^n \frac{x_{i-1}}{x_i} = 1 \tag{10.8}$$

then:

$$\prod_{i=1}^n k_i = \prod_{i=1}^n (\mu + d_i) \tag{10.9}$$

Considering that  $d_i < \mu$ , we can write:

$$\prod_{i=1}^n k_i \simeq \mu^n + \mu^{n-1} \sum_{i=1}^n d_i \tag{10.10}$$

that is:

$$\frac{\mu^n}{\prod_{i=1}^n k_i} \left( 1 + \frac{\sum_{i=1}^n d_i}{\mu} \right) \simeq 1 \tag{10.11}$$

which gives:

$$\frac{\mu}{(\prod_{i=1}^n k_i)^{1/n}} \left( 1 + \frac{\sum_{i=1}^n d_i}{\mu} \right)^{1/n} \simeq 1 \tag{10.12}$$

By taking the Taylor expansion of the function  $\left( 1 + \sum_{i=1}^n d_i/\mu \right)^{1/n}$  in the neighbourhood of zero we obtain:

$$\mu \left( 1 + \sum_{i=1}^n d_i/(n\mu) \right) \simeq \left( \prod_{i=1}^n k_i \right)^{1/n} \tag{10.13}$$

Finally:

$$\boxed{\mu \simeq (\prod_{i=1}^n k_i)^{1/n} - \frac{1}{n} \sum_{i=1}^n d_i} \tag{10.14}$$

# Bibliography

- Akaike, H. Information theory and an extension of the maximum likelihood principle. In *Selected Papers of Hirotugu Akaike*, pages 199–213. Springer, 1998. 18
- Amarasekare, P. Effects of temperature on consumer–resource interactions. *Journal of Animal Ecology*, 84(3):665–679, 2015. 146
- Angilletta, M. J. Thermal adaptation. *Oxford University Press, Oxford*, 2009. 7, 45
- Antoine, D. and Morel, A. Oceanic primary production: 1. adaptation of a spectral light-photosynthesis model in view of application to satellite chlorophyll observations. *Global biogeochemical cycles*, 10(1):43–55, 1996. 2
- Arnold, F. H., Wintrode, P. L., Miyazaki, K., and Gershenson, A. How enzymes adapt: lessons from directed evolution. *Trends in biochemical sciences*, 26(2):100–106, 2001. 81
- Arrhenius, S. On the reaction velocity of the inversion of cane sugar by acids. *Zeitschrift für Physikalische Chemie*, 4:226–248, 1889. 24
- Arthur, H. and Watson, K. Thermal adaptation in yeast: growth temperatures, membrane lipid, and cytochrome composition of psychrophilic, mesophilic, and thermophilic yeasts. *Journal of Bacteriology*, 128(1):56–68, 1976. 56
- Baldauf, S. L. An overview of the phylogeny and diversity of eukaryotes. *J. Syst. Evol.*, 46:263–273, 2008. 2
- Banks, B. E. C., Damjanovic, V., and Vernon, C. A. The so-called thermodynamic compensation law and thermal death. *Nature*, 240:147–149, 1972. 81
- Banse, K. Cell volumes, maximal growth rates of unicellular algae and ciliates, and the role of ciliates in the marine pelagial. *Limnology and Oceanography*, 27(6):1059–1071, 1982. 69
- Baranyi, J., Robinson, T., Kaloti, A., and Mackey, B. Predicting growth of brochothrix thermosphacta at changing temperature. *International journal of food microbiology*, 27(1):61–75, 1995. 37, 38



## BIBLIOGRAPHY

---

- Baranyi, J., Jones, A., Walker, C., Kaloti, A., Robinson, T., and Mackey, B. A combined model for growth and subsequent thermal inactivation of brochothrix thermosphacta. *Applied and environmental microbiology*, 62(3):1029–1035, 1996. 41
- Baranyi, J. and Roberts, T. A. Mathematics of predictive food microbiology. *International journal of food microbiology*, 26(2):199–218, 1995. 37
- Baroukh, C. *Metabolic modeling under non-balanced growth. Application to microalgae for biofuels production*. PhD thesis, Université Montpellier 2, 2014. 150, 151
- Bechet, Q., Shilton, A., Fringer, B., Munoz, R., and Guieysse, B. Mechanistic modeling of broth temperature in outdoor photobioreactors. *Environmental science and technology*, 44:2197–2203, 2010. 7
- Béchet, Q., Shilton, A., Park, J. B., Craggs, R. J., and Guieysse, B. Universal temperature model for shallow algal ponds provides improved accuracy. *Environmental science & technology*, 45(8):3702–3709, 2011. 7, 8
- Béchet, Q., Shilton, A., and Guieysse, B. Modeling the effects of light and temperature on algae growth: State of the art and critical assessment for productivity prediction during outdoor cultivation. *Biotechnology advances*, 31(8):1648–1663, 2013. 36, 37
- Behrenfeld, M. J., OMalley, R. T., Siegel, D. A., McClain, C. R., and Sarmiento, J. L. Climate-driven trends in contemporary ocean productivity. *Nature*, 44:752–755, 2006. 4, 6
- Bendif, E. M., Probert, I., Schroeder, D. C., and de Vargas, C. On the description of tisochrysis lutea gen. nov. sp. nov. and isochrysis nuda sp. nov. in the isochrysidales, and the transfer of dicrateria to the prymnesiales (haptophyta). *Journal of applied phycology*, 25(6):1763–1776, 2013. 114
- Benedetti, F., Gasparini, S., and Ayata, S.-D. Identifying copepod functional groups from species functional traits. *Journal of Plankton Research*, 38(1):159–166, 2016. 153
- Bennett, A. F. and Lenski, R. E. Evolutionary adaptation to temperature ii. thermal niches of experimental lines of escherichia coli. *Evolution*, pages 1–12, 1993. 113
- Bernard, O. and Rémond, B. Validation of a simple model accounting for light and temperature effect on microalgal growth. *Bioresource Technology*, 123:520–527, 2012. xv, 4, 16, 21, 36, 37, 46, 109, 115, 137, 141, 149, 151
- Bischof, J. C. and He, X. Thermal stability of proteins. *N. Y. Acad. Sci.*, 1066:12–33, 2005. 27, 81
- Bissinger, J. E., Montagnes, D. J., Atkinson, D., et al. Predicting marine phytoplankton maximum growth rates from temperature: Improving on the eppley curve using quantile regression. *Limnology and Oceanography*, 53(2):487–493, 2008. 17, 61, 62, 70

- Blanchard, G. F., Guarini, J.-M., Richard, P., Gros, P., and Mornet, F. Quantifying the short-term temperature effect on light-saturated photosynthesis of intertidal microphytobenthos. *Marine Ecology Progress Series*, 134:309–313, 1996. 21, 25
- Boersma, M., Grüner, N., Signorelli, N. T., González, P. E. M., Peck, M. A., and Wiltshire, K. H. Projecting effects of climate change on marine systems: is the mean all that matters? In *Proc. R. Soc. B*, volume 283, page 20152274. The Royal Society, 2016. 145
- Bonnefond, H. *Amélioration de microalgues à vocation énergétique par pression de sélection continue*. PhD thesis, Université Pierre et Marie Curie, 2015. 11, 12
- Bonnefond, H., Moelants, N., Talec, A., Bernard, O., and Sciandra, A. Temperature: a key parameter in microalgae biochemical mechanisms. *Algal Research*, 14:72–78, 2016. 115, 151
- Bonnefond, H., Grimaud, G., Rumin, J., Pruvost, E., Bernard, O., and Sciandra, A. Continuous pressure of selection to improve temperature response of *tisochrysis lutea*. *Plos One*, subm. 56, 114, 115, 116, 117, 118, 152
- Boudouresque, C. F. Taxonomy and phylogeny of unicellular eukaryotes. *Environmental Microbiology: Fundamentals and Applications*, pages 191–257, 2015. 1
- Bougaran, G., Rouxel, C., Dubois, N., Kaas, R., Grouas, S., Lukomska, E., Le Coz, J.-R., and Cadoret, J.-P. Enhancement of neutral lipid productivity in the microalga *isochrysis affinis galbana* (t-iso) by a mutation-selection procedure. *Biotechnology and bioengineering*, 109(11):2737–2745, 2012. 114
- Boyd, P. W. and Doney, S. C. *The impact of climate change and feedback processes on the Ocean Carbon Cycle*. Fasham MJR editor. Ocean Biogeochemistry the role of the ocean carbon cycle in global change. Springer-Verlag, Berlin. pp. 157187., 2003. 1
- Boyd, P. W., Rynearson, T. A., Armstrong, E. A., Fu, F., Hayashi, K., Hu, Z., Hutchins, D. A., Kudela, R. M., Litchman, E., Mulholland, M. R., Passow, U., Strzepek, R. F., Whittaker, K. A., Yu, E., and Thomas, M. K. Marine phytoplankton temperature versus growth responses from polar to tropical waters outcome of a scientific community-wide study. *PLoS ONE*, 8:e63091, 2013. doi: 10.1371/journal.pone.0063091. 22, 93, 136, 150
- Brauer, V., Jonge, V., Buma, A., and Weissing, F. Does universal temperature dependence apply to communities? an experimental test using natural marine plankton assemblages. *Oikos*, 118:1102–1108, 2009. 153
- Brauer, V., Stomp, M., Rosso, C., van Beusekom, S., Emmerich, B., Stal, L., and Huisman, J. Low temperature delays timing and enhances the cost of nitrogen fixation in the unicellular cyanobacterium cyanothece. *The ISME journal*, 13:1–11, 2013. 151

## BIBLIOGRAPHY

---

- Brown, J. H., Gillooly, J. F., Allen, A. P., Savage, V. M., and West, G. B. Toward a metabolic theory of ecology. *Ecology*, 85(7):1771–1789, 2004. 61, 69
- Brush, M. J., Brawley, J. W., Nixon, S. W., and Kremer, J. N. Modeling phytoplankton production: problems with the eppley curve and an empirical alternative. *Marine ecology. Progress series*, 238:31–45, 2002. 70
- Butler, G. and Freedman, H. Predator-prey system with periodic coefficients. *Mathematical biosciences*, 55:27–38, 1981. 102
- Butler, G., Hsu, S., and Waltman, P. A mathematical model of the chemostat with periodic washout rate. *SIAM J. Appl. Math.*, 45:435–449, 1985. 102
- Cade, B. S. and Noon, B. R. A gentle introduction to quantile regression for ecologists. *Frontiers in Ecology and the Environment*, 1(8):412–420, 2003. 18
- Campbell, A. Synchronization of cell division. *Bacteriological Reviews*, 21(4):263, 1957. 15, 22
- Carvalho, A. P. and Malcata, F. X. Kinetic modeling of the autotrophic growth of *pavlova lutheri*: study of the combined influence of light and temperature. *Biotechnology progress*, 19(4):1128–1135, 2003. 37
- Caspeta, L., Chen, Y., Ghiaci, P., Feizi, A., Buskov, S., Hallström, B. M., Petranovic, D., and Nielsen, J. Altered sterol composition renders yeast thermotolerant. *Science*, 346(6205):75–78, 2014. 56, 114, 150
- Champagnat, N., Ferrière, R., and Ben Arous<sup>4</sup>, G. The canonical equation of adaptive dynamics: a mathematical view. *Selection*, 2(1-2):73–83, 2002. 152
- Chen, B. Patterns of thermal limits of phytoplankton. *Journal of Plankton Research*, 37(2):285–292, 2015. 4, 136, 145
- Chen, B., Landry, M. R., Huang, B., and Liu, H. Does warming enhance the effect of microzooplankton grazing on marine phytoplankton in the ocean? *Limnology and oceanography*, 57(2):519–526, 2012. 146
- Chen, P. and Shakhnovich, E. I. Thermal adaptation of viruses and bacteria. *Biophysical journal*, 98(7):1109–1118, 2010. 31, 33, 45
- Chollet, S. F. *The role of diatoms in the global carbon cycle*. PhD thesis, University of East Anglia, 2011. 61, 70
- Coello-Camba, A., Agustí, S., Holding, J., Arrieta, J. M., and Duarte, C. M. Interactive effect of temperature and co<sub>2</sub> increase in arctic phytoplankton. *Front Mar Sci*, 1:49, 2014. 146

- Cooper, V. S., Bennett, A. F., and Lenski, R. E. Evolution of thermal dependence of growth rate of *escherichia coli* populations during 20,000 generations in a constant environment. *Evolution*, 55:889–896, 2001. 45
- Corkrey, R., McMeekin, T. A., Bowman, J. P., Ratkowsky, D. A., Olley, J., and Ross, T. Protein thermodynamics can be predicted directly from biological growth rates. *PLoS one*, 9(5):e96100, 2014. 14, 20, 21, 31, 41, 80, 149, 150
- Corradini, M. G. and Peleg, M. On modeling and simulating transitions between microbial growth and inactivation or vice versa. *International journal of food microbiology*, 108(1):22–35, 2006. 41, 42
- Corradini, M. G. and Peleg, M. A weibullian model for microbial injury and mortality. *International journal of food microbiology*, 119(3):319–328, 2007. 41, 43
- Costas, E., Basegla-Cervera, B., Garcia-Balboa, C., and Lopez-Roda, V. Estimating the genetic capability of different phytoplankton organisms to adapt to climate warming. *Environmental Science group, Oceanography Open Access*, 2014a. 7, 114, 132, 136
- Costas, E., Huertas, E., Basegla-Cervera, B., Garcia-Balboa, C., and Lopez-Roda, V. Phytoplankton ability to physiological acclimatization and genetic adaptation to global warming. *International Journal of Biology*, 6:24, 2014b. 7, 114, 132, 136
- Couñago, R., Wilson, C. J., Peña, M. I., Wittung-Stafshede, P., and Shamoo, Y. An adaptive mutation in adenylate kinase that increases organismal fitness is linked to stability–activity trade-offs. *Protein Engineering Design and Selection*, 21(1):19–27, 2008. 81
- Dallinger, W. The president’s address. *Journal of the Royal Microscopical Society*, 7: 185–199, 1887. 7, 9
- Daniel, R. M., Van Eckert, R., Holden, J. F., Truter, J., and Crowan, D. A. The stability of biomolecules and the implications for life at high temperatures. *The Subseafloor Biosphere at Mid-Ocean Ridges*, pages 25–39, 2004. 56
- De Rosbo, G. K. and Bernard, O. *Évaluation du gisement potentiel de ressources algales pour l’énergie et la chimie en France à horizon 2030*. PhD thesis, ADEME, 2014. 7
- DeLong, J. P., Okie, J. G., Moses, M. E., Sibly, R. M., and Brown, J. H. Shifts in metabolic scaling, production, and efficiency across major evolutionary transitions of life. *Proceedings of the National Academy of Sciences*, 107(29):12941–12945, 2010. 69
- Dermoun, D., Chaumont, D., Thebault, J.-M., and Dauta, A. Modelling of growth of porphyridium cruentum in connection with two interdependent factors: light and temperature. *Bioresource technology*, 42(2):113–117, 1992. 37
- Dieckmann, U. A beginners guide to adaptive dynamics. in *Mathematical modelling of population dynamics*, R. Rudnicki (ed.). *Banach Center Publications*, no. 63. Polish Academy of Sciences, Warsaw, 2004. 96

## BIBLIOGRAPHY

---

- Dieckmann, U. and Law, R. The dynamical theory of coevolution: A derivation from stochastic ecological processes. *Journal of Mathematical Biology*, 34:579–612, 1996. 94, 96, 139
- Dill, K. A., Ghosh, K., and Schmit, J. D. Physical limits of cells and proteomes. *Proceedings of the National Academy of Sciences*, 108(44):17876–17882, 2011. 21, 80
- Doemel, W. N. and Brock, T. The physiological ecology of cyanidium caldarium. *Microbiology*, 67(1):17–32, 1971. 70
- Dougherty, D. P., Breidt Jr, F., McFeeters, R. F., and Lubkin, S. R. Energy-based dynamic model for variable temperature batch fermentation by lactococcus lactis. *Applied and environmental microbiology*, 68(5):2468–2478, 2002. 38
- Droop, M. Vitamin b12 and marine ecology. iv. the kinetics of uptake, growth and inhibition in monochrysis lutheri. *J. Mar. Biol. Assoc. UK*, 48(3):689–733, 1968. 38, 95, 151
- Duarte, P. A mechanistic model of the effects of light and temperature on algal primary productivity. *Ecological Modelling*, 82(2):151–160, 1995. 151
- Dutkiewicz, S., Scott, J. R., and Follows, M. Winners and losers: ecological and biogeochemical changes in a warming ocean. *Global Biogeochemical Cycles*, 27(2):463–477, 2013. 136
- Eppley, R. W. Temperature and phytoplankton growth in the sea. *Fish. Bull.*, 70:1063–1085, 1972. 34, 61, 62, 70, 150
- Falconer, D. S., Mackay, T. F., and Frankham, R. Introduction to quantitative genetics (4th edn). *Trends in Genetics*, 12(7):280, 1996. 94
- Falkowski, P. G. and Raven, J. A. *Aquatic photosynthesis*. Princeton University Press, 2013. 1
- Falkowski, P., Barber, R., and Smetacek, V. Biogeochemical controls and feedbacks on ocean primary production. *Science*, 281:200–206, 1998. 136
- Falkowski, P. and Raven, J. A. *Aquatic photosynthesis*. Princeton University Press, New Jersey., 2007. 136
- Feller, G., d’Amic, D., and Gerday, C. Thermodynamic stability of a cold-active  $\alpha$ -amylase from the antarctic bacterium alteromonas haloplanctis. *Biochemistry*, 38(14):4613–4619, 1999. 79
- Field, C. B., Behrenfeld, M. J., Randerson, J. T., and Falkowski, P. G. Primary production of the biosphere: integrating terrestrial and oceanic components. *Science*, 281:237, 1998. 1

- Fielding, S. R. *Emiliana huxleyi* population growth rate response to light and temperature: a synthesis. *AQUATIC MICROBIAL ECOLOGY*, 73(2):163–170, 2014. 146
- Finkel, Z. V., Beardall, J., Flynn, K. J., Quigg, A., Rees, T. A. V., and Raven, J. A. Phytoplankton in a changing world: cell size and elemental stoichiometry. *Journal of Plankton Research*, 32(1):119–137, 2009. 3
- Flombaum, P., Gallegos, J. L., Gordillo, R. A., Rincón, J., Zabala, L. L., Jiao, N., Karl, D. M., Li, W. K., Lomas, M. W., Veneziano, D., et al. Present and future global distributions of the marine cyanobacteria prochlorococcus and synechococcus. *Proceedings of the National Academy of Sciences*, 110(24):9824–9829, 2013. 1
- Follows, M. J., Dutkiewicz, S., Grant, S., and Chisholm, S. W. Emergent biogeography of microbial communities in a model ocean. *science*, 315(5820):1843–1846, 2007. 35, 36
- Galmes, J., Kapralov, M., Copolovici, L., Hermida-Carrera, C., and Niinemets, Ü. Temperature responses of the rubisco maximum carboxylase activity across domains of life: phylogenetic signals, trade-offs, and importance for carbon gain. *Photosynthesis research*, 123(2):183–201, 2015. 73
- Garrido, M., Cecchi, P., Vaquer, A., and Pasqualini, V. Effects of sample conservation on assessments of the photosynthetic efficiency of phytoplankton using pam fluorometry. *Deep Sea Research Part I: Oceanographic Research Papers*, 71:38–48, 2013. 152
- Geider, R. J., MacIntyre, K. L., and Kana, T. M. A dynamic regulatory model of phytoplankton acclimation to light, nutrients, and temperature. *Limnology and Oceanography*, 43:679–694, 1998. 38
- Geider, R. Light and temperature dependence of the carbon to chlorophyll a ratio in microalgae and cyanobacteria: implications for physiology and growth of phytoplankton. *New Phytol*, 106(1):1–34, 1987. 38
- Geritz, S., Kisdi, E., Meszéna, G., and Metz, J. Evolutionarily singular strategies and the adaptive growth and branching of the evolutionary tree. *Evolutionary Ecology*, 12: 35–57, 1998. 94, 106
- Ghosh, K. and Dill, K. Cellular proteomes have broad distributions of protein stability. *Biophysical journal*, 99(12):3996–4002, 2010. 32, 33
- Gibbs, S. J., Bown, P. R., Ridgwell, A., Young, J. R., Poulton, A. J., and ODea, S. A. Ocean warming, not acidification, controlled coccolithophore response during past greenhouse climate change. *Geology*, 44(1):59–62, 2016. 146
- Gillooly, J. F., Brown, J. H., West, G. B., Savage, V. M., and Charnov, E. L. Effects of size and temperature on metabolic rate. *Science*, 293:2248–2251, 2001a. 45

## BIBLIOGRAPHY

---

- Gillooly, J. F., Brown, J. H., West, G. B., Savage, V. M., and Charnov, E. L. Effects of size and temperature on metabolic rate. *science*, 293(5538):2248–2251, 2001b. 69, 73
- Grimaud, G. M., Mairet, F., and Bernard, O. Modelling thermal adaptation in microalgae: an adaptive dynamics point of view. *19th IFAC World Congress, Cape Town (South Africa)*, 2014a. 137, 138, 140
- Grimaud, G. M., Rabouille, S., Dron, A., Sciandra, A., and Bernard, O. Modelling the dynamics of carbon–nitrogen metabolism in the unicellular diazotrophic cyanobacterium *crocospaera watsonii* wh8501, under variable light regimes. *Ecological Modelling*, 291:121–133, 2014b. 151
- Guillard, R. R. Culture of phytoplankton for feeding marine invertebrates. In *Culture of marine invertebrate animals*, pages 29–60. Springer, 1975. 11
- Guyot, S., Pottier, L., Hartmann, A., Ragon, M., Hauck Tiburski, J., Molin, P., Ferret, E., and Gervais, P. Extremely rapid acclimation of *escherichia coli* to high temperature over a few generations of a fed-batch culture during slow warming. *MicrobiologyOpen*, 3(1):52–63, 2014. 114
- Guyot, S., Gervais, P., Young, M., Winckler, P., Dumont, J., and Davey, H. M. Surviving the heat: heterogeneity of response in *saccharomyces cerevisiae* provides insight into thermal damage to the membrane. *Environmental microbiology*, 2015. 114
- Han, B.-P. Photosynthesis–irradiance response at physiological level: a mechanistic model. *Journal of theoretical biology*, 213(2):121–127, 2001. 151
- Harisson, G. Global stability of predator-prey interactions. *J. Math. Biology*, 8:159–171, 1979. 94
- Harris, P. S. Compensation effect and experimental error. *Nature*, 243:401, 1973. 81
- Hinshelwood, C. N. On the chemical kinetics of autotrophic systems. *J Chem Soc (Resumed)*, 136:745–755, 1952. 78, 156
- Hinshelwood, C. N. The chemical kinetics of bacterial cells. *Oxford at the Clarendon press*, 1945. 27
- Hobbs, J. K., Jiao, W., Easter, A. D., Parker, E. J., Schipper, L. A., and Arcus, L. V. Change in heat capacity for enzyme catalysis determines temperature dependence of enzyme catalyzed rates. *ACS Chemical Biology*, 8:2388–2393, 2013. 33
- Hofmann, G. E. and Todgham, A. E. Living in the now: physiological mechanisms to tolerate a rapidly changing environment. *Annual review of physiology*, 72:127–145, 2010. 7
- Hoppenrath, M. and Leander, B. S. Dinoflagellate phylogeny as inferred from heat shock protein 90 and ribosomal gene sequences. *PloS one*, 5(10):e13220, 2010. 3

- Howell, S. C., Inampudi, K. K., Bean, D. P., and Wilson, C. J. Understanding thermal adaptation of enzymes through the multistate rational design and stability prediction of 100 adenylate kinases. *Structure*, 22(2):218–229, 2014. 81
- Huertas, I. E., Rouco, M., and Lopez-Rodas, V. Warming will affect phytoplankton differently: evidence through a mechanistic approach. *Proceedings of the Royal Society B: Biological Sciences*, 278:3534–3543, 2011. 7, 13, 45, 114, 118, 136, 145, 146
- Huey, R. B. and Kingsolver, J. G. Evolution of thermal sensitivity of ectotherm performance. *Trends in Ecology & Evolution*, 4(5):131–135, 1989. 55
- Irwin, A. J., Finkel, Z. V., Müller-Karger, F. E., and Ghinaglia, L. T. Phytoplankton adapt to changing ocean environments. *Proceedings of the National Academy of Sciences*, 112(18):5762–5766, 2015. 146
- Ispolatov, I., Madhok, V., and Doebeli, M. Individual-based models for adaptive diversification in high-dimensional phenotype spaces. *Journal of theoretical biology*, 390:97–105, 2016. 152
- Iyer-Biswas, S., Wright, C. S., Henry, J. T., Lo, K., Burov, S., Lin, Y., Crooks, G. E., Crosson, S., Dinner, A. R., and Scherer, N. F. Scaling laws governing stochastic growth and division of single bacterial cells. *Proceedings of the National Academy of Sciences*, 111(45):15912–15917, 2014. 78
- Jensen, S. and Knutsen, G. Influence of light and temperature on photoinhibition of photosynthesis in *Spirulina platensis*. *Journal of applied phycology*, 5(5):495–504, 1993a. 37
- Jensen, S. and Knutsen, G. Influence of light and temperature on photoinhibition of photosynthesis in *Spirulina platensis*. *Journal of applied phycology*, 5(5):495–504, 1993b. 151
- Johnson, F. H. and Lewin, I. The growth rate of *E. coli* in relation to temperature, quinine and coenzyme. *Journal of Cellular and Comparative Physiology*, 28(1):47–75, 1946. 21, 26, 29
- Johnson, M. D., Völker, J., Moeller, H. V., Laws, E., Breslauer, K. J., and Falkowski, P. G. Universal constant for heat production in protists. *Proceedings of the National Academy of Sciences*, 106(16):6696–6699, 2009. 69
- Julou, T. *Evolution, competition and cooperation in bacterial populations*. PhD thesis, Ecole Normale Supérieure de Paris-ENS Paris, 2011. 9, 78, 114
- Karshikoff, A., Nilsson, L., and Ladenstein, R. Rigidity versus flexibility: the dilemma of understanding protein thermal stability. *FEBS Journal*, 2015. 81
- Kempes, C. P., Dutkiewicz, S., and Follows, M. J. Growth, metabolic partitioning, and the size of microorganisms. *Proceedings of the National Academy of Sciences*, 109(2):495–500, 2012. 69



## BIBLIOGRAPHY

---

- Kimura, H., Mori, K., Yamanaka, T., and Ishibashi, J. Growth temperatures of archaeal communities can be estimated from the guanine-plus-cytosine contents of 16s rrna gene fragments. *Environmental microbiology reports*, 5:468–474, 2013. 141
- Kingsolver, J. G. The well-temperated biologist. *The American Naturalist*, 174:755–768, 2009. 3, 45, 55, 114
- Kleiber, M. et al. Body size and metabolic rate. *Physiol. rev*, 27(4):511–541, 1947. 69
- Knies, J. L., Kingsolver, J. G., and Burch, C. L. Hotter is better and broader: thermal sensitivity of fitness in a population of bacteriophages. *The American Naturalist*, 173(4):419–430, 2009. 7, 10, 114
- Koch, A. L. Overall controls on the biosynthesis of ribosomes in growing bacteria. *Journal of theoretical biology*, 28(2):203–231, 1970. 79
- Koenker, R. and Bassett, G. Regression quantiles. *Econometrica: journal of the Econometric Society*, pages 33–50, 1978. 62
- Koenker, R. and Machado, J. A. Goodness of fit and related inference processes for quantile regression. *Journal of the american statistical association*, 94(448):1296–1310, 1999. 18
- Koenker, R. W. and d’Orey, V. Algorithm as 229: Computing regression quantiles. *Journal of the Royal Statistical Society. Series C (Applied Statistics)*, 36(3):383–393, 1987. 18
- Kooijman, S. A. L. M. *Dynamic energy budget theory for metabolic organisation*. Cambridge university press, 2010. 29
- Kovarova, K., Zehnder, A., and Egli, T. Temperature-dependent growth kinetics of escherichia coli ml 30 in glucose-limited continuous culture. *Journal of bacteriology*, 178(15):4530–4539, 1996. 38
- Kremer, C. T. and Klausmeier, C. A. Coexistence in a variable environment: Eco-evolutionary perspectives. *Journal of theoretical biology*, 339:14–25, 2013. 152
- Kuwabara, T., Minaba, M., Ogi, N., and Kamekura, M. *Thermococcus celericrescens* sp. nov., a fast-growing and cell-fusing hyperthermophilic archaeon from a deep-sea hydrothermal vent. *International journal of systematic and evolutionary microbiology*, 57(3):437–443, 2007. 62
- Laidler, K. J. The development of the arrhenius equation. *Journal of Chemical Education*, 61:494–498, 1984. 24
- Liberles, D. A., Teichmann, S. A., Bahar, I., Bastolla, U., Bloom, J., Bornberg-Bauer, E., Colwell, L. J., De Koning, A., Dokholyan, N. V., Echave, J., et al. The interface of protein structure, protein biophysics, and molecular evolution. *Protein Science*, 21(6):769–785, 2012. 56

- Lin, H., Kuzminov, F. I., Park, J., Lee, S., Falkowski, P. G., and Gorbunov, M. Y. The fate of photons absorbed by phytoplankton in the global ocean. *Science*, 351(6270): 264–267, 2016. 2
- Listmann, L., LeRoch, M., Schlüter, L., Thomas, M. K., and Reusch, T. B. Swift thermal reaction norm evolution in a key marine phytoplankton species. *Evolutionary Applications*, 2016. 136
- Liu, L. and Guoa, Q.-X. Isokinetic relationship, isoequilibrium relationship, and enthalpy-entropy compensation. *Chemical Review*, 101:673–695, 2001. 80
- Liu, L., Yang, C., and Guo, X.-Q. A study on the enthalpy-entropy compensation in protein unfolding. *Biophysical Chemistry*, 84:239–251, 2000. 81
- Lobry, J. R., Rosso, L., and Flandrois, J. P. A fortran subroutine for the determination of parameter confidence limits in non-linear models. *Binary*, 3:86–93, 1991. 25
- Longurst, A. R. *Ecological geography of the sea*. Academic Press. 527p., 1998. 2
- Lorius, C., Jouzel, J., Raynaud, D., Hansen, J., and Le Treut, H. The ice-core record: climate sensitivity and future greenhouse warming. *Nature*, 347(6289):139–145, 1990. 3
- Los, D. A., Mironov, K. S., and Allakhverdiev, S. I. Regulatory role of membrane fluidity in gene expression and physiological functions. *Photosynthesis research*, 116(2-3):489–509, 2013. 56
- Mafart, P., Couvert, O., Gaillard, S., and Leguérinel, I. On calculating sterility in thermal preservation methods: application of the weibull frequency distribution model. *International journal of food microbiology*, 72(1):107–113, 2002. 39
- Mairet, F., Bernard, O., Masci, P., Lacour, T., and Sciandra, A. Modelling neutral lipid production by the microalga *Isochrysis* aff. *galbana* under nitrogen limitation. *Bioresource Technology*, 102:142–149, 2010. 38
- Marañón, E., Cermeño, P., Huete-Ortega, M., López-Sandoval, D. C., Mouriño-Carballido, B., and Rodríguez-Ramos, T. Resource supply overrides temperature as a controlling factor of marine phytoplankton growth. *PloS one*, 9(6):e99312, 2014. 70, 136, 145
- Marchetti, J., Bougaran, G., Le Dean, L., Megrier, C., Lukomska, E., Kaas, R., Olivo, E., Baron, R., Robert, R., and Cadoret, J.-P. Optimizing conditions for the continuous culture of *isochrysis affinis galbana* relevant to commercial hatcheries. *Aquaculture*, 326:106–115, 2012. 13, 115
- Martiny, A. C., Pham, C. T., Primeau, F., Vrugt, J. A., and Moore, J. Strong latitudinal patterns in the elemental ratios of marine plankton and organic matter. *Nature Geoscience*, 6:279–283, 2013. 6

## BIBLIOGRAPHY

---

- Masci, P., Bernard, O., and Grogard, F. Continuous selection of the fastest growing species in the chemostat. In *17th IFAC World Congress*, pages 9707–9712, 2008. 114
- Massera, J. The existence of periodic solutions of systems of differential equations. *Duke Math. J.*, 17:457–475, 1950. 102
- Mata, T., Martins, A. A., and S., C. N. Microalgae for biodiesel production and other applications: a review. *Renew Sustainable Energy Rev*, 14:217–232, 2010. 7
- Metz, J. A. J., Nisbet, R., and Geritz, S. How should we define fitness for general ecological scenarios ? *Trends in Ecology and Evolution*, 7:4222–4229, 1992. 94, 106
- Metz, J., Mylius, S., and Diekmann, O. When does evolution optimize? *Evolutionary Ecology Research*, 10(5):629–654, 2008. 140
- Metz, J. A., Geritz, S. A., Meszéna, G., Jacobs, F. J., Van Heerwaarden, J. S., et al. Adaptive dynamics, a geometrical study of the consequences of nearly faithful reproduction. *Stochastic and spatial structures of dynamical systems*, 45:183–231, 1996. 94
- Miller, S. R., McGuirl, M. A., and Carvey, D. The evolution of rubisco stability at the thermal limit of photoautotrophy. *Molecular biology and evolution*, 30(4):752–760, 2013. 73
- Miller, S. Evidence for the adaptive evolution of the carbon fixation gene *rbcl* during diversification in temperature tolerance of a clade of hot spring cyanobacteria. *Molecular ecology*, 12(5):1237–1246, 2003. 73
- Miller, S. and Castenholz, R. Evolution of thermotolerance in hot spring cyanobacteria of the genus *Synechococcus*. *Appl. and Env. Micr.*, 66:4222–4229, 2000. 73, 74
- Mirrahimi, S., Perthame, B., and Wakano, J. Evolution of species trait through resource competition. *J. Math. Biol.*, 64:1189–1223, 2011. doi: 10.1007/s00285-011-0447-z. 109
- Moats, W. A. Kinetics of thermal death of bacteria. *Journal of Bacteriology*, 105(1): 165–171, 1971. 39, 40
- Monastersky, R. Monster el nino probed by meteorologists. *Nature*, 529(7586):267–268, 2016. 4
- Monod, J. The growth of bacterial cultures. *Selected Papers in Molecular Biology by Jacques Monod*, page 139, 2012. 22
- Muñoz-Tamayo, R., Mairet, F., and Bernard, O. Optimizing microalgal production in raceway systems. *Biotechnology progress*, 29(2):543–552, 2013. 38
- Murphy, K. P. and Gill, S. J. Solid model compounds and the thermodynamics of protein unfolding. *Journal of molecular biology*, 222(3):699–709, 1991. 31

- Murphy, K. P., Privalov, P. L., and Gill, S. J. Common features of protein unfolding and dissolution of hydrophobic compounds. *Science*, 247(4942):559–561, 1990. 29
- Nelder, J. A. and Mead, R. A simplex method for function minimization. *The computer journal*, 7(4):308–313, 1965. 18
- Nielsen, S. L. Size-dependent growth rates in eukaryotic and prokaryotic algae exemplified by green algae and cyanobacteria: comparisons between unicells and colonial growth forms. *Journal of Plankton Research*, 28(5):489–498, 2006. 61
- Niklas, K. J. A phyletic perspective on cell growth. *Cold Spring Harbor perspectives in biology*, 7(5):a019158, 2015. 69
- Norberg, J. Biodiversity and ecosystem functioning: A complex adaptive systems approach. *Limnol Oceanogr*, 49:1269–1277, 2004. 21, 34, 35, 61, 70, 137
- Olenina, I. Biovolumes and size-classes of phytoplankton in the baltic sea. 2006. 15
- Padfield, D., Yvon-Durocher, G., Buckling, A., Jennings, S., and Yvon-Durocher, G. Rapid evolution of metabolic traits explains thermal adaptation in phytoplankton. *Ecology Letters*, 1:1, 2015a. 153
- Padfield, D., Yvon-Durocher, G., Buckling, A., Jennings, S., and Yvon-Durocher, G. Rapid evolution of metabolic traits explains thermal adaptation in phytoplankton. *Ecology letters*, 2015b. 7, 136
- Parvinen, K., Dieckmann, U., and Heino, M. Function-valued adaptive dynamics and the calculus of variations. *Journal of Mathematical Biology*, 52(1):1–26, 2006. 152
- Peeters, J. and Eilers, P. The relationship between light intensity and photosynthesis a simple mathematical model. *Hydrobiological Bulletin*, 12(2):134–136, 1978. 37
- Pena, M. I., Davlieva, M., Bennett, M. R., Olson, J. S., and Shamoo, Y. Evolutionary fates within a microbial population highlight an essential role for protein folding during natural selection. *Molecular systems biology*, 6(1), 2010. 29
- Pfaundler, L. Beiträge zur chemischen statik. *Pogg. Ann. Phys. Chem.*, 131:55–85, 1867. 23
- Pittera, J., Humily, F., Thorel, M., Grulois, D., Garczarek, L., and Six, C. Connecting thermal physiology and latitudinal niche partitioning in marine synechococcus. *The ISME Journal*, 118:1751–7370, 2014. 73, 74, 101
- Poertner, H.-O. Integrating climate-related stressor effects on marine organisms: unifying principles linking molecule to ecosystem-level changes. *Marine Ecology Progress Series*, 470:273–290, 2012. 149
- Privalov, P. L. Stability of proteins small globular proteins. *Advances in protein chemistry*, 33:167–241, 1979. 29

## BIBLIOGRAPHY

---

- Privalov, P. and Khechinashvili, N. A thermodynamic approach to the problem of stabilization of globular protein structure: a calorimetric study. *Journal of molecular biology*, 86(3):665–684, 1974. 31
- Qin, Z., Balasubramanian, S. K., Wolkers, W. F., Pearce, J. A., and Bischof, J. C. Correlated parameter fit of arrhenius model for thermal denaturation of proteins and cells. *Annals of biomedical engineering*, 42(12):2392–2404, 2014. 39, 81
- Quinn, J., De Winter, L., and Bradley, T. Microalgae bulk growth model with application to industrial scale systems. *Bioresource technology*, 102(8):5083–5092, 2011. 38
- Ras, M., Steyer, J.-P., and Bernard, O. Temperature effect on microalgae: a crucial factor for outdoor production. *Reviews in Environmental Science and Bio/Technology*, 12(2):153–164, 2013. 3, 7, 36, 41, 151
- Ratkowsky, D., Lowry, R., McMeekin, T., Stokes, A., and Chandler, R. Model for bacterial culture growth rate throughout the entire biokinetic temperature range. *Journal of Bacteriology*, 154:1222–1226, 1983. 21, 25
- Ratkowsky, D., Olley, J., McMeekin, T. A., and Ball, A. Relationship between temperature and growth rate of bacterial cultures. *Journal of Bacteriology*, 149(1):1–5, 1982. 24, 25
- Ratkowsky, D. A., Olley, J., and Ross, T. Unifying temperature effects on the growth rate of bacteria and the stability of globular proteins. *Journal of theoretical biology*, 233(3):351–362, 2005. 29, 31
- Raven, J. A., Beardall, J., Larkum, A. W., and Sánchez-Baracaldo, P. Interactions of photosynthesis with genome size and function. *Philosophical Transactions of the Royal Society of London B: Biological Sciences*, 368(1622):20120264, 2013. 70
- Reboud, X., Majerus, N., Gasquez, J., and Powles, S. *Chlamydomonas reinhardtii* as a model system for pro-active herbicide resistance evolution research. *Biological Journal of the Linnean Society*, 91(2):257–266, 2007. 13
- Redfield, A. C. *On the proportions of organic derivatives in sea water and their relation to the composition of plankton*. university press of liverpool Liverpool, UK, 1934. 1
- Reuman, D. C., Holt, R. D., and Yvon-Durocher, G. A metabolic perspective on competition and body size reductions with warming. *Journal of Animal Ecology*, 83(1): 59–69, 2014. 136
- Reusch, T. B. and Boyd, P. W. Experimental evolution meets marine phytoplankton. *Evolution*, 67:1849–1859, 2012. 114, 136
- Riebesell, U. and Gattuso, J.-P. Lessons learned from ocean acidification research. *Nature Climate Change*, 5(1):12–14, 2015. 6

- Ripa, J. and Dieckmann, U. Mutant invasions and adaptive dynamics in variable environments. *Evolution*, 67:1279–1290, 2013. doi: 10.1111/evo.12046. 103, 139
- Robertson, A. D. and Murphy, K. P. Protein structure and the energetics of protein stability. *Chemical reviews*, 97(5):1251–1268, 1997. 29
- Rogelj, J., Meinshausen, M., and Knutti, R. Global warming under old and new scenarios using ipcc climate sensitivity range estimates. *Nature climate change*, 2(4):248–253, 2012. 4, 5
- Rose, J. M. and Caron, D. A. Does low temperature constrain the growth rates of heterotrophic protists? evidence and implications for algal blooms in cold waters. *Limnology and Oceanography*, 52(2):886–895, 2007. 61, 146
- Rosenberg, B., Kemeny, G., Switzer, R. C., and Hamilton, T. C. Quantitative evidence for protein denaturation as the cause of thermal death. *Nature*, (232):471 – 473, 1971. 29, 80, 81, 82
- Ross, T. *A philosophy for the development of kinetic models in predictive microbiology*. PhD thesis, University of Tasmania, 1993. 29, 31
- Rosso, L., Lobry, J., and Flandrois, J. An unexpected correlation between cardinal temperatures of microbial growth highlighted by a new model. *J Theor Biol*, 162: 447–463, 1993. 21, 25, 26, 46, 48, 52, 56, 150
- Rosso, L., Lobry, J., Bajard, S., and Flandrois, J. Convenient model to describe the combined effects of temperature and ph on microbial growth. *Applied and environmental microbiology*, 61(2):610–616, 1995. 106
- Rothschild, L. J. and Rocco, L. M. Life in extreme environments. *Nature*, 409:1092–1101, 2001. 45
- Ruoff, P., Zakhartsev, M., and Westerhoff, H. V. Temperature compensation through systems biology. *FEBS journal*, 274(4):940–950, 2007. 149
- Sal, S., Alonso-Sáez, L., Bueno, J., García, F. C., and López-Urrutia, Á. Thermal adaptation, phylogeny, and the unimodal size scaling of marine phytoplankton growth. *Limnology and Oceanography*, 2015. 61, 70
- Sandnes, J., Kllqvist, T., Wenner, D., and Gislerod, H. Combined influence of light and temperature on growth rates of *Nannochloropsis oceanica*: linking cellular responses to large-scale biomass production. *Journal of Applied Phycology*, 17:515–525, 2005. doi: 10.1007/s10811-005-9002-x. 100
- Sauterey, B., Ward, B. A., Follows, M. J., Bowler, C., and Claessen, D. When everything is not everywhere but species evolve: an alternative method to model adaptive properties of marine ecosystems. *Journal of plankton research*, page fb078, 2014. 146

## BIBLIOGRAPHY

---

- Sawle, L. and Ghosh, K. How do thermophilic proteins and proteomes withstand high temperature? *Biophysical journal*, 101(1):217–227, 2011. 33
- Schipper, L. A., Hobbs, J. K., Ruedge, S., and Arcus, V. L. Thermodynamic theory explains the temperature optima of soil microbial processes and high q10 values at low temperatures. *Global Change Biology*, 20:3578–3586, 2014. 21, 33, 34
- Schlüter, L., Lohbeck, K. T., Gutowska, M. A., Gröger, J. P., Riebesell, U., and Reusch, T. B. Adaptation of a globally important coccolithophore to ocean warming and acidification. *Nature Climate Change*, 4(11):1024–1030, 2014. 146
- Siddiqui, K. S. and Cavicchioli, R. Cold-adapted enzymes. *Annu. Rev. Biochem.*, 75: 403–433, 2006. 79, 81
- Smelt, J. P., Hellemons, J. C., Wouters, P. C., and van Gerwen, S. J. Physiological and mathematical aspects in setting criteria for decontamination of foods by physical means. *International Journal of Food Microbiology*, 78(1):57–77, 2002. 39
- Smelt, J. and Brul, S. Thermal inactivation of microorganisms. *Critical reviews in food science and nutrition*, 54(10):1371–1385, 2014. 39
- Smith, J. M. *Evolution and the Theory of Games*. Cambridge university press, 1982. 94
- Sommer, U. A comparison of the droop and the monod models of nutrient limited growth applied to natural populations of phytoplankton. *Functional Ecology*, pages 535–544, 1991. 95
- Stal, L. J. Is the distribution of nitrogen-fixing cyanobacteria in the oceans related to temperature? *Environmental microbiology*, 11(7):1632–1645, 2009. 151
- Storch, D., Menzel, L., Frickenhaus, S., and Portner, H. O. Climate sensitivity across marine domains of life: Limits to evolutionary adaptation shape species interactions. *Global change biology*, 2014. 64
- Sunagawa, S., Coelho, L. P., Chaffron, S., Kultima, J. R., Labadie, K., Salazar, G., Djahanschiri, B., Zeller, G., Mende, D. R., Alberti, A., et al. Structure and function of the global ocean microbiome. *Science*, 348(6237):1261359, 2015. 2, 19
- Taucher, J., Jones, J., James, A., Brzezinski, M., Carlson, C., Riebesell, U., and Passow, U. Combined effects of co2 and temperature on carbon uptake and partitioning by the marine diatoms *thalassiosira weissflogii* and *dactyliosolen fragilissimus*. *Limnology and Oceanography*, 2015. 35
- Thomas, M., Kremer, C., Klausmeier, C., and Litchman, E. A global pattern of thermal adaptation in marine phytoplankton. *Science*, 338:1085–1088, 2012. 14, 38, 93, 94, 136, 137, 141, 145, 146, 153
- Thomas, M. *The effect of temperature on the ecology, evolution, and biogeography of phytoplankton*. PhD thesis, MICHIGAN STATE UNIVERSITY, 2013. 3

- Thomas, M. K., Kremer, C. T., and Litchman, E. Environment and evolutionary history determine the global biogeography of phytoplankton temperature traits. *Global Ecology and Biogeography*, 2015. xi, xv, 4, 14, 53, 54, 55, 58, 70, 71, 137, 145
- Thompson, P. A., Guo, M.-x., and Harrison, P. J. Effects of variation in temperature. i. on the biochemical composition of eight species of marine phytoplankton1. *Journal of Phycology*, 28(4):481–488, 1992. 150
- Tikhonov, A. N. Systems of differential equations containing a small parameter multiplying the derivative. *Matematicheskii Sbornik*, 31:575–586, 1952. 138
- Ting, C. S., Rocap, G., King, J., and Chisholm, S. W. Cyanobacterial photosynthesis in the oceans: the origins and significance of divergent light-harvesting strategies. *Trends in microbiology*, 10:134–142, 2002. 1
- Tollefson, J. 2015 declared the hottest year on record. *Nature*, 529(7587):450, 2016. 4
- Toseland, A., Daines, S. J., Clark, J. R., Kirkham, A., Strauss, J., Uhlig, C., Lenton, T. M., Valentin, K., Pearson, G. A., Moulton, V., et al. The impact of temperature on marine phytoplankton resource allocation and metabolism. *Nature Climate Change*, 3(11):979–984, 2013. 56, 136
- Valdramidis, V., Geeraerd, A., and Van Impe, J. Stress-adaptive responses by heat under the microscope of predictive microbiology. *Journal of applied microbiology*, 103(5):1922–1930, 2007. 39
- Valik, L., Medvedova, A., Cizniar, M., and Liptakova, D. Evaluation of temperature effect on growth rate of lactobacillus rhamnosus gg in milk using secondary models. *Chemical Papers*, 67(7):737–742, 2013. 16, 26
- Van Uden, N. Temperature profiles of yeasts. *Advances in microbial physiology*, 25:195–251, 1985. 21, 41
- van't Hoff, J. Etudes de dynamiques chimiques. *F. Mullet and Co*, Amsterdam, 1889. 23
- Volk, T. and Hoffert, M. I. Ocean carbon pumps: Analysis of relative strengths and efficiencies in ocean-driven atmospheric co2 changes. *The Carbon Cycle and Atmospheric CO: Natural Variations Archean to Present*, pages 99–110, 1985. 1
- Ward, B. A. Temperature-correlated changes in phytoplankton community structure are restricted to polar waters. *PloS one*, 10(8):e0135581, 2015. 146
- Wei, Y., Wu, X., Xu, Z., Tan, Z., and Jia, S. A thermotolerant acetobacter pasteurianus t24 achieving acetic acid fermentation at high temperature in self-adaption experiment. In *Advances in Applied Biotechnology*, pages 287–293. Springer, 2015. 114



## BIBLIOGRAPHY

---

- Wijffels, R., Kruse, O., and Hellingwerf, K. Potential of industrial biotechnology with cyanobacteria and eukaryotic microalgae. *Current Opinion in Biotechnology*, 24:405–413, 2013. 7
- Wijffels, S., Roemmich, D., Monselesan, D., Church, J., and Gilson, J. Ocean temperatures chronicle the ongoing warming of earth. *Nature Climate Change*, 6(2):116–118, 2016. 4
- Wilhelmy, L. Über das gesetz, nach welchem die einwirkung der säuren auf den rohrzucker stattfindet. *Pogg. Ann.*, 81:413–433, 1850. 23
- Willey, J. *Prescott, Harley, and Klein's Microbiology-7th international ed./Joanne M. Willey, Linda M. Sherwood, Christopher J. Woolverton*. New York [etc.]: McGraw-Hill Higher Education, 2008. 53
- Winder, M. and Sommer, U. Phytoplankton response to a changing climate. *Hydrobiologia*, 698(1):5–16, 2012. 4
- Wright, J. J., Konwar, K. M., and Hallam, S. J. Microbial ecology of expanding oxygen minimum zones. *Nature Reviews Microbiology*, 10(6):381–394, 2012. 6
- Young, J. N., Goldman, J. A., Kranz, S. A., Tortell, P. D., and Morel, F. M. Slow carboxylation of rubisco constrains the rate of carbon fixation during antarctic phytoplankton blooms. *New Phytologist*, 205(1):172–181, 2015. 37
- Yvon-Durocher, G., Dossena, M., Trimmer, M., Woodward, G., and Alle, P. A. Temperature and the biogeography of algal stoichiometry. *Global Ecol Biogeogr*, 1:1, 2015. 4, 136, 153
- Zakhartsev, M., Yang, X., Reuss, M., and Pörtner, H. O. Metabolic efficiency in yeast *saccharomyces cerevisiae* in relation to temperature dependent growth and biomass yield. *Journal of thermal biology*, 52:117–129, 2015. 149
- Zavodszky, P., Kardos, J., Svingor, Á., and Petsko, G. A. Adjustment of conformational flexibility is a key event in the thermal adaptation of proteins. *Proceedings of the National Academy of Sciences*, 95(13):7406–7411, 1998. 81
- Zeldovich, K. B., Chen, P., and Shakhnovich, E. I. Protein stability imposes limits on organism complexity and speed of molecular evolution. *Proceedings of the National Academy of Sciences*, 104(41):16152–16157, 2007. 29, 31, 33, 45
- Zhang, J. Protein-length distributions for the three domains of life. *Genome Analysis*, 16(3):107–109, 2000. 33
- Zwietering, M. H., De Koos, J. T., Hasenack, B. E., De Witt, J. C., and Van't Riet, K. Modeling of bacterial growth as a function of temperature. *Applied and Environmental Microbiology*, 57(4):1094–1101, 1991. 16

## Abstract

Unicellular photosynthetic organisms forming the phytoplankton are the basis of primary production. Because these organisms cannot regulate their inner temperature, the medium temperature strongly constrains their growth. Understanding the impact of this factor is topical in a global change context. In this PhD thesis we have investigated how phytoplankton adapts to temperature. By analyzing the growth rate as a function of temperature for hundreds of species we highlighted the characteristics that can be accurately described by a mathematical model. We have identified the links between the cardinal temperatures as well as their thermodynamical fundament using the mechanistic Hinshelwood model. We then challenged the Eppley hypothesis ‘hotter is faster’ for 5 phylogenetic phytoplankton groups and determined the evolutionary limits for each of them. We have also studied the adaptation mechanisms associated to long term temperature variations by developing an evolutionary model using the adaptive dynamics theory allowing to predict the evolutionary outcome of species adaptation to a simple temperature cycle. Our results have been compared to a selection experiment carried out in a controlled device on *Tisochrysis lutea*. Our method has been extended to predict the adaptation of a strain to periodic temperature profiles and study phytoplankton adaptation at the global ocean scale. *In situ* data of sea surface temperature have been used as a forcing variable and have permitted to show that the elevation of temperature will be critical for several species in particular for those living in areas where the annual temperature fluctuation is high such as the Mediterranean sea.

## Résumé

Les organismes unicellulaires photosynthétiques formant le phytoplancton sont la base de la production primaire marine. Ne pouvant pas réguler leur température, ce facteur physique contraint fortement leur croissance. L'étude de son impact est d'une actualité brûlante dans un contexte de changement climatique. Dans cette thèse nous nous sommes efforcés de comprendre comment le phytoplancton s'acclimate à la température. En analysant la réponse du taux de croissance à la température de centaines d'espèces, nous avons mis en évidence les liens existant entre les températures cardinales ainsi que leurs fondements thermodynamiques grâce au modèle mécaniste de Hinshelwood. Nous avons testé l'hypothèse de Eppley 'plus chaud implique plus rapide' pour 5 groupes phylogénétiques de phytoplancton et défini leurs limites évolutives intrinsèques. Nous avons examiné les mécanismes d'adaptation induits à long terme par des variations de température et construit un modèle évolutif en utilisant la théorie de la dynamique adaptative afin de prévoir l'issue évolutive de l'adaptation d'une espèce à un cycle de température simple. Nos résultats ont été confrontés à une expérience de sélection réalisée en laboratoire sur *Tisochrysis lutea*. Notre méthode a été étendue pour prédire l'adaptation d'une souche soumise à un profil de température périodique et étudier l'adaptation thermique du phytoplancton à l'échelle de l'océan mondial. Des données *in situ* de température de surface de l'océan ont permis de forcer le modèle et de montrer qu'une augmentation de température sera critique pour certains groupes dans les zones où l'amplitude thermique annuelle est grande, comme par exemple la mer Méditerranée.